NANYANG TECHNOLOGICAL UNIVERSITY

SYNTHESIS, CHARACTERIZATION AND APPLICATION OF N-DITHIENO[3,2-B:2',3'-D]PYRROLES/FLUORENE DERIVATIVES BASED CONJUGATED MOLECULES/POLYMERS

LU YONG

A THESIS SUBMITTED

FOR THE OF DOCTOR OF PHILOSOPHY

DIVISION OF CHEMICAL & BIOMOLECULAR ENGINEERING

NANYANG TECHNOLOGICAL UNIVERSITY

2010

SYNTHESIS, CHARACTERIZATION AND APPLICATION OF N-DITHIENO[3,2-B:2',3'-D]PYRROLES/FLUORENE DERIVATIVES BASED CONJUGATED MOLECULES/POLYMERS

LU YONG

(M Sc)

A THESIS SUBMITTED

FOR THE OF DOCTOR OF PHILOSOPHY

DIVISION OF CHEMICAL & BIOMOLECULAR ENGINEERING

NANYANG TECHNOLOGICAL UNIVERSITY

2010

Acknowledgements

First and foremost, I wish to express my sincere gratitude to my supervisor, Professor Ng Siu Choon for his invaluable guidance and constant advice throughout my project. Moreover, his keen and vigorous academic observation enlightens me not only in my research work but also in my future study.

I would like to express my heartfelt thanks to Professor Hu Xiao from MSE for his instructive advice and useful suggestion pertaining to my research work. With his help in so many ways, my project can be completed with competence.

Special thanks go to Dr Chen Hui who has unreservedly devoted his valuable time and experience to help me fulfil the project. Thanks also go to other members in our team for their advice and friendship.

I would also like to gratefully acknowledge Nanyang Technological University for providing me the opportunity to take the PhD program with financial support. The supports and research facilities provided by the Division of Chemical and Biomolecular Engineering, NTU are greatly appreciated.

Last but not the least, I would like to express my thanks to my parents without whose supports I could not have arrived at this point.

Table of Contents

Summary

Semiconducting conjugated materials have attracted intensive interests during recent decades due to their potential applicability in organic electronics, such as organic photovoltaics and organic transistors. The structural modification of conjugated materials significantly influences their optical and electronic properties. This dissertation examined novel conjugated materials based on N-functionalized dithieno[3,2-b:2’,3’-d]pyrrole (DTP) and fluorene derivatives. The study was focused on the preparation and characterization of donor and acceptor (p- and n-type) materials which are potential candidates in organic electronics.

For the p-type materials, polymers based on N-functionalized DTP units have been prepared using Stille coupling reactions with good yields in Chapter 3 and 4. Their structures are confirmed by NMR and elemental analyses. They are soluble in common organic solvents such as chloroform and THF. TGA results showed that they have good thermal stability. The investigation of their optical and electrical properties revealed that these polymers (discussed in chapter 3 and chapter 4) are low band gap (<1.8 eV) polymers. Polymers with such low band gaps are beneficial for light harvesting and are promising donor materials for organic solar cells. Consequently, organic photovoltaic devices based on the blend of selected polymers (donor) and PCBM (acceptor) are fabricated and investigated and preliminary results show that a PCE of 0.51% can be achieved based on polymer containing DTP moiety as donor material. In addition, in order to investigate side chain influence on polymer’s properties, in Chapter 5, a series of DTP and fluorene copolymers were prepared. The polymers physical, optical and electrical properties are characterized and discussed.

The results indicate that the side chain of the polymer can influence the polymer's solubility as well as their optical and electrical properties. It is generally believed that the rigid and planar structures of these polymers can facilitate charge transfer. Accordingly, these polymers are potential candidates in the application of organic electronics such as OFETs.

For the n-type materials, novel bisfluorenyl substituted perylene diimide (Chapter 6) has been prepared and investigated. Its structure characterized by NMR and MS analysis. The oligomer is soluble in common organic solvents such as chloroform, THF and toluene. TGA results show that it has good thermal stability, whilst the electrical results indicate that the oligomer is a comparable accepter material to PCBM. Organic photovoltaic devices based on the blend of P3HT (donor) and the oligomer (acceptor) are fabricated and their device characteristic investigated. So far power conversation efficiency of 0.13% can be achieved based on the device. In addition, polymers based on tetrabenzo[5,5] and fluorone (Chapter 7 and Chapter 8) have been synthesized and their structures characterized. These polymers are soluble in common organic solvents and thermally stable. Investigations on the electrical properties of these polymers shows that they all have electron accepting characteristics, and thus are potential candidates for acceptor materials in organic electronics.

Publications

[1] Y. Lu, H. Chen, F. Qiao, X. Hu and S. C. Ng. Synthesis, Characterization and Photovoltaic Application of N, N'-Bisfluorenyl Substituted Perylene Bisimide. Sol. Energy Mater. Sol. Cells, (2010), 94, 2034-2041.

[2] Y. Lu, H. Chen, X. Hou, X. Hu and S. C. Ng. A Novel Low Band Gap Polymer Based on N-Substituted Dithino[3,2-b:2',3'-d]pyrrole. Synth. Met., (2010), 160, 1438-1441.

[3] F. Qiao, X. Hou, Y. Lu, H. Chen, A. Liu, X. Hu and S. C. Ng. Photovoltaic Characterization of Poly(2,5-bis(3-dodecylthiophen-2-yl)-2,2''-biselenophene) for Organic Solar Cells. Sol. Energy Mater. Sol. Cells, (2010), 94, 442-445.

[4] H. Chen, Y. Lu, T. T. Ong, X. Hu and S. C. Ng. Synthesis, Characterization and Properties of Regioregular Conjugated Polymers Containing Quaterthiophene and an Acceptor Repeating Unit. J. Polym. Sci .Part A: Polym. Chem., (2009), 47, 2163-2171.

[5] Y. Lu, H. Chen, F. Qiao, X. Hou, X. Hu and S. C. Ng. Synthesis, Characterization and Photovoltaic Application of Low Band Gap N-Functionalized Dithienopyrrole Based Conjugated Polymers. To be submitted.

[6] Y. Lu, H. Chen, X. Hou, X. Hu and S. C. Ng. A New Generation of Acceptor Polymeric Materials Based on Tetrabenzo[5,5']fulvalene: Synthesis, Characterization and Their Photovoltaic Performances. To be submitted.

Chapter 1
General Introduction

1.1 Conjugated polymers

Conjugated polymers (or semiconductive polymers) are materials comprising a sequence of alternating single and double (or triple) bonds along the polymer skeleton, forming an extended π-conjugated system. Since the first discovery of polyacetylene (PA) film with electrical conductivity by Shirakawa, MacDiarmid, Heeger and coworkers[1], conjugated polymers have been attracting increasing interest during the past 30 years. Polyacetylene (PA) is an organic polymer with a repeat unit $(C_2H_2)_n$. In its natural state, PA is not conductive, which indicates that the π-conjugated system does not contribute to the conductivity. However, after treated with chlorine, bromine or iodine vapor, the conductivity of PA films is 10^9 times higher than it is originally. Such treatment with oxidants to PA films is analogous with the doping of inorganic semiconductors and this process is the major factor for the highly accentuated electrical conductivity in PA films. This discovery of PA's conductive characteristics opened the modern era of conjugated polymers. Since polymers were already known for their outstanding physical properties, such as low density, high mechanical strength, low cost and easy processability, the combination of electrical conductivity with these favorable physical properties make conjugated polymers ideal materials in many fields. Since then, a large numbers of conjugated polymers have been synthesized and studied, including polyaniline (PAN), polypyrrole (PPyR), polythiophene (PT), poly(p-phenylene) (PPP) and poly(p-phenylene vinylene) (PPV),

etc. The electrical conductivity of these polymers ranges from 10^{-10} S/cm (typical of insulators) to 10^{4} S/cm (nearly the conductivity of a metal such as copper). Some of the common conjugated polymers are depicted in **Table 1.1**.

Table 1.1 Examples of Conjugated Polymers.

Polymers	Abbreviation	Formula
trans-Polyacetylene	PA	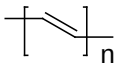
Poly(p-phenylene)	PPP	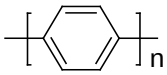
Poly(p-phenylenevinylene)	PPV	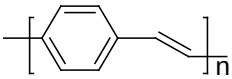
Polypyrrole	PPyR	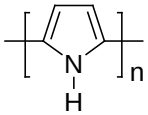
Polyaniline	PAN	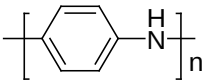
Polythiophene	PT	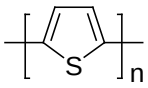

1.1.1 Bandgap and energy levels of conjugated polymers

In order to understand the optical and electrical properties of conjugated polymers, the simple band theory[2] provides an apt basis. According to the difference in conductivity, solid materials are usually classified as conductors (usually metals), insulators and semi-conductors.

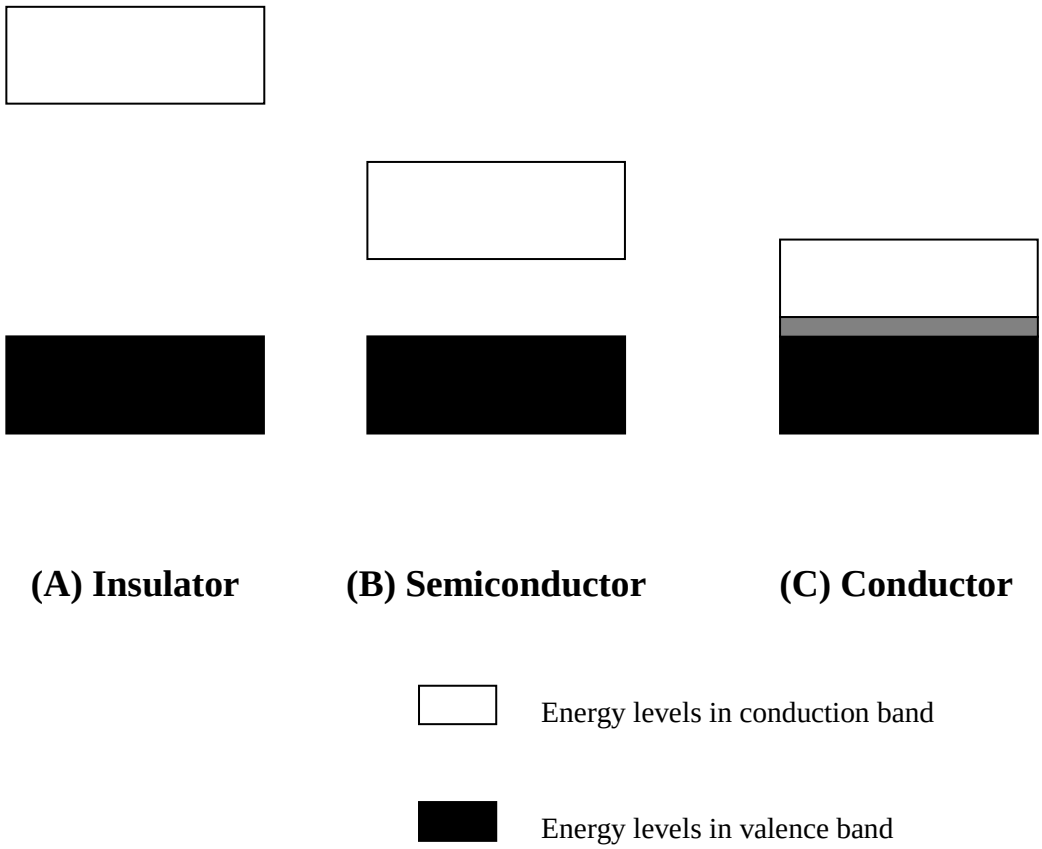

Figure 1.1 A schematic representation of energy gap in (A) insulator (B) semiconductor (C) conductor

An efficient way of visualizing the difference of the three materials is to plot the available energies for electrons in them. Instead of having discrete energies as in the case of free atoms, the available energy states form bands. The migration of electrons in the conduction band is crucial to the conduction. In insulators, the electrons in the valence band are separated by a large gap from the conduction band. In conductors like metals the valence band overlaps with the conduction band. In semiconductors the gap between the valence and conduction bands is narrow enough that thermal or other excitations can bridge the gap. With such a small gap, the presence of a certain percentage of a doping material can increase conductivity dramatically. **Figure 1.1** shows the energy gap of respective materials.

The electrical and optical properties of conjugated polymers are mainly determined by their π-electron systems. By analogy, the bonding π and anti-bonding π^* orbitals generate energy bands that are fully occupied (π band) and empty (π^* band). The π-electron level with highest energy is referred as the highest occupied molecular orbital (HOMO) and is known as the valence band. The lowest energy π^*-electron level is referred as the lowest unoccupied molecular orbital (LUMO) and is also known as the conduction band. The HOMO and LUMO level are regarded as the frontier orbitals in a π- π^* system of the conductive polymer. The energy difference between HOMO and LUMO is referred to as HOMO-LUMO gap of a conjugated polymer and it can be determined using cyclic voltammetry (CV) by the difference between the standard potentials in solution. The determination of bandgap can be effected using optical or electrochemical methods, through UV-visible absorption spectra and cyclic voltammetry (CV) respectively. In addition, CV can afford the onset values of the oxidation and reduction potentials of a material in solution relative to a reference redox couple and the values of HOMO and LUMO can be calculated accordingly.

In addition, Jablonski diagrams are common representations of the possible energetic states and transitions as molecules enter and leave the excited state. Jablonski diagrams describe the electronic states of molecules, transitions and associated light emitting phenomena. The y-axis, labeled E, indicates the relative energies of the electronic states. Within each electronic state a range of vibrational levels exist and can be considered as HOMO and LUMO levels in conjugated polymers, as shown in **Figure 1.2**. Molecules can progress from one state to another via either radiative or nonradiative processes. Graphically, nonradiative transitions are shown as straight lines and radiative transitions are shown with squiggly lines on a Jablonski diagram.

Many photo-physical processes can occur if the molecules are excited. For example, once the molecule is excited by photons, the electron at HOMO level will gain energy and jump to LUMO level. Since the electron at LUMO level is metastable, it comes down to the vibrational levels and releases energy. The released energy can be radiative (eg. fluorescence) or non-radiative, which can be tuned according to the characteristics of particular organic electronics.

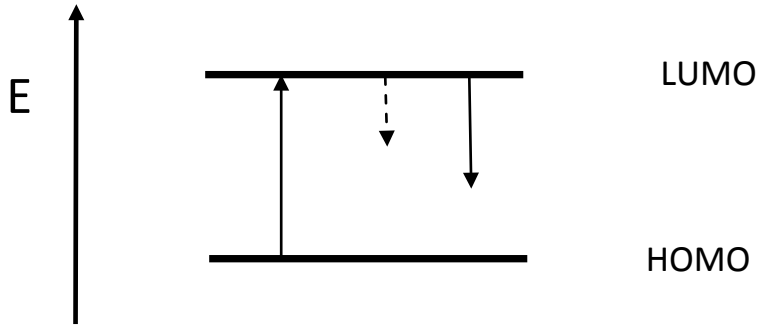

Figure 1.2 A simple Jablonski diagrams representation of energy level.

1.1.2 Conductivity of conjugated polymers

In order to make conjugated polymers conductive, charge carriers have to be introduced and the following three approaches are invariably used: 1) doping-induced charge carriers. 2) photo- and radiation-induced charge carriers. 3) charge carriers from suitable electrodes. However, in comparison with metals and traditional semiconductors, the conduction mechanism of conjugated polymers is notably different. In metals, the intrinsic presence of free electrons accounts for high conductivity. For traditional semiconductors such as silicon, coordination of each atom to its neighbour via covalent bands leads to a rigid structure and electronic excitation can be usually considered in the context of this rigid structure leading to the conventional concepts of electrons and holes as the dominant excitation. However, the

structural characteristic of conjugated polymers is a conjugated π system extending over repeating units along the backbone and the twofold coordination makes these systems generally more susceptible to structural distortion, resulting in low-dimensional materials with a high anisotropy in conductivity, which is higher along the chain direction. The value of conductivity (σ) of conjugated polymers can be determined by the following equation[3] in solid state physics:

$$\sigma = n e \mu$$

where n is the number of mobile charge carriers, e is the elementary charge and μ is the mobility of the charge carriers, so the number and mobility of charge carriers are the two major factors contributing to the conductivity of polymers.

1.1.3 Stability and processibility of conjugated polymers

The possibility of conjugated polymers of neutral state is very crucial for commercial use because it is imperative that the candidate materials exhibit good environmental stability and be amenable to a wide variety of processing techniques. The stability of a conjugated polymer of neutral state depends on a number of factors, which include the susceptibility to external chemical species, the reactivity of its doped sites and the conformational states of its backbone, etc. The investigation of the polymer's stability is of importance to the successful utilization of these materials in commercial applications.

Soluble conjugated polymers can be processed by wet techniques such like spin-coating, which is a straightforward procedure used to fabricate uniform thin films on flat substrates. However, some conjugated polymers with rigid planar backbones severely limit the possibilities of processing using wet techniques due to their poor

solubility. Novel processing schemes have been developed and are conveniently divided into four categories. The first category is the manipulation of soluble precursor polymers. This scheme is based on the synthesis and manipulation of a processable, non-conducting precursor polymer that, once fabricated into a suitable form using the conventional polymer processing technique, can be converted into an insoluble electrically conducting polymer. The second processing scheme is the manipulation of soluble conducting polymer derivatives and copolymers. This scheme is to modify the structure of the polymer in such a way to improve the processability without compromising its electrical and optical properties. The third processing scheme is the in-situ polymerization of monomers in insulating matrix polymers. This processing scheme focuses on the growth of insoluble, intractable conjugated polymers with a performed polymer matrix. In this case, a processible, insulating polymer impregnated with a catalyst system is fabricated into a desirable form such as a thin film or fiber. This activated polymer matrix is then exposed to the monomer, usually in the form of a gas or vapor, resulting in a blend comprised of an isolated or semi-continuous conjugated polymer phase dispersed throughout a continuous phase of the host polymer. The last processing scheme is the manipulation of conducting polymers via the Langmuir-Blodgett technique. This technique relies on the ability of the LB trough to manipulate surface active molecules into highly ordered thin films with structures and film thickness that is controllable at the molecular level. The true promise of the LB processing technique is its unique ability to allow control over the molecular architecture of conducting polymer thin films.

1.2 Application of conjugated materials: organic photovoltaics (solar cell) (OPVs)

1.2.1 Introduction

In the early years of 19th century, Becquerel discovered that a photocurrent could be generated when platinum electrodes, covered with silver bromide or silver chloride, were illuminated in aqueous solution. Thereafter, Smith made the first reports on photoconductivity in 1873. The scientific interests as well as the commercial potential led to increased research into photoconductivity and related subjects. In 1954 the first inorganic solar cell was developed at Bell Laboratories[4]. It was based on silicon and had power conversion efficiency of 6%. Over the years the power conversion efficiency of crystalline silicon solar cells has reached 24% in the laboratory[5]. Today the silicon based solar cells are by far the most dominant type of photovoltaics (PVs) used and account for 99% of all PVs[6]. In the past 20 years, as the evidence for global warming continues to build up and the exhaustion of fossile resources, the demand for solar energy has grown consistently with growth rates of 20–25% per annum. Fifty years of research and innovation have dramatically reduced the cost of silicon based PVs while the technology of further reducing silicon based PVs is confined to niches. The high cost of the silicon PVs limits its competition with conventional energy sources[7] and thus the semiconductor PVs account for < 0.1% of the total world energy production. Organic semiconductors including conjugated polymers and oligomers are a less expensive alternative to inorganic semiconductors like silicon. In addition, most of organic semiconductors can be processed from solution, which is commonly known as wet techniques. In particular, conjugated polymers are attractive in this respect due to their superior material properties combined with a large number of facile and low-cost processing techniques. Thus, even a rather low efficiency (5%) of

organic photovoltaics (OPVs) would be good enough to compete with the silicon based inorganic PVs. In addition, the fact that conjugated polymers are flexible and thin opens a whole range of possibilities. Among organic solar cells there is another class of dye-sensitized OPV, which are attractive due to their favourable efficiencies. In this work only conjugated polymers based OPVs will be discussed and reviewed.

1.2.2 Structure of OPVs

A simple structure of a solar cell is shown in **Figure 1.3**. The devices are fabricated in sandwich geometry including substrates, active layer and electrodes. For substrates, conducting electrodes such as transparent glass or plastics covered with indium tin oxide (ITO) are commonly used. The ITO electrodes are transparent with good conductivity. In addition, poly(ethylenedioxythiophene) (PEDOT) doped with polystyrenesulfonic acid (PSS) is coated on ITO surface from an aqueous solution. This PEDOT : PSS layer improves the surface quality of the ITO electrode as well as facilitates the hole injection/extraction. Furthermore, the work function of this electrode can be changed by chemical or electrochemical redox reactions of the PEDOT layer[8]. For OPVs, the active layers can be systems of donor-acceptor blends such as polymer/polymer, polymer/small molecule, or small molecule/small molecule, which are coated from solution. The top electrode is evaporated using a lower work-function metal than that of ITO such as aluminium with an ultrathin lithium fluoride underlayer. The exact role of this LiF underlayer is unknown yet. Generally, in photoelectron spectroscopy studies, it has been shown that the metal work function can be considerably reduced by evaporation of LiF layers.

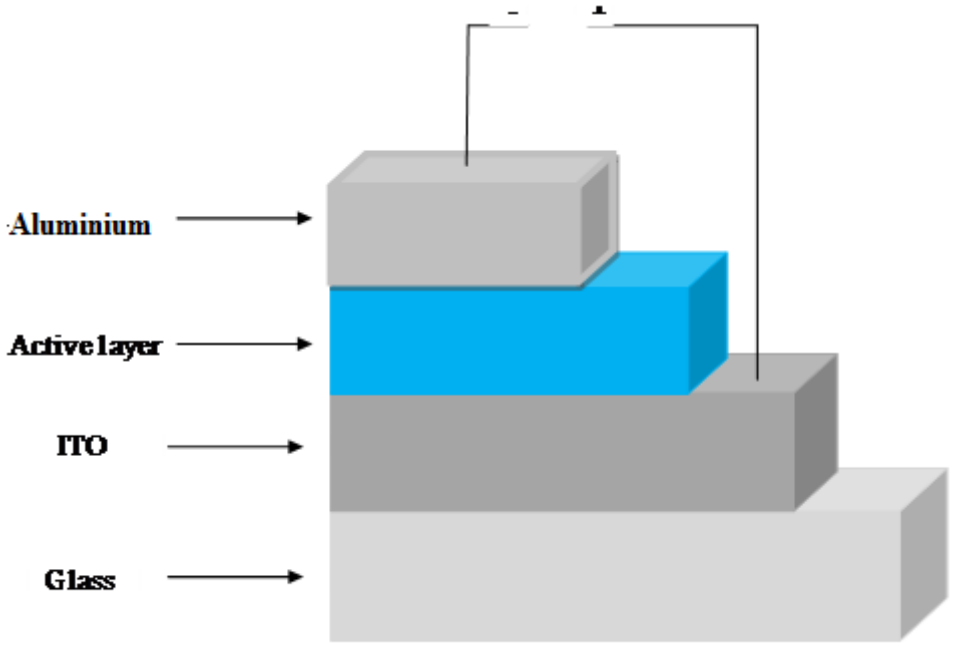

Figure 1.3 Structure of an organic solar cell device.

1.2.3 Materials used in OPV active layer

The active layer of OPVs consists of the electron donating materials (p-type) and the electron accepting materials (n-type) that introduce free charge carriers by photo induced electron transfer. Important representatives of p-type semiconducting polymers are (i) derivatives of phenylene vinylene backbones such as poly[2-methoxy-5-(3,7-dimethyloctyoxy)]-1,4-phenylenevinylene (MDMO-PPV); (ii) derivatives of thiophene chains such as poly(3-hexylthiophene) (P3HT); and (iii) derivatives of fluorene backbones such as poly[9,9'-dioctylfluorene-co-bis-N,N'-(4-butylphenyl-1,4-phenylenediamine)] (F8T2). For n-type semiconducting materials, C_{60} fullerene is known to a good electron acceptor and can be electrochemically reduced with up to six electrons[9]. However, the solubility of C_{60} is quite poor. Wudl et al. developed a soluble derivative of C_{60}, PC61BM[10], which has been widely used in conjugated polymers based OPVs due to its improved solubility. Rylenes, such as

naphthalene, perylene, etc. can be easily converted into the corresponding anhydrides or diimides derivatives , which have been used as n-type materials due to their good electron accepting ability[11]. Some examples of the materials used in active layer of OPVs are shown in **Figure 1.4.**

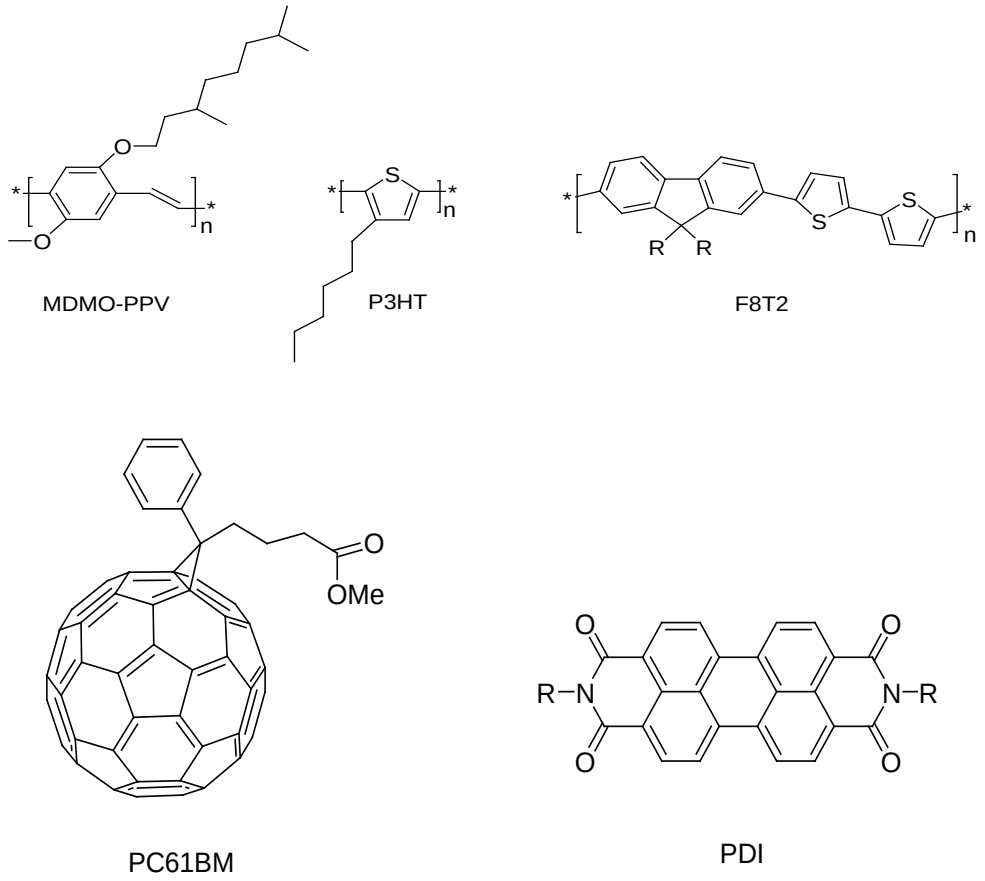

Figure 1.4 Examples of p-type and n-type materials used in OPVs.

The common architectures of active layer in OPVs can be divided into two types, bilayer and heterojunction. In a bilayer device, p-type and n-type organic semiconductors are sequentially stacked on top of each other and the organic semiconductors used are combinations of many different materials[12-16]. In such

devices, only excitons created within a distance of 10-20 nm from the interface are able to reach the heterojunction interface. Absorbed photons further away from the interface are lost, resulting in low quantum efficiencies[17]. Consequently, the efficiency of bilayer solar cells is limited by the charges generated within 10-20 nm of the donor-acceptor interface. Using thicker films creates optical filter effects of the absorbing material before light gets to the interface, leading to a reduced photocurrent[18]. Further, the film thicknesses have to be optimized for interference effects in the multiple stacked thin film structure[19]. Arising from the efficiency limitation of bilayer device and excitions dissociation difficulty in most organic semiconductors, the bulk heterjunction (BHJ) concept came up in the 1990's and widely explored since then. Currently BHJ organic solar cells are mostly used in OPV fabrication and investigation. In a BHJ device, a blend of the donor and acceptor components in bulk phase is used. It exhibits a donor-acceptor phase separation in a 10-20 nm (perhaps a bit more in reality) length scale. In such a nanoscale interpenetrating network, each interface is within a distance less than the exciton diffusion length from the absorbing site. The concept of BHJ has substantively increased (by several orders of magnitude) the interfacial area between the donor and acceptor phases and resulted in improved solar cells efficiency[20]. In contrast to the bilayer architecture where the donor and acceptor phases are completely separated from each other and selectively in contact with the anode and cathode, in the BHJ both phases are intimately intermixed. This mixture has no symmetry breaking in the volume. There is no preferred direction for the internal fields of separated charges; that is, the electrons and holes created within the volume have no net direction they should move. Therefore, a symmetry breaking condition (like using different work-

function electrodes) is essential in BHJ. Otherwise, only concentration gradient (diffusion) can act as driving force. Furthermore, separated charges require percolated pathways for the hole and electron transporting phases to the contacts. In other words, the donor and acceptor phases have to form a nanoscale, bi-continuous, and interpenetrating network[21]. BHJ devices are much more sensitive to the nanoscale morphology in the blend. BHJ OPVs can be achieved by co-deposition or solution casting of donor and acceptor blends[9-10].

1.2.4 Operation Principles of OPVs

Figure 1.5 shows the simplified operation principles in OPVs. When light is absorbed by the active layer, an electron is promoted from the HOMO level to the LUMO level in the donor material, forming an exciton. The primary excitation is a coulombically bound electron-hole pair in organic conjugated polymers and does not directly and quantitatively lead to free charge carrier. It is estimated that only 10% of the primary excitations lead to free charge carriers in conjugated polymers[22]. However, exciton dissociation must be followed up so that the electron can reach one electrode while the hole can reach the other electrode. In order to achieve efficient charge separation an electrical field is necessary. Such local fields can be supplied via externally applied electrical fields as well as via interfaces of the two materials. At an interface, strong enough local electrical fields are possible if abrupt changes of the potential energy occur. When the exciton has reached such an interface, photoinduced charge transfer occurs.

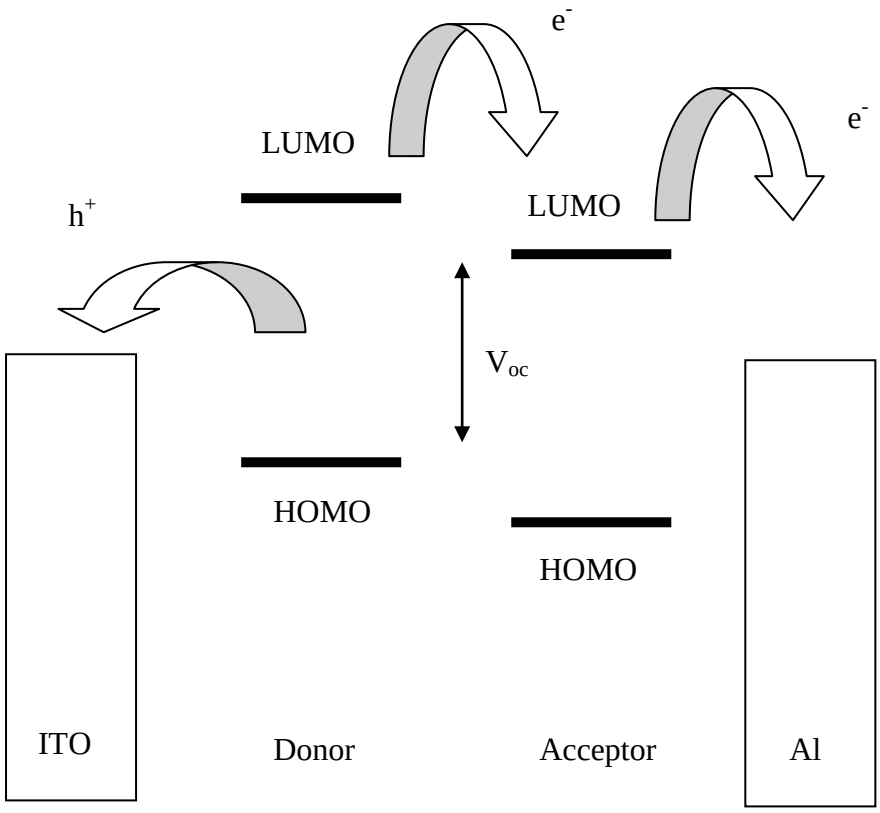

Figure 1.5 Scheme of operation principle in OPVs.

In a BHJ OPVs, a conjugated polymer and an electron-acceptor material are blended as the active layer. Studies show that PC61BM is a very ideal acceptor material for excitons dissociation. Excitons can separate into free charge carriers at the interfaces of the conjugated polymer and PC61BM with high efficiency. The created charges then need to be transported to the appropriate electrodes so that a driving force for such transport is needed. A gradient in the chemical potentials of electrons and holes exists in donor-acceptor junction and it is determined by the difference between HOMO level of the donor and the LUMO level of the acceptor. This internal electrical field determines the open circuit voltage (V_{oc}) of a device and contributes to a field-induced drift of charge carriers. In addition, the asymmetrical ionisation energy/work functions of the electrodes are proposed to lead to an external field in

short circuit condition. Another driving force can be the concentration gradients of the respective charges, which lead to a diffusion current. At the same time, the transport of charges is affected by recombination on the pathway to the electrodes, particularly if the same material serves as transport medium for both electrons and holes[23]. Finally, the free charge carriers are extracted from the device through two selective electrodes. One is the electrode of transparent ITO, which matches the HOMO levels of most of the conjugated polymers. The other electrode is evaporated aluminium metal, which matches the LUMO of acceptor PC61BM. Consequently, electricity is generated in the external lead between the two electrodes.

1.2.5 Characteristics of OPV

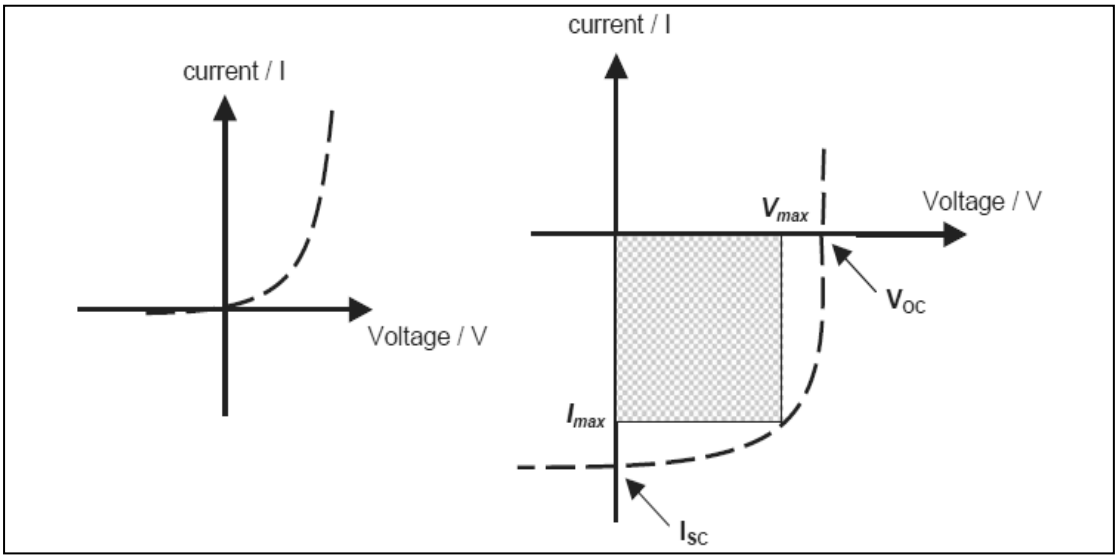

Figure 1.6 I–V curves of OPV in the dark (left) and under illumination (right). The opencircuit voltage (V_{oc}) and the short-circuit current (I_{sc}) are shown. The maximum output is given by the square $I_{max} \times V_{max}$.

The current-voltage characteristics of an organic solar cell in the dark and under illumination are shown in **Figure 1.6**. In the dark, there is almost no current flowing, until the electrodes start to inject at forward bias for voltages larger than V_{oc}. Under illumination, the OPV device generates power. At maximum power point, the product

of current and voltage is the largest[24]. The photovoltaic power conversion efficiency of an OPV is determined by the following formula:

$$\eta = \frac{V_{oc} \times I_{sc} \times FF}{P_{in}}$$

$$FF = \frac{I_{max} \times V_{max}}{I_{sc} \times V_{oc}}$$

where V_{oc} is the open circuit voltage, I_{sc} is the short circuit current, FF is the fill factor and P_{in} is the incident light power density. This light intensity is standardized at 1000 W/m^2, which is called as the AM 1.5 spectrum[25]. I_{max} and V_{max} are the current and voltage at the maximum power point.

Generally, the V_{oc} in an OPV is found to be linearly dependent on the HOMO level of the donor material and the LUMO level of the acceptor material by theory[26-27]. However, V_{oc} will be affected by many factors in practice. Charge carrier losses at electrodes lower the open circuit voltage[28]. V_{oc} is also affected by the nano morphology of the active layer in the polymer fullerene BHJ OPVs[29]. Interfacial effects at the metal/organic semiconductor interface such as the formation of metal oxide change the work function of the electrodes and influence V_{oc}[30]. In brief, the V_{oc} of an OPV is a sensitive function of energy levels of the used materials as well as their interfaces.

The I_{sc} is determined by the product of the photo induced charge carrier density and the charge carrier mobility within the organic semiconductors:

$$I_{sc} = ne\mu E$$

where n is the density of charge carriers, e is the elementary charge, μ is the mobility and E is the electric field. Assuming the 100% efficiency for the photo induced charge generation in the active layer of a BHJ OPV, n is the number of absorbed photons per

unit volume. For a given material, the bottleneck is the mobility of charge carriers. Mobility is not a material parameter but a device parameter. It is sensitive to the nanoscale morphology of the organic semiconductor thin film[31-33]. The final nano morphology of the film depends on many parameters of preparation, such as solvent type, the solvent evaporation time, the temperature of the substrate, and/or the deposition method[34-35]. The architecture of a bulk heterojunction enlarges the interfacial area between donor and acceptor phases dramatically. However, the down side to this would be the complicated nano morphology of a blend that is difficult to optimize and control[36]. Fill factor is determined by charge carriers reaching the electrodes, when the built-in field is lowered toward the open circuit voltage. In fact, there is a competition between charge carrier recombination and transport. Consequently, the product of the lifetime (σ) times the mobility (μ) has to be maximized. Furthermore, the series resistances influence the filling factor considerably and should be minimized. The external quantum efficiency (EQE) or incident photon to current efficiency (IPCE) is also a useful parameter in an OPV device and is simply the number of electrons collected under short circuit conditions, divided by the number of incident photons. IPCE is calculated using the following formula:

$$IPCE = \frac{1240 I_{sc}}{\lambda P_{in}}$$

Where λ (nm) is the incident photon wavelength, I_{sc} ($\mu A/cm^2$) is the photocurrent of the device, and P_{in} (W/m^2) is the incident power.

1.3 Application of conjugated materials: organic field - effect transistors (OFETs)

1.3.1 Introduction

The principle of the field effect transistor (FET) was first proposed by Lilienfeld in 1930[37]. Essentially, a FET operates as an on/off switch as well as a capacitor where one plate is a conducting channel between the source and drain electrodes. The density of charge carriers in the channel is modulated by the voltage applied by the second plate of the capacitor, the gate electrode. Thus with no voltage between the source and the gate electrodes the FET is in its insulating state. By application of a voltage between these electrodes, the device can be switched to its conducting state, resulting in the creation of charge carriers. Three types of FETs can be distinguished: metal-insulator-semiconductor FETs, metal-semiconductor FETs and thin film transistor FETs. Organic field effect transistors (OFETs) were first described in 1986 by Koezuka and co-workers[38-39]. The conjugated polymer used was polythiophene (PT) and a carrier mobility of 10^{-5} $cm^2 \cdot V^{-1} \cdot S^{-1}$ was observed. Today, soluble conjugated polymers based OFETs are still the focus of many research activities. It is mainly driven by the promise of fabricating low-cost organic electronics with wet patterning and deposition techniques. High performance polymer OFETs based on thiophene, fluorene and their derivatives have been explored and a carrier mobility of 0.1-0.2 $cm^2 \cdot V^{-1} \cdot S^{-1}$ has been achieved with the regioregular poly(3, 3’’’-dialkyl-quaterthiophene) (PQT)[40].

1.3.2 Structures of OFETs

Figure 1.7 shows two common architectures of OFETs. The OFET device usually consists of a gate electrode, a dielectric layer, and an organic semiconducting material

sandwiched between the source and drain electrodes. Devices can be constructed in either top or bottom contact geometry, each with their respective advantages. In top contact geometry, the organic film is deposited on a uniform dielectric surface, and then the source and drain electrodes are deposited on top by metal evaporation through a shadow mask. In bottom contact devices, the source and drain electrodes are lithographically pre-patterned on the substrate and the organic layer is deposited last. In top contact device, contact resistance is usually minimal due to intimate contact between the semiconductor and the electrodes, and the charge mobility tends to be higher. However, due to shadowing effects, such devices have a limit as to how small the channel dimensions can be (usually >5 μm channels), and this process is not readily amenable to large-scale manufacturing. Bottom contact devices typically exhibit less than half the effective drive current of top contact devices due to contact resistance and the difficulty in preparing highly ordered films on an irregular surface[41-43]. However, bottom contact devices are more easily integrated into low-cost manufacturing processes, and smaller device feature sizes can be realized through photolithographic techniques.

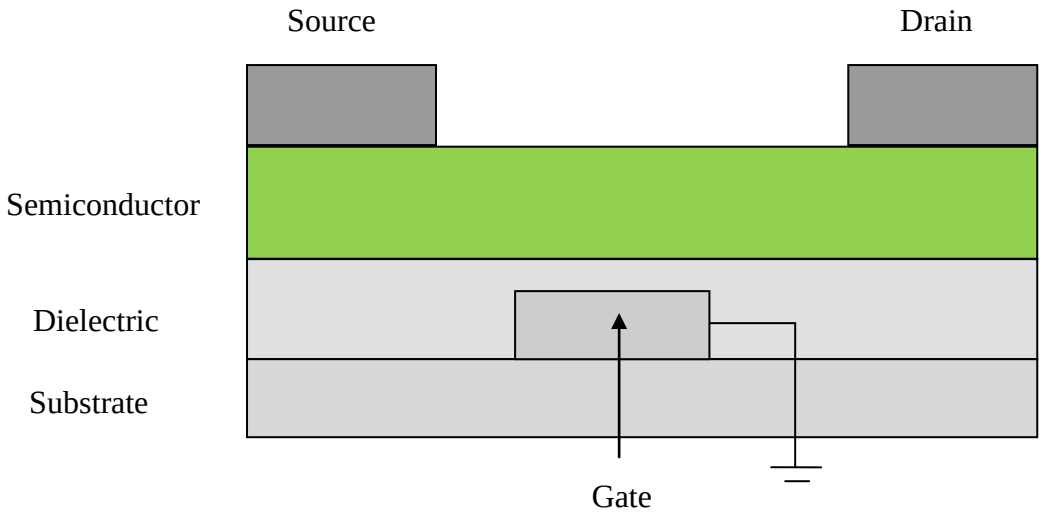

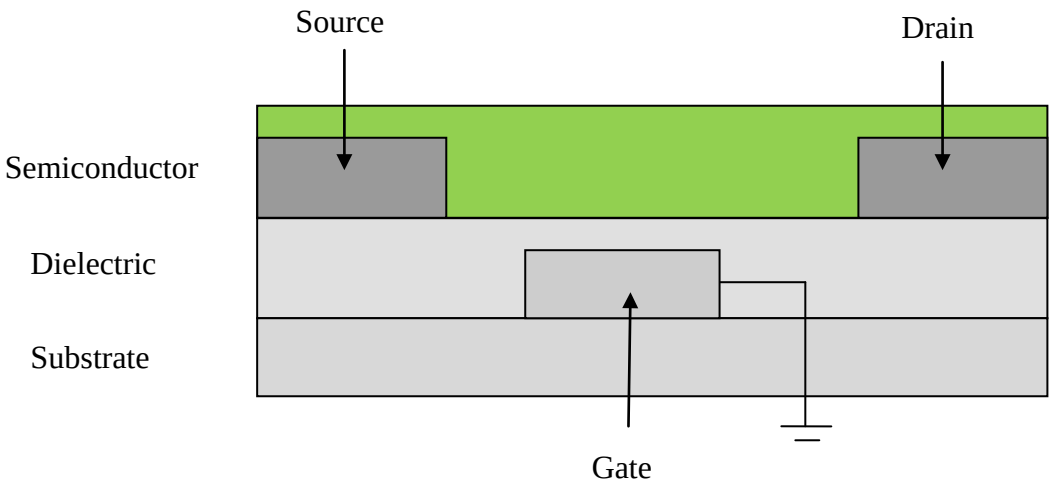

Figure 1.7 Structures of (a) top contact and (b) bottom contact OFET devices.

1.3.3 Operation Principles of OFETs

The organic conjugated polymers used in these devices are not intentionally doped, so there should be a near-zero current between the source and drain electrodes when there is no voltage applied to the gate electrode. When a negative or positive bias is applied to the gate, a large electric field is produced at the semiconductor-dielectric interface. This field causes a shift between the HOMO and LUMO energy levels in the organic semiconductor. Depending on the work function of the electrodes relative to the HOMO/LUMO levels, electrons will either flow out of the HOMO level into the electrodes (leaving behind holes) or flow from the electrodes into the LUMO, forming a conducting channel between the source and drain. Current can be driven through the device by applying a voltage between the source and drain. In most cases, however, a conductive channel is not immediately formed because usually energy level mismatches with the electrodes and the presence of traps that must be overcome before charges are transferred.

The quality of the interface between the dielectric and the conjugated polymer film is a crucial parameter, because it has been reported that the majority of charge carriers

are generated in the first one to two monolayers of semiconductor nearest to the dielectric surface[44]. Charge transfer between molecules is also strongly dependent on the trap concentrations at the dielectric-semiconductor interface and at the grain boundaries in the film[45]. Tight packing of adjacent molecules is desired to maximize the π-orbital overlap between neighbouring molecules, thus increasing charge delocalization and minimizing trapping at defect sites[46]. This can be achieved by increasing the crystallinity of the bulk materials by using planar aromatic molecules with little or no other steric bulk. It is also essential that the materials to be pure, because impurities can introduce charge carriers or traps within the material leading to erroneous results.

1.3.4 Characteristics of OFETs

The most critical parameters of an OFET are the charge mobility and I_{on}/I_{off} ratio. The charge mobility is the average drift velocity per unit electric field and can be calculated in the saturation regime using following formula:

$$I_{ds} = \frac{WC_i}{2L} \times \mu\left(V_g - V_0\right)^2$$

where W is channel width, L is channel length, C_i is capacitance of the insulator, μ is field-effect mobility, V_g is gate voltage and V_0 is threshold voltage. This equation assumes that the mobility of a material is constant. However, mobility of organic semiconductors has been found to be dependent on the gate voltage, which suggests that a larger gate voltage leads to a higher density of charge at the dielectric-semiconductor interface, resulting in an increased charge mobility[47]. The temperature dependence on charge mobility in organic semiconductors has been experimentally

measured, and it has been determined that mobility is thermally activated at temperatures > 25 K but is thermally independent < 25 K. In an OFET, the I_{on}/I_{off} ratio can be defined as the ratio of current flow between the source and drain when there is no gate bias and the current flow at maximum gatebias. However, this value is highly dependent on the voltages used, the device geometry, and the dielectric material. Therefore, this value provides a qualitative measure of semiconductor performance, but identical parameters must be used to quantify the results when comparing different materials. The I_{on}/I_{off} ratio is also a useful index of material purity, because a high off current can be indicative of high extrinsic doping levels in the semiconductor. To be useful in optoelectronic devices such as active matrix displays that require sharp turn-on and fast switching, charge mobility of above 0.1 $cm^2/(V \cdot s)$ and an I_{on}/I_{off} ratio above 10^6 for the semiconducting material are needed[48].

1.4 Conjugated materials for the application of OPVs and OFETs

In this section, different conjugated polymers for the application of OPVs and OFETs will be discussed in general and in details.

1.41 Summary

PPV-type materials: Soluble derivatives of phenylene-vinylenes are important representatives of hole conducting donor-type semiconducting polymers utilized in BHJ solar cells. For example, a power conversion efficiency of 2.5% has been achieved by the device based on poly[2- methoxy-5-(3',7'-dimethyloctyloxy)-1,4-phenylene vinylene) (MDMO-PPV) mixed with PC61BM (w:w=1:4) by using chlorobenzene as a solvent for spincasting[49]. Such BHJ solar cells have 80 wt % of PC61BM. From the investigation of Van Duren et al. it also indicates that, in solar

cells based on MDMO-PPV as a donor and PC61BM as an acceptor, the nanoscale phase separation at approximately 67 wt % PC61BM giving rise to almost pure PC61BM domains in a surrounding matrix[50]. Since PC61BM has almost no absorption in the visible-near-infrared region, the polymer MDMO-PPV is supposed to be the main light absorber in these solar cells. Therefore, it is better to increase the volume concentration of MDMO-PPV for better absorption of solar light. The limitation of volume concentration of PPV type materials restrains the improved performance of these devices.

Thiophene chain-type materials: Poly(3-alkylthiophenes) are important and traditional conjugated polymers as donor materials in BHJ solar cells. The power conversion efficiencies based on regioregular poly(3-alkylthiophenes) and PC61BM are up to 5%. The influence of the alkyl side chain length on the electrochemical and optical properties of regioregular P3HT (poly 3-hexyl thiophene), P3OT (poly 3-octyl thiophene), and P3DDT (poly 3-dodecyl thiophene) has been investigated by Al Ibrahim et al[51]. Energy levels for P3OT, P3HT and P3DDT107 are almost the same with the optical band gap energy around 1.9 eV. With longer side chain length, their electrochemical band gaps were slightly increased. The absorption coefficient undergoes a systematic decrease by longer side chain polythiophenes due to chromophore dilution. Using regioregular P3HT as donor and PC61BM as acceptor, bulk heterojunction solar cells have been realized with external quantum efficiencies of around 75% and power conversion efficiencies up to 5%. The high efficiency of these devices is proposed to be due to a microcrystalline lamellar stacking in the solid state packing and a high hole mobility up to ca. 0.1 $cm^2/V \cdot s$, resulting in reduced

recombination. In addition, interchain interactions cause a red shift of the optical absorption of P3HT due to this stacking.

Low bandgap materials: The design, synthesis and use of low bandgap materials for solar cell applications have greatly developed in the past two decades. Solar cells based on regioregular P3HT as donor material can only absorb sunlight below a wavelength of 650 nm and thus only 22.4% of the total amount of photons can be harvested. Hence, solar cells based on polymers with decreasing bandgap increases the total amount of photons that can be harvested from the solar spectrum. The bandgap of the absorbing polymer can be tuned and modified via six parameters in the conjugated polymer. The design and synthesis of most low bandgap polymers reported in literature, is rationally based on these parameters, which are: molecular weight, bond length alternation, torsion angle, aromatic resonance energy, substituents, and intermolecular interactions. All these parameters have an influence on the bandgap of a (macro)-molecule, but also affect each other and the rest of the chemical, mechanical, and physical properties. For example, the torsion angle is influenced by steric hindrance, thus also by the size and nature of the substituents. By using large substituents not only the solubility increases, but also the torsion angle is increased due to the steric hinderance, since these substituents are often (a)-symmetric (branched) alkyl/alkoxy chains, which make these conjugated polymers quite soluble. However, narrowing of the polymeric bandgap will eventually result in a decrease in power conversion efficiency (PCE) due to a decrease in open circuit voltage (V_{oc}). For a single bandgap material the optimal bandgap equals 1.4 eV as predicted by the detailed balance limit. In practice the optimal bandgap will depend on the restrictions placed on the energy needed to induce charge separation, the absorbing properties of

the donor and restrictions on the acceptor used. In the case of absorbing the conjugated polymer in combination with the most used acceptor PC61BM, an optimal bandgap of 1.3 to 1.9 is reported for the absorbing conjugated polymer. Some examples are shown in **Figure 1.8**.

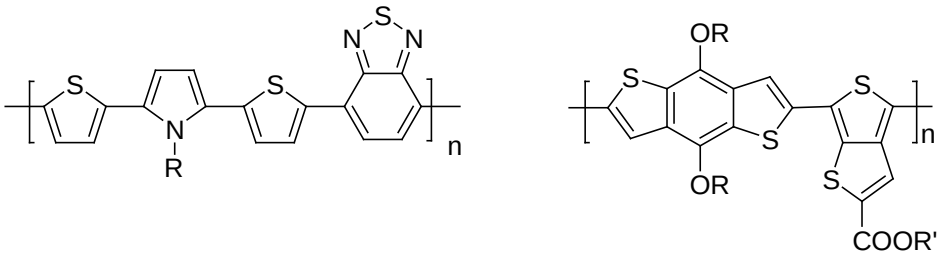

Figure 1.8 Examples of conjugated polymers with low bandgap for OPV application.

Fused aromatic rings contained materials: Introduction of fused aromatic rings into the conjugated polymer backbone has been widely used to design novel materials for FET application and high charge carrier mobility has been already achieved. On the one hand, the incorporation of fused rings can lead to a more rigid and planar polymer backbone, thereby enhancing effective π conjugation, preventing chain-folding, and lowering the band gap. Furthermore, the rigid fused ring structure can lower the reorganization energy of the molecule, facilitating intermolecular hopping and charge carrier mobility[52-53]. Various aromatic fused ring-based conjugated polymers have been developed for their use in potential field effect transistors applications. In particular, FET performance can be greatly improved by incorporating thiophene based fused rings into polymers, such as thienothiophene, benzodithiophene, and cyclopentadithiophene. Some examples are shown in **Figure 1.9**.

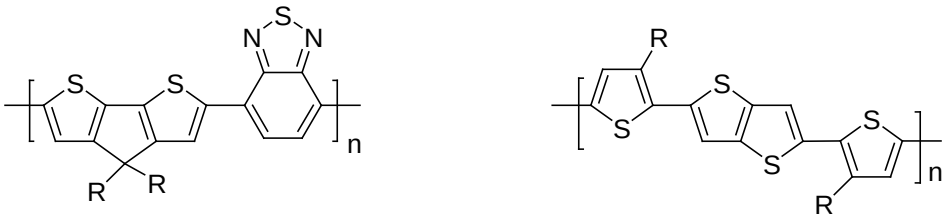

Figure 1.9 Examples of conjugated polymers incorporated with fused aromatic rings for OFET application.

1.4.2 p-Type material for OPV application based on poly(3-hexylthiophene) (P3HT)

Scheme 1.1 The synthetic approach to P3HT

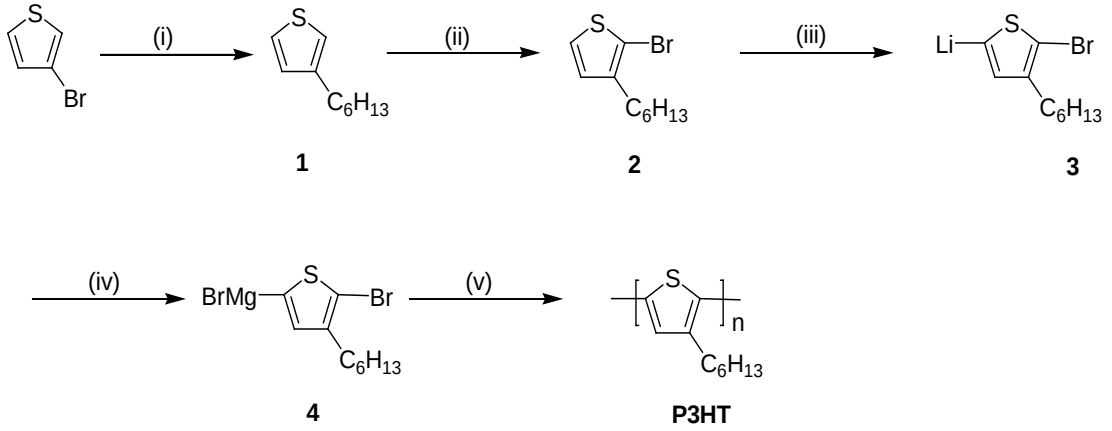

Conditions and reagents: (i) Mg, $C_6H_{13}Br$, dry ether; (ii) NBS, DMF; (iii) LDA, THF; (iv) CH_3MgBr, dry ether; (v) $Ni(dppp)Cl_2$.

Poly(3-hexylthiophene) (P3HT) is a conjugated polymer with good solubility and processability[54]. Organic BHJ photovoltaic cells based on regioregular P3HT (donor)/ PCBM (acceptor) with record power conversion efficiency up to 5%, which is one of the top performances for OPVs[55]. The synthesis of regioregular P3HT was first investigated by McCollough[56-57] and the yield is almost 100% (**Scheme 1.1**). It is based on region-specific metallation of 2-bromo-3-hexylthiophene **2** with lithium diisopropylamide (LDA) at position 5 and its further transformation into Grignard

derivative **4**. The latter is polymerized with catalytic amount of $Ni(dppp)Cl_2$ using the Kumada cross-coupling method. An important modification of this synthetic route replaces the lithiation reaction by treatment of dibromothiophene derivative with methylmagnesium or vinylmagnesium bromide, affording the Grignard intermediate in one step[58].

The onset UV-vis absorption of P3HT in film state is ca. 650 nm with the optical band gap energy around 1.9 eV. External quantum efficiencies (EQE) of around 75% and power conversion efficiencies (PCE) up to 5% can be achieved by using regioregular P3HT as donor material and PC61BM as acceptor material in BHJ solar cells[59-60]. The high efficiency of these devices is proposed to be due to a microcrystalline lamellar stacking in the solid state[59]. Such stacking thus results in reduced recombination[61] of the dissociated charges in P3HT based OPV devices.

Moreover, the efficiency of solar cells based on P3HT has been improved by a thermal annealing step. It has been demonstrated that, by annealing the devices, the characteristics of such plastic solar cells are improved[62]. Annealing not only causes recrystallization of the polymer but also reduces the free volume and the density of defects at the interfaces[63]. Reported by Erb et al., the sample shows one single peak at $2\theta = 5.4^{o}$ after being annealed and corresponding lattice constant d can be calculated by Bragg's Law. When $\lambda = 0.154$ nm of the incident beam is used, d = 1.61 nm is obtained. It can be concluded the detect peak originates from the polymer crystallites with α-axis orientation, which is main chain parallel and side chain perpendicular to the substrate. The height of the peak is proportional to the number of P3HT nanodomains per unit volume. The non-annealed sample exhibited no crystallites whereas the annealed sample showed pronounced crystallinity. Furthermore, the

optical absorption coefficient of the annealed sample is larger than that of the non-annealed sample over the whole spectral range. This is related to the aggregation state of P3HT from amorphous to crystalline. BHJ solar cells benefit from the process of the enhanced absorption properties of the P3HT crystallites. Additionally, the findings for P3HT/PC61BM films are very different to those of pristine P3HT films. Thin films processed from pristine P3HT solutions exhibit the same red-shifted absorption typical of polymer aggregates and nanocrystallites. Annealing of pristine P3HT films can result in slightly increased crystallinity, depending on the drying conditions of the cast films. In P3HT/PCBM composites, PC61BM seems to suppress the formation of polymer crystallites. PCBM is finely dispersed on a molecular basis between P3HT chains, thus prevent P3HT aggregation or crystallization. On the other hand, P3HT recrystallization has a positive effect on the mobility of holes. Annealing at 80 °C resulted in the formation of crystalline P3HT fibrils and enhanced the hole mobility by an order of magnitude. Thermal annealing under chloroform vapor or simple thermal treatment leads to an overall increase in power conversion efficiency. The optical absorption spectrum shows a pronounced red shift upon thermal annealing and the processing conditions have different effects of on the light absorption of P3HT:PCBM cells. Films cast from chloroform and chlorobenzene solutions have absorption maxima at 600 and 630 nm, respectively[64]. It was argued that this difference indicated a higher degree of P3HT side chain ordering using chlorobenzene. The increased structural order can be created by thermal annealing and/or by changing the solvent from chloroform to chlorobenzene[64].

1.4.3 p-Type material for OFET application based on poly{(N-alkyl-dithieno[3,2-b:2',3'-d]pyrrole)-co-[thiophene derivatives]} (PDTP-THs)

Scheme 1.2 The synthetic approach to PDTP-THs.

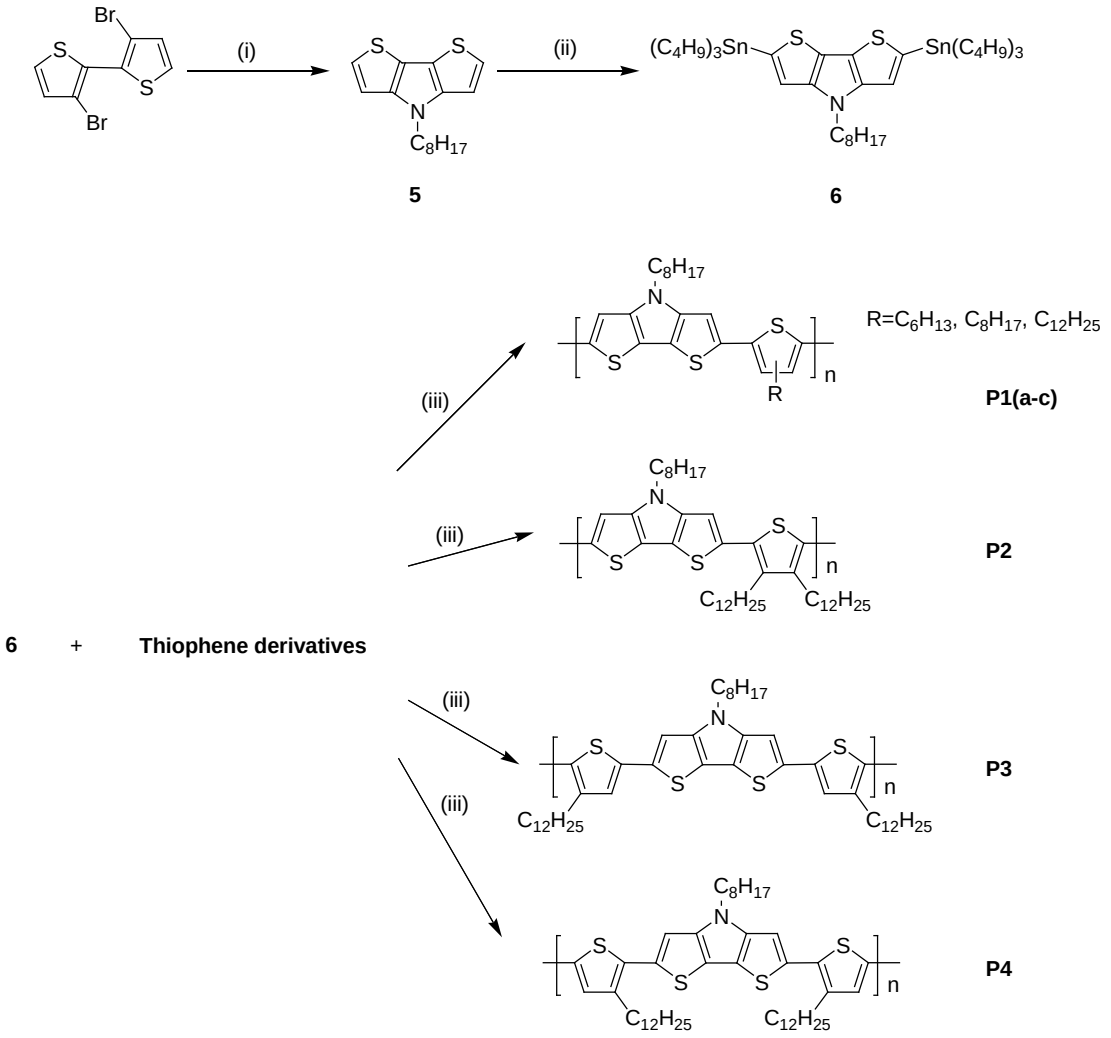

Reagents and conditions: (i) Pd_2dba_3, BuONa, BINAP, C_8H_{17}-NH_2, toluene; (ii) n-Butyl lithium, (trimethyl)tin chloride, dry THF,; (iii) Pd catalyst, chlorobenzene.

N-alkyl-dithieno[3,2-b:2',3'-d]pyrrole based oligomers/polymers have shown interesting optical and electrical properties and have been investigated by many research groups[65-69]. Amongst them, poly{(N-alkyl-dithieno[3,2-b:2',3'-d]pyrrole)-co-[thiophene derivatives]} (PDTP-THs) are a series of low bandgap copolymers prepared by Richard D. McCullough's group[70] and their OFET behaviours were

explored as well. N-functionalized dithieno[3,2-b:2’,3’-d]pyrrole (DTP) can be achieved by reacting 3,3’-dibromo-2,2’-bithiophene and corresponding primary amine. The functionalized thiophene derivatives are widely explored and reported so the monomers can be obtained easily. The Stille coupling method is used the polymerization and the synthetic approach is shown in **Scheme 1.2**.

The polymer structure is affected by the thiophene substitution patterns on the DTP-*co*-THs backbone and the effect can be examined by calculating the energy from various conformation models for each linkage. Model compounds of **P1**, **P3**, and **P4** containing methyl side groups were designed for the calculations. The results revealed that all the adjacent rings prefer to be trans to each other. If the adjacent thiophene rings have a tail-tail (TT) linkage or if the tail of the thiophene rings is linked with adjacent DTP rings, the two adjacent rings prefer trans coplanarity. In all other cases, the two adjacent rings twist in their minimum energy conformation. The energy of the different torsion angles of these twisted adjacent rings was calculated using density functional theory a. The minimum energy geometries thus can be determined and the energy barriers for adopting a planar conformation can be calculated. For model compounds **P1** and **P4**, the minimum-energy geometries twisted with an angle of 160° and 140°, respectively. The calculated energy barrier for adopting a trans planar conformation is less than 0.2 kcal/mol. Because of the low energy barrier, the adjacent DTP and TH rings can display trans planarity. In contrast, the minimum energy geometry of model compound **P3** is highly twisted at the HH linkage with dihedral angle of 120°, in which up to 5.5 kcal/mol is required to adopt a trans coplanar conformation from this minimum energy geometry. Therefore, it may be unlikely for HH coupling thiophene rings to adopt planarity. This result indicates that the HH

linkages in the polymer backbone decrease conjugation, increase the band gap, and inhibit intrachain charge transfer. Except for the polymer **P4**, the bandgaps of polymer **P1**-**P3** are all lower than that of P3HT. In case of solid states, fluorescence is only detected from **P4** and the fluorescence quenching of polymer **P1**-**P3** is due to their relatively rigid structures, which facilitate aggregation in the solid state and favour the interchain excitation instead of giving emission. Amongst these polymers, it has been shown that the polymer **P4** exhibits the best OFET performance with the highest mobility of 0.21 $cm^2 \cdot V^{-1} \cdot s^{-1}$, which is even higher than the highest reported field effect mobilities of P3HT[71]. Furthermore, the measured values of **P4** OFET mobility are highly consistent with good batch-to-batch reproducibly. The mobility in sample **P3** is more than one order of magnitude lower because its structure does not allow extensive conjugation.

The investigation of the polymers **DTP-Th**s indicates that enhanced backbone-to-backbone contacts would facilitate effective interchain hopping. DTP based polymers can be good candidates for low-cost plastic electronics. Particular interest arises when it comes to the applications of these materials in FETs, OPVs, and OLEDs as they demonstrated possibility to tailor their π conjugation by the introduction of a fused ring system and stereochemistry.

1.4.4 p-Type material for OFET application based on poly(9,9'-dioctyl-fluorene-co-bithiophene) (F8T2)

Poly(9,9'-dioctyl-fluorene-co-bithiophene) (F8T2) is a conjugated co-polymer with good solubility and processability. In addition, it is relatively air stable and can be fabricated to OFET devices with high performances. F8T2 can be easily prepared by Suzuki method with high yield. The synthesis can be started from converting 2,7-

dibromofluorene, which is converted to its boronic ester **6** after 2 steps. The other monomer **8** can be obtained by the bromination of bithophene **7** in DMF. Monomers **6** and **8** go through the classic Suzuli coupling polymerization to achieve F8T2. The synthetic approach is shown in **Scheme 1.3**.

Scheme 1.3 Synthetic approach to F8T2.

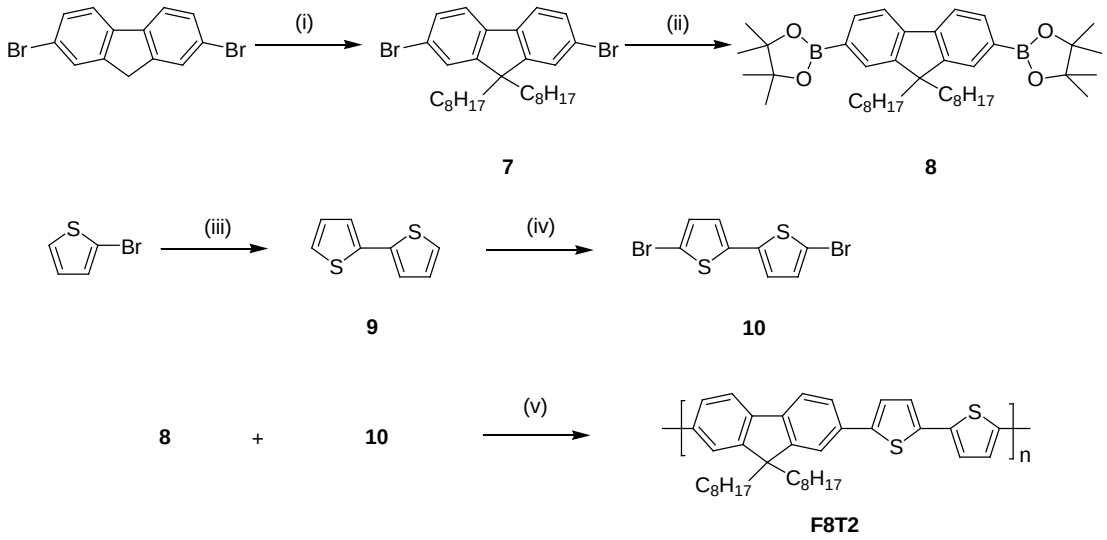

Conditions and reagents: (i) NaOH, $C_8H_{17}Br$, DMSO; (ii) n-butyllithium, 2-isopropoxy -4,4,5,5-tetramethyl-1,3,2-dioxaborolane, anhydrous THF; (iii) Mg, I_2, dry ether; (iv) NBS, DMF; (v) $Pd(PPh_3)_4$, 2 M Na_2CO_3, toluene.

It has been shown that F8T2 possesses a thermotropic, nematic liquid crystal phase above 265 °C and orients into a monodomain on an alignment layer[72]. In order to afford alignment of LC semiconducting layers of F8T2, a mechanically rubbed polyimide alignment layer is prepared on the glass substrate first, followed by the deposition of gold as source-drain electrodes. The F8T2 film is then spin coated and aligned parallel to the rubbing direction of the underlying polyimide by annealing in the LC phase at high temperature. During this annealing step the alignment of the polymer chains is preserved but crystallization is suppressed[73]. The degree of alignment can be quantified by polarized optical absorption spectra. In the spectral

region of the F8T2, π–π* transition the dichroic ratio of the absorption coefficients for incident light polarized parallel (perpendicular) to the rubbing direction is 5–12 depending on film thickness and details of the annealing and rubbing procedure. Because on the same substrates TFT devices are oriented parallel and perpendicular to the alignment direction, high mobilities of μ = 0.009– 0.02 $cm^2/V \cdot s$ are obtained if current flow is parallel to the alignment direction. Significantly lower values μ = 0.001– 0.002 $cm^2/V \cdot s$ can be determined for perpendicular device orientation. Values for the anisotropy of the field-effect mobility are 5–8 varying between devices on the same substrate. The corresponding dichroic ratio is slightly higher but is always of the same order of magnitude as the mobility anisotropy. The mobility values can be compared to those of isotropic TFT devices that underwent the same thermal treatment as the aligned devices, but exhibit no monodomain alignment. These isotropic devices are prepared on areas of the substrate that are not coated by polyimide, and typically exhibit mobilities μ = 0.0030 – 0.005 $cm^2/V \cdot s$. In the multidomain, isotropic devices the domain sizes are on the order of 0.1–1mm, as estimated from optical micrographs, that is, the TFT channel contains several LC domain boundaries. The annealed, isotropic devices exhibit significantly higher mobilities and better turn-on voltage stability than devices in which the F8T2 film underwent no thermal treatment. This may indicate that LC domain boundaries in the nematic glass do not act as carrier traps to the same extent as microcrystalline grain boundaries in as-spun films. This predicts the mobility anisotropy to be of the same order of magnitude as the dichroic ratio in good agreement with experimental observations. In F8T2 the octyl chains on the sp^3-carbon atom of the fluorene bridge emanate perpendicularly to the conjugated planes and prevent close p-p interchain

stacking. However, such liquid crystallinity of F8T2 provides an elegant way of fabricating OFFTs with uniaxial alignment and rapid charge transport along the polymer chains can be exploited. These fluorene based block copolymers are a promising new class of materials for OFETs.

1.4.5 n-Type material for OPV application based on tetrabenzo[5.5]fulvalene (TBF) backbone

Materials based on tetrabenzo[5.5]fulvalene (TBF) backbone which are promising new electron acceptors in organic electronics has been recently reported by Fred Wudl, etc. recently. TBF is forced to be coplanar in the ground state because of the presence of the double bond, but the repulsive interaction between the protons at H1– H1' and H8–H8' affords the twist structure of the dimer[74]. The addition of one electron across the C9–C9' bond is highly favourable for such TBF structures and attributable to two main reasons: the relief of steric strain and gain in aromaticity in affording a 14-π electron system[75].

In comparison to widely explored and common acceptor materials such as fullerene (C_{60}) and its derivatives PC61BM, TBF scaffold is considered to be much more versatile since theoretically, it has twelve different sites for functionalization by substitution. **Scheme 1.4** shows some examples of materials bearing the TBF backbone[76].

Scheme 1.4 Compounds based on TBF backbone.

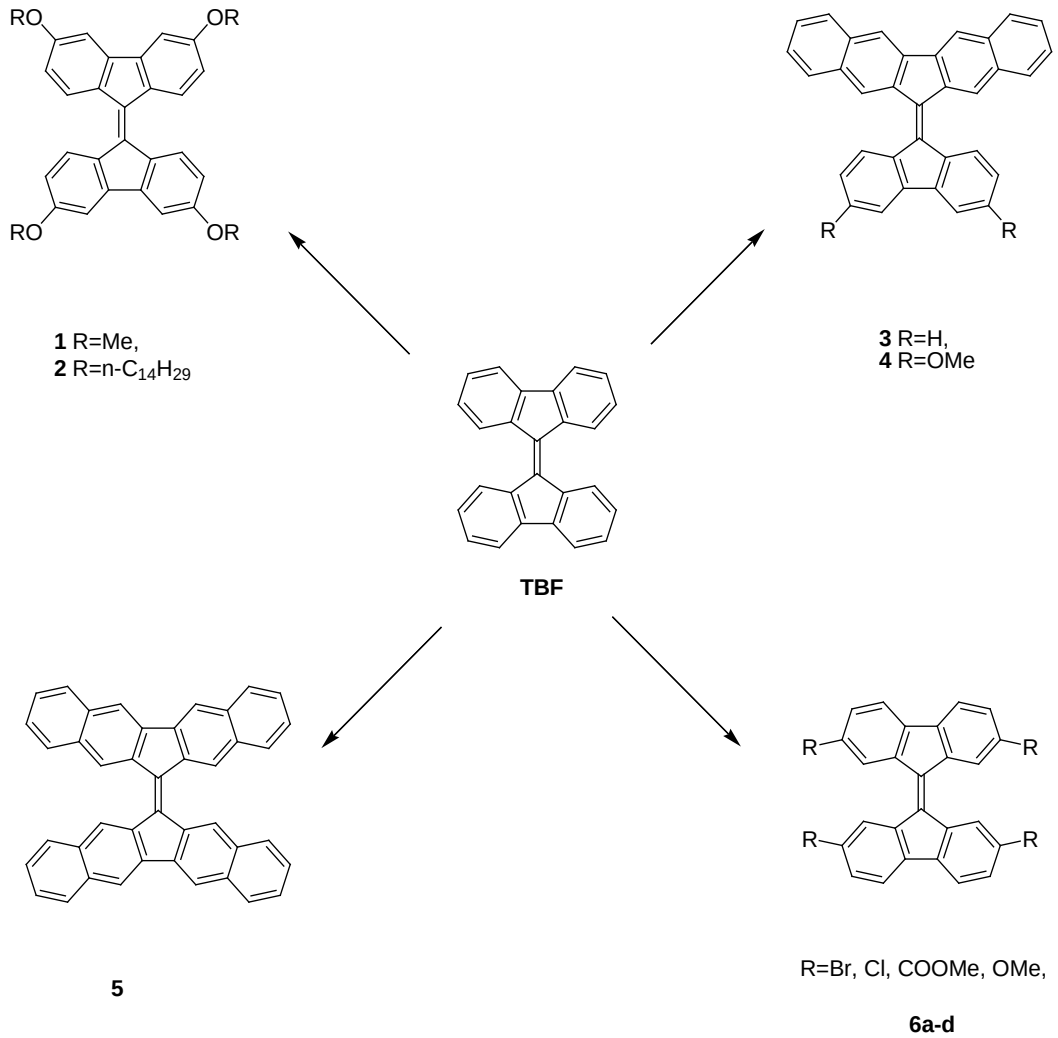

The thermal investigation of compounds **1**–**5** clearly indicates that all of them have good thermal stabilities, which is one of the basic requirements for long lifetime in organic devices. Optical studies show that compound **5** has the strongest light absorption of this set of compounds because of its enhanced π-electron delocalization. The absorption of these dimmers is much stronger than that of PCBM and thus a better light harvesting ability is expected from these TBF backbone based compounds. Additionally, an edge-to-face π-π stacking motif was observed in the solid state of compound **4**, along with a minimal intermolecular distance of 3.61 Å between the dibenzofluorenylidene fragment and the 3,6-dimethoxyfluorene unit of a neighboring

molecule, probably because of the asymmetry of the molecule and the electron density difference of each fragment. However, the solid-state interactions in this arrangement could facilitate the intermolecular delocalization of the negative charge during the migration to the electrode. As in the crystal structure of TBF[77], X-ray diffraction studies reveal that compound **4** is significantly distorted from planarity with a torsional angle of 36.51^{o}, in contrast to 39.3^{o} for TBF. This difference can be attributed to the presence of donor groups that increase the length of the double bond between C9 and C9' from 1.364 Å to 1.382 Å and consequently decrease the repulsive interaction between the neighboring protons.

OPV devices based on the blends of compound **4** as n-type material and P3HT as p-type material have been fabricated and the performances have been tested. By employing Ba/Al as cathode, an open-circuit voltage (V_{oc}) of 1.10 V, which is almost double that of PCBM, a fill factor (FF) of 0.40, and power conversion efficiency (PCE) of 1.7% can be achieved.

1.5 Aim of the project

BHJ OPVs, which use P3HT as the electron-donating (p-type) material and PCBM as the electron-accepting material (n-type) have been widely investigated. However, despite the fact that P3HT has good charge carrier photogeneration and charge transport properties, the absorption spectra of the polymer overlap poorly with the solar emission spectrum which extends deeply into the infrared region. Thus, the design and exploration of low band gap conjugated polymers, which are better able to absorb sunlight across the full spectrum in solar radiation, have been the recent focus to achieve high performance OPVs. In addition, although the PCBM acceptor material has brought good progresses in OPV devices performance, PCBM still has

shortcomings, such as viably poor light harvesting ability and difficulty in tuning the energy levels, etc. The preparation and investigation of novel acceptor materials as viable alternatives to PC61BM would be of tremendous interests and importance. In addition, the design and development of new materials for OFETs with high device mobility (via p-/n-channel) present ongoing challenges for researchers for the application in organic electronics with enhanced efficiency.

On the basis of guiding principles outline in this chapter, conjugated polymers/oligomers based on DTP units or fluorene/fluorene derivatives units will likely be strong candidates for organic electronics (OPVs and OFETs) due to their outstanding electronic and optical properties as well as the excellent physical properties. Furthermore, their electronic and optical properties can easily be adjusted at the molecule level on the basis of the structure of conjugated polymers. Given this impetus, the attention of this dissertation would be focused on:

I. Designing and synthesizing novel, solution processable conjugated polymers as electron-donating materials (p-type) for application in organic electronics.
    - N-Dodecyl DTP based polymer.
    - N-Octylnony DTP based polymers.
    - N-Functionalized DTP and 9,9'-functionalized fluorene based polymers.

II. Designing and synthesizing novel, processable and stable materials as electron-accepting materials (n-type) for application in organic electronics.
    - Bisfluorene substituted perylene bisimides.
    - TBF based polymers.
    - Fluorene derivatives (fluorone and TBF) based polymers.

In this project, the design and synthesis of novel conjugated materials have been presented. The structures and properties of the synthesized materials have been fully characterized and investigated. In addition, an outline for possible future work is presented in the last chapter of this thesis.

Chapter 2
Experimental

2.1 Materials

All starting organic materials were purchased from Aldrich and used without further purification unless otherwise stated. Anhydrous tetrahydrofuran (THF), diethyl ether and toluene were collected from the solvents drying machine. Other organic solvents such as hexane, N, N-dimethylformamide (DMF) and ethanol, etc, were purchased from Merck and used as received.

2.2 Instrumentation

NMR spectroscopy: ^{1}H NMR and ^{13}C NMR spectra were recorded on a 300 MHz, Bruker Avance DPX 300 apparatus in solution of deuterated solution at 25 ^{o}C

Mass spectroscopy: The Maldi-TOF mass was tested using a Bruker Autoflex II with THF as the solvent and 2,5- dihydroxybenzoic acid (DHB) as the matrix.

Gel Permeation Chromatography (GPC): Number-average (M_n) and weight-average (M_w) molecular weights were determined by Gel Permeation Chromatography (GPC) system on a Shimadzu LC-20A equipped with a pump (LC-20-AD) and a refractive index (RI) detector (RID-10A). The analysis was performed on a PL Gel column (Agilent) using THF (HPLC grade) as mobile phase.

Thermogravimetry analysis (TGA): TG measurements of polymer powders were performed on Perkin Elmer Diamond TG/DTA analyzer under nitrogen/air atmosphere at a heating rate of 20 ^{o}C/min.

Differential scanning calorimetry (DSC): The DSC measurements of polymers were performed under a nitrogen atmosphere at a heating rate of 10 ^{o}C/min from 25 ^{o}C to 250 ^{o}C with a TA 2920 analyzer. The weight of polymers powders was 3-7 mg.

UV-Vis spectroscopy: UV-visible absorption spectra were recorded on a Shimadzu UV 3101 spectrophotometer in dilute solution or in film state.

Fluorescence spectroscopy: Photoluminescence (PL) measurements were done on a Perkin-Elmer LS 45 in chloroform at room temperature

Elemental analysis: Elemental analyses were performed with a Vario EL III Elementor analyzer for C, H and N determination.

X-ray diffraction (XRD): XRD patterns of films were recorded on a Bruker AXS D8 diffractometer (under ambient conditions) using a filtered Cu-Kα radiation. Diffraction data were collected between 0º and 30º (2θ) with a resolution of 0.02º (2θ).

Cyclic votammetry (CV): Cyclic voltammetry measurements were conducted on a three-electrode electrochemistry workstation (Model CHI006B) in 0.1 M anhydrous acetonitrile solution of Bu_4NBF_4 at 25 ^{o}C under nitrogen atmosphere. All experimental potentials were recorded with respect to standard calomel electrode (SCE).

2.3 Synthesis

2.3.1 Synthesis of the polymer PBTDTP

2,2'-Bithophene (2)[78]

2-Bromothiophene (59.3 g, 0.364 mol) in dry ether (160 ml) was added to Mg (10.5 g, 0.437 mol) activated with iodine in 50 ml ether in a dry, oxygen free atmosphere at room temperature and refluxed for 1 h. The resultant Grignard reagent **1** was cooled and added to a second portion of 2-bromothiophene (49 g, 0.3 mol) in ether containing $NiCl_2$(dppp) (1.6 g, 3.04 mmol) at 0 ^oC. The mixture was stirred over night at room temperature. The mixture was poured into ice cooled water and treated with NH_4Cl solution. The ether layer was collected, dried with $MgSO_4$ and the ether removed to give 47.6 g white solid.

Yield: 96%. ^1H NMR (300 MHz, $CDCl_3$): δ (ppm) 7.23-7.02 (m, 4H), 7.00 (dd, 2H). Anal. Calcd for $C_8H_6S_2$: C, 57.79; H, 3.64; S, 38.57. Found: C, 57.75; H, 3.74.

3,3',5,5'-Tetrabromo-2,2'-bithiophene (3)[78]

Bromine (19.74 g, 123 mmol) in chloroform (120 ml) was added over 40 min to an ice-cooled solution of **2** (10g, 60.2 mmol) in glacial acetic acid (200 ml) and chloroform (150 ml). To the resultant mixture was added a second portion of bromine solution over 1 h at room temperature. The mixture was stirred over night at room temperature and refluxed for 24 h. The reaction solution was cooled and the solvent was removed. The crystalline product was collected by cold filtration, recrystallized with ethanol and dried in vacuo at room temperature.

Yield: 95%. ^1H NMR (300 MHz, $CDCl_3$): δ (ppm) 6.91 (s, 2H).

3,3'-Dibromo-2,2'-bithiophene (4)[78]

Zinc dust (20.8 g, 318 mmol) was added in small portion over 5 h to a refluxing solution of **3** (28 g, 57.8 mmol) in ethanol (700ml), glacial acetic acid (30 ml) and 10 ml concentrated HCl. When the reaction was completed, the solvent was removed and the product was extracted with ether, washed with deionized water, saturated $NaHCO_3$ solution and brine. After drying with $MgSO_4$, the ether was removed to give a white solid.

Yield: 87%. ^{1}H NMR (300 MHz, $CDCl_3$): δ (ppm) 7.42 (d, 2H), 6.80 (d, 2H).

N-1-dodecyl-dithieno[3,2-b:2',3'-d]pyrrole (5)[79]

A solution of **4** (2.00 g, 6.18 mmol), NaOtBu (1.42 g, 14.8 mmol), Pd_2dba_3 (0.142 g, 0.155 mmol), and BINAP (0.386 g, 0.620 mmol) in dry toluene (12 ml) was purged with nitrogen for 20 min. 1-dodecyl-amine (1.15 g, 6.18 mmol) was added via syringe, and the mixture was stirred at 110 ^{o}C under nitrogen until completion of the reaction. After cooling, water was added and the layers were separated. The water phase was extracted twice with diethyl ether. The combined organic layers were dried over $MgSO_4$, and the solvents were removed via rotary evaporation. The crude product was purified by column chromatography and the desired product was obtained as yellow oil.

Yield: 87%. ^{1}H NMR (300 MHz, $CDCl_3$): δ (ppm) 7.13 (d, J=5.3Hz, 2H), 6.98 (d, J=5.3Hz, 2H), 4.06 (t, 2H), 1.94 (m, 2H), 1.22-1.4 (m, 18H), 0.82 (m, 3H).

2,6-Di(tributyltin)-N-dodecyl dithieno[3,2-b:2',3'-d]pyrrole (6)[79]

Under a nitrogen atmosphere, compound **5** (0.956 g, 2.75 mmol) was dissolved in dry THF (12 ml) was cooled to -78 ^{o}C with a dry ice-acetone bath and n-butyllithium (1.6 M in hexane, 4.3 ml, 6.78 mmol) was added dropwise. The reaction mixture was

stirred at -78 ^{o}C for 1 h and then brought to room temperature. The stirring was continued for 20 min and then the reaction mixture was cooled to -78 ^{o}C again. A solution of tributylstannyl chloride (2.2 g, 6.78 mmol) in dry THF (7 ml) was added dropwise. The mixture was slowly brought to room temperature and stirred for another 2 h. Water was subsequently added to the reaction mixture and the aqueous phase was extracted with diethyl ether twice. The combined organic layers were dried over $MgSO_4$ and concentrated to afford dark-green viscous oil. The product **6** is obtained and used for next reactions without further purification.

Yield: 95%. ^{1}H NMR (300 MHz, $CDCl_3$): δ (ppm) 6.97 (s, 2H), 4.10 (m, 2H), 2.01 (m, 2H), 1.21-1.68 (m, 72H), 0.81 (t, 3H).

4,7-Dibromo-2,1,3-benzothiadiazole (8)[80]

To a 1000 ml two-necked flask were added benzothiadiazole **7** (20.0 g, 146.8 mmol) and HBr (300 ml, 48%). A solution of bromine (70.4 g, 440.6 mmol) in 200 ml HBr was added dropwise. After completion of the addition, the solution was heated to reflux for 6 h. The mixture was cooled to room temperature and excess bromine was removed. The mixture then was poured into ice water and filtered under vacuum. The resulting solid was washed exhaustively with water and dried under vacuum. The product of **8** was recrystalized in the mixture of chloroform and hexane. Pure **8** was obtained as a pale yellow needle crystal.

Yield: 95%. ^{1}H NMR (300 MHz, $CDCl_3$): δ (ppm) 7.73 (s, 2 H). Anal. Calcd for $C_6H_2Br_2N_2S$: C, 24.52; H, 0.69; Br, 54.36; N, 9.53; S, 10.91; Found: C, 24.62; H, 0.78; N, 9.59.

Poly{[N-dodecyl-dithieno(3,2-b:2',3'-d)pyrrole-2,6-diyl]-alt-[2,1,3-benzothiadiazole-4,7-diyl]} (PBTDTP)

Dichlorobis(triphenylphosphine)palladium (2.4 mg, 0.0034 mmol) was added to a stirred solution of a mixture of **6** (0.315 g, 0.34 mmol) and **8** (0.1 g, 0.34 mmol) in dry THF (4 ml) under a nitrogen atmosphere. The mixture was stirred at 90 ^{o}C for 40 h. After completion of the reaction, the mixture was poured into methanol under vigorous stirring. A dark colored powdery solid was separated and filtered. The resulting polymer was washed with methanol and hexane for 24 h through a Soxhlet apparatus. Finally, the crude polymer was purified by extracting with chloroform. The chloroform solution was concentrated, and the polymer re-precipitated in methanol and the resulting solid collected by filtration. After drying in vacuum, a dark purple solid of 57 mg was obtained.

Yield: 47%. ^{1}H NMR (300 MHz, $CDCl_3$): δ (ppm) 8.2 (br, 2H), 7.5 (br, 2H), 4.10 (br, 2H), 1.95-0.5 (br, 23H). Anal. Calcd for $C_{26}H_{31}N_3S_3$: C, 64.82; H, 6.49; N, 8.72. Found: C, 64.73; H, 6.61; N, 8.65.

2.3.2 Synthesis of the polymer PT2-DTP8, PBT-DTP8, PT2-BT -DTP8

1-Octylnonanol (10)[79]

A solution of ethyl formate **9** (18.52 g, 250 mmol) in 40 ml anhydrous ether was added dropwise to a freshly prepared octylmagnesium bromide in 250 ml diethyl ether. The addition was at such a rate to maintain the reaction mixture gentle reflux. When the addition was finished, stirring was continued for 10 min and this was followed by the addition of 36 ml H_2O. A solution of 15.5 ml sulfuric acid in 135 ml H_2O was added to the reaction mixture. The solids were filtered off by suction filtration and

washed with diethyl ether. The combined organic phase was washed with a saturated $NaHCO_3$ solution, brine and then dried over $MgSO_4$. The diethyl ether was removed and the product was purified by recrystallization from acetonitrile. The pure product of **10** is a white crystal.

Yield: 80%. ^{1}H NMR (300 MHz, $CDCl_3$): δ (ppm) 3.63 (m, 1H), 1.21-1.53 (m, 29H), 0.87 (t, 6H). ^{13}C NMR (300 MHz, $CDCl_3$): δ (ppm) 71.8, 38.6, 32.8, 31.0, 31.5, 31.8, 26.8, 23.4, 14.9.

***N*-1-Octylnonyl-phthalimide (11)**[79]

To a solution of triphenylphosphine (26.2 g, 100 mmol), phthalimide (14.72 g, 100 mmol) and **10** (25.6 g, 100 mmol) in 100 ml of anhydrous ether, a solution of DIAD (19.4 ml, 100 mmol) in 20 ml ether was slowly added. After stirring overnight, the precipitate was filtered off and washed with diethyl ether. After removal of the ether by rotary evaporation, the residue was purified by column chromatography (eluent: hexanes). The product of **11** was a colorless oil.

Yield: 54%. ^{1}H NMR (300 MHz, $CDCl_3$): δ (ppm) 7.80 (dd, 2H), 7.67 (dd, 2H), 4.20 (m, 1H), 2.03 (m, 2H), 1.75 (m, 2H), 1.1-1.4 (m, 24H), 0.85 (t, 6H).

9-Aminoheptadecane (12)[79]

To a solution of **11** (15.8 g, 42 mmol) in 40 ml absolute ethanol hydrazine monohydrate (2.00 ml, 42 mmol) was added dropwise. The mixture was heated to reflux for 2 h. 10 ml of concentrated HCl was added and the mixture was refluxed for another 10 min. After the mixture was cooled to room temperature, the precipitate was filtered off. Excess NaOH solution (2 M) was added into the filtrate. The mixture was extracted with ether for 3 times. The organic phase was dried over $MgSO_4$ and

the solvents were removed by rotary evaporation. The amine was isolated by vacuum distillation. The product of **12** was a colorless oil.

Yield: 50%. ^{1}H NMR (300 MHz, CDCl3): δ (ppm) 2.69 (m, 1H), 1.23-1.51 (m, 28H), 1.11 (s, 2H), 0.88 (t, 6H).

N-1-Octylnonyl-dithieno[3,2-*b*:2',3'-*d*]pyrrole (14)

The same procedure was followed as described for the synthesis of **5**, starting from **13** and **12**. The product of **14** is a white solid.

Yield: 68%. ^{1}H NMR (300 MHz, $CDCl_3$): δ (ppm) 7.12 (d, 2H), 7.05 (d, 2H), 4.20 (m, 1H), 2.03 (m, 2H), 1.85 (m, 2H), 1.01-1.48 (m, 24H), 0.86 (t, 6H).

2,6-Di(tributyltin)-*N*-1-octylnonyl-dithieno[3,2-*b*:2',3'-*d*]pyrrole (15)

The same procedure was followed as described for the synthesis of **6**, starting from **14**. The product of **15** is green oil.

Yield: 92%. ^{1}H NMR (300 MHz, CDCl3): δ (ppm) 7.01 (s, 2H), 4.20 (m, 1H), 2.00 (m, 2H), 1.85 (m, 2H), 1.21-1.68 (m, 94H), 0.84 (t, 6H).

5,5'-Dibromo-2,2'-bithiophene (17)[78]

In the absence of light, NBS (2.25 g, 12.7 mmol) was added in one portion at room temperature to a solution of bithiophene **16** (1.0 g, 6 mmol) in 25 ml of DMF. The mixture was stirred for 3 h and poured into ice water. The white precipitate was filtered and washed with water for 3 times. After drying in vacuum at 60 ^{o}C, the crude product was recrystallized in ethanol to afford a white crystal of **17**.

Yield: 85%. ^{1}H NMR (300 MHz, $CDCl_3$): δ (ppm) 6.95 (d, 2H) 6.88 (d, 2H). ^{13}C NMR (300 MHz, $CDCl_3$): δ (ppm) 139.8, 131.2, 129.5, 111.8.

4,7-Di(thiophen-2-yl)-2,1,3-benzothiadiazole (20)[81]

A solution of 2-(tributyltin)thiophene (6.34 g,17 mmol), **19** (2.5 g, 8.5 mmol) and dichlorobis(triphenylphosphine)palladium (6.0 mg, 0.0085 mmol) in 30 ml of anhydrous THF was stirred at 90 ^{o}C for 40 h. After being cooled to room temperature, the mixture was poured into water and extracted with chloroform for 3 times. The organic phase was dried over $MgSO_4$ and the solvents were removed by reduced pressure. The residue was purified by column chromatography (eluent: dichloromethane /hexanes=1:2, v:v). The pure product of **20** was a red solid.

Yield: 86%. ^{1}H NMR (300 MHz, $CDCl_3$): δ (ppm) 8.15 (d, 2H), 7.87(s, 2H), 7.46 (d, 2H), 7.24 (dd, 2H). ^{13}C NMR (300 MHz, $CDCl_3$): δ (ppm) 153.5, 141.2, 129.4, 128.3, 127.9, 126.8, 126.5. Anal. calcd for $C_{14}H_8N_2S_3$: C, 55.97; H, 2.68; N, 9.32; S, 32.02. Found: C, 55.85; H, 2.78; N, 9.40.

4,7-Bis(5-bromothiophen-2-yl)benzo-2,1,3-thiadiazole (21)[82]

NBS (6.6 g, 37 mmol) was added to a solution of **20** (5.0 g, 16.5 mmol) in acetic acid/chloroform (1:1, v:v). The mixture was refluxed for 12 h. After the solution was cooled to room temperature, the mixture was poured onto ice water. The solid was filtered and washed thoroughly with water. The red solid was recrystallized from chloroform and 6.2 g of red crystals were obtained. The pure product of **21** was a red crystal.

Yield: 83 %. ^{1}H NMR (300 MHz, $CDCl_3$): δ 7.74 (d, 4H), 7.12 (d, 2H). ^{13}C NMR (300 MHz, $CDCl_3$): 152.71, 141.34, 132.13, 129.02, 126.95, 126.42, 115.38. Anal. calcd for $C_{14}H_6Br_2N_2S_3$: C, 36.70; H, 1.32; N, 6.11; S, 20.99. Found: C, 36.88; H, 1.58; N , 6.03.

General synthesis of polymers: PT2-DTP8, PBT-DTP8, PT2-BT -DTP8

Dichlorobis(triphenylphosphine)palladium (4.4 mg, 0.0062 mmol) was added to a stirred solution of a mixture of **15** (615 mg, 0.62 mmol) and the other monomer (0.62 mmol) in dry THF (10 ml) under nitrogen atmosphere. The mixture was stirred at 90 ^{o}C for 40 h. After completion of the reaction, the mixture was cooled to room temperature and dropped into methanol with vigorous stirring. A powdery solid was separated and filtered. The resulting polymer was washed with methanol and hexane for 24 h through a Soxhlet apparatus. Finally, the crude polymer was purified by extracting with chloroform. The chloroform solution was concentrated under reduced pressure, and the polymer re-precipitated in methanol and the resulting solid collected by filtration.

Poly{[N-1-octylnonyl-dithieno(3,2-b:2',3'-d)pyrrole-2,6-diyl]-alt-[2,2'-bithiophene-5,5'-diyl]} (PT2-DTP8)

Yield: 38%. ^{1}H NMR (300 MHz, $CDCl_3$): δ (ppm) 7.3 (br, 2H), 7.1-6.9 (br, 4H), 3.90 (br, 1H), 2.0-1.8 (br, 4H), 1.5-0.6 (br, 29H). Anal. Calcd for $C_{33}H_{43}NS_4$: C, 68.11; H, 7.45; N, 2.41. Found: C, 67.83; H, 7.81; N, 2.25.

Poly{[N-1-octylnonyl-dithieno(3,2-b:2',3'-d)pyrrole-2,6-diyl]-alt-[2,1,3-benzothiadiazole-4,7-diyl]} (PBT-DTP8)

Yield: 43%. ^{1}H NMR (300 MHz, $CDCl_3$): δ (ppm) 8.4 (br, 2H), 7.9 (b, 2H), 4.40 (br, 1H), 2.2-1.9 (br, 4H), 1.5-0.7 (br, 29H). Anal. Calcd for $C_{31}H_{41}N_3S_3$: C, 67.47; H, 7.49; N, 7.61. Found: C, 67.03; H, 7.61; N, 7.65.

Poly{[N-1-octylnonyl-dithieno(3,2-b:2',3'-d)pyrrole-2,6-diyl]-alt-[bis(thiophen-2-yl)-2,1,3-benzothiadiazole-4,7-diyl]} (PT2-BT -DTP8)

Yield: 56%. ^{1}H NMR (300 MHz, $CDCl_3$): δ (ppm) 8.1 (br, 2H), 7.9 (br, 2H), 7.5-7.0 (br, 4H), 4.10 (br, 1H), 2.1-1.9 (br, 4H), 1.5-0.5 (br, 29H). Anal. Calcd for $C_{39}H_{45}N_3S_5$: C, 65.41; H, 6.33; N, 5.87. Found: C, 65.23; H, 6.71; N, 5.65.

2.3.3 Synthesis of the polymer PF12-DTP12, PF8-DTP12, PF6-DTP12, PF8-DTP8, PF8-DTP6, PF8-DTP4

General synthesis of 9,9'-dialkyl-2,7-dibromofluorene (23a-c)

A mixture of 2, 7-dibromofluorene **22** (5 g, 15.4 mmol) and DMSO (20 ml) was stirred at room temperature, to which 20 g of 50% (w/w) KOH solution was slowly added. The color of the reaction mixture changed into purple immediately and 1–bromoalkane (2.2 equv.) was added dropwise. After stirring at room temperature for 3 h, the reaction mixture was poured into water and extracted with dichloromethane. The organic extract was washed with brine, dried over $MgSO_4$ and then concentrated. Further purification was accomplished by column chromatography with hexane, providing product of white solid.

9,9'-Dihexyl-2,7-dibromofluorene (23a)

Yield: 93%. ^{1}H NMR (300 MHz, $CDCl_3$): δ (ppm) 7.53 (d, 2H), 7.47 (d, 2H), 7.43 (d, 2H), 1.93 (m, 4H), 1.3-1.0 (m, 12H), 0.82 (t, 6H), 0.56 (m, 4H).

9,9'-Dioctyl-2,7-dibromofluorene (23b)

Yield: 95%. ^{1}H NMR (300 MHz, $CDCl_3$): δ (ppm) 7.52 (d, 2H), 7.45 (d, 2H), 7.42 (d, 2H), 1.91 (m, 4H), 1.25-1.05 (m, 20H), 0.83 (t, 6H), 0.58 (m, 4H).

9,9'-Didodecyl-2,7-dibromofluorene (23c)

Yield: 91%. ^{1}H NMR (300 MHz, $CDCl_3$): δ (ppm) 7.52 (d, 2H), 7.42 (d, 2H), 7.40 (d, 2H), 1.91 (m, 4H), 1.25-1.05 (m, 36H), 0.86 (t, 6H), 0.55 (m, 4H).

The synthesis of N-alkyl-dithieno[3,2-*b*:2',3'-*d*]pyrrole (25a-c)

The processure was described for the synthesis of **5**.

N-1-butyl-dithieno[3,2-b:2',3'-d]pyrrole (25a)

Yield: 83%. ^{1}H NMR (300 MHz, $CDCl_3$): δ (ppm) 7.13 (d, 2H), 6.97 (d, 2H), 4.08 (t, 2H), 1.98 (m, 2H), 1.22-1.4 (m, 2H), 0.85 (t, 3H).

N-1-hexyl-dithieno[3,2-b:2',3'-d]pyrrole (25b)

Yield: 85%. ^{1}H NMR (300 MHz, $CDCl_3$): δ (ppm) 7.19 (d, 2H), 7.02 (d, 2H), 4.09 (t, 2H), 1.95 (m, 2H), 1.22-1.4 (m, 6H), 0.87 (t, 3H).

N-1-octyl-dithieno[3,2-b:2',3'-d]pyrrole (25c)

Yield: 78%. ^{1}H NMR (300 MHz, $CDCl_3$): δ (ppm) 7.10 (d, 2H), 6.92 (d, 2H), 4.03 (t, 2H), 1.97 (m, 2H), 1.22-1.4 (m, 10H), 0.88 (t, 3H).

The synthesis of 2,6-di(tributyltin)-N-alkyl-dithieno[3,2-*b*:2',3'-*d*]pyrrole (26a-c)

The processure was described for the synthesis of **6**.

2,6-Di(tributyltin)-N-butyl dithieno[3,2-b:2',3'-d]pyrrole (26a)

Yield: 92%. ^{1}H NMR (300 MHz, $CDCl_3$): δ (ppm) 6.95 (s, 2H), 4.08 (m, 2H), 1.98 (m, 2H), 1.23-1.70 (m, 56H), 0.85 (t, 3H).

2,6-Di(tributyltin)-N-hexyl dithieno[3,2-b:2',3'-d]pyrrole (26b)

Yield: 93%. ^{1}H NMR (300 MHz, $CDCl_3$): δ (ppm) 6.98 (s, 2H), 4.13 (m, 2H), 2.04 (m, 2H), 1.20-1.69 (m, 60H), 0.83 (t, 3H).

2,6-Di(tributyltin)-N-octyl dithieno[3,2-b:2',3'-d]pyrrole (26c)

Yield: 90%. ^{1}H NMR (300 MHz, $CDCl_3$): δ (ppm) 6.94 (s, 2H), 4.15 (m, 2H), 2.00 (m, 2H), 1.25-1.72 (m, 64H), 0.82 (t, 3H).

General synthesis of polymers: PF12-DTP12, PF8-DTP12, PF6-DTP12, PF8-DTP8, PF8-DTP6, PF8-DTP4

Dichlorobis(triphenylphosphine)palladium (3%mol) was added to a stirred solution of a mixture of 9,9'-dialkyl-2,7-dibromofluorene and 2,6-di(tributyltin)-N-alkyl dithieno[3,2-b:2',3'-d]pyrrole (1:1, mol:mol) in anhydrous THF under a nitrogen atmosphere. The mixture was stirred at 90 ^{o}C for 40 h. After completion of the reaction, the mixture was poured into methanol under vigorous stirring. A powdery solid was separated and filtered. The resulting polymer was washed with methanol and hexane for 24 h through a Soxhlet apparatus. Finally, the crude polymer was purified by extracting with chloroform. The chloroform solution was concentrated, and the polymer re-precipitated in methanol and the resulting solid collected by filtration. After drying in vacuum, a colored solid was obtained.

Poly {[9,9'-dihexyl-fluoren-2,7-yl]-alt-[N-dodecyl-dithieno(3,2-b:2',3'-d)pyrrole-2,6-diyl]} (PF6-DTP12)

Yield: 57%. ^{1}H NMR (300 MHz, $CDCl_3$): δ (ppm) 7.9-7.6 (br, 6H), 7.3 (br, 2H), 4.25 (br, 2H), 2.21-1.80(br, 6H), 1.5-0.6 (br, 43H). Anal. Calcd for $C_{45}H_{61}NS_2$: C, 79.47; H, 9.04; N, 2.06. Found: C, 79.30; H, 9.23; N, 1.84.

Poly{[9,9'-dioctyl-fluoren-2,7-yl]-alt-[N-dodecyl-dithieno(3,2-b:2',3'-d)pyrrole-2,6-diyl]} (PF8-DTP12)

Yield: 42%. ^{1}H NMR (300 MHz, $CDCl_3$): δ (ppm) 7.72-7.55 (br, 6H), 7.33 (br, 2H), 4.25 (br, 2H), 2.15-1.90(br, 6H), 1.5-0.7 (br, 51H). Anal. Calcd for $C_{49}H_{69}NS_2$: C, 79.94; H, 9.45; N, 1.90. Found: C, 79.75; H, 9.63; N, 1.86.

Poly{[9,9'-didodecyl-fluoren-2,7-yl]-alt-[N-dodecyl-dithieno(3,2-b:2',3'-d)pyrrole-2,6-diyl]} (PF12-DTP12)

Yield: 38%. ^{1}H NMR (300 MHz, $CDCl_3$): δ (ppm) 7.8-7.5 (br, 6H), 7.3 (br, 2H), 4.22 (br, 2H), 2.19-1.78(br, 6H), 1.5-0.5 (br, 59H). Anal. Calcd for $C_{57}H_{85}NS_2$: C, 80.69; H, 10.10; N, 1.65. Found: C, 80.53; H, 10.23; N, 1.48.

Poly{[9,9'-dioctyl-fluoren-2,7-yl]-alt-[N-butyl-dithieno(3,2-b:2',3'-d)pyrrole-2,6-diyl]} (PF8-DTP4)

Yield: 52%. ^{1}H NMR (300 MHz, $CDCl_3$): δ (ppm) 7.8-7.6 (br, 6H), 7.26 (br, 2H), 4.22 (br, 2H), 2.2-1.85 (br, 6H), 1.5-0.6 (br, 35H). Anal. Calcd for $C_{41}H_{53}NS_2$: C, 78.92; H, 8.56; N, 2.24. Found: C, 79.18; H, 8.73; N, 2.04.

Poly{[9,9'-dioctyl-fluoren-2,7-yl]-alt-[N-hexyl-dithieno(3,2-b:2',3'-d)pyrrole-2,6-diyl]} (PF8-DTP6)

Yield: 39%. ^{1}H NMR (300 MHz, $CDCl_3$): δ (ppm) 7.7-7.5 (br, 6H), 7.35 (b, 2H), 4.2 (br, 2H), 2.21-1.80(br, 6H), 1.5-0.55 (br, 39H). Anal. Calcd for $C_{43}H_{57}NS_2$: C, 79.21; H, 8.81; N, 2.15. Found: C, 79.30; H, 9.03; N, 1.94.

Poly{[9,9'-dioctyl-fluoren-2,7-yl]-alt-[N-octyl-dithieno(3,2-b:2',3'-d)pyrrole-2,6-diyl]} (PF8-DTP8)

Yield: 40%. ^{1}H NMR (300 MHz, $CDCl_3$): δ (ppm) 7.7-7.45 (br, 2H), 7.3 (br, 2H), 4.23 (br, 2H), 2.05-1.75(br, 6H), 1.5-0.6 (br, 43H). Anal. Calcd for $C_{45}H_{61}NS_2$: C, 79.47; H, 9.04; N, 2.06. Found: C, 79.60; H, 9.28; N, 1.92.

2.3.4 Synthesis of the oligomer BFPBF

2-Bromo-9,9'-dioctyl-fluorene (28)[83]

A mixture of 2-bromofluorene (2 g, 8.16 mmol) and DMSO (12 ml) was stirred at room temperature, to which 12 g of 50% (w/w) KOH solution was slowly added. The color of the reaction mixture changed into purple immediately and 1–bromooctane was added dropwise. After stirring at room temperature for 3 h, the reaction mixture was poured into water and extracted with dichloromethane. The organic extract was washed with brine, dried over $MgSO_4$ and then concentrated. Further purification was accomplished by column chromatography with hexane, providing product of oil. Yield: 75%. ^{1}H NMR (300 MHz, $CDCl_3$): δ (ppm) 7.60-7.35 (m, 7H), 2.00 (m, 4H), 1.25-1.12 (m, 20H), 0.78 (t, 6H), 0.60 (m, 4H).

2-(4,4,5,5-Tetramethyl-1,3,2-dioxanborolan-2-yl)fluorene (29)[84]

The solution of **37** (1.0 g, 2.1 mmol) in 20 ml anhydrous THF was cooled to -78 ^{o}C, to which was added 1.6 ml of n-butyllithium (1.6M in hexane). The reaction mixture was kept at this temperature for 1 h and then warmed up to 0 ^{o}C with further stirring for 15 min. The reaction solution was cooled to -78 ^{o}C again and 0.5 ml of 4,4,5,5-tetramethyl-1,3,2-dioxanborolane (2.63 mmol) was added. The reaction mixture was slowly warmed to room temperature and stirred over night. The work up was done as usual procedure to afford product **38** as a white solid.

Yield: 72%. ^{1}H NMR (300 MHz, $CDCl_3$): δ (ppm) 7.77-7.34 (m, 7H), 2.00 (m, 4H), 1.41 (s, 12H), 1.1-1.0 (m, 20H), 0.86 (t, 6H), 0.65 (m, 4H).

7-Iodo-2-nitrofluorene (31)[85]

To a solution of 2-nitrofluorene (3.2 g, 0.015 mol) in 100 ml glacial acetic acid was added iodine (2.0 g, 0.008 mol). The solution was stirred at room temperature for 10 min, after which were added 10 ml of concentrated H_2SO_4 and $NaNO_2$ (1.1 g, 0.015 mol). The solution was heated under reflux for 30 min and then poured into 100 g of ice. The yellow solid was collected by filtration to get the product **40** of 4.91 g.

Yield: 95%. Mp 242.5 (Lit. 243.5-245).

7-Iodo-9,9-dioctyl-2-nitrofluorene (32)[83]

A mixture of 7-iodo-2-nitrofluorene (2.0 g, 5.9 mmol) and 12 ml DMSO was stirred at room temperature, to which 12 g of 50% (w/w) KOH solution was slowly added. After the addition of KOH solution, 1–bromooctane was added dropwise. The reaction mixture was stirred at room temperature for 1 h and poured into water, followed by extracting with dichloromethane. The organic extract was washed with brine, dried over $MgSO_4$ and concentrated. The crude product was purified by column chromatography with hexane as the eluent to give a yellow solid.

Yield: 75%. ^{1}H NMR (300 MHz, $CDCl_3$): δ (ppm) 8.3-7.53 (m, 6H, H), 2.00 (m, 4H), 1.24-1.07 (m, 20H), 0.84 (t, 6H), 0.60 (m, 4H).

2 – Nitro-9, 9, 9', 9'-tetraoctyl-bisfluorene (33)[84]

2-Iodo-9,9'-bisoctyl-7-nitrofluorene (1 g, 1.78 mmol), 2-(4,4,5,5-tetramethyl-1,3,2-dioxanborolan-2-yl)fluorene (0.92 g, 1.78 mmol) and $Pd(PPh_3)_4$ (2 mol%) were dissolved in a mixture solution of toluene and aqueous 2M K_2CO_3. The solution was heated at 95 ^oC with vigorous stirring for 48 h. The resulting mixture was poured into dilute HCl and extracted with chloroform for 3 times. The organic extract was washed with brine and then dried over anhydrous $MgSO_4$. The solvent was removed under

reduced pressure and the residue was purified by chromatography with hexane/dichloromethane (5:1) as eluent to get the product of **42** as yellow oil.

Yield: 65%. ^{1}H NMR (300 MHz, $CDCl_3$): δ (ppm) 8.30-7.37 (m, 13H), 2.00 (m, 8H), 1.31-1.11 (m, 40H), 0.82 (t, 12H), 0.65 (m, 8H).

2 – Animo-9, 9, 9', 9'-tetraoctyl-bisfluorene (34)[86]

Compound **28** (1.0 g, 1.21 mmol) was added to 6 ml EtOH:EtOAc (v:v = 1:1). The reaction mixture was purged with nitrogen for 10 mins and then anhydrous $SnCl_2$ (2.30 g, 12.1 mmol) was added. The reaction mixture was refluxed under nitrogen for 40 h, poured into EtOAc and then washed with 1M NaOH, water, and brine. The organic layer was dried over $MgSO_4$ and the solvent was removed by reduced pressure. The product was purified by flash chromatography with hexane/ dichloromethane (3:1) as eluent to obtain the product as brown oil.

Yield: 90%. ^{1}H NMR (300 MHz, $CDCl_3$): δ (ppm) 7.70-7.32 (m, 13H), 6.81 (s, 2H), 2.01 (m, 8H), 1.33-0.75 (m, 60H).

N, N' – Bis(9, 9, 9', 9'-tetraoctyl-bisfluoren-2-yl)-3, 4 : 9, 10-perylene bisimide (BFPBF)[87]

0.1 g (0.255 mmol) Perylene-3,4:9,10-tetracarboxylic acid bisanhydride (in short, **PTCDA**), 1.62 g of **43** (2.04 mmol) and 0.514 g (0.281 mmol) $Zn(OAc)_2$ were mixed with 30 ml of quinoline and the reaction mixture was stirred under nitrogen for 2 days at 180 ^{o}C. After cooling to room temperature, the reaction mixture was poured into 300 ml 1M HCl solution. The mixture was extracted with CH_2Cl_2 for 3 times. The organic layer was collected, washed with brine and dried over $MgSO_4$. After the solvent was removed under vacuum, the residue was purified by chromatography with hexane/dichloromethane (3:1) as eluent and a red solid was obtained.

Yield: 78%. ^{1}H NMR (300 MHz, $CDCl_3$): δ (ppm) 8.83 (d, 4H), 8.77 (d, 4H), 7.85-7.36 (m, 26H), 2.07 (m, 16H), 1.27-0.87 (m, 120H). Anal. Calcd for $C_{140}H_{170}N_2O_4$: C, 86.46; H, 8.81; N, 1.44. Found: C, 86.35; H, 8.97; N, 1.38. MALDI-TOF MS (m/z): calcd for $C_{140}H_{170}N_2O_4$, 1944.86; found, 1944.45.

2.3.5 Synthesis of the polymer PTBF-FL, PTBF-CZ and PTBF-DTP

2,7-Dibromofluorenone (36)[88]

To a solution of 2,7-dibromofluorene (5.0 g, 15.5 mmol) in 150 ml of acetic anhydride was added powdered CrO_3 (3.85 g, 39 mmol) slowly. The mixture was stirred for 6 h at room temperature and poured into 200 ml of 1 M HCl. The solid was collected by filtration and washed with water thoroughly. The crude product was crystallized from 2-propanol to give the pure product of a yellow solid.

Yield: 90 %. ^{1}H NMR (300 MHz, $CDCl_3$): δ (ppm) 7.82 (d, 2 H) 7.68 (dd, 2 H), 7.42 (d, 2 H).

2,7-Dibromotetrabenzo[5,5']fulvalene (37)[89]

A solution of fluorene (18 mmol, 3.00 g) in 100 ml of anhydrous THF was cooled to -78 °C under nitrogen atmosphere and 11.3 ml of n-butyllithium (18 mmol, 1.6 M in hexanes) was added in dropwise. The solution was stirred for 10 min at this temperature. Trimethylsilyl chloride (1.95 g, 18 mmol) was then added and the solution was stirred for an additional 10 min. A second equivalent of n-butyllithium solution was added in. After the solution was stirred for 20 min, 2,7-dibromofluorenone (18 mmol, 6.1 g) in 50 ml of THF was added. The reaction mixture was allowed to warm to room temperature and to stir overnight. The reaction

mixture was poured into saturated NH_4Cl solution and extracted with ether for 3 times. The organic phase was dried with $MgSO_4$ and the solvent was removed. The crude product was recrystallized from a mixture solvent of chloroform and hexane. A red solid was obtained as the desired compound.

Yield: 60 %. ^{1}H NMR (300 MHz, $CDCl_3$): δ (ppm) 8.51 (s, 2H), 8.23 (d, 2H), 7.71 (d, 2H), 7.55 (d, 2H), 7.45 (d, 2H), 7.35 (t, 2H), 7.25 (d, 2H).

Toluene-4-sulfonic acid 1-decylundecyl ester (39)[90]

To a solution of 1-decylundecanol (25 g, 80 mmol), triethyl amine (28 ml, 200mmol) and $Me_3N{\cdot}HCl$ (7.7 g, 80 mmol) in 110 ml of anhydrous CH_2Cl_2 was added p-toluenesulfonyl chloride (23 g, 120 mmol) in 90 ml of anhydrous CH_2Cl_2 at 0 ^{o}C. The reaction mixture was warmed to room temperature and stirred for 2 h. Water was added to the mixture and extraction was done with CH_2Cl_2 for 3 times. The organic phase was dried over with $MgSO_4$ and the solvent was removed. The crude product was purified by chromatography with eluent of dichloromethane/hexane (1:5). Pure compound of **48** was colorless liquid.

Yield: 83 %. ^{1}H NMR (300 MHz, $CDCl_3$): δ (ppm) 7.77 (d, 2H), 7.28 (d, 2H), 4.52 (m, 1H), 2.40 (s, 3H), 1.55 (m, 4H), 1.32-1.02 (br, 32H), 0.83 (t, 6H).

4,4'-Dibromo-2,2'-dinitrobiphenyl (41)[91]

A mixture of **49** (24 g, 86 mmol) and activated copper powder (17.2 g, 300 mmol) was stirred in 150 ml of DMF for 2 h at 130 ^{o}C. After cooling to room temperature, 300 ml of toluene was added and the mixture was stirred for 10 min. The solid was filterd off and the organic layer was washed with water for several times. The organic

phase was dried over $MgSO_4$ and the solvent was removed by reduced pressure. The crude product was recrystallized in ethanol. The pure product of **50** was brown crystal.

Yield: 80 %. ^{1}H NMR (300 MHz, $CDCl_3$): δ (ppm) 8.35 (d, 2H), 7.78 (dd, 2H), 7.15 (d, 2H).

4,4'-Dibromo-2,2'-diaminobiphenyl (42)[91]

Small portions of tin powder (4.8 g, 40.5 mmol) were added to a stirred solution of **50** (4.0 g, 9.8 mmol) in a mixture of 20 ml of concentrated HCl and 50 ml of ethanol. The reaction mixture was refluxed for 3 h and then cooled to room temperature. The reaction mixture was poured into cold water and 2 M NaOH solution was added until pH of the solution was 8. The solution was extracted with ether for several times. The organic layer was washed with water, brine and dried over $MgSO_4$. The solvent was removed and the residue was purified by collumn chromatography with the eluent of dichloromethane/hexane (30:1). The pure product of **51** was a pale brown solid.

Yield: 70 %. ^{1}H NMR (300 MHz, $CDCl_3$): δ (ppm) 7.08 (d, 2H), 6.89 (d, 2H), 6.82 (dd, 2H), 5.01 (br, 4H).

2,7-Dibromocarbazole (43)[91]

A mixture of **51** (3.5 g, 10.5 mmol) and 80 ml of concentrated H_3PO_4 was refluxed at 190 ^oC for 24 h. The crude product was filter off and washed with water thoroughly. The residue was recrystallized in toluene. Pure product of **52** was a white solid.

Yield: 58 %. ^{1}H NMR (300 MHz, $CDCl_3$): δ (ppm) 8.08 (br, H), 7.85 (d, 2H), 7.55 (d, 2H), 7.33 (d, 2H).

2,7-Dibromo-N-(1-decylundecyl)carbazole (44)[90]

A mixture of **52** (3.25 g, 10 mmol) and potassium hydroxide (2.8 g, 50 mmol) were dissolved in 50 ml of anhydrous DMSO. A solution of 7.0 g (60 mmol) of **48** in DMSO (20 ml) and THF (10 ml) was added dropwise at room temperature. The mixture was stirred overnight. Water was added and the mixture was extracted with hexane for 3 times. The organic phase was dried over with $MgSO_4$ and the solvent was reduced under reduced pressure. The crude product was purified by collumn chromatography with the eluent of hexane. Pure product of **53** was a white solid.

Yield: 75 %. ^{1}H NMR (300 MHz, $CDCl_3$): δ (ppm) 7.85 (m, 2H), 7.65 (s, 1H), 7.53 (s, 1H), 7.30 (m, 2H), 4.4 (m, 1H), 2.19 (m, 2H), 1.88 (m, 2H), 1.35-0.9 (br, 32H), 0.85(t, 6H).

2, 7-Bis(4,4,5,5-tetramethyl-1,3,2-dioxaborolan-2-yl)-N-(1-decylundecyl)carbazole (45)[90]

53 (1.86 g, 3 mmol) was dissolved in 40 ml of anhydrous THF and cooled to -78 ^{o}C. To this solution, n-butyllithium (3.95 ml, 1.6 M in hexane) was added in dropwise. The reaction mixture was kept at this temperature for 1 h and then warmed up to 0 ^{o}C with further stirring for 15 min. The solution was cooled to -78 ^{o}C again and 2-isopropoxy-4,4,5,5-tetramethyl-1,3,2-dioxaborolane (1.38 ml, 6.6 mmol) was added rapidly. The reaction mixture was allowed to warm to room temperature and stirred overnight. The mixture was poured into water and extracted with ether for 3 times. The combined organic layer was dried over $MgSO_4$ and the solvent was removed. The crude product was purified by column chromatography with the eluent of hexane. The pure product of 46 was a colorless solid.

Yield: 65 %. ^{1}H NMR (300 MHz, $CDCl_3$): δ (ppm) 8.15 (m, 2H), 8.0 (s, 1H), 7.85 (s, 1H), 7.65 (m, 2H), 4.6 (m, 1H), 2.3 (m, 2H), 1.9 (m, 2H), 1.38 (s, 24H), 1.36-1.0 (br, 32 H), 0.83 (t, 6H).

2, 7-Bis(4,4,5,5-tetramethyl-1,3,2-dioxaborolan-2-yl)-9,9'-dioctylfluorene (47)

The same synthsis procedure as described for **45**.

Yield: 72 %. ^{1}H NMR (300 MHz, $CDCl_3$): δ (ppm) 7.54 (d, 2H), 7.46 (d, 2H), 7.41 (d, 2H), 1.98 (m, 4H), 1.4 (s, 24H), 1.25-1.05 (m, 20H), 0.86 (t, 6H), 0.56 (m, 4H).

General synthesis of polymers: PTBF-FL and PTBF-CZ

The compound **46** (300 mg, 61.7 mmol) and the other equvilent mole monomer **56** or **54** were dissolved in a mixture of THF (15 ml) and 2 M aqueous solution of Na_2CO_3 (8 ml). $Pd(PPh_4)_4$ (3% mol) was added and the mixture was heated at 125 oC for 48 h. Phenylboric acid (100 mg) was added and the mixture was stirred for 3 h. Then bromobenzene (1 ml) was injected and the mixture was stirred for another 3 h. The reaction mixture was extracted with chloroform and the organic phase was dried over $MgSO_4$. The mixture was concentrated to a few volume of solution by the removal of solvent. The polymer was precipitated by adding the mixture into methanol. A colored powdery solid was separated and filtered. The resulting polymer was washed with methanol and hexane for 24 h through a Soxhlet apparatus. Finally, the crude polymer was purified by extracting with chloroform. The chloroform solution was concentrated, and the polymer re-precipitated in methanol and the resulting solid collected by filtration. After drying in vacuum, a solid of the polymer was obtained.

Poly{[9,9'-dioctylfluorene-2,7-diyl]-alt-[tetrabenzofulvalene(5,5')-2,7-diyl]}

Yield: 42 %. ^{1}H NMR (300 MHz, $CDCl_3$): δ (ppm) 8.75 (br, 2H), 8.55 (br, 2H), 7.9-7.2 (br, 16H), 1.9 (br, 4H), 1.0-0.55 (br, 30H). Anal. Calcd for $C_{55}H_{54}$: C, 92.39; H, 7.61. Found: C, 92.09; H, 7.98.

Poly{[N-(1-decylundecyl)carbazole-2,7-diyl]-alt-[tetrabenzofulvalene(5,5')-2,7-diyl]}

Yield: 50 %. ^{1}H NMR (300 MHz, $CDCl_3$): δ (ppm) 8.65 (br, 2H), 8.4 (br, 2H), 7.8-7.1 (br, 16H), 4.0 (br, 1H), 2.05-1.8 (br, 4H), 1.35-0.32 (br, 30H). Anal. Calcd for $C_{55}H_{55}N$: C, 90.49; H, 7.59; N, 1.92. Found: C, 89.60; H, 8.28; N, 1.53.

The synthesis of polymer PTBF-DTP

The synthetic procedure of **PTBF-DTP** was the same as described for the synthesis of polymer **PBTDTP**.

Poly{[N-1-octylnonyl-dithieno(3,2-b:2',3'-d)pyrrole-2,6-diyl]-alt-[tetrabenzofulvalene(5,5')-2,7-diyl]}

Yield: 36 %. ^{1}H NMR (300 MHz, $CDCl_3$): δ (ppm) 8.7 (br, 2H) 8.4 (br, 2H), 7.8-7.1 (br, 12H), 4.15 (br, 1H), 2.1-1.85 (br, 4H), 1.3-0.3 (br, 30H). Anal. Calcd for $C_{51}H_{51}NS_2$: C, 82.54; H, 6.93; N, 1.89; S, 8.64. Found: C, 81.60; H, 7.28; N, 1.62.

2.3.6 Synthesis of the polymer PTBF-AOT and PFO-AOT

3-Methoxythiophene (51)

8.1 g (150 mmol) of sodium methoxide was suspended in 15 ml methanol. To this mixture 16.3 g (100 mmo) of 3-bromothiophene and 1.44g (10 mmol) copper bromide were successively added. The reaction mixture was heated under gentle reflux with stirring. After 6 h the reaction had finished. The mixture was extracted with ether for

3 times and the organic layer was dried over $MgSO_4$. The solvent was removed and the pure product was obtained by vacuum distillation. The product of 50 is colorless oil.

Yield: 80 %. ^{1}H NMR (300 MHz, $CDCl_3$): δ (ppm) 7.2 (dd, 1H), 6.8 (dd, 1H), 6.3 (d, 1H), 3.9 (s, 3H).

3-Dodecyloxythiophene (52)[92]

A mixture of **28** (12g, 105 mmol), 1-dodecanol (47 ml, 210 mmol), p-toluenesulfonic acid monohydrate (2g, 0.2 eq) and 100 ml toluene was heated at 130 ^{o}C under nitrogen and the reaction mixture was stirred over night. The mixture was poured into water and extracted with dichloromethane for 3 times. The organic layer was dried over MgSO4. After solvent evaporation, the residue was purified by column chromatography to give the desire compound. The pure product of **29** was a colorless solid.

Yield: 50 %. ^{1}H NMR (300 MHz, $CDCl_3$): δ (ppm) 7.18 (dd, 1H), 6.78 (dd, 1H), 6.26 (d, 1H), 3.94 (t, 2H), 1.8 (m, 2H), 1.45 (m, 2H), 1.3 (br, 16H), 0.85 (t, 3H).

2-Bromo-3-dodecyloxythiophene (53)[92]

NBS (3.56 g, 20 mmol) was added in one portion to the compound **29** (5.4 g, 20 mmol) in 20 ml $CHCl_3$ at 0 ^{o}C and kept from dark for 1 h. Then the mixture was warmed to room temperature and stirred for 3 h. The chloroform was removed by rotary evaporation and the residue was diluted with hexane. After the filtration, the filtrate was concentrated and purified by column chromatography. The eluent is pure hexane. Pure product of **30** was white solid.

Yield: 88 %. ^{1}H NMR (300 MHz, $CDCl_3$): δ (ppm) 7.15 (d, 1H), 6.7 (d, 1H), 3.98 (t, 2H), 1.82 (m, 2H), 1.4 (m, 2H), 1.3 (br, 16H), 0.83 (t, 3H).

5,5'-Dibromo-4,4'-didodecyloxyl-2,2'-bithiophene (54)[93]

Compound **30** (8.0 g, 23 mmol), $PdCl_2(PhCN)_2$ (77.5 mg, 0.20 mmol), potassium fluoride (2.70 mg, 46 mmol), and DMSO (100 mL) was added into a 250 ml round bottom flask. $AgNO_3$ (7.8 g, 46 mmol) was added in one portion and the resulting mixture was heated with stirring at 60 °C for 12 h. Additional $AgNO_3$ (7.8 g, 46 mmol) and potassium fluoride (2.7 mg, 46 mmol) was then added and stirring was continued for further 12 h. The reaction mixture was passed through a Celite pad to remove a solid residue and the cake was washed repeatedly with ethyl acetate. The filtrate was washed with water for 3 times and the organic layer was dried over $MgSO_4$. The solvent was removed under reduced pressure and the crude solid was purified by column chromatography on silica gel with hexane. The pure product of **31** was pale green solid.

Yield: 58 %. ^{1}H NMR (300 MHz, $CDCl_3$): δ (ppm) 6.74 (s, 2H), 4.05 (t, 4H), 1.8 (m, 4H), 1.5-1.2 (br, 36H), 0.9 (t, 6H). Anal. Calcd for $C_{32}H_{52}Br_2O_2S_2$: C, 55.49; H, 7.57. Found: C, 54.86; H, 8.03.

5,5'-Bis(trimethylstannyl)-4,4'-didodecyloxyl-2,2'-bithiophene (55)

To a solution of **31** (1.8 g, 2.6 mmol) in 40 ml of anhydrous THF, n-butyllithium (3,25 ml, 5.2 mmol, 1.6 M in hexane) was added dropwise at -78 ^{o}C. The solution was stirred at -78 ^{o}C for 1 h and warmed to room temperature for further 0.5 h stirring. The solution was then cooled -78 ^{o}C again and a 1 M solution of trimethyltin chloride in THF (5.5 ml, 5.5 mmol) was added in one potion. The solution was warmed to

room temperature and stirred overnight. The mixture was poured into water and extracted with EA for 3 times. The organic phase was dried over $MgSO_4$ and the solvent was removed from reduced pressure. The product of **33** was a dark green solid.

Yield: 92 %. ^{1}H NMR (300 MHz, $CDCl_3$): δ (ppm) 6.7 (s, 2H), 3.95 (t, 4H), 1.9 (m, 4H), 1.55-1.23 (br, 36H), 0.85 (t, 6H), 0.45 (s, 18H).

The synthesis of polymers: PFO-OAT and PTBF-AOT

The synthesis procedure of polymers **PFO-OAT** and **PTBF-AOT** was the same as described for polymer **PBTDTP**.

Poly{ 2,7-bis(3-decyloxythien-2-yl)tetrabenzofulvalene(5,5')-5,5'-diyl]}

Yield: 53 %. ^{1}H NMR (300 MHz, $CDCl_3$): δ (ppm) 8.7 (br, 2H), 8.5 (br, 2H), 7.8-7.25 (br, 10H), 6.78 (br, 2H), 4.05 (br, 4H), 1.88 (br, 4H), 1.55-0.6 (br, 42H). Anal. Calcd for $C_{58}H_{66}O_2S_2$: C, 81.07; H, 7.74. Found: C, 79.68; H, 8.38.

Poly{ 2,7-bis(3-decyloxythien-2-yl)fluorone-5,5'-diyl]}

Yield: 37 %. ^{1}H NMR (300 MHz, $CDCl_3$): δ (ppm) 7.9-7.2 (br, 6H), 6.8 (br, 2H), 4.0 (br, 4H), 1.8 (br, 4H), 1.5-0.7 (br, 42H). Anal. Calcd for $C_{45}H_{58}O_3S_2$: C, 76.01; H, 8.22. Found: C, 75.20; H, 9.08.

Chapter 3

A Low Bandgap Conjugated Polymer Based On N-Dodecyl-dithieno[3,2-b:2',3'-d]pyrrole

3.1 Introduction

As already discussed in chapter one, semiconducting polymer materials have attracted intensive interests during recent decades due to their applicability in organic photovoltaics. Amongst these polymers, low band gap conjugated polymers[94-99] are of considerable scientific and technological importance because of their improved light harvesting ability from the solar emission spectrum in photovoltaic devices[100-103]. Thus, reducing polymer bandgap is a simple and efficient way to obtain active materials with high performance in organic photovoltaics.

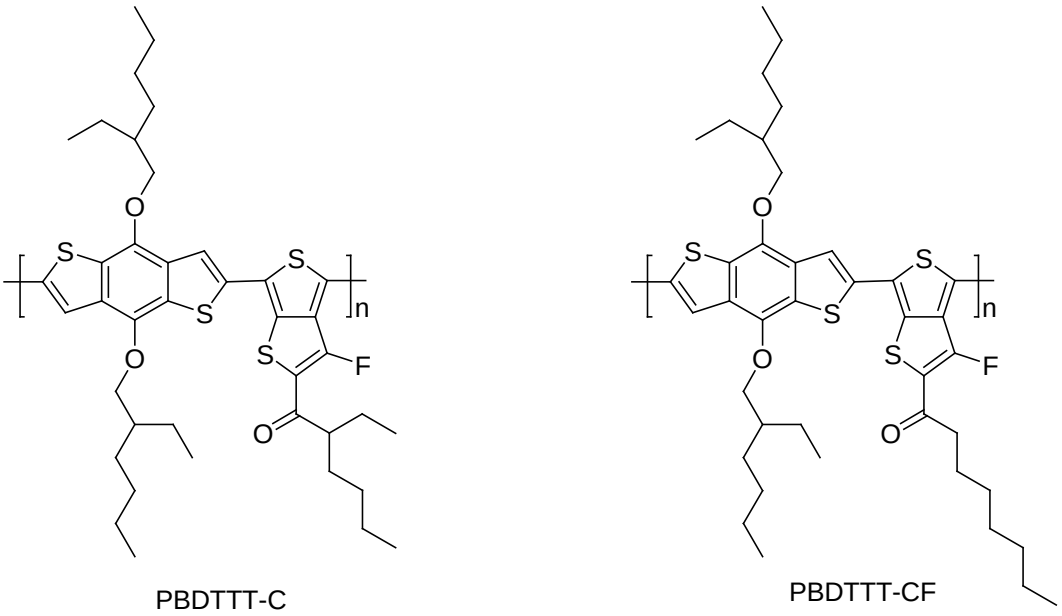

Figure 3.1 Low bandgap polymers based on benzo[1,2-b:4,5-b']dithiophene and thieno[3,4-b]thiophene.

Recently, BHJ OPV devices fabricated by using PC71BM and low band gap polymers[104] based on benzo[1,2-b:4,5-b']dithiophene and thieno[3,4-b]thiophene (shown in **Figure 3.1**) has been reported and PCE of ca. 8% has been achieved. In these PSC devices, the blend of the polymer and PC71BM are used as the active material with the optimized weight ratios of 1:1.5 for both polymers. A V_{oc} as high as 0.76 V can be obtained in devices based on PBDTTT–CF. Consequently, combined with its high J_{sc} and fill factor (FF), a high PCE of 7.38+0.4% was thus achieved in the PBDTTT–CF system. Additionally, the external quantum efficiency (EQE) of the devices based on the two polymers were also measured and all the devices show rather efficient photoconversion efficiency in the range 400–700 nm, with EQE values of 50–70%. In the PBDTTT–CF device, the highest EQE value was 68.7% at 630 nm, which is the highest achieved in a low bandgap PSCs system. The calculated J_{sc} values are 14.1 and 15.0 mA cm^{-2} for devices based on PBDTTT–C and PBDTTT–CF, respectively. The average internal quantum efficiency (IQE) higher than 90% in the range 400–700 nm can be obtained from the device based on PBDTTT–CF, which indicating a highly efficient overall photo conversion process in the cell. From the results above, it can be concluded that high performance PSCs can be realized by using low bandgap polymers and V_{oc}, or in another word energy level, can be tuned by means of molecular design as well. One significant design approach towards low band gap polymers is to introduce rigid and planar unit such as molecules with fused ring structures into the polymer backbones. Generally, these fused components are structurally planar and lead to a substantive extension of the polymers conjugation[66,105]. Another powerful approach towards designing low band gap polymers is to arrange alternating donor and acceptor units along the polymer

backbone[106]. The alternation of donor and acceptor units increases the double bond character between the repeating units and stabilizes the quinoid form of the polymer[107]. Furthermore, such donor-acceptor system enables an increased intra-chain charges transfer, which would accentuate the performance of low band gap polymers in organic electronics[108-109].

Conjugated polymers based on functionalized thiophenes or fused thiophene rings have been widely explored as the active materials of organic electronics, due to their outstanding optical properties, electrical properties[110-114] and facile synthetic approaches/ methodology towards their preparations. These thiophene/ functional thiophene based polymers can be easily obtainable via oxidative polymerization, Stille cross-coupling or Suzuki cross-coupling[115-117]. N-Functionalized dithieno[3,2-b:2',3'-d]pyrroles (**Chart 3.1, a**), in short DTPs, having structures of fused thiophene rings, are structurally planar molecules. Homopolymers of DTPs have been investigated (**Chart 3.1 b**) with details by several research groups[118-119]. A few samples of DTP copolymers have been reported as well[70,120]. From the reported polymers, there are indications that DTPs are promising molecules towards ideal materials for multipurpose organic electronics. In this chapter, the synthesis of a new DTP based donor-acceptor copolymer via Stille coupling reaction will be discussed. The DTP unit was selected as the donor unit based on the premise that N-alkylated DTP would allow for better solubility without changing the planarity[121]. In addition, the nitrogen atom in DTP molecule enhances the electron-donating nature in the resulting polymer[118]. On the other hand, benzothiadiazole moiety is selected as the acceptor unit, which is driven by consideration of its high electron affinity as well as the good performance of the benzothiadiazole incorporated materials in organic

electronics[122-124]. Herein, the detail synthesis of DTP based copolymer via Stille-cross coupling method is reported in this chapter and the thermal, optical and electrochemical properties of the polymer were investigated.

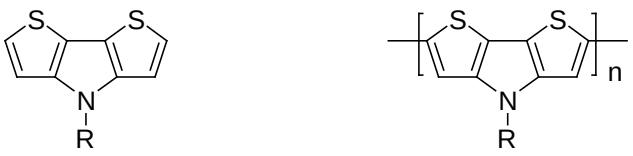

(a) DTPs (b) PDTPs

R= Alkyl chain

Chart 3.1 Structures of DTPs and PDTPs.

3.2 Synthesis and characterization

3.2.1 Monomer synthesis

The synthetic approach to produce monomers **6** and **8** is shown in **Scheme 3.1**. The compound **2** was obtained by the Kumada coupling of 2-bromothiophene. 3,3',5,5'-Tetrabromo-2,2'-bithiophene (**3**) was synthesized by the bromination of **2** in chloroform solution and then reduced to 3,3'-dibromo-2,2'-bithiophene **4** by reacting with the zinc dust. The target compound **5** was obtained by reacting compound **4** with 1-dodecyl amine in presence of the catalyst tris(dibenzylideneacetone)dipalladium (Pd_2dba_3). Subsequently, compound **5** was treated with n-butyllithium to form the dilithiated intermediate which was then quenched with tributyltin chloride to afford compound **6**. 4,7-Dibromo-2,1,3-benzothiadiazole **8** was synthesized by refluxing the compound **7** with bromine in the hydrobromic acid. The structures of the synthesized compounds are confirmed by ^{1}H NMR and reported in the experimental section.

Scheme 3.1 Synthetic approach of the monomers **6** and **8**.

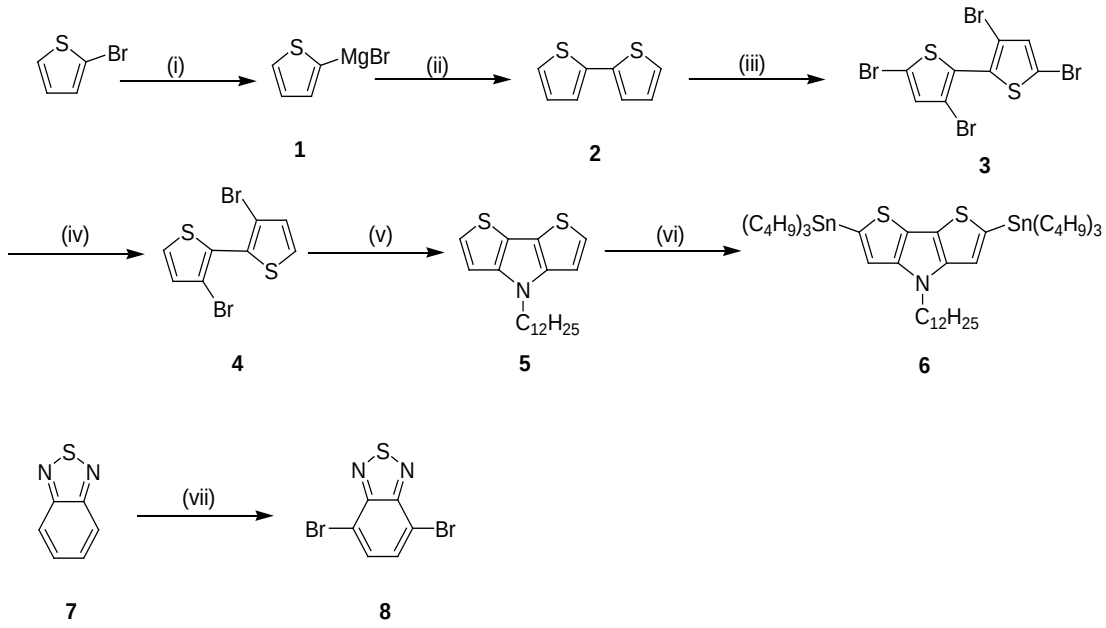

Reagents and conditions: (i) Mg, I_2, dry ether; (ii) Ni(dppp)Cl_2, dry ether; (iii) Br_2, chloroform; (iv) Zinc dust, ethanol; (v) Pd_2dba_3, BuONa, BINAP, $C_{12}H_{24}$-NH_2, toluene; (vi) n-Butyl lithium, dry THF, -78 ^oC; (vii) Br_2, HBr, reflux.

3.2.2 Polymer synthesis

Stille coupling reaction is effective for the preparation of conjugated alternative copolymers between distannyl aromatic compounds and dihalogenated compounds, so it was chosen for the polymer synthesis. As shown in **Scheme 3.2**, the building blocks of **6** and **8** were polymerized in anhydrous THF using the palladium-catalyzed Stille coupling reaction to afford the desired polymer (**PBTDTP**).

Scheme 3.2 Synthetic approach of the polymer **PBTDTP**.

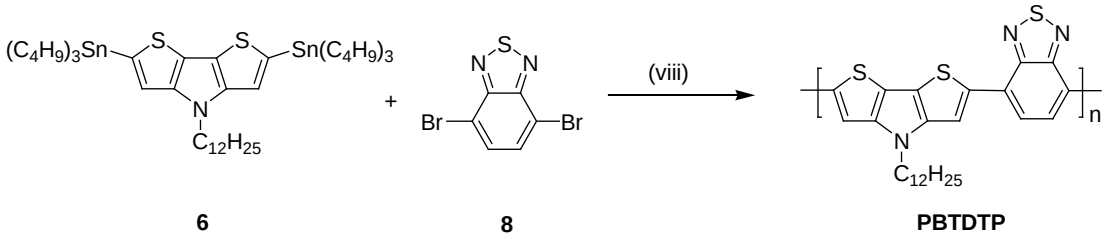

Reagents and conditions: (viii) $Pd(PPh_3)_2Cl_2$, THF, 90 ^oC, 48 h.

3.2.3 Polymer structure

The structure of **PBTDTP** was confirmed by ^{1}H NMR spectroscopy and elemental analysis. The chemical shift of the protons at DTP ring in **PBTDTP** is manifested at δ 7.5 ppm while the protons of benzothiadiazole moiety appear at δ 8.2 ppm. The peak at δ 4.2 is attributed to the hydrogens at the methylene group attached to the nitrogen atom. The chemical shifts from δ 0.5 to 1.95 ppm are assigned to the protons of N-dodecyl chain attached to DTP. In addition, elemental analysis of the polymer is roughly in agreement with the expected formula.

3.3 Results and discussion

3.3.1 Polymer preparation

The Suzuki coupling reaction utilized in the preparation of **PBTDTP** offered a possibility of preparing alternative copolymers in good yields. Furthermore, the reaction conditions are mild and can be carried out in homogeneous phase without the need of a phase transfer catalyst. After completion of the polymerization, extraction with different solvents (methanol and hexane) in a Soxhlet apparatus is necessary to remove oligomers and impurities that would significantly degrade the performances of the polymer based devices. Finally, thorough drying of the polymer was performed and the obtained polymer was stored under an inert atmosphere.

3.3.2 Physical properties

The resulting polymer is soluble in common organic solvents such as $CHCl_3$ and THF. The molecular weights and the polydispersity of the polymer were measured by GPC

(THF eluent, calibrated with polystyrene stands). The number average molecular weight of **PBTDTP** is found to be 4.1 KDa with a polydispersity index of 1.1.

3.3.3 Thermal properties

The thermal stability of the polymer **PBTDTP** was evaluated using TGA under nitrogen atmosphere. An apparent one-step degradation curve is observed during the measurements and a weight loss (~ 5 %) occurrs at ca. 270 ^{o}C, indicating that the novel polymer has fair thermal stability under inert atmosphere.

3.3.4 Optical properties

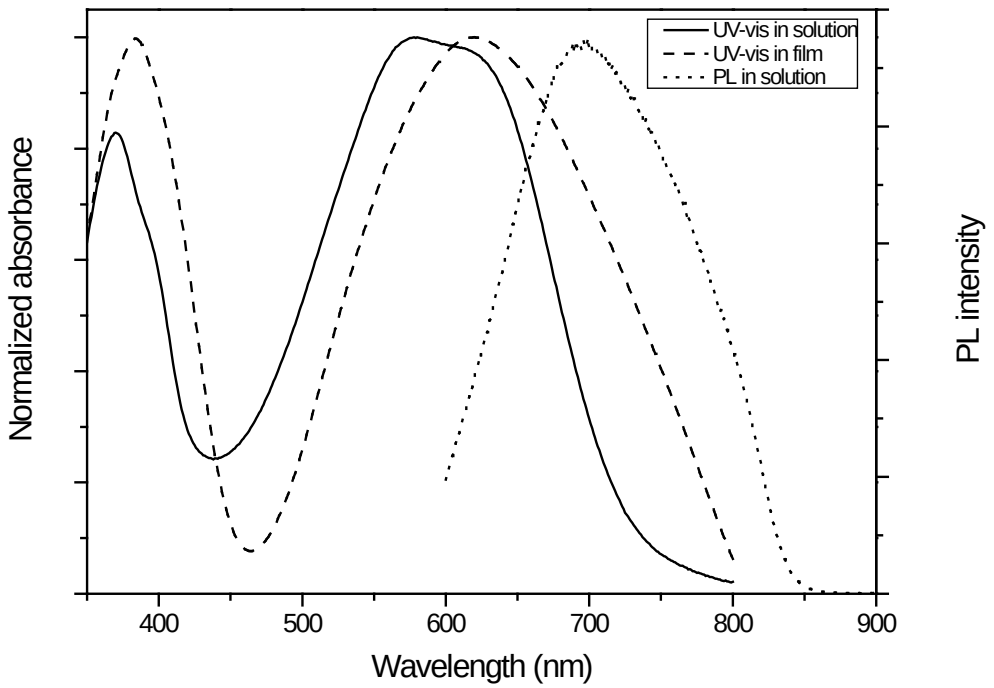

Figure 3.2 UV-vis and PL spectra of **PBTDTP** in solution and UV-vis spectra in solid state.

The optical properties of the polymer were characterized by UV-visible spectroscopy. In $CHCl_3$ dilute solution, the UV-visible absorption spectrum shows two absorption

peaks at 375 and 596 nm (**Figure 3.2**), which are attributed to π-π* transition of benzothiadiazole and DTP units, respectively[125]. The maximum absorption of **PBTDTP** in solution is red-shifted by approx 40 nm in comparison to the homopolymer of DTP (**Chart 3.1 b**, R = dodecyl, λ_{max} = 552 nm in solution). The results suggest that extended conjugation is achievable in **PBTDTP**.

In addition, the optical absorption of the polymer in solid state was also investigated (**Figure 3.2**). In solid state, the polymer shows two broader absorption peaks at 390 and 620 nm. The maximum absorption at longer wavelength in film state is red-shifted by 24 nm compared to that in dilute solution, which implies weak inter-chain interactions in its solid state. The onset of absorption for **PBTDTP** in the solid state is extended beyond 800 nm, corresponding to a 1.55 eV of the optical band gap (E_g^{opt}), which is lower than that of DTP homopolymer (1.7 eV). This value of the optical bandgap from the film state clearly indicates that a low bandgap polymer is achieved in the donor-acceptor architecture. As such, this new polymer would be anticipated to be able to harvest more photons due to its broader absorption in the visible light region. Accordingly, **PBTDTP** is potentially a good donor candidate in BHJ organic solar cells.

The photoluminescence spectroscopy of the polymer in dilute chloroform solution is depicted in **Figure 3.2**. The polymer **PBTDTP** displays a maximum emission at λ = 695 nm, which indicates a Stokes shift of 3333333 cm^{-1}. As for the homopolymer of DTP (**Chart 3.1 b**, R = dodecyl), the maximum emission appeared at λ = 614 nm and the Stokes shift value is about 20666666 cm^{-1}. The greater Stokes shift of **PBTDTP** indicates a more effective charge transfer compared to the DTP homopolymer.

3.3.5 Electrochemical properties

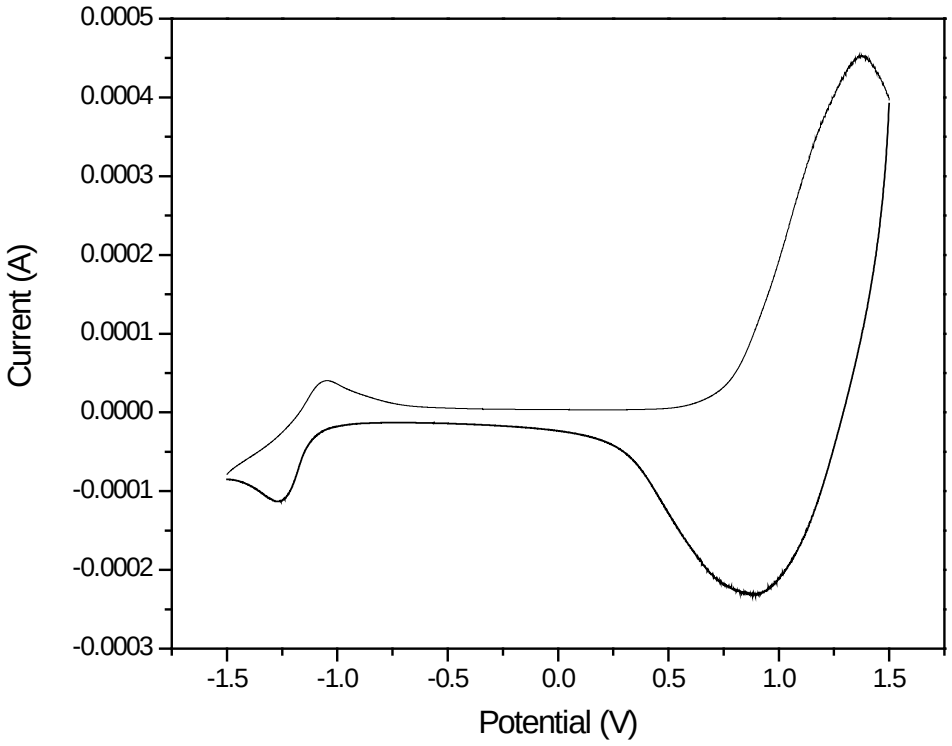

Figure 3.3 Cyclic voltammogram of **PBTDTP** film casted on a glass carbon electrode in Bu_4NBF_4/acetonitrile at scan rate of 100 $mV \cdot s^{-1}$.

The electrochemical property of **PBTDTP** was determined by cyclic voltammetry (CV) (**Figure 3.3**). The measurements were performed under a nitrogen atmosphere in anhydrous acetonitrile solution of 0.1 M Bu_4NBF_4. A glassy carbon disk coated with the thin polymer film was used as work electrode, a silver wire as pseudo-reference electrode and a platinum wire as counter electrode. The redox potentials were calibrated against the ferrocene/ ferrocenium couple as an internal standard. All potentials were converted to the standard calomel electrode (SCE) scale using a value of $E_{1/2}(Fc^+/Fc)$ = 0.40 V vs. SCE[126]. The cyclic voltammograms reveal a chemically quasi-reversible oxidation (p-doping) and reduction (n-doping) of the polymer. An oxidation potential of $E_{ox\ onset}$ = 0.6 V (versus SCE) and a reduction potential of E_{re}

$_{onset}$ = -1.1 V were observed for **PBTDTP**. A HOMO energy level of -5.0 eV, a LUMO energy level of -3.3 eV and an electrochemical band gap of 1.7 eV are calculated from the CV values. The oxidization potential of **PBTDTP** is about 0.3 V higher than that of the DTP homopolymer, which indicates a more stable neutral state for **PBTDTP** than that of the DTP homopolymer.

It is generally considered that a donor material serving in a bulk heterojunction solar cell should have a bandgap lower than 1.80 eV in order to achieve a better harvesting of solar photons, whose maximum flux is around 1.77 eV[127]. Meanwhile, the HOMO levels of donor materials should be between -5.7 and -4.8 eV for large open-circuit voltages as well as good air stability. The LUMO level of donor should be higher than that of [6,6]-phenyl C_{61} butyric acid methyl ester (PC61BM, -4.3 eV) for effective charge transfer. The new polymer **PBTDTP**, whose bandgap, LUMO and HOMO level are 1.7, -3.3 and -5.0 eV, meets these requirements. The CV results further suggest the potential of **PBTDTP** as a donor material in bulk heterojunction solar cells.

3.4 Summary

A novel donor-acceptor polymer **PBTDTP** based on a N-dodecyldithieno[3,2-b:2',3'-d]pyrrole and a 2,1,3-benzothidadiazole units was successfully prepared by a Stille cross-coupling approach. This new polymer has good solubility in common organic solvents and good thermal stability. The optical characteristics of the polymer indicate that **PBTDTP** has an optical bandgap as low as 1.55 eV in the solid state. Cyclic voltammetry measurements reveal an electrochemical band gap of 1.7 eV and a HOMO energy level of -5.0 eV of the polymer. From these results, N-functionalized

dithieno[3,2-b:2’,3’-d]pyrroles (DTPs) are promising candidates for achieving low band gap polymers. The optical and electrical characteristics of **PBTDTP** enable the potentiality of the polymer to serve as donor material in BHJ organic solar cells.

Chapter 4

Conjugated Polymers Based on N- 1 - Octylnonyl-dithieno[3,2-b:2’,3’-d]pyrrole

4.1 Introduction

In chapter 3, a novel low band gap polymer based on N-dodecyldithieno[2,2-b:2’,3’]pyrrole was synthesized and shown to have interesting optical and electrochemical properties, making it a potential p-type material in organic photovoltaics. The N-dodecyldithieno[2,2-b:2’,3’]pyrrole based donor-acceptor polymer possess a low bandgap and exhibits broad light absorption capabilities in the UV-vis region extending into the near IR region. The polymer having such excellent light absorption would benefit light harvesting and would be suitable for application in organic solar cell devices.

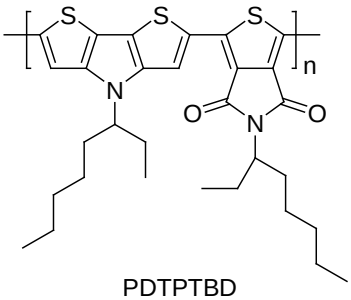

PDTPTBD

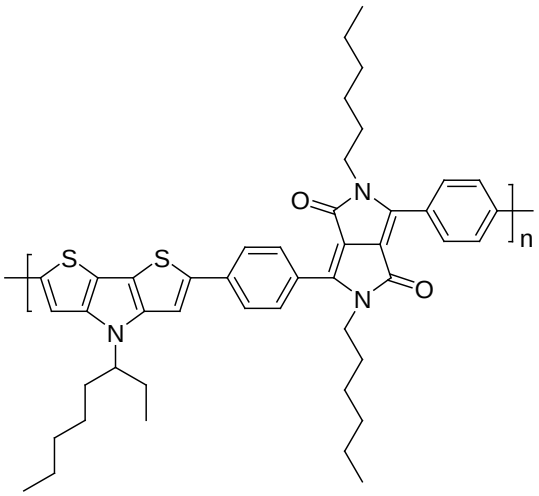

PDTPDTD

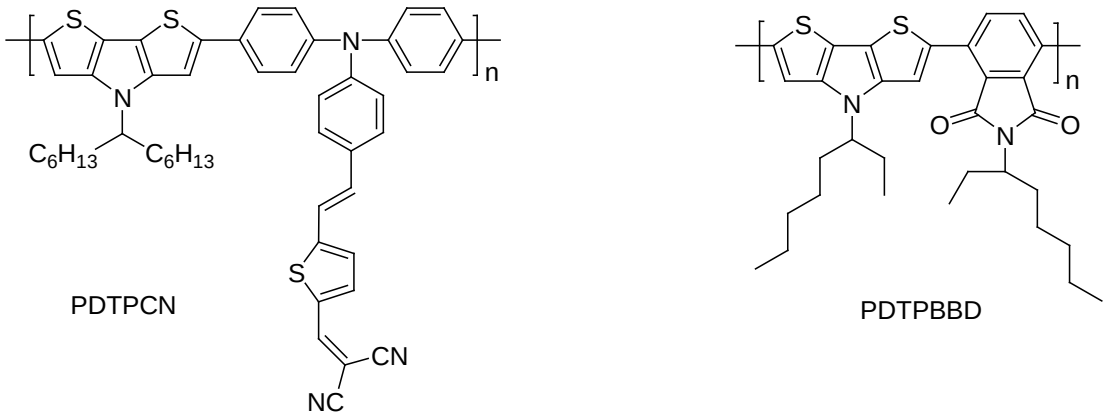

Figure 4.1 DTP based polymers that used in BHJ solar cells as donor materials.

Recently, some of low bandgap polymers based on DTP have been reported for the photovoltaic application and the polymer structures are shown in **Figure 4.1**. Among these polymers, solar cells based on PDTPTBD and PC61BM has the highest V_{oc} and J_{sc} associated with a PCE of 1.90 %, which might be due to it is good charge interchain transfer. The PCEs based on the rest polymers and PC61BM or PC71BM range from 0.25 ~ 0.76%. The device characteristics of these reported polymers for OPV application are summarized in **Table 4.1**.

Table 4.1 Device Characteristics of the BHJ Solar Cells Based on Reported Polymer with PC61BM or PC71BM.

Active layer	J_{sc} (mA/cm^2)	V_{oc} (V)	FF	PCE (%)
PDTPTPD:PC60BM [128]	6.97	0.7	0.39	1.9
PDTPDTD:PC60BM [129]	3.6	0.69	0.31	0.76
PDTPCN:PC60BM [130]	1.78	0.63	0.30	0.34
PDTPBBD:PC70BM[128]	1.22	0.78	0.26	0.25

On the other hand, the characteristics of conjugated polymers, such as HOMO/LUMO levels, need to be optimized in order to achieve optimal photovoltaic performance. In general, the band gap of the polymer should be minimized to increase photon absorption. At the same time, the gap between the HOMO of the donor polymer and the LUMO of the electron acceptor should be maximized in order to increase the open-circuit voltage (V_{oc}). In addition, the LUMO of the polymer (donor) should be positioned above the LUMO of the acceptor such as fullerene derivatives by at least 0.2-0.3 eV to ensure efficient electron transfer. In order to further investigate N-alkyl dithieno[2,2-b:2',3']pyrroles suitability as for donor candidates in OPV devices, a series of alternating polymers based on N-1-octylnonydithieno[2,2-b:2',3']pyrrole were synthesized (see **Chart 4.1)**, which would include donor-acceptor and donor-donor arrangements. N-1-octylnonyldithieno[2,2-b:2',3']pyrrole is chosen as the donor building unit with the expectation for higher molecular weights associated with its better solubility due to presence of branched pendant chains.

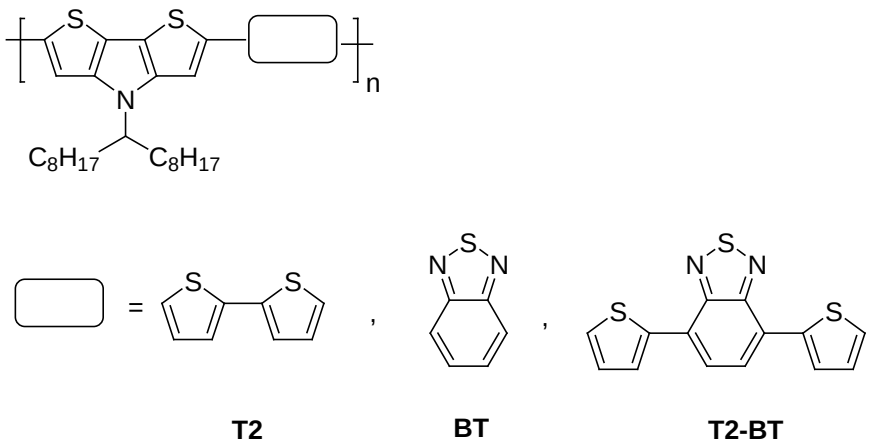

Chart 4.1 Polymer structures based on N-1-octylnonyldithieno[2,3-b:2',3'-d] pyrrole

4.2 Synthesis and characterization

4.2.1 Monomer synthesis

Scheme 4.1 The synthetic approach of the monomers **15**, **17**, **19** and **21**.

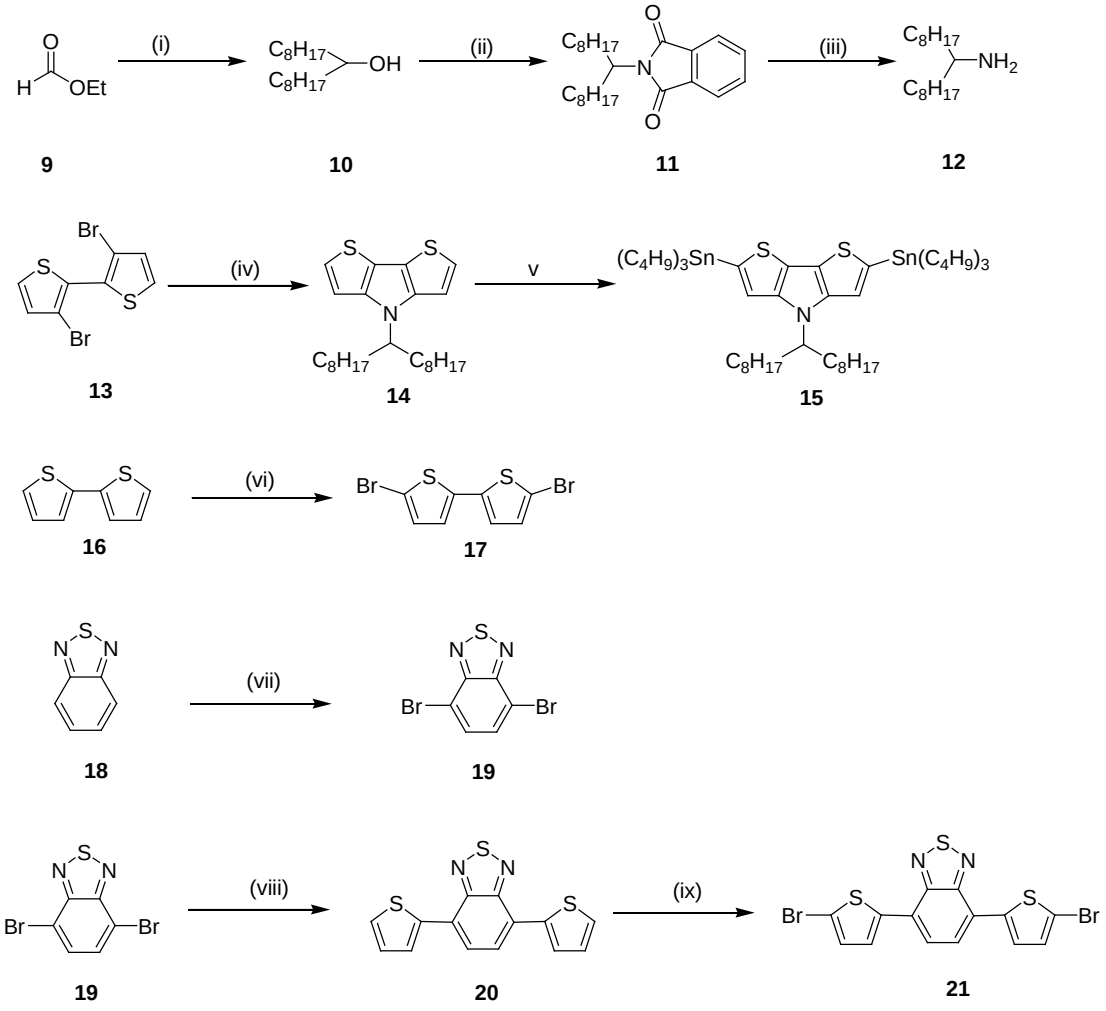

Reagents and conditions: (i) Mg, I_2, n-bromooctane, dry ether; (ii) phthalimide, PPh_3, DIAD, dry ether; (iii) hydrazine monohydrate, concentrated HCl, abs. ethanol; (iv) Pd_2dba_3, BuONa, BINAP, **12**, toluene; (v) n-Butyl lithium, dry THF, -78 ^oC; (vi) NBS, DMF; (vii) Br_2, HBr, reflux; (viii) 2-tri(butyltinyl)thiophene, $Pd(PPh_3)_2Cl_2$; (ix) NBS, acetic acid/chloroform.

The synthetic approach to monomers **15**, **17**, **19** and **21** is shown in **Scheme 4.1**. The preparation of amine **12** with branched chain was started from ethyl formate **9**, which was converted to 1-octylnonanol **10** firstly and followed *N*-1-octylnonylphthalimide

11. Compound **11** was refluxed with hydrazine under the strongly acidic conditions to form the primary amine with branched chain. The DTP monomer **15** was obtained by a series of similar synthesis steps to compound **6** (Chapter 3). The preparation of monomer **17** was effected by the reaction of NBS and 2,2'-bithiophene in DMF solution with a high yield. The two acceptor monomers **19** and **21** were synthesized following literature procedures. The structures and purity of monomers were verified using ^{1}H NMR spectroscopy and elemental analyses.

4.2.2 Polymer synthesis

Scheme 4.2 The synthetic approach for the polymer **PT2-DTP8, PBT-DTP8** and **PT2-BT-DTP8**.

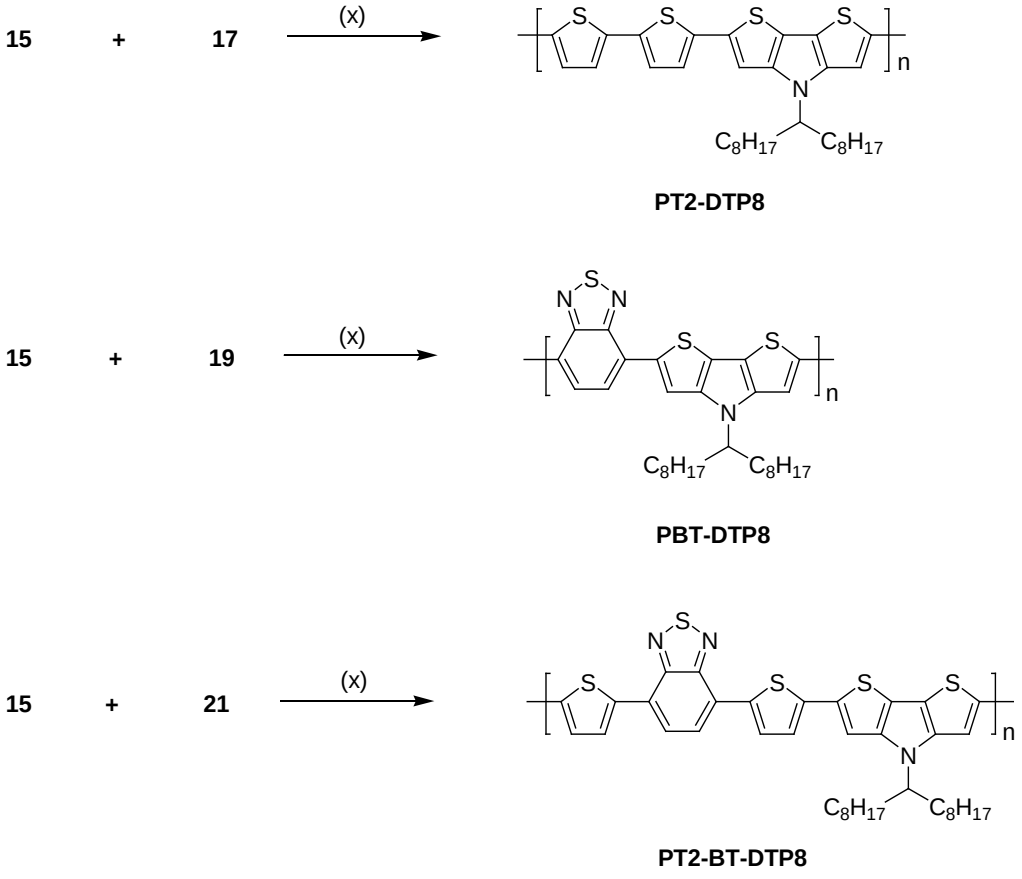

Reagents and conditions: (x) $Pd(PPh_3)_2Cl_2$, THF, 90 ^{o}C, 48 h.

The Stille coupling methodology is used for the polymerization, following the same conditions outlined in Chapter 3. The detail synthetic approach is shown in **Scheme 4.2**. During the reaction, a red colour solution for polymer **PT2-DTP8** and a dark blue colour for **PBT-DTP8**, **PT2-BT-DTP8** were observed. All polymerizations proceeded smoothly and target polymers were obtained as powdery solids after purification by Soxhlet extraction.

4.2.3 Polymer structure

The structures of **PBT-DTP8**, **PBT-DTP8** and **PT2-BT-DTP8** were confirmed by ^{1}H NMR spectroscopy and elemental analyses. For **PT2-DTP8**, the chemical shift of the protons at DTP ring appears at δ 7.3 ppm and the protons of bithiophene moiety are at δ 7.1-6.9 ppm. The peak at δ 3.9 belongs to the hydrogen connected to the tertiary carbon which is attached to the nitrogen atom. The two broad peaks at δ 2.2-1.9 are the hydrogens of methylene groups which are adjacent to the tertiary carbon. Chemical shifts from δ 0.7 to 1.5 ppm are assigned to the rest protons of the branched chains. For the polymers **PBT-DTP8** and **PT2-BT-DTP8**, the chemical shifts of the protons at DTP ring are manifested at δ 7.9 and 7.85 ppm while the protons of benzothiadiazole moiety appear at δ 8.4 and 8.1 ppm, respectively. The peak at δ 4.4 and 4.2 ppm is attributed to the hydrogen connected to the tertiary carbon which is attached to the nitrogen atom. The broad chemical shifts at δ 2.2-0.6 are assigned to the hydrogens of the branched chains. Compared to donor-donor type polymer **PT2-DTP8**, arising from the electron accepting characteristic of benzothiadiazole and thiophenyl benzothiadiazole, the chemical shifts of hydrogens at DTP groups as well as chemicals shifts of hydrogens connected to the tertiary carbon in **PBT-DTP8** and

PT2-BT-DTP8 are both moved downfield. Arising from the extent of downfield chemical shift, it can be deduced that the sequence of the electron accepting ability in these three polymers would be T2 << T2-BT < BT.

4.3 Results and discussion

4.3.1 Physical properties

All three polymers derived were soluble in common organic solvents such as $CHCl_3$, THF and toluene. The molecular weights and the polydispersity of the polymers as measured by GPC (using THF eluent, calibrated with polystyrene standards) are summarized in **Table 4.2**. The polymers have polydispersity indexes (PDI) ranging from 1.27 to 1.55 and M_n values in the range of 4.7 to 14.5 × 10^3 Da. The polymer, **PT2-BT-DTP8**, based on the combination of benzothiadiazole unit and two thiophene units (T2-BT) achieved much higher molecular weight than the polymer based on just benzothiadiazole unit while similar electron-accepting characteristic were achievable at the same time.

Table 4.2 GPC Results of **PBT-DTP8**, **PBT-DTP8** and **PT2-BT-DTP8**.

Polymer	M_n (×10^3)	M_w (×10^3)	PDI	n[a]
PT2-DTP8	6.9	8.8	1.27	48
PBT-DTP8	4.7	7.3	1.55	26
PT2-BT-DTP8	14.5	19.6	1.35	103

[a] Number of aromatic rings in the polymer chain.

4.3.2 Thermal properties

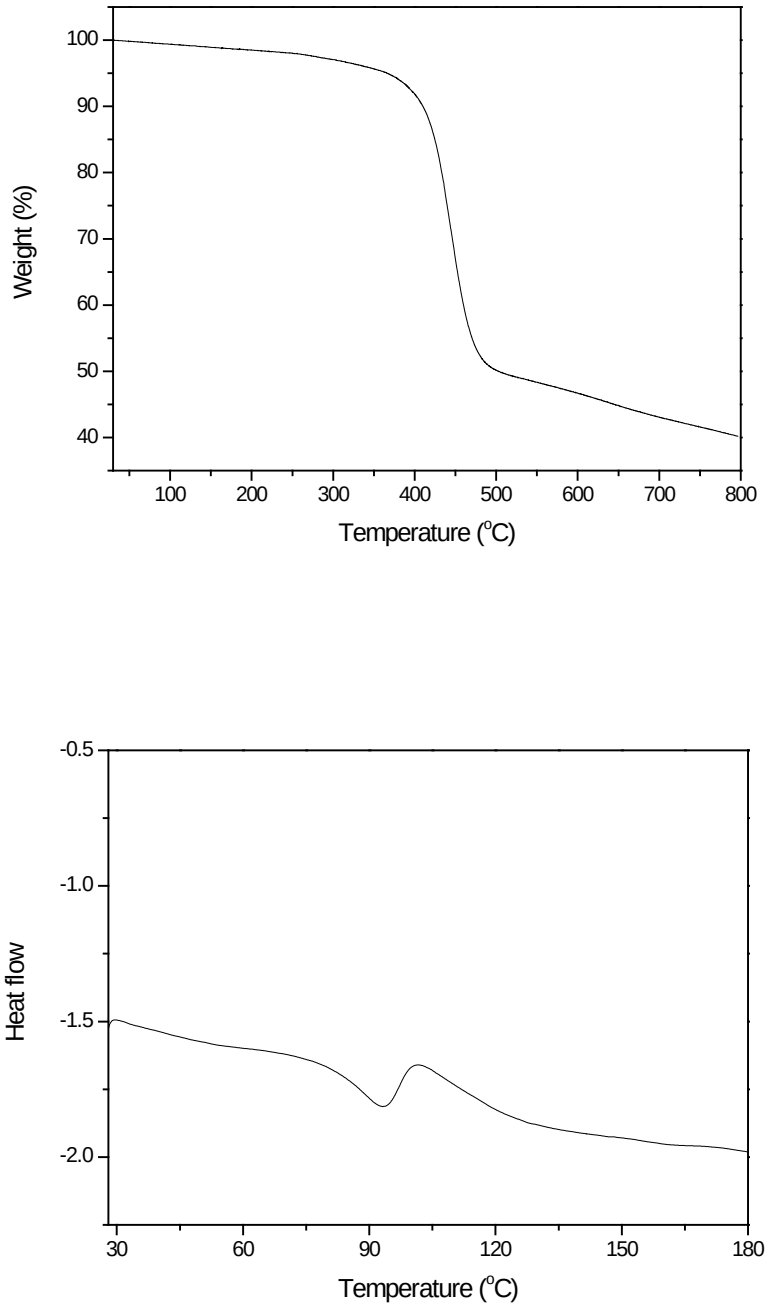

Figure 4.2 Representative TGA and DSC curve of **PT2-BT-DTP8** under nitrogen atmosphere.

The thermal properties of **PBT-DTP8**, **PBT-DTP8** and **PT2-BT-DTP8** were evaluated by TGA and DSC under nitrogen atmosphere. The results are summarized in **Table 4.3**. In nitrogen atmosphere, an apparent one-step degradation attributable to the cleavage of side chain group is observed with the onset of degradations (a weight loss ~ 5 %) for all the three polymers observed at above 300 ^{o}C. DSC measurements revealed that the glass transition temperatures of **PT2-DTP8** and **PT2-BT-DTP8** are at 66 and 93 ^{o}C respectively. No obvious glass transition is observed for the polymer **PBT-DTP8**, which might be due to its low molecular weight. TGA and DSC analysis indicated that the novel polymers were thermally stable under inert atmosphere. **Figure 4.2** depicts the representative TGA and DSC curves of **PT2-BT-DTP8**.

Table 4.3 TGA and DSC Results of **PBT-DTP8**, **PBT-DTP8** and **PT2-BT-DTP8**.

Polymer	T_d [a] (^{o}C)	T_g (^{o}C)
PT2-DTP8	300	66
PBT-DTP8	320	--
PT2-BT-DTP8	340	93

[a] Weigth loss ~ 5 %, T_d: temperature of decomposition, T_g: temperature of glass transition.

4.3.3 Optical properties

The optical properties of the polymers were investigated by UV-visible spectroscopy in solution phase and film state as well as by photoluminescence spectroscopy in solution phase at room temperature. The results are summarized in **Table 4.4**. In $CHCl_3$ dilute solution, the UV-visible absorption spectrum of **PT2-DTP8** shows one absorption peak at 521 nm while those of **PBT-DTP8** and **PT2-BT-DTP8** show two

absorption peaks (**Figure 4.3**), which can be attributed to π-π* transition of the benzothiadiazole and DTP units.

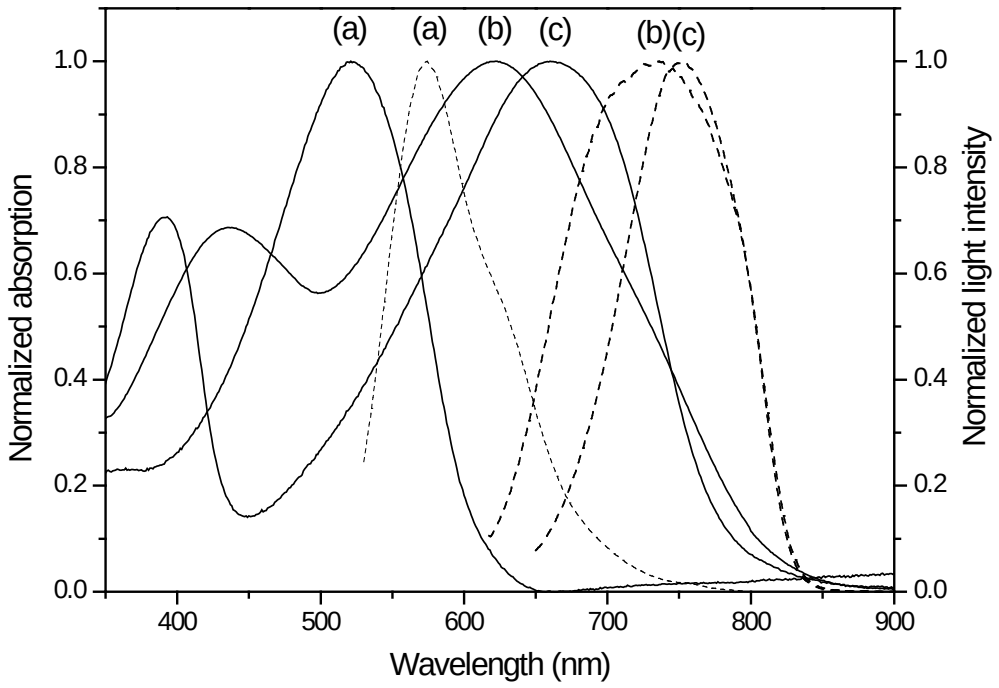

Figure 4.3 UV-vis (solid line) and PL (dash line) spectra of **PT2-DTP8 (a)**, **PBT-DTP8 (b)** and **PT2-BT-DTP8 (c)** in dilute $CHCl_3$ solution.

The maximum absorption of **PT2-DTP8** in solution is 520 nm which is red-shifted approx 40 nm in comparison with that of **P3HT** (λ_{max} = 480 nm in solution). The results suggest that an extended conjugation is achieved in **PT2-DTP8** while the maximum absorption for **PBT-DTP8** and **PT2-BT-DTP8** are 674 and 659 nm, which can be attributed to the introduction of the strongly electron withdrawing benzothiadiazole unit. The photoluminescence spectroscopy of the polymers in dilute chloroform solution is depicted in **Figure 4.3**. **PT2-DTP8**, **PBT-DTP8** and **PT2-BT-DTP8** display maximum emissions at λ = 576, 754 and 736 nm, which indicate

Stokes shifts of 1833333, 3133333 and 3800000 cm^{-1}, respectively. The higher Stokes shifts for **PBT-DTP8** and **PT2-BT-DTP8** would be indicative of greater charge transfer in these two polymers than **PT2-DTP8**.

Table 4.4 Optical Properties of the Polymers in Solution and Film States.

Polymer	UV (solution) λ (nm)	PL (solution) λ (nm)	UV (film) λ (nm))	Bandgap[a] (opt.) E_g (eV)
PT2-DTP8	521	576	548	1.73
PBT-DTP8	393, 660	754	397, 674	1.41
PT2-BT-DTP8	436, 622	736	442, 659	1.46

[a] Estimated from the onset of absorption of the polymers in film states.

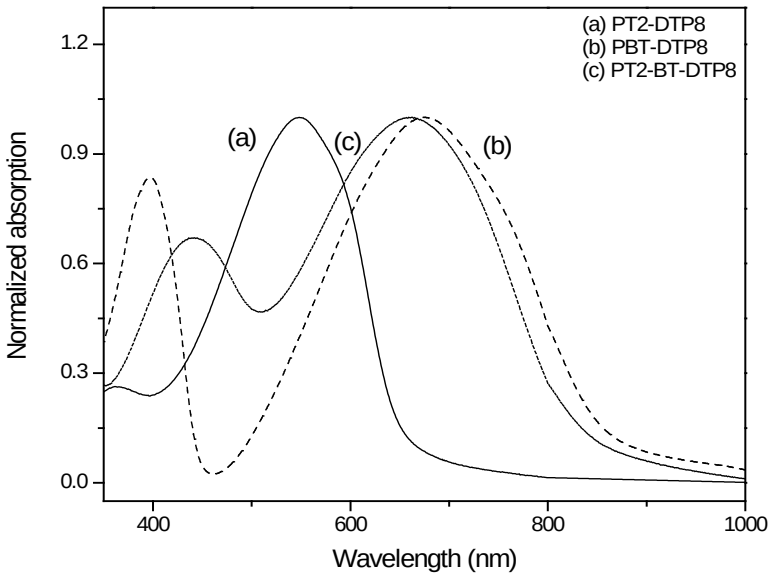

Figure 4.4 UV-vis spectra of **PBT-DTP8**, **PBT-DTP8** and **PT2-BT-DTP8** in solid states.

In addition, the optical absorption of the three polymers in solid phase was also investigated (**Figure 4.4**), where the polymers depicted ~~broader~~ absorptions than when in solution. The absorption maxima for all the three polymers in solid phase are red-shifted by around 20 nm than those in dilute solution. This observation implies that there were no significant conformational changes in the polymer chains in going from solution to film because of the high rigidity of the polymer backbones. The absorption onset of **PBT-DTP8** and **PT2-BT-DTP8** in solid states is around 900 nm and the calculated values of optical band gap (E_g^{opt}) of the two polymers are 1.41 and 1.46 eV. Such values of the optical band gap clearly indicate that **PBT-DTP8** and **PT2-BT-DTP8** are low bandgap polymers and the broad absorption in visible region would benefit their light harvesting greatly. Even for the polymer **PT2-DTP8**, the optical band gap is about 1.7 eV and is lower than that of P3HT (1.9 eV) as well. The optical characteristics suggest that these novel polymers would be good donor candidates for use in BHJ organic solar cells.

4.3.4 Electrochemical properties

The electrochemical properties of **PT2-DTP8**, **PBT-DTP8** and **PT2-BT-DTP8** were determined by cyclic voltammetry (CV) and the CV curves are shown in **Figure 4.5**. These measurements were performed under nitrogen atmosphere in anhydrous acetonitrile solution of 0.1 M Bu_4NBF_4. A glassy carbon disk coated with a thin polymer film was used as work electrode, a silver wire as pseudo-reference electrode and a platinum wire as counter electrode. The redox potentials were calibrated against the ferrocene/ ferrocenium couple as an internal standard.

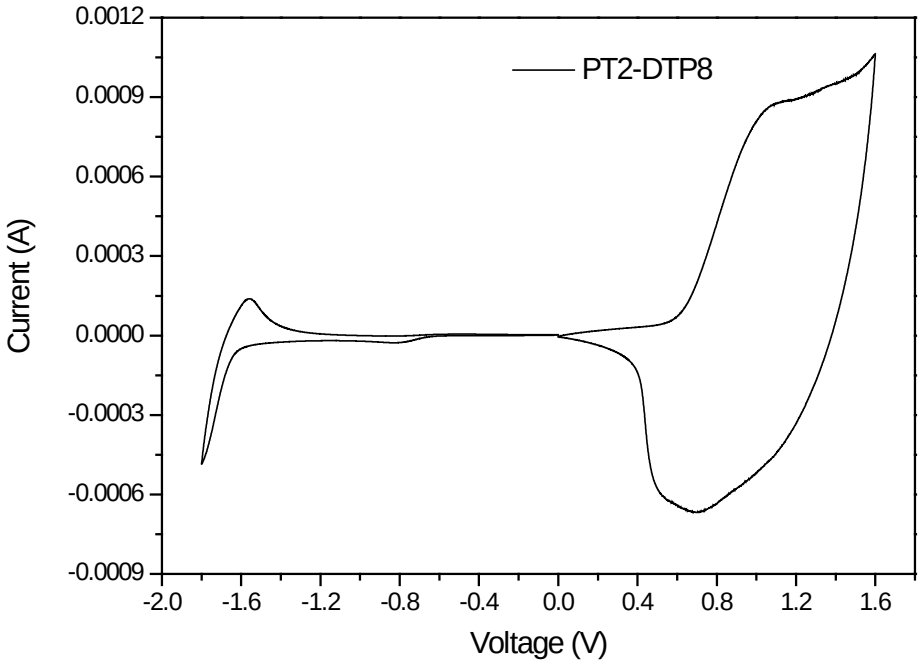
PT2-DTP8
Current (A)
Voltage (V)
0.0012
0.0009
0.0006
0.0003
0.0000
-0.0003
-0.0006
-0.0009
-2.0
-1.6
-1.2
-0.8
-0.4
0.0
0.4
0.8
1.2
1.6

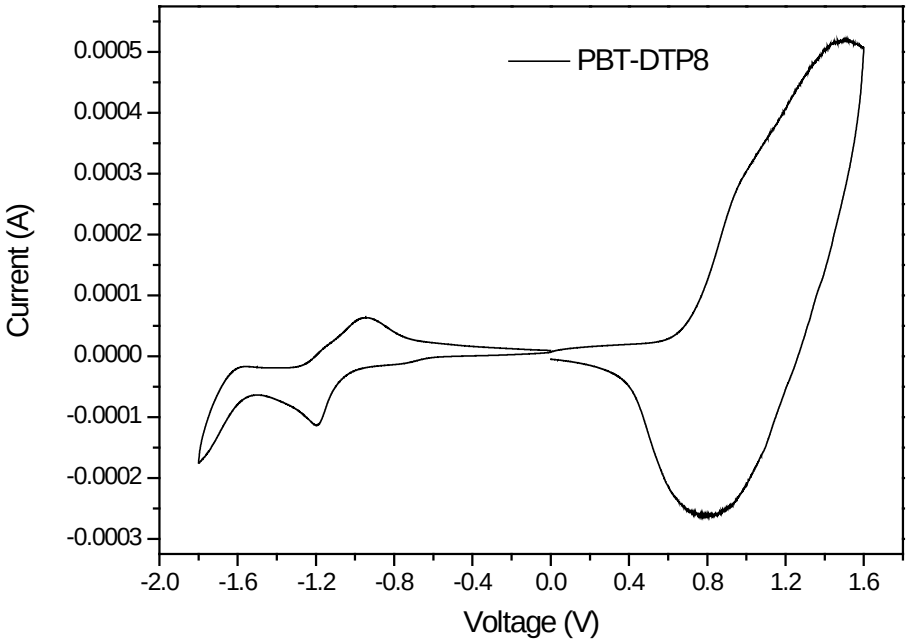
PBT-DTP8
Current (A)
Voltage (V)
0.0005
0.0004
0.0003
0.0002
0.0001
0.0000
-0.0001
-0.0002
-0.0003
-2.0
-1.6
-1.2
-0.8
-0.4
0.0
0.4
0.8
1.2
1.6

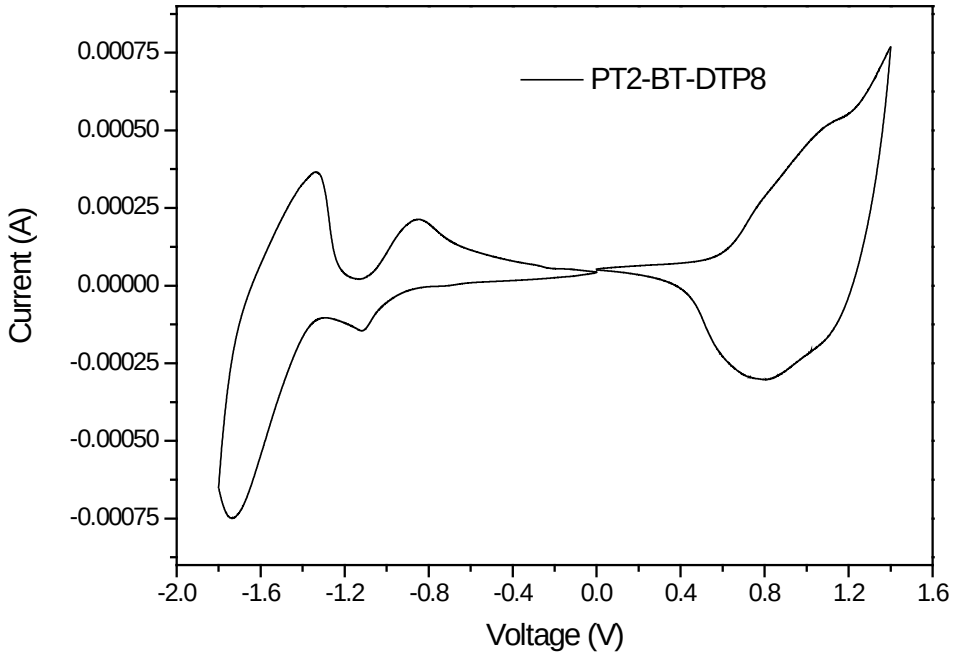

Figure 4.5 Cyclic voltammogram of **PT2-DTP8**, **PBT-DTP8** and **PT2-BT-DTP8** in Bu_4NBF_4/acetonitrile at a scan rate of 100 $mV \cdot s^{-1}$.

For **PT2-DTP8**, an onset oxidation potential of 0.52 V and an onset reduction potential of -1.42 V are observed respectively, corresponding to a HOMO level of -4.92 and a LUMO level of -2.98 eV. For **PBT-DTP8**, an onset oxidation potential of 0.57 V and an onset reduction potential of -1.0 V was observed, corresponding to a HOMO level of -4.97 and a LUMO level of -3.4 eV. Due to the electron donating characteristic of DTP and thiophene moieties in **PT2-BT-DTP8**, multi-oxidation and corresponding reverse reduction peaks were observed and an onset oxidation potential of 0.6 V is shown in in the cyclic voltammogram. At the same time, **PT2-BT-DTP8** shows an onset reduction potential of -0.95 V. A HOMO energy level of -5.0 eV and a LUMO level of -3.45 eV are calculated for **PT2-BT-DTP8**. In comparison with **PBT-DTP8** and **PT2-BT-DTP8**, a higher HOMO level is achieved for **PT2-DTP8** because of the electron-donating characteristic of the bithiophene moiety and thus a

higher V_{oc} would be expected for **PT2-DTP8** based OPV devices. On the other hand, due to the strongly electron withdrawing characters of BT and T2-BT moieties, **PBT-DTP8** and **PT2-BT-DTP8** show lower LUMO level than that of **PT2-DTP8** and thus lower band gaps are achieved for the two polymers. The electrochemical band gaps of 2.04, 1.57 and 1.55 eV for **PT2-DTP8**, **PBT-DTP8** and **PT2-BT-DTP8** are calculated from the CV results.

Table 4.5 Onset and Peak Potentials of p- and n-Doping Process of the Polymers.

Polymer	p-Doping			n-Doping			Bandgap
	E_{on} (V)	E_{pa} (V)	HOMO (eV)	E_{on} (V)	E_{pc} (V)	LUMO (eV)	E_g (eV)[a]
PT2-DTP8	0.52	1.06	-4.92	-1.42	-1.77	-2.98	1.99
PBT-DTP8	0.57	1.45	-4.97	-1.0	-1.2, -1.78	-3.4	1.57
PT2-BT-DTP8	0.6	0.81, 1.37	-5.0	-0.95	-1.11, -1.74	-3.45	1.55

[a] Electrochemical band gap

4.3.5 Photovoltaic characteristics

From the investigation of optical properties, all three polymers are anticipated to be able to harvest light effectively. Accordingly, organic BHJ solar cells were fabricated using an active layer based on mixture of these polymers with PC61BM. The active layer of 100 nm thickness was spin-coated onto the substrates from dichlorobenzene solution of the polymer (**PT2-DTP8**, **PBT-DTP8** or **PT2-BT-DTP8)**:**PC61BM** (1:1, w/w) inside a nitrogen glove box. Post device annealing was carried out at 145 ^{o}C for 15 min in a N_2 glove box. The photovoltaic characteristics of the organic solar cells were determined by a Source-Meter (Keithley, model 2400) under a Xe lamp

illumination with power density of 100 mW/cm^2 (AM 1.5). All the measurements were performed under nitrogen atmosphere at room temperature.

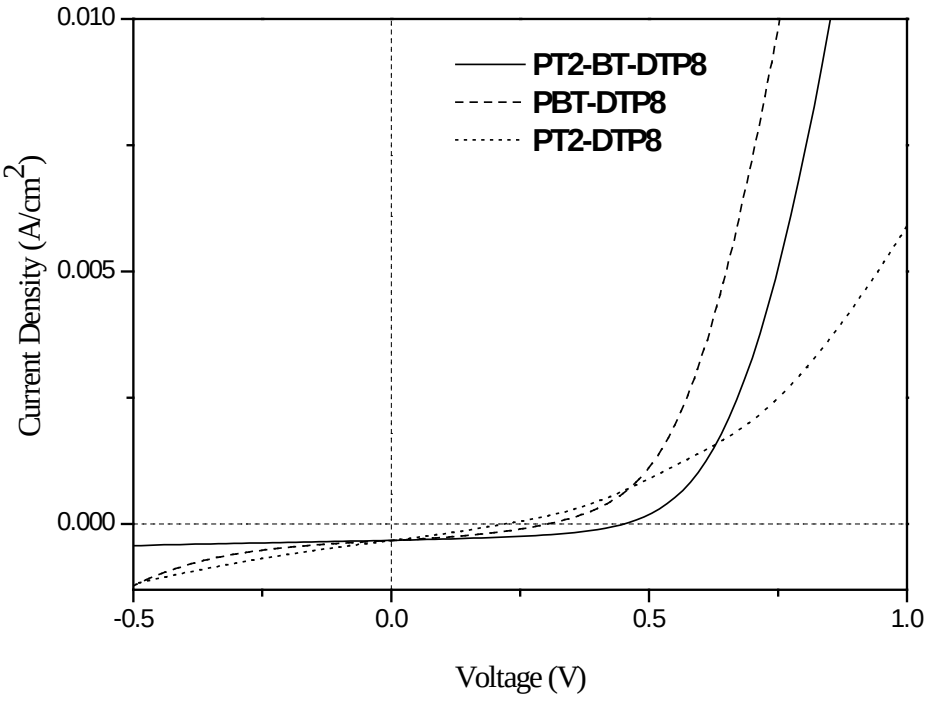

Figure 4.6 Current density-voltage characteristics of the three polymers based photovoltaic devices under simulated AM 1.5 illumination.

The I-V characteristics of the photovoltaic devices fabricated from the blend of polymer/PCBM were measured under simulated AM 1.5 (**Figure 4.6**). The power conversion efficiencies (PCE), open-circuit voltages (V_{oc}), short-circuit current densities (J_{sc}) and fill factors (FF) of the three polymers based BHJ devices have been listed in **Table 4.6** for the non-optimized solar cell device.

Table 4.6 Photovoltaic Parameters of the BHJ Solar Cells Based on Polymer:PCBM under Illumination (100 mW/cm^2, AM 1.5).

Active layer	J_{sc} (mA/cm^2)	V_{oc} (V)	FF	PCE (%)
PT2-DTP8:PCBM	0.320	0.16	0.28	0.14
PBT-DTP8:PCBM	0.321	0.24	0.33	0.26
PT2-BT-DTP8:PCBM	0.316	0.40	0.40	0.51

Under the same fabrication conditions, BHJ devices based on **PT2-BT-DTP8:PCBM** showed the highest power conversion efficiency (PCE) of 0.51 %. This may be due to its broad absorption in the UV-vis light region. The polymer **PT2-DTP8** based devices are supposed to have the highest V_{oc} from the theoretical calculation because it has the lowest HOMO level among the three polymers. However, devices based on a blend of **PT2-BT-DTP8:PC61BM** afforded the highest V_{oc} from experimental results. This may perhaps be attributable to a better nano-morphology achieved using the blend of **PT2-BT-DTP8:PC61BM** than with the blend of **PT2-DTP8:PC61BM**.

Because the performances of devices based on the prepared polymers were only preliminarily tested, the PCE is a bit lower than those of the reported polymers as well as lower than that of P3HT (~5%). However, fabrication parameters such as annealing temperature, selection of casting solvent, selection of acceptor materials and mixture ratio can be further optimized. Thus, the PCE based on the novel polymers is expected to increase greatly.

Additionally, spectral responses of photovoltaic behaviour, the external quantum efficiency (EQE) of **PT2-DTP8**, **PBT-DTP8** and **PT2-BT-DTP8** were explored subsequently and are shown in **Figure 4.7**. It is obvious the wavelength range response of solar cells is similar to the broad optical absorption spectra. The highest EQE of 13% at wavelength around 570 nm was obtained for the device using active layer of **PT2-DTP8** and PC61BM (1:1, wt%). At the same time, the EQE of 7.0% and 8.4% were obtained for the devices using active layers of **PBT-DTP8** with PC61BM and **PT2-BT-DTP8** with PC61BM (both 1:1, wt%). The EQE curves of the devices using **PBT-DTP8** and **PT2-BT-DTP8** extended to around 1000 nm, which indicated the possibilities of good conversion efficiency in the near infrared region. The EQE data further demonstrated the π-π^* energy transition within these polymers and it is believed that such transition is beneficial for the photovoltaic conversion.

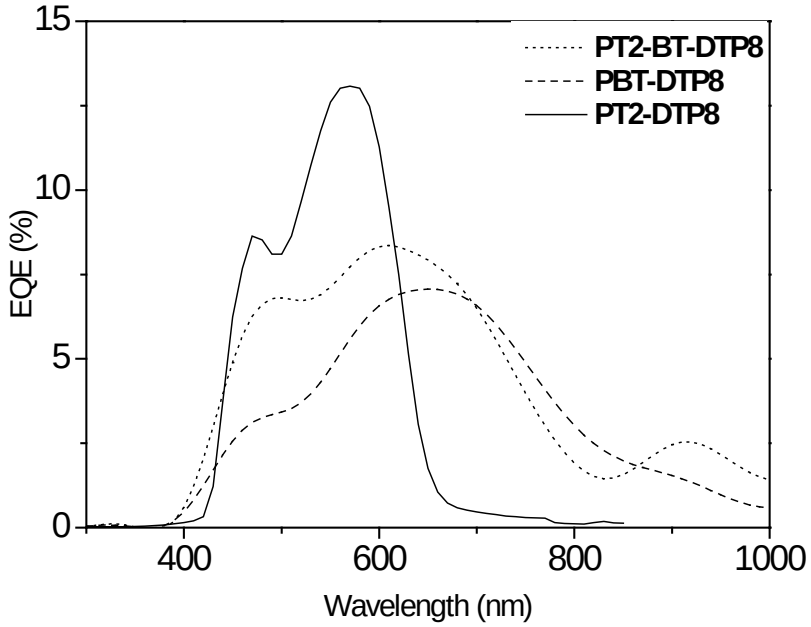

Figure 4.7 External quantum efficiency of active layers based on the three polymers.

4.4 Summary

A series of polymers based on a N-1-octylnonyldithieno[3,2-b:2',3'-d]pyrrole, **PT2-DTP8**, **PBT-DTP8** and **PT2-BT-DTP8**, have been successfully prepared via Stille cross-coupling polymerization. These new polymers show good solubility in common organic solvents and good thermal stability. Their optical characteristics indicate that all the three polymers can harvest light effectively and the optical band gaps of **PBT-DTP8** and **PT2-BT-DTP8** can be as low as 1.4 eV. Cyclic voltammetry measurements reveal the HOMO energy levels of -5.02, -4.97 and -5.0 eV for **PT2-DTP8**, **PBT-DTP8** and **PT2-BT-DTP8**. The light harvesting abilities and HOMO levels of the three polymers make them apt donor materials for use in organic BHJ solar cells. OPV devices based on the blend of three polymers and PC61BM were fabricated and power conversion efficiencies were measured. Preliminary results show that device based on **PT2-BT-DTP8**/PC61BM blend has the highest power conversion efficiency of 0.51% amongst the three polymers while the power conversion efficiencies for **PT2-DTP8**/**PCBM** and **PBT-DTP8**/PC61BM based devices are 0.14 and 0.26% respectively. These results indicate that these N-1-octylnonyldithieno[3,2-b:2',3'-d]pyrrole based polymers are promising candidates as donor materials in organic BHJ solar cells.

Chapter 5

Conjugated Polymers Based on N- substituted dithieno[3,2-b:2',3'-d]pyrroles and 9,9'-Dialkyl-fluorenes

5.1 Introduction

Conjugated polymers can be engineered through molecular design to afford tunable electronic and optical properties[131-132]. The key to this approach would be the ability to control the dimensional π conjugation and connectivity essentially through synthesis and assembly[133]. One important strategy would be the introduction of fused aromatic rings into the conjugated polymer backbone, which would afford a more rigid and planar polymer backbone, thereby enhancing effective π conjugation, preventing chain-folding and lowering the band gap. Furthermore, the rigid fused ring structure can lower the reorganization energy of the molecule, thus facilitating intermolecular hopping and charge carrier mobility[52-53]. Consequently, this strategy has been widely deployed in the synthesis of polymers with high charge carrier mobility[134]. A variety of fused ring-based aromatic conjugated polymers have been developed for potential applications in field effect transistors (OFETs)[135-137]. Among these materials, OFET performance was found to be greatly improved by incorporating thiophene based fused rings into polymers, such as thienothiophene[134], benzodithiophene[138] and cyclopentadithiophene[139].

On the other hand, the nature of the alkyl substituent (side chain of the polymers) also plays an important role in determining the electronic and physical properties of the

materials. For instance, the side chain length directly affects the solubility of the polymer, its ability to form interchain order in deposited films and the interchain stacking order structure in these films[140]. Additionally, electronic energies, surface tension, and thermal properties can also vary depending on the alkyl substituent[141]. In particular, important properties for organic electronic devices such as charge mobility and the degree of phase separation can be tuned by varying the pendant chains. Yang et al. studied the effects of side chain variation on a naphtho[2,1-b:3,4-b0]dithiophene-co-4,7-di(thiophen-2-yl)benzothiadiazole system and observed differences in the V_{oc} and J_{sc} for BHJ solar cells. These were quantitatively correlated with a pre-exponential dark current term, which they claimed accounts for the intermolecular interactions in the polymer/fullerene blend. Biniek et al. studied the effect of side chain variation and site of attachment on a benzo[1,2-b:4,5-b']dithiophene-co-thieno[3,4-b]thiophene polymer. They found an increased solar cell efficiency using ethylhexyl chains over linear dodecyl chains. Szarko et al. very recently reported on the effect of side chain variation on thieno[3,-b]thiophene-co-benzodithiophene polymer systems, which have given record breaking PCEs. They found that varying the degree of alkyl chain branching affected the π-π stacking distance which they suggested allowed a varying amount of fullerene intercalation to occur. In addition, a study on the variation of the side chain on the acceptor portion of a N-alkylthieno[3,4-c]pyrrole-4,6-dione polymer demonstrated that the highest solar cell efficiency was achieved with a linear chain[142]. **Figure 5.1** shows the structures of indacenodithiophene-co-benzothiadiazole based polymers which are reported recently on the properties optimization by different alkyl chains[143].

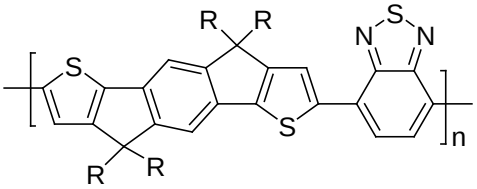

P1 R= MethylButyl
P2 R= EthylHexyl
P3 R= Octyl
P4 R= HexylDecyl

Figure 5.1 The indacenodithiophene-co-benzothiadiazole based polymer structures with alkyl chain optimization.

In solution, polymers **P2** - **P4** display absorption maxima at around 660 nm. The absorption maximum of **P1** is at a slightly shorter wavelength (645 nm) which is attributed to the lower molecular weight of the material. A slight shoulder can be observed at a shorter wavelength in all these polymers and it believes to be attributed to solution aggregation. In thin film, polymers **P1**, **P3**, and **P4** display red-shifted absorbance maxima (~10 ~ 15 nm) and the shoulder at a shorter wavelength (~575 nm) is clearly more pronounced for all polymers due to solid state. However, there is no significant red-shift in the absorbance of **P2**, and only a slight shoulder is observed at shorter wavelengths and it might be due to a lack of thin film crystallinity and subsequent backbone planarization.

Table 5.1 OFET Characteristics of the Copolymers

Polymer	On/Off ratio	Hole mobility ($cm^2V^{-1}s^{-1}$)
P1	10^2	0.003
P2	10^5	0.57
P3	10^4	0.15
P4	10^4	1.2

Additionally, OFET devices were fabricated from **P1**-**P4** by bottom-contact architecture and the results are shown collected in **Table 5.1**. **P2**-**P4** all display extremely high hole mobility (>0.1 cm^2V^{-1} s^{-1}) and the highest is the material with the longest alkyl chains (**P4**). The slightly lower mobility of **P3** which contains linear

alkyl chains can be attributed to the difficulty in obtaining good quality films due to the lower solubility of this sample. **P1** displays significantly poor hole mobility, which is probably, in part, a result of its significantly lower molecular weight. The extremely high hole mobility measured for **P2** is remarkable considering the absence of any observed aggregation effects in the solid-state absorption spectrum and the presence of only short bulky side chains. One possible reason is that molecular weight plays a more vital role in obtaining high hole mobilities than choice of side chain in this polymer.

In chapters 3 & 4, polymers based on *N*-alkyldithieno[3,2-*b*:2′,3′-*d*]pyrroles were shown to have low band gaps. This was attributable to the planar structures of DTP molecules. In this chapter, a series of polymers comprising alternating functionalized fluorene and DTP with side chains of varying carbon chain lengths were synthesized and characterized. The introduction of the fused-ring fluorene and DTP units into polymer backbone would extend π conjugation and afford a rigid polymer structure, which would be amenable for attainment of high charge mobility. Meanwhile, the combination of different side chains in the fluorene and DTP units can also be used in tuning the polymer's properties. In this chapter, the thermal, optical and electrochemical properties of various fluorene-DTP copolymers having different pendant chains are investigated.

5.2 Synthesis and characterization

5.2.1 Monomer synthesis

The syntheses of the monomers **23 (a-c)** and **25 (a-d)** are shown in **Scheme 5.1**. The fluorene derivatives with different alkyl chain length can be easily prepared in high

yields by reacting fluorene and n-bromoalkane under alkaline conditions. The DTP monomer derivatives **25 (a-d)** were obtained by reacting 3,3'-dibromo-2,2'-bithiophene with the corresponding primary amine, using the same synthetic procedure reported for compound **6**. The structures and purity of the newly synthesized monomers are confirmed by characterization with ^{1}H NMR spectroscopy.

Scheme 5.1 Synthetic scheme for the monomers **23 (a-c)** and **26 (a-d)**.

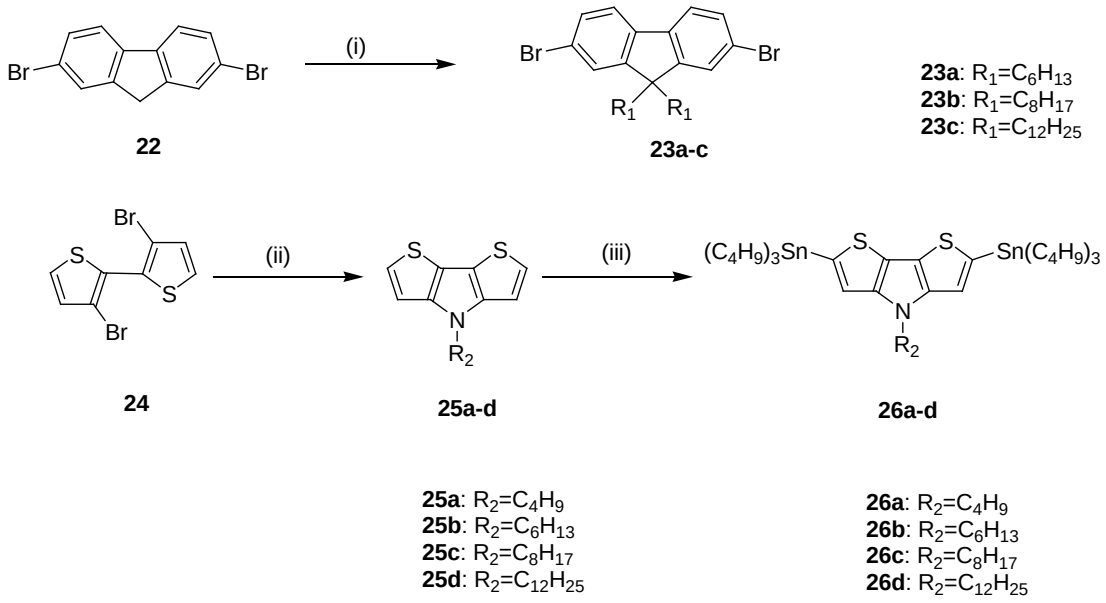

Reagents and conditions: (i) KOH, n-bromoalkane, DMSO; (ii) Pd_2dba_3, BuONa, BINAP, primary amine, toluene; (iii) n-Butyl lithium, dry THF, -78 ^{o}C.

5.2.2 Polymer synthesis

The Stille coupling reaction was applied for the polymerization of fluorene-DTP copolymers. The synthetic approach is shown in **Scheme 5.2**. All polymerization proceeded smoothly and the reaction solution became sticky as the reactions progressed. The crude polymers were precipitated by pouring the reaction mixture in methanol with vigorous stirring and then subjected to Soxhlet extractions sequentially

with methanol, hexane and then chloroform. The fraction from chloroform was then concentrated to a small volume and reprecipitated in methanol again. The target polymers were collected as powdery solids after filtration.

Scheme 5.2 Synthetic scheme for the polymers **PF-DTPs**.

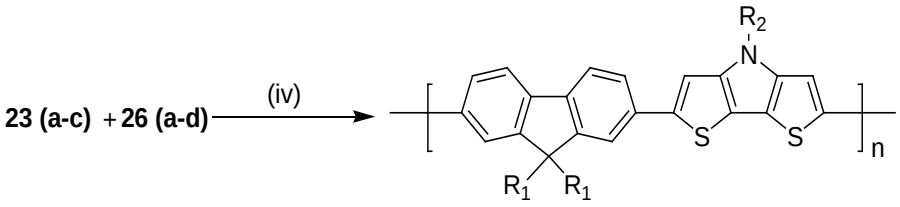

PF6-DTP12: $R_1=C_6H_{13}$, $R_2=C_{12}H_{25}$
PF8-DTP12: $R_1=C_8H_{17}$, $R_2=C_{12}H_{25}$
PF12-DTP12: $R_1=C_{12}H_{25}$, $R_2=C_{12}H_{25}$
PF8-DTP8: $R_1=C_8H_{17}$, $R_2=C_8H_9$
PF8-DTP6: $R_1=C_8H_{17}$, $R_2=C_6H_{13}$
PF8-DTP4: $R_1=C_8H_{17}$, $R_2=C_4H_9$

Reagents and conditions: (iv) $Pd(PPh_3)_2Cl_2$, THF, 90 ^oC, 48 h.

5.2.3 Polymer structures

The structures of **PF-DTP**s are confirmed by ^1H NMR spectroscopy and elemental analyses. The chemical shifts of these fluorene-DTP copolymers are almost identical since the different alkyl chain lengths have little effects on aromatic environment. The characteristic peaks of these polymers are around δ 4.2, which were ascribed to the hydrogens on the adjacent methylene group to DTP. The chemical shifts from δ 0.5 to 1.95 ppm were assigned to the protons alkyl chains attached to fluorene and DTP units. In addition, elemental analysis of the polymer was consistent with the expected formula.

5.3 Results and discussion

5.3.1 Physical properties

The alkylated fluorene and DTP moieties based copolymers are soluble in common organic solvents such as $CHCl_3$, THF and toluene. The molecular weights were determined by the GPC method at room temperature, using THF as eluant. The GPC results are summarized in **Table 5.2**. The **PF-DTP** polymers afforded molecular weights from 3.2 to 6.1 KDa and PDIs from 1.3 to 2.0. The data revealed that **PF12-DTP12** has the lowest weight molecular weight amongst these polymers which may be attributable to the steric hindrance of its polymer backbone. On the other hand, **PF8-DTP8** has the highest molecular weights and the largest PDI value amongst the polymers.

Table 5.2 GPC Results of Polymers **PF-DTP**s.

Polymer	M_n (10^3)	M_w (10^3)	PDI	n[a]
PF6-DTP12	4.7	6.4	1.38	37
PF8-DTP12	4.5	5.8	1.28	31
PF12-DTP12	3.2	5.1	1.6	20
PF8-DTP8	6.1	12.1	2.0	72
PF8-DTP6	3.8	5.3	1.4	32
PF8-DTP4	4.1	5.4	1.3	33

[a] Number of aromatic rings

5.3.2 Thermal properties

The thermal stabilities of **PF-DTP**s were determined by TGA measurements over the temperature range from 25 to 700 ^{o}C. The glass transition behaviours of the polymers were investigated using DSC measurements over a temperature range from 25 to 200 ^{o}C under N_2 atmosphere. The TGA curves of the polymers are shown in **Figure 5.2** and the corresponding TGA results of the polymers are summarized in **Table 5.3**. In nitrogen atmosphere, the onset temperatures of degradation of all the polymers are above to 300 ^{o}C, among which **PF8-DTP8** showed the highest T_d of 387 ^{o}C.

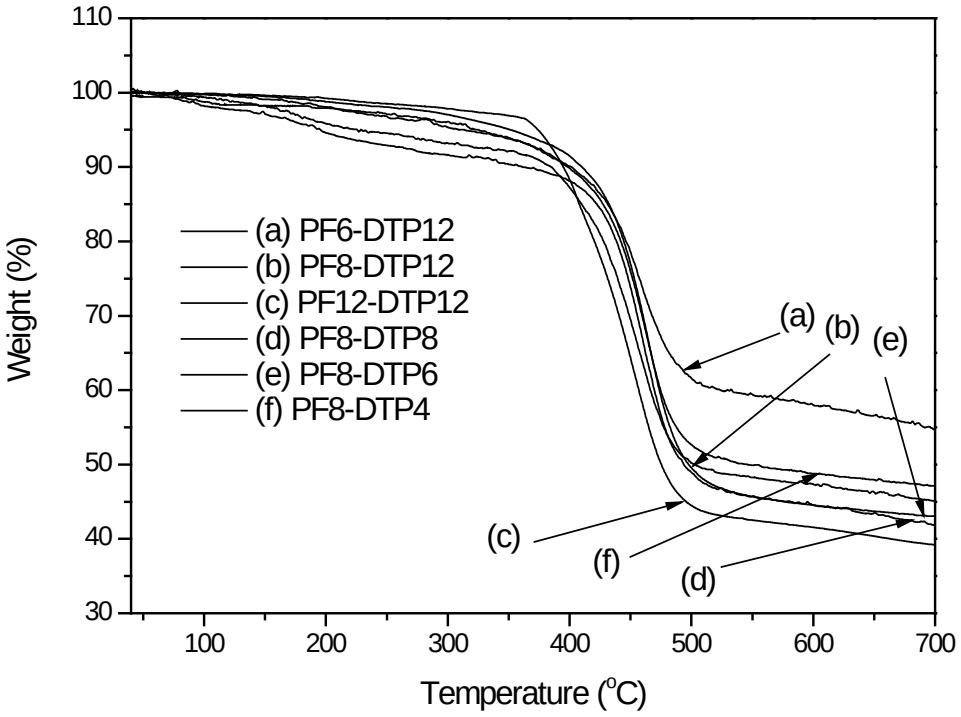

Figure 5.2 TGA curves of polymers **PF-DTP**s under nitrogen atmosphere.

DSC measurements do not reveal obvious glass transition for these polymers. TGA analyses indicate that these novel polymers are thermally stable under inert atmosphere and this would meet the basic requirement for fabrication of organic electronic devices.

Table 5.3 TGA Results of Polymers **PF-DTP**s.

Polymer	T_d [a] (^oC)
PF6-DTP12	360
PF8-DTP12	355
PF12-DTP12	356
PF8-DTP8	387
PF8-DTP6	340
PF8-DTP4	322

[a] estimated from the differentiation of the TGA curves.

5.3.3 Optical properties

The optical properties of the polymers were investigated by UV-visible spectroscopy at room temperature in dilute solution and in solid states, which are depicted in **Figures 5.3** and **5.4** respectively and the results are summarized in **Table 5.4**. When the alkyl chains length of the DTP moieties are fixed at 12 carbons and the length of alkyl chain of fluorene moieties are increased from 6 to 12 methyl units, the UV-visible absorption maxima of **PL6-DTP12, PL8-DTP 12** and **PL12-DTP12** are respectively 468, 465 and 462 nm in dilute chloroform solutions. When the alkyl chains on the fluorene moieties are shortened, slight red shifts of the absorption

maxima can be observed. This may be attributed to reduced steric hindrance with shorter alkyl substituent which would accord a more planar polymer backbone. In contrast, when the alkyl chain lengths of the fluorene moieties are fixed at 8 carbons and the alkyl chains of DTP moieties are decreased from 8 to 4 carbons, the absorption maxima for **PL8-DTP8, PL8-DTP6** and **PL8-DTP4** diminishes from 479, 470 to 466 nm, respectively. This may be due to the lower molecular weights of **PL8-DTP6** and **PL8-DTP4** than that of **PL8-DTP8** because Ogawa et al. have reported that the possible conjugation length of N-substituted PDTPs is higher than the number of repeating units present and the λ_{max} would therefore depend on its molecular weight[68]. Amongst the six polymers, the UV-vis absorption maximum of **PL8-DTP8** is at the longest wavelength, which would indicate that the best co-planarity (or the highest conjugation) is attained in **PL8-DTP8** as compared to the other polymers.

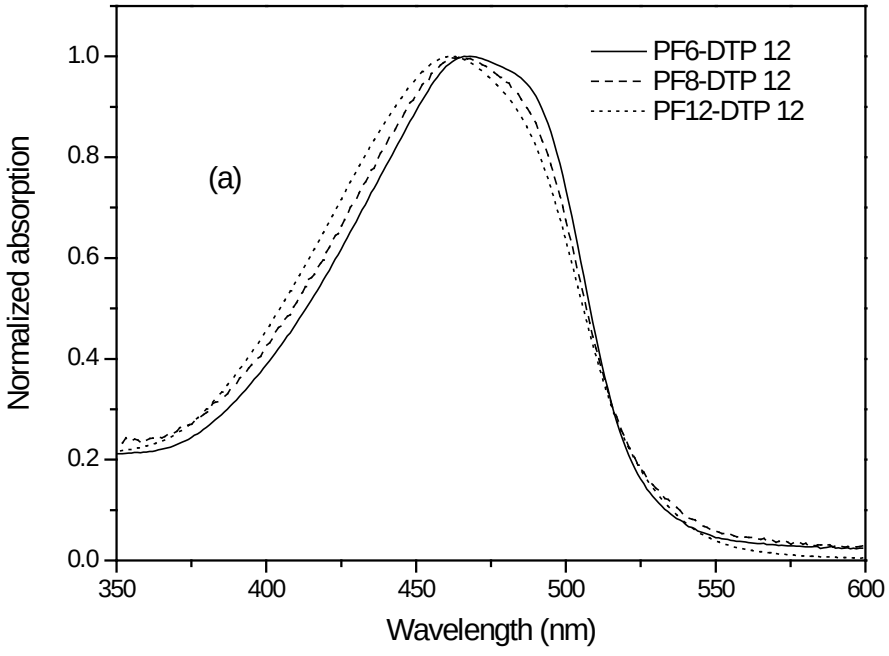

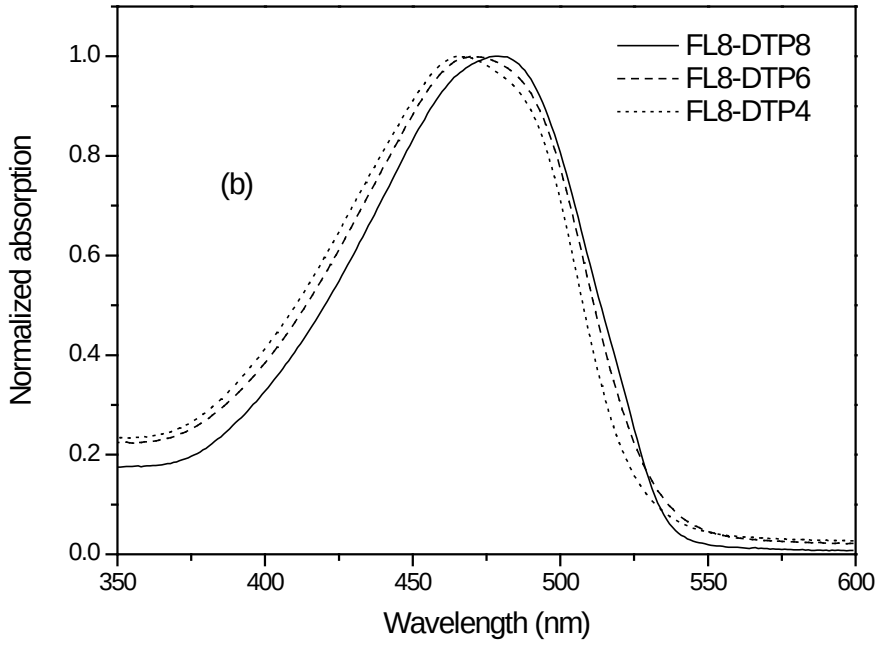

Figure 5.3 UV-vis spectra of **(a) PF6-DTP12** (solid line), **PF8-DTP12** (dash line) and **PF12-DTP12** (dot line) in dilute chloroform solution; **(b) PF8-DTP8** (solid line), **PF8-DTP6** (dash line) and **PF12-DTP4** (dot line) in dilute chloroform solution.

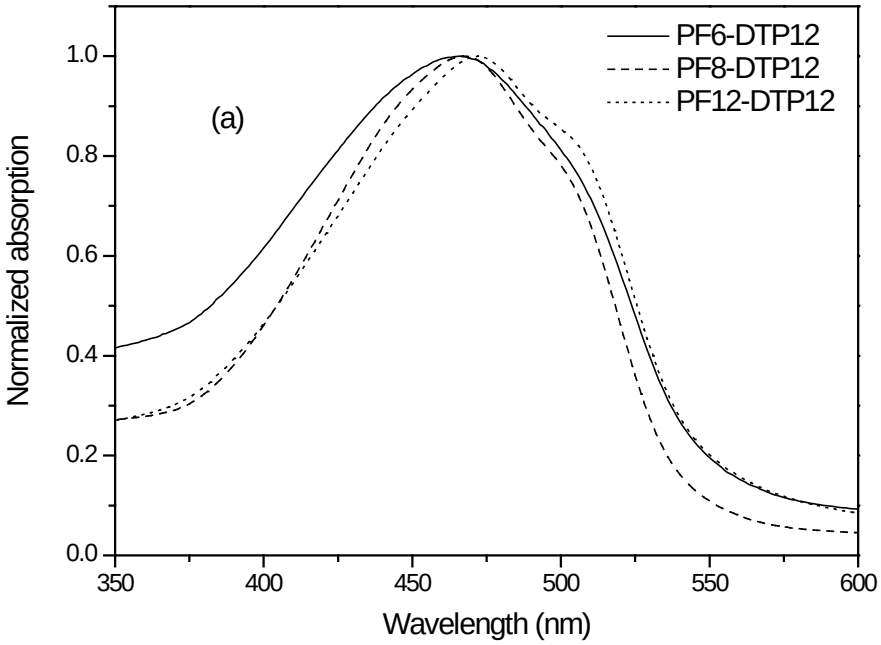

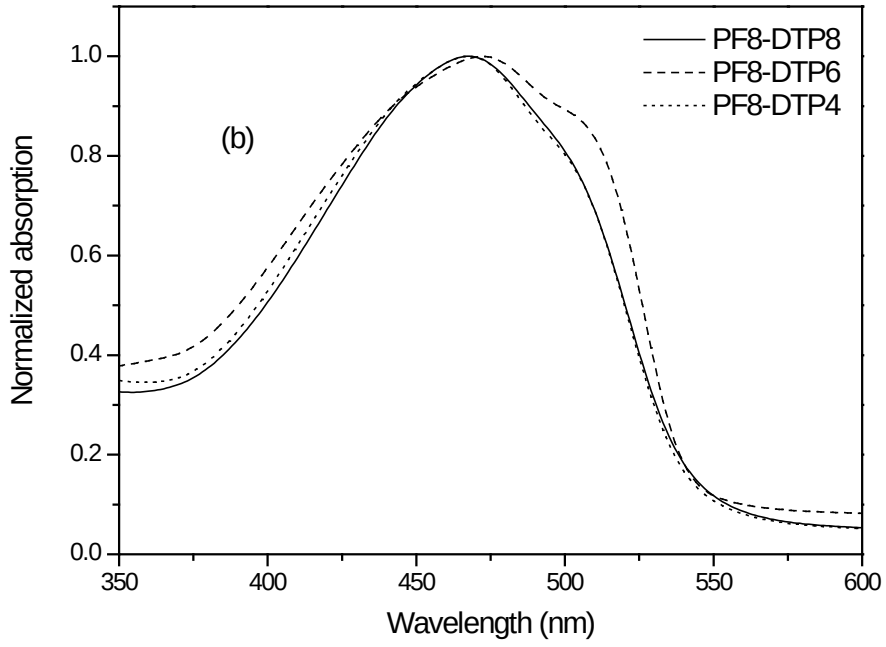

Figure 5.4 UV-vis spectra of **(a) PF6-DTP12** (solid line), **PF8-DTP12** (dash line) and **PF12-DTP12** (dot line) in sold states**; (b) PF8-DTP8** (solid line), **PF8-DTP6** (dash line) and **PF12-DTP4** (dot line) in solid states.

In addition, the optical absorption of the polymers in film phases was also investigated (**Figure 5.4**). All the polymers depicted broader absorption in solid states than in solution. In thin films, **PF-DTP**s also showed shoulder-like absorptions, which indicates vibronic features for these polymers. The absorption maxima of all the polymers are almost identical in dilute solution and in films, indicating weak inter-chain interactions between the polymer backbones in solid state, which may be ascribable to the rigid molecular structures of the fluorene and DTP backbone units. The optical bandgaps calculated from UV-vis absorption in film showed that these polymers have bandgaps of between 2.21 and 2.27 eV.

Table 5.4 Optical Properties of the Polymers in Solution and Film States.

Polymer	UV (solution) λ (nm)	UV (film) λ (nm)	Bandgap (opt.) ΔE (eV)
PF6-DTP12	468	472	2.21
PF8-DTP12	465	467	2.25
PF12-DTP12	462	466	2.21
PF8-DTP8	479	472	2.25
PF8-DTP6	470	468	2.27
PF8-DTP4	466	466	2.25

5.3.4 Electrochemical properties

The electrochemical properties of copolymers **PL-DTP**s were investigated by cyclic voltammetry (CV). The measurements were performed in anhydrous acetonitrile solution of 0.1 M Bu_4NBF_4 under nitrogen. A glassy carbon disk coated with the thin polymer film was used as work electrode, a silver wire as pseudo-reference electrode and a platinum wire as counter electrode. The redox potentials were calibrated against the ferrocene/ferrocenium couple as an internal standard and the results are summarized in **Table 5.5**. The CV of the representative polymer **PFL8-DTP8** under three repeated scans is depicted in **Figure 5.5**.

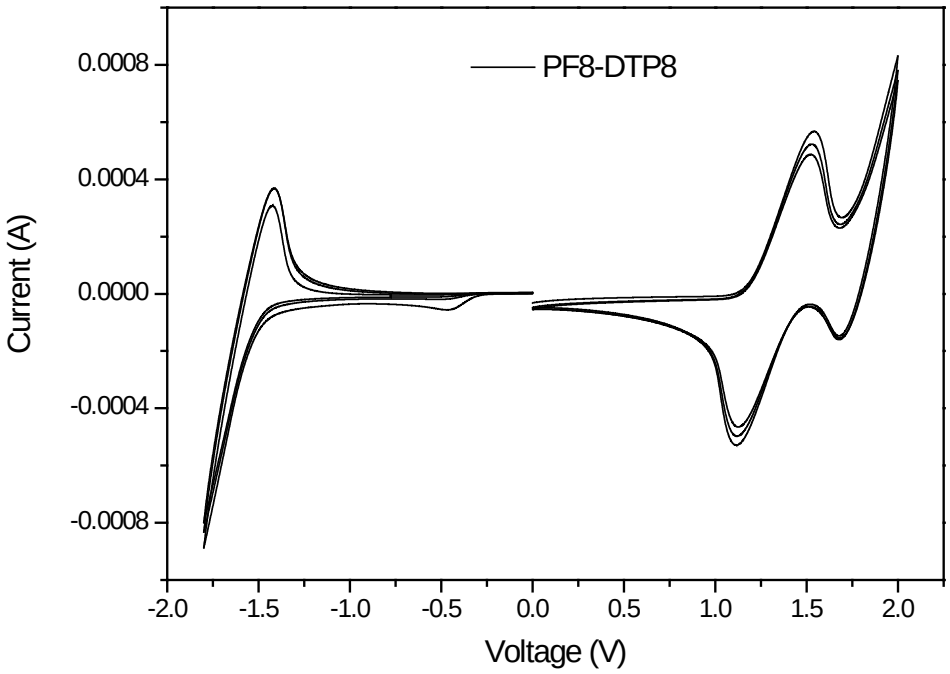

Figure 5.5 Cyclic voltammogram of polymer **PF8-DTP8** film coated on a glassy carbon electrode in Bu_4NBF_4/acetonitrile at scan rate of 100 $mV \cdot s^{-1}$.

All the polymers of **PFL-DTP**s depicted similar electrochemical behaviours. Arising from the electron-donating character of fluorene and DTP moieties, redox processes are observed clearly for these polymers. An onset oxidation potential of ca. 1.1 V appear in the cyclic voltammogram due to the oxidation of the polymers. On the other hand, an onset reduction potential of at ca. -1.4 V are obtained for these polymers. Accordingly, a HOMO level of ca. -5.5 eV and a LUMO level of ca. -3.0 eV can be calculated. The electrochemical bandgaps for **PFL-DTP**s are calculated to be between 2.41 and 2.53 eV. In particular, this series of polymers showed good electrochemical stability and reproducible results can be achieved (**Figure 5.5**).

Table 5.5 Onset and Peak Potentials of p- and n-Doping Processes of the Polymers.

Polymer	p-Doping			n-Doping			Bandgap
	E_{on} (V)	E_{pa} (V)	HOMO (eV)	E_{on} (V)	E_{pc} (V)	LUMO (eV)	E_g (eV)[a]
PF6-DTP12	1.11	1.55	-5.51	-1.35	-1.62	-3.05	2.46
PF8-DTP12	1.05	1.51	-5.45	-1.38	-1.65	-3.02	2.43
PF12-DTP12	1.06	1.57	-5.46	-1.35	-1.69	-3.05	2.41
PF8-DTP8	1.1	1.53	-5.5	-1.43	-1.79	-2.97	2.53
PF8-DTP6	1.07	1.57	-5.47	-1.39	-1.75	-3.01	2.46
PF8-DTP4	1.08	1.58	-5.48	-1.44	-1.78	-2.96	2.52

[a] Electrochemical band gap

5.4 Summary

A series of fluorene-dithieno[3,2-b:2',3'-d]pyrrole copolymers attached with alkyl pendants of different carbon chain length have been prepared using the Stille cross-coupling approach. All new polymers derived are soluble in common organic solvents and found to be thermally stable under inert atmosphere. Different alkyl chains of fluorene and DTP units affect the solubility of these polymers, thereby affording varying degrees of polymerization. Moreover, the optical properties can be slightly tuned by the alkyl substituent as seen by shifts in the UV-vis absorption maxima. On account of the rigidity of the fluorene and DTP units in the polymer backbone, only minor shifts of the UV-vis absorption between states in solution and in film were

observed for the **PFL-DTP** polymers. It is generally believed that structural planarity and rigidity would facilitate charge transport, making these polymers promising candidates for application in organic electronics such as OFETs. The polymers' optical bandgaps as determined from the onset of absorptions in the film state range between 2.21 and 2.27 eV. Cyclic voltammetry measurements revealed that all polymers have a HOMO energy level below -5.45 eV and the measurements are reproducible. This would imply that the polymers are fairly stable electrochemically. In addition, the electrochemical band gaps ranging from 2.41 to 2.53 eV were calculated accordingly from the HOMO and LUMO level.

Chapter 6

An Oligomer Based On N,N'-Bisfluorenyl Substituted Perylene Bisimide

6.1 Introduction

In the previous chapters, p-type conjugated polymers which can be used as donor materials in OPVs have been investigated. Currently, research interest on organic electronics is continuously focused on exploring both novel p- and n-type organic molecules and polymers on account of their advantages as alternatives to inorganic semiconductors. The BHJ architecture is by far the most used architecture for organic photovoltaics due to its efficient charge separation. Since the active layer in a BHJ solar cell invariably comprises a blend of the p-type donor and n-type acceptor materials, research into novel p-/n- type molecules / polymers has been a subject of importance. Dye-linked oligomers/polymers have also attracted interests because of their unique optical and physical properties[144-147]. The appropriate connection of dye molecules and individual functional oligomers/polymers enables new *n*-type materials for organic photovoltaic cell applications. On the other hand, in comparison to numerous studies done on the p-type organic materials used in BHJ solar cells, investigation of new n-type organic semiconductors[148] is relatively rare. [6,6]-Phenyl C_{61} butyric acid methyl ester (PC61BM) is the most commonly used n-type material in BHJ photovoltaic devices. However, the PC61BM moiety has a relatively weak molar absorption coefficient in the visible region and the morphology of donor/PCBM

blends is difficult to be controlled. Consequently, the exploration of novel *n*-type materials in organic BHJ solar cells remains attractive and challenging.

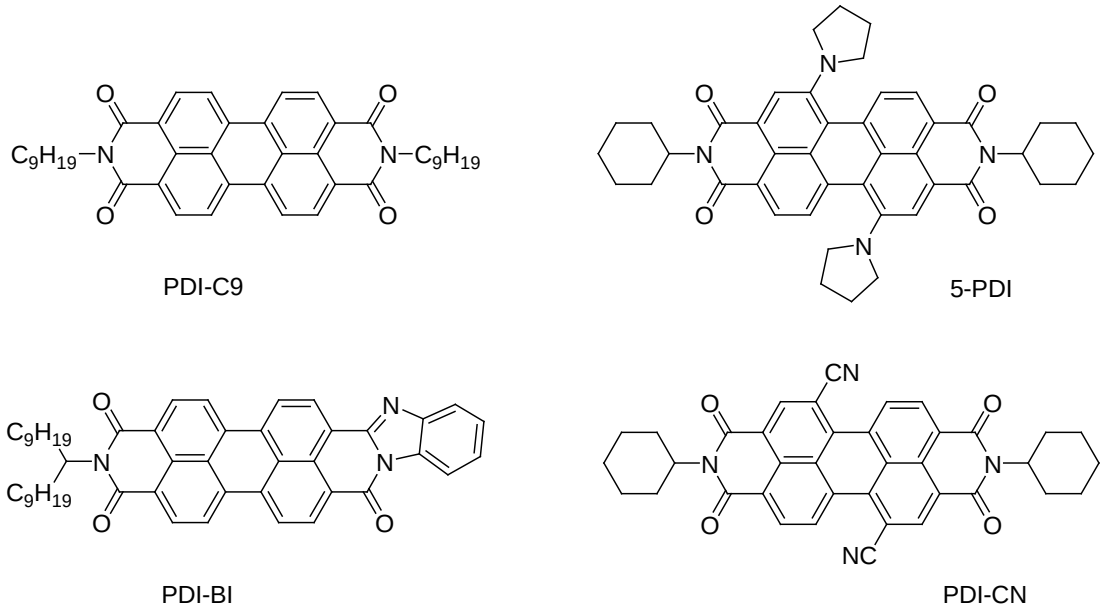

Figure 6.1 Examples of perylene bisimdes and perylene bisimides derivatives used as acceptor materials in BHJ solar cells.

Amongst *n*-type organic materials, perylene bisimide derivatives which are widely used dyes in industry, are considered to be of importance[42,149-150]. Perylene bisimide derivatives have large molar absorption coefficients, excellent electron accepting properties and a conducting direction along π-π stacking axis[149,151]. In addition, soluble alkyl substituted perylene bisimides can readily be synthesized by a coupling reaction of aliphatic primary amines with perylene tetracarboxylic acid bisanhydride[152]. Accordingly, perylene bisimide derivatives would be potential n-type candidates for application in photovoltaic devices. Some examples of perylene bisimides and perylene bisimides derivatives are shown in **Figure 6.1** and BHJ solar cells based on perylene bisimide, PDI-C9, have been reported and power conversion efficiency of 0.18% under AM 1.5 (100mW/cm^2) was achieved using P3HT and PDI-C9 blend as active layer[151]. Additionally, power conversion efficiencies of 0.043%,

0.044% and 0.061% have been achieved based on the devices using P3HT and 5-PDI, PDI-BI or PDI-CN as active layers. Recently, a power conversion efficiency of 1.32% has been achieved by using P3HT and annulated thiophene perylene bisimide analogues[153]. However, applications of perylene bisimides with chromophoric substituents to the BHJ photovoltaic devices are limited. In chapter 3 and 4, a series of polymers as p-type materials for organic solar cells have been synthesized and their photovoltaic characteristics were investigated. In this chapter, the synthesis of a novel donor-acceptor-donor compound incorporating perylene bisimide and bisfluorenyl moieties is presented. The studies of the molecule's properties indicated that it can be adopted as n-type material in organic photovoltaics.

6.2 Synthesis and characterization

The synthetic route to the alkyl fluorenyl substituted perylene bisimide (**BFPBF**) is depicted in **Scheme 6.1**. The synthesis of the bifluorenyl amine started from fluorene derivatives, 2-bromo-fluorene and 2-nitro-fluorene. The active postions (9 and 9') of both fluorene derivatives were modified by octyl chains to eliminate the active positions of the fluorene derivatives as well as increase the solubility of the compounds. The yields of compounds **29** and **32** were 72% and 75% respectively. The preparation of the compound **33** was conducted by reacting **29** and **32** via Suzuki coupling and a yield of 65% was achieved. Reduction of **33** afforded amino-tetraoctyl bisfluorenyl compound **34** with a high yield of 90%. Compound **34** was reacted with the commercially available **PTCDA** to afford **BFPBF**. Catalytic amounts of $Zn(AcO)_2$ was added to accelerate the reaction[87]. After purification by

chromatography, the final product **BFPBF** was obtained as a red solid with a yield of 78%.

Scheme 6.1 The synthetic approach of **BFPBF**.

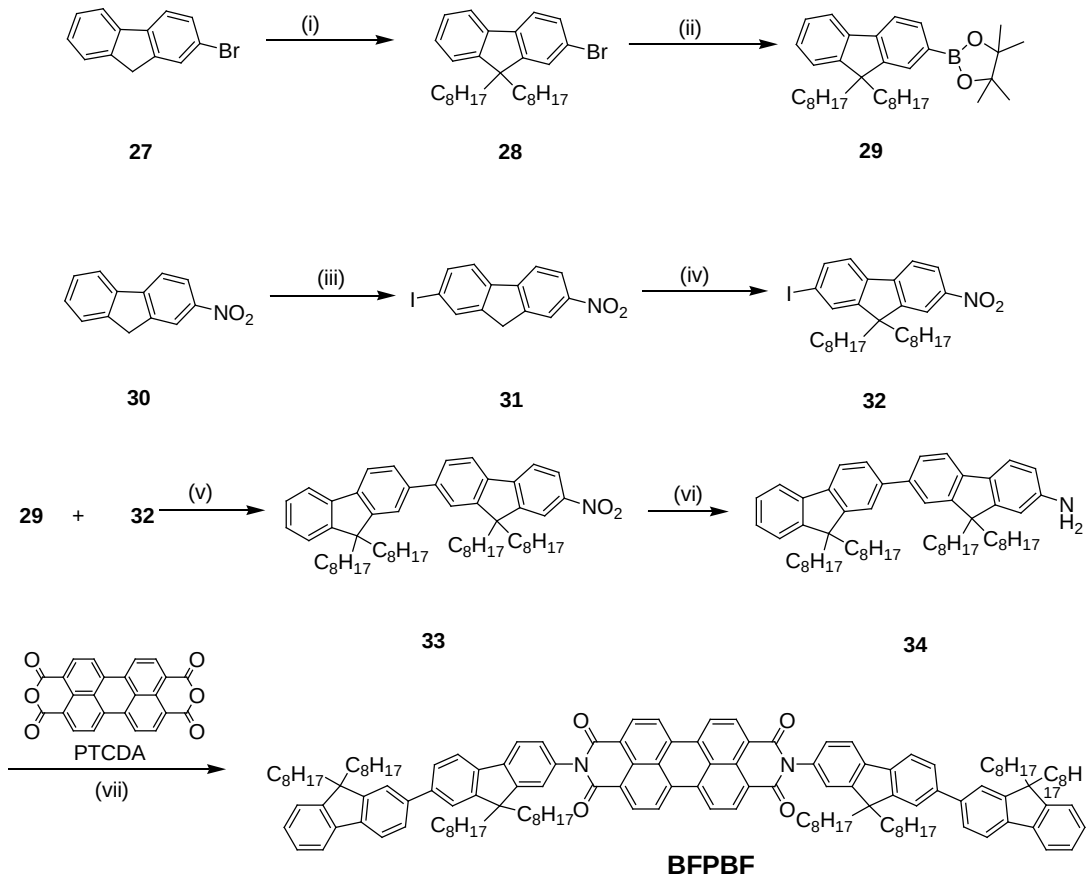

Reagents and conditions: (i) NaOH, n-bromooctane, DMSO; (ii) n-Butyllithium, -78 ^{o}C, THF; (iii) I_2, AcOH, H_2SO_4; (iv) NaOH, n-bromooctane, DMSO; (v) $Pd(PPh_3)_4$, 2 M Na_2CO_3, toluene; (vi) $SnCl_2$, EA/EtOH; (vii) PTCDA, quinoline.

BFPBF is characterized by ^{1}H NMR, MALDI-TOF mass spectrometry and elemental analysis. The NMR spectrum and mass spectrum of **BFPBF** are shown in **Figure 6.2**. From the ^{1}H NMR spectrum, the chemical shifts of hydrogens on perylenyl and bisfluorenyl segments are clearly identified. The doublet at δ=8.83 is attributed to the 4 hydrogens at position 1, 6, 7 and 12 of the perylene unit and the doublet at δ=8.77 is

attributed to the 4 hydrogens at position 2, 5, 8 and 11 of the perylene unit. The signals ranging from δ 7.85 to δ 7.36 belong to the hydrogens at fluorenyl rings. The chemical shifts at ca. δ 2.0 belong to the hydrogens of CH_2 which connect with fluorene cores. The chemical shifts from 1.3 to 0.5 are attributed to the rest hydrogens on the saturated alkyl chains. The molecule was examined by MALDI-TOF mass spectrometry as well and the measured molecular weight of 1944.4 is accorded well with the calculated value of 1944.8. Furthermore, elemental analysis was conducted and the result confirmed that a pure product was obtained desirably. **BFPBF** is soluble in common organic solvents such as dichloromethane, chloroform and toluene, so that it can be easily processed from solution by wet techniques such as spin-coating.

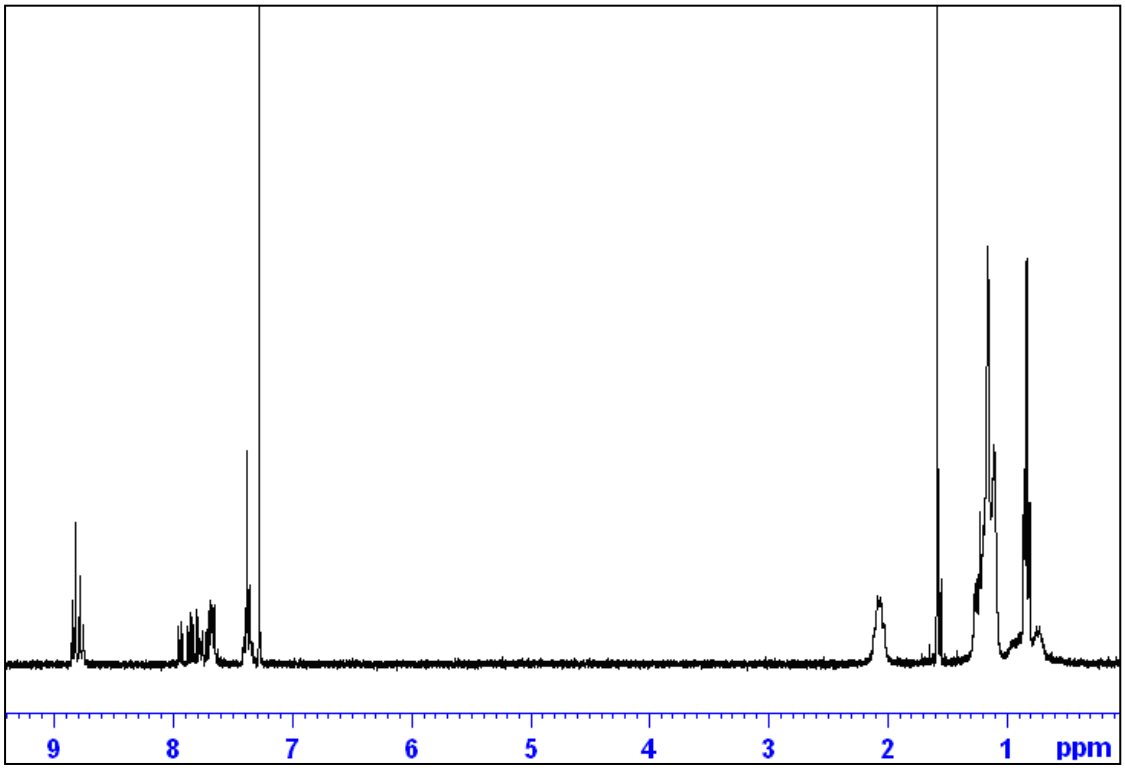

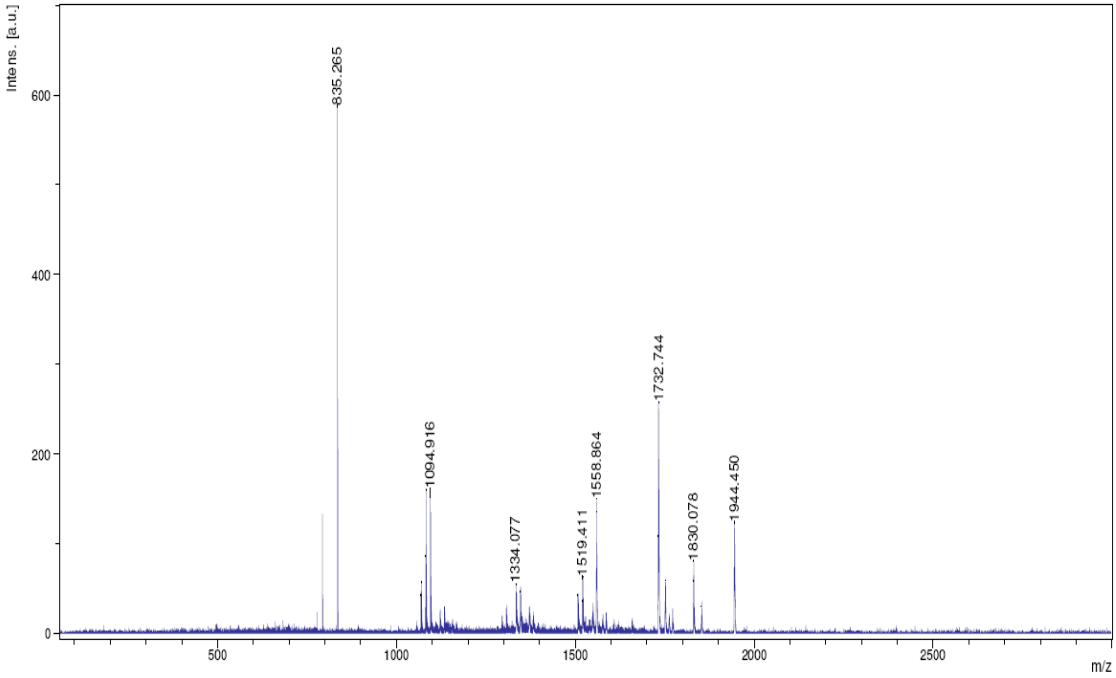

Figure 6.2 ^{1}H NMR spectrum and MALDI-TOF mass spectrum of **BFPBF**.

6.3 Results and discussion

6.3.1 Thermal properties

Figures 6.2 and **6.3** depicted the TGA and DSC curves of **BFPBF**. TGA analysis was performed under nitrogen or air atmosphere. The results reveal that **BFPBF** has a thermal stability up to 438 ^{o}C in nitrogen and 385 ^{o}C in air. In nitrogen atmosphere, a one-step degradation was observed, which was attributed to the cleavage of side chain. On the other hand, **BFPBF** in air had a lower onset temperature of degradation and was a two-step decomposition. The first weight loss step corresponded to the cleavage of the side chain. The second weight loss step was attributed to the degradation of the main chain (bond of C-N) and by-product was probably the perylene bisimide type residues. A glass transition temperature (T_g) of **BFPBF** is observed at 160 ^{o}C by DSC measurement.

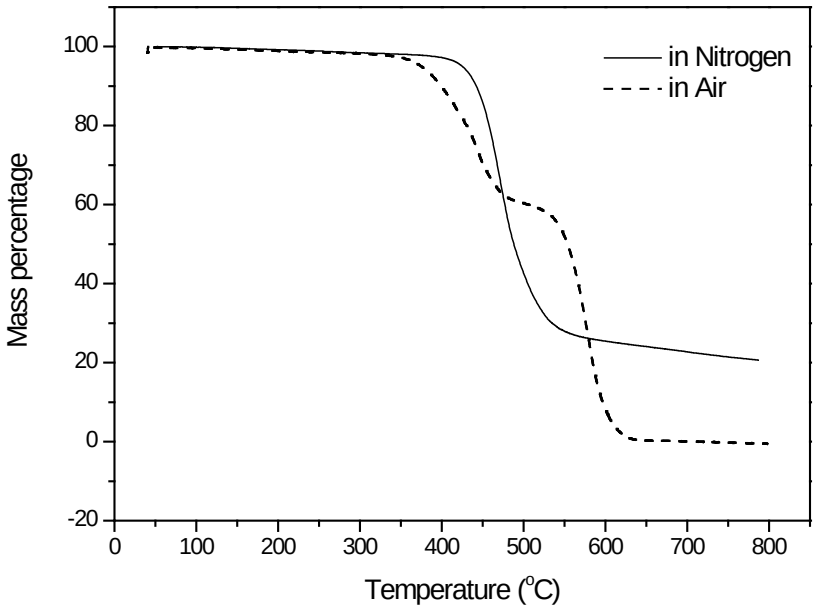

Figure 6.3 TGA thermograms of **BFPBF** at a heating temperature rate of 10 °C/min under nitrogen or air atmosphere.

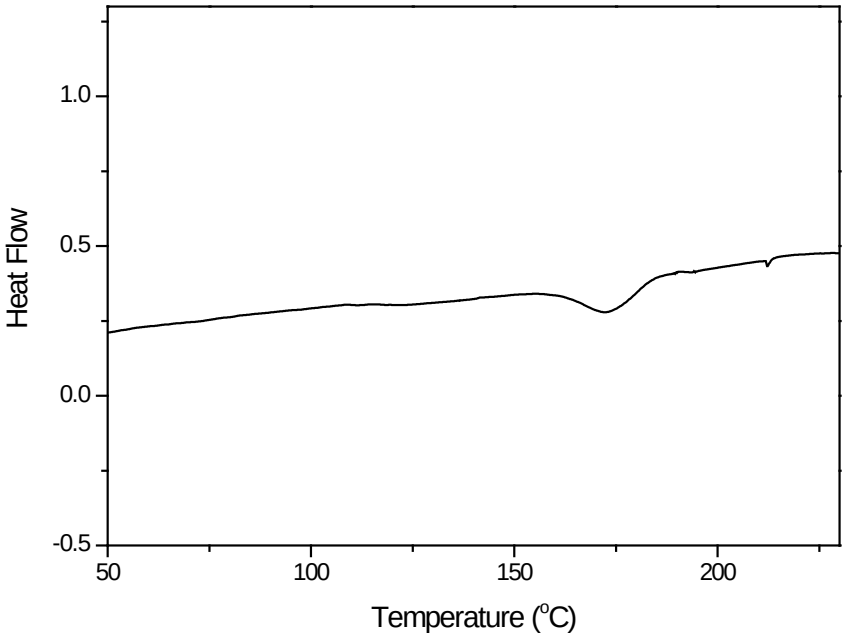

Figure 6.4 DSC curve of **BFPBF** at a heating temperature rate of 10 °C/min under nitrogen atmosphere.

6.3.2 Optical properties

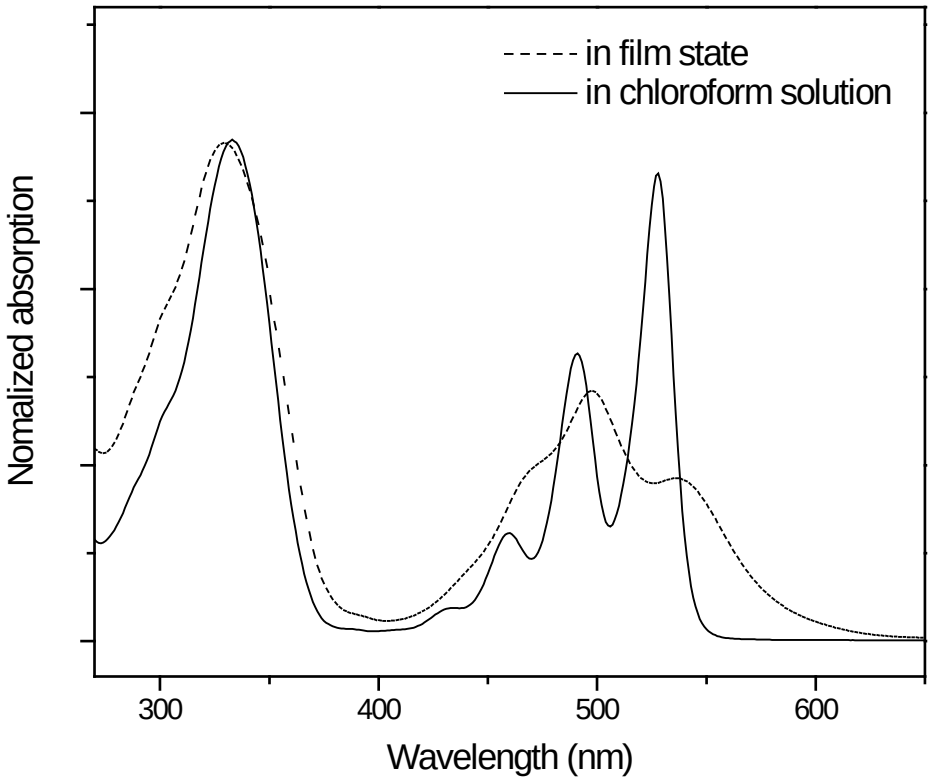

Figure 6.5 UV-vis spectra of **BFPBF** in solution and in film state.

The optical properties of **BFPBF** were investigated by UV-vis absorption (**Figure 6.5**) and photoluminescence spectroscopy (**Figure 6.6**). In dilute chloroform solution, **BFPBF** exhibits two strong UV-visible absorption bands from 280 to 380 nm and 420 to 550 nm. The absorption band with maxima at λ = 333 nm originates from the bisfluorenyl chromophore[154], whilst that at λ = 550 nm is assigned to S0-S1 transition[155] which has three well-resolved vibronic peaks attributed to breathing vibrations of the perylene unit. In the long wavelength region, the absorption band of the perylenyl moiety in **BFPBF** and the absorption of the alkyl perylene bisimide are almost identical, which demonstrates that the three segments (Bisfluorene-Perylene-

Bisfluorene) are only weakly electronically coupled[156]. The absorption of the bisfluorenyl chromophores of **BFPBF** in the visible region indicates that **BFPBF** has improved photon harvesting in comparison with alkyl substituted perylene bisimide derivatives. In solid state, the absorption of **BFPBF** is only red shifted by a few nanometers in comparison with the absorption in solution and it indicates that there is a weak inter-chain interaction of **BFPBF** in the solid state. The onset of absorption for **BFPBF** film is located at 620 nm, which corresponds to an optical band gap (E_g) of 2.0 eV.

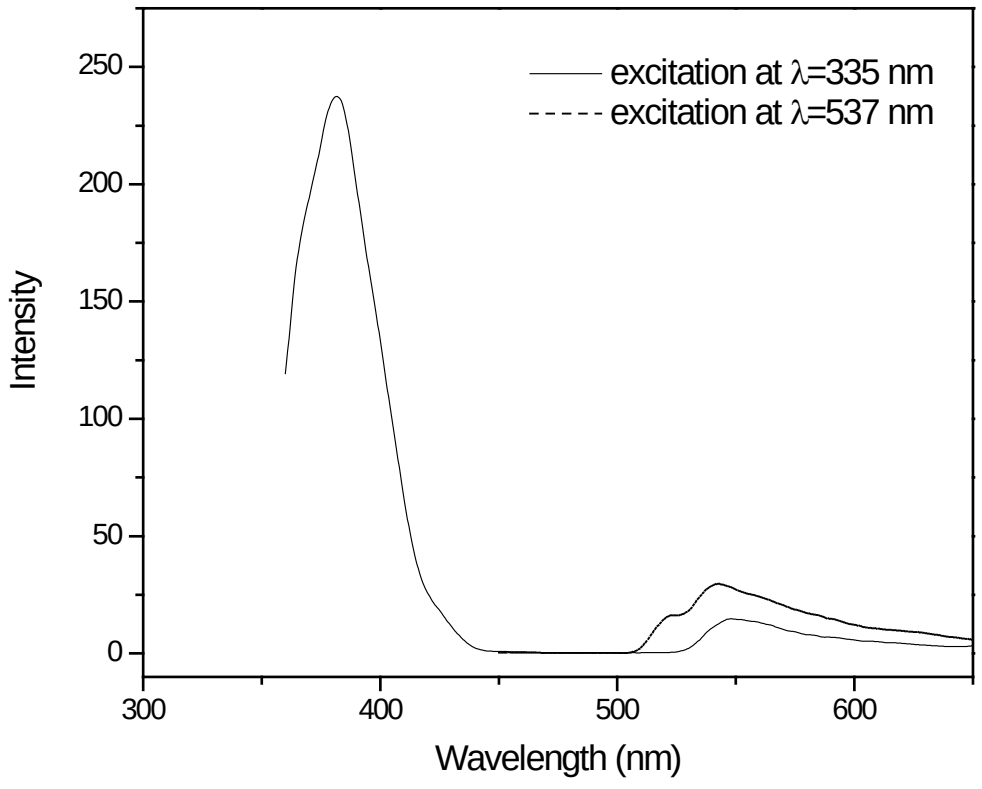

Figure 6.6 PL spectra of **BFPBF** in chloroform solution.

Photoluminescence (PL) measurements of **BFPBF** were conducted in chloroform solution at room temperature. The photoluminescence spectra are shown in **Figure 6.6**. As can be seen, under excitation at 530 nm, only a weak fluorescence band around 550 nm corresponding to the perylene bisimide core is observed. Upon excitation at 335nm, **BFPBF** exhibits an additional emission peak at around 380 nm originating from the bisfluorenyl units. Studies have shown that alky substituted perylene bisimides are themselves characterized by a high fluorescence quantum yield. Decrease of the fluorescence intensity in **BFPBF** (quantum yields < 1% when **BFPBF** was excited at wavelength of 335 or 530 nm) suggests an intramolecular photoinduced electron transfer from the fluorenyl group to the perylene system.

6.3.3 Electrochemical properties

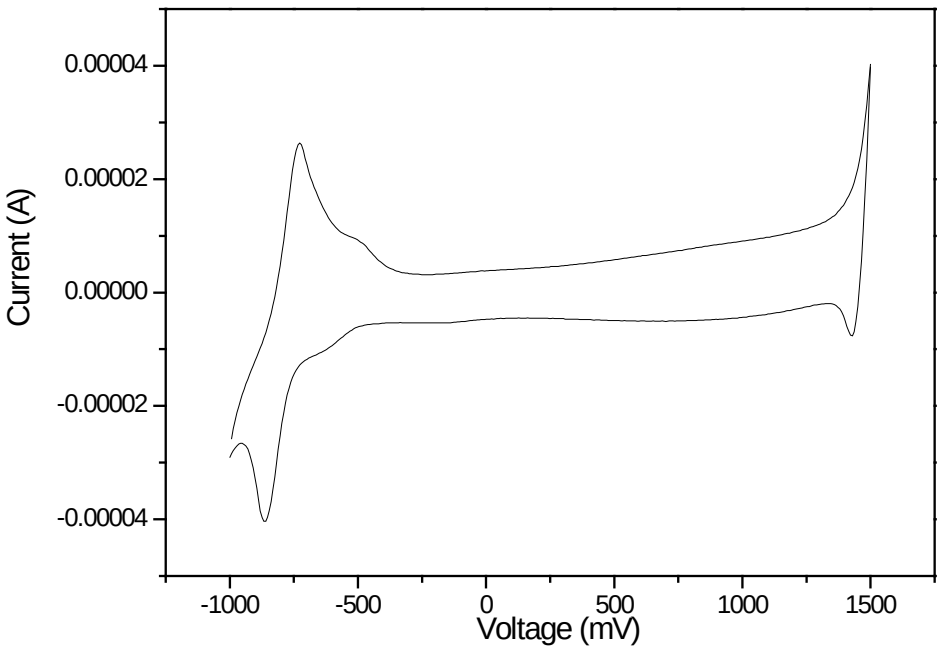

Figure 6.7 Cyclic voltammogram of **BFPBF** film coated on a glassy carbon electrode in Bu_4NBF_4/acetonitrile at scan rate of 100 $mV \cdot s^{-1}$.

The electrochemical behavior of the **BFPBF** was investigated by cyclic voltammetry (CV) measurements (**Figure 6.7)**. A glassy carbon disk coated with **BFPBF** thin film was used as working electrode, a silver wire as reference electrode and a platinum wire as counter electrode. The cyclic voltammogram revealed an oxidation (p-doping) and reduction (n-doping) process clearly. An oxidation potential ($E_{ox\ onset}$ = 1.3 V versus SCE) and a reduction potential ($E_{re\ onset}$ = -0.4 V versus SCE) were observed. Thus, an electrochemical band gap ($E_{electrochem}$) of 1.7 eV was calculated for **BFPBF**. The highest occupied molecular orbital (HOMO) energy level of -5.7 eV and the lowest unoccupied molecular orbital (LUMO) energy level of -4.0 eV were calculated as well. The LUMO level of **BFPBF** is comparable with that of PC61BM (LUMO = -4.0 eV). The results indicate that **BFPBF** can be utilized as an *n*-type material in a BHJ photovoltaic device.

6.3.4 Photovoltaic characteristics

The organic solar cells were fabricated on the indium tin oxide (ITO) coated glass substrates. The ITO glass was thoroughly cleaned by an ultrasonic treatment in acetone, ethanol and deionized water sequentially. A thin layer of poly(3,4-ethylenedioxythiophene):poly(styrene-sulfonate) (PEDOT: PSS) was spin-coated onto the substrate, followed by heating for 15 min at 150 ^{o}C. Subsequently, the active layer was spin-coated onto the substrates from dichlorobenzene solution of **P3HT**:**BFPBF** (1:1, w/w) inside a nitrogen glove box. The active area of the device is 0.9 cm^2. The aluminum (Al) top electrodes were thermally devaporated on the active layer under vacuum at 1×10^{-4} Pa. Post device annealing was carried out for 15 min at 170 ^{o}C inside a nitrogen glove box. The photovoltaic characteristics of the organic solar cells were determined by a Source- Meter (Keithley, model 2400) under a Xe lamp

illumination with power density of 100 mW/cm^2 (AM 1.5). All the measurements were performed under nitrogen atmosphere at room temperature.

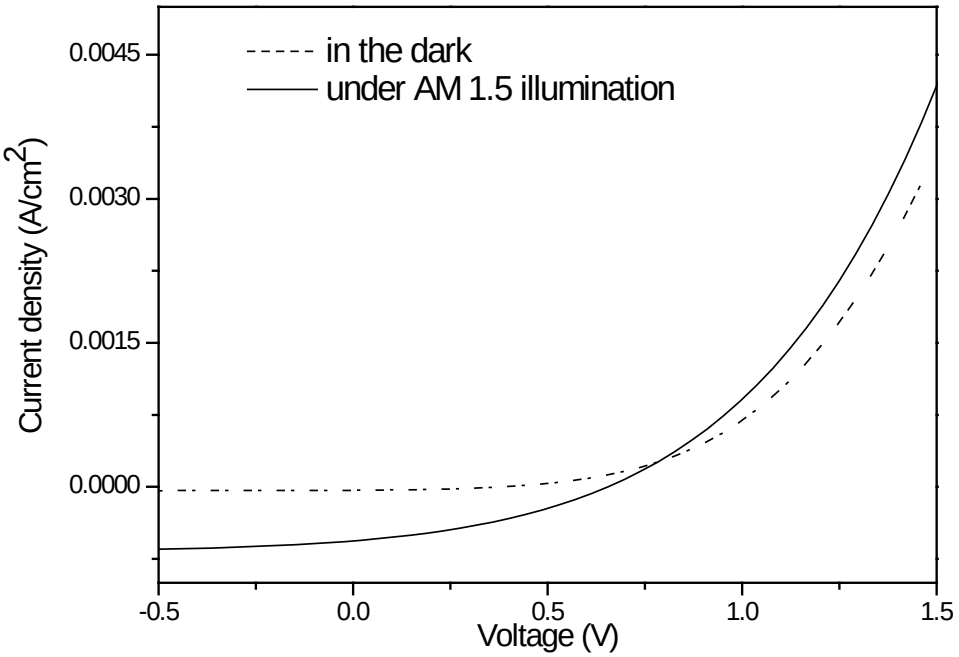

Figure 6.8 Current density-voltage characteristics of photovoltaic device (ITO/PEDOT:PSS/ P3HT:**BFPBF**/Al) in the dark and under simulated AM 1.5 illumination.

Organic BHJ solar cell was fabricated using a blend of **P3HT** and **BFPBF** (w:w, 1:1) as active layer. The I-V characteristics of the photovoltaic device was measured both in the dark and under simulated AM 1.5 (**Figure 6.8**). The power conversion efficiency (PCE) of 0.135% under AM 1.5 with an open-circuit voltage (V_{oc}) of 0.66 V, a short-circuit current density (J_{sc}) of 0.6 mA/cm^2 and a fill factor (FF) of 0.33 has been achieved for the non-optimized solar cell device.

PDI-C9 is bisnonyl substituted perylene bisimide and the BHJ device based on PDI-C9/P3HT as active layer was reported[157]. Under the same fabrication conditions, the device showed power conversion efficiency (PCE) of 0.036 %, V_{oc} of 0.26 V, J_{sc} of

0.45 mA/cm^2, and FF of 0.31. Both the values of J_{sc} and V_{oc} of **BFPBF** based BHJ device are higher than the reference perylene bisimide, contributing to a higher PCE of **BFPBF** based device than that of PDI-C9 based device. Although one reason for this improved power conversion efficiency of **BFPBF** based device is probably due to the extended absorption of **BFPBF** in visible region than that of PDI-C9, other factors such as annealing temperature, the morphology of active layer should be taken into account as well. Since the power conversion efficiency of PDI-C9 based devices was increased from 0.036 % to 0.182% by device optimization, higher PCE of **BFPBF** based device can be expected after optimization of device fabrication.

6.4 Summary

A novel dye-crossing molecule, bisfluorenyl chromophores substituted perylene bisimide (**BFPBF)**, has been successfully prepared via a condensation reaction. **BFPBF** is soluble in common organic solvents and thermally stable under ambient atmosphere. The optical properties investigation indicates that **BFPBF** has an improved light harvesting ability than alkyl substituted perylene bisimides due to the absorption of bisfluorenyl chromophores. The optical band gap of 2.0 eV is calculated for **BFPBF**. Photoluminescence measurements imply a photoinduced electron transfer from the fluorenyl group to the perylene system, resulting in an intra-molecular fluorescence quenching in **BFPBF**. Organic BHJ photovoltaic device was fabricated using a blend of P3HT/**BFPBF** (1:1, w:w) as the active layer. Power conversion efficiency of 0.13% and a V_{oc} of 0.66 V were achieved for the un-optimized solar cell device.

Chapter 7

Conjugated Polymers Based on Tetrabenzo[5.5] fulvalene

7.1 Introduction

Although great progresses have been made in organic photovoltaic devices (OPVs), the design and synthesis of novel organic p-/n type of oligomers/polymers to serve as donor/acceptor materials in OPVs is still attracting escalatory research and technical interests. In particular, the investigation on n-type materials is comparatively rare and huge challenges remain. C_{60} and its derivative PC61BM[158] are currently the most widely used electron-acceptor materials. However, C_{60} derivatives have relatively weak molar absorption coefficient in the visible region. In addition, the C_{60} and its derivatives are difficult to be modified and the ensuing structures have limited scope for energy level tuning. Accordingly, the syntheses of novel acceptors with energy levels significantly different from those of current C_{60} derivatives are urgently required.

In Chapter 6, the n-type material comprising bisfluorene substituted preylene bisimide has been prepared and shown to have interesting properties. Herein, a new series of acceptor polymers based on tetrabenzo[5,5']fulvalene (TBF), which is potentially a new generation of acceptor compounds, are investigated. The addition of one electron across the C9–C9' bond would be highly favourable for TBF due to the steric strain relief and gain in aromaticity in attainment of a 14-π electron system[75]. Thus, it is envisaged that TBF based polymers could reasonably be possessive of electron

accepting characteristics. Furthermore, incorporation of both TBF and chromophoric units in the polymer backbone will enhance light absorption of the resulting materials. The structures of TBF and analogous polymers are shown in **Chart 7.1**.

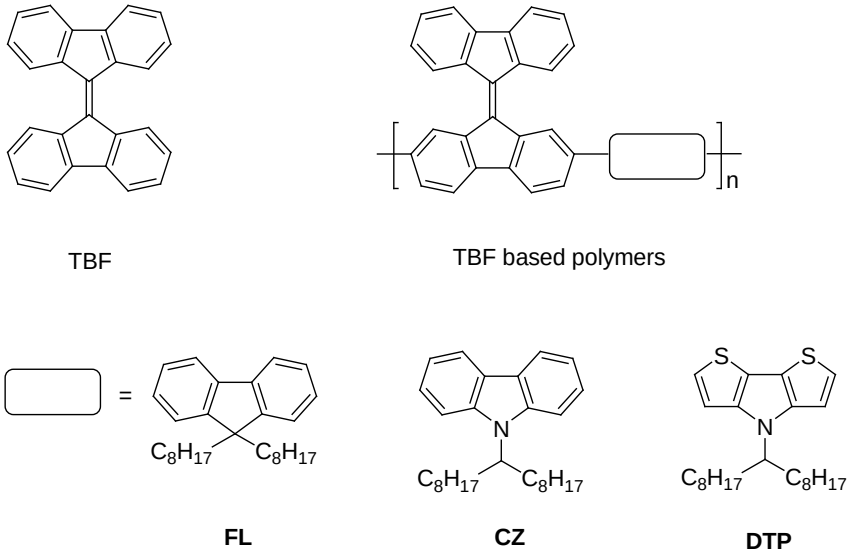

Chart 7.1 Structures of TBF and polymers having TBF.

7.2 Synthesis and characterization

7.2.1 Monomer synthesis

As shown in **Scheme 7.1**, the synthesis of 2,7-dibromo-tetrabenzo[5.5]fulvalene was started from 2,7-dibromofluorene, which was first oxidized to 2,7-dibromofluorone with CrO_3 in DMSO solution. Compound **36** was then converted to tetrabenzo[5.5]fulvalene derivative under strongly basic conditions. The target molecule was obtained by two steps with high yields.

Scheme 7.1 Synthetic approach of the monomers **45**, **47** and **49**.

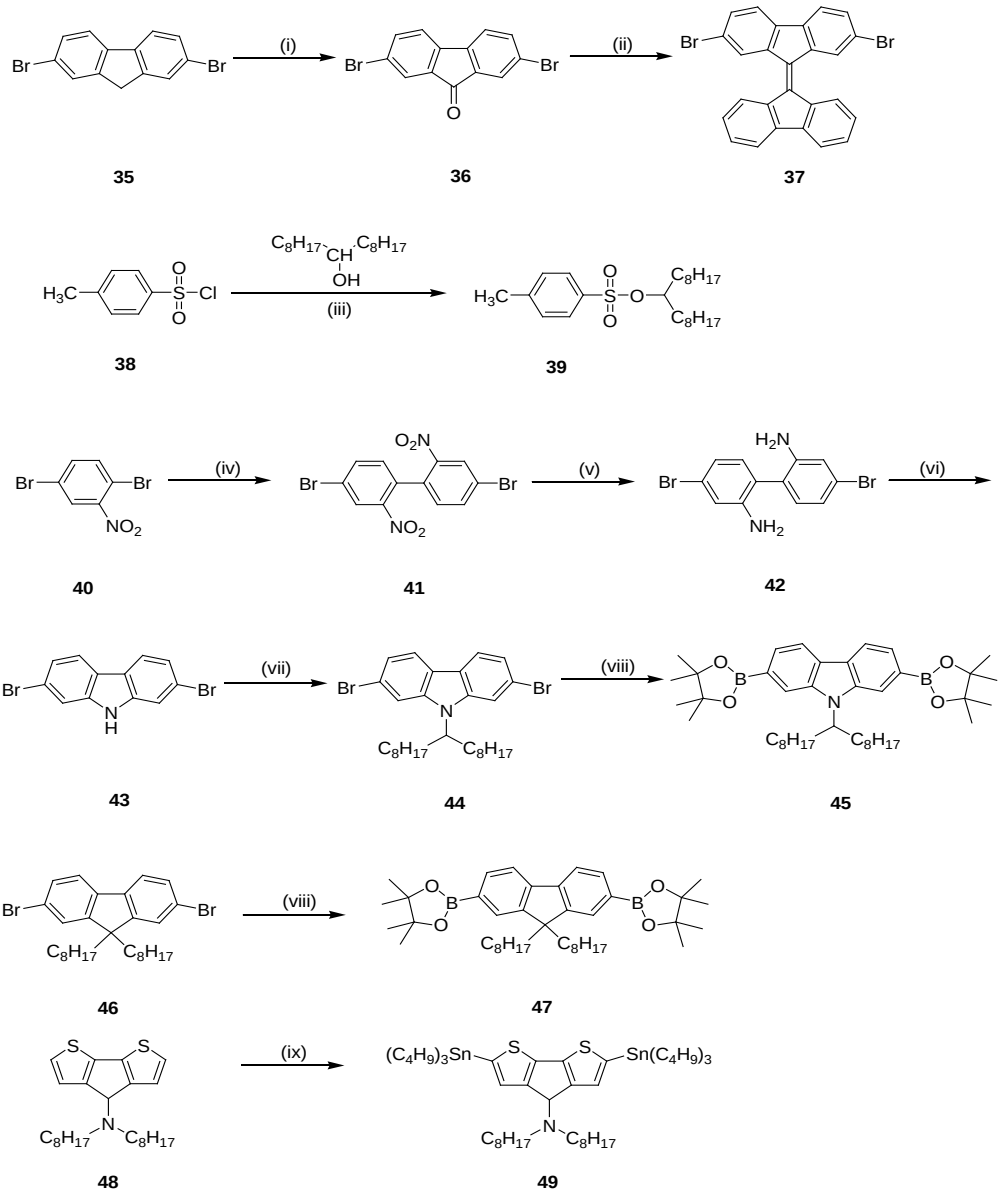

Reagents and conditions: (i) CrO_3, DMSO; (ii) n-BuLi, $(CH_3)_3SiCl$, THF; (iii) Et_3N, $Me_3N{\cdot}HCl$, CH_2Cl_2; (iv) Cu, DMF; (v) Sn powder, conc. HCl, ethanol; (vi) Conc. H_3PO_4; (vii) KOH, DMSO; (viii) n-BuLi, -78 ^oC, 2-isopropoxy-4,4,5,5-tetramethyl-1,3,2-dioxaborolane, anhydrous THF; (ix) n-BuLi, -78 ^oC, $(C_4H_9)_3SnCl$, dry THF.

2,7-Dibromocarbazole **44** cannot be obtained directly by the bromination of carbazole, from which only 3,6-dibromocarbazole is formed. The target molecule was prepared

by the indirect synthesis through a series of steps, starting from compound **40**. Finally, compound **45**, **46** and **48** were converted to their respective derivatives of boronic ester or stannyl reagent for use in the ensuing polymerization steps.

7.2.2 Polymer synthesis

Scheme 7.2 The synthetic approach of the polymer **PTBF-FL**, **PTBF-CZ** and **PTBF-DTP**.

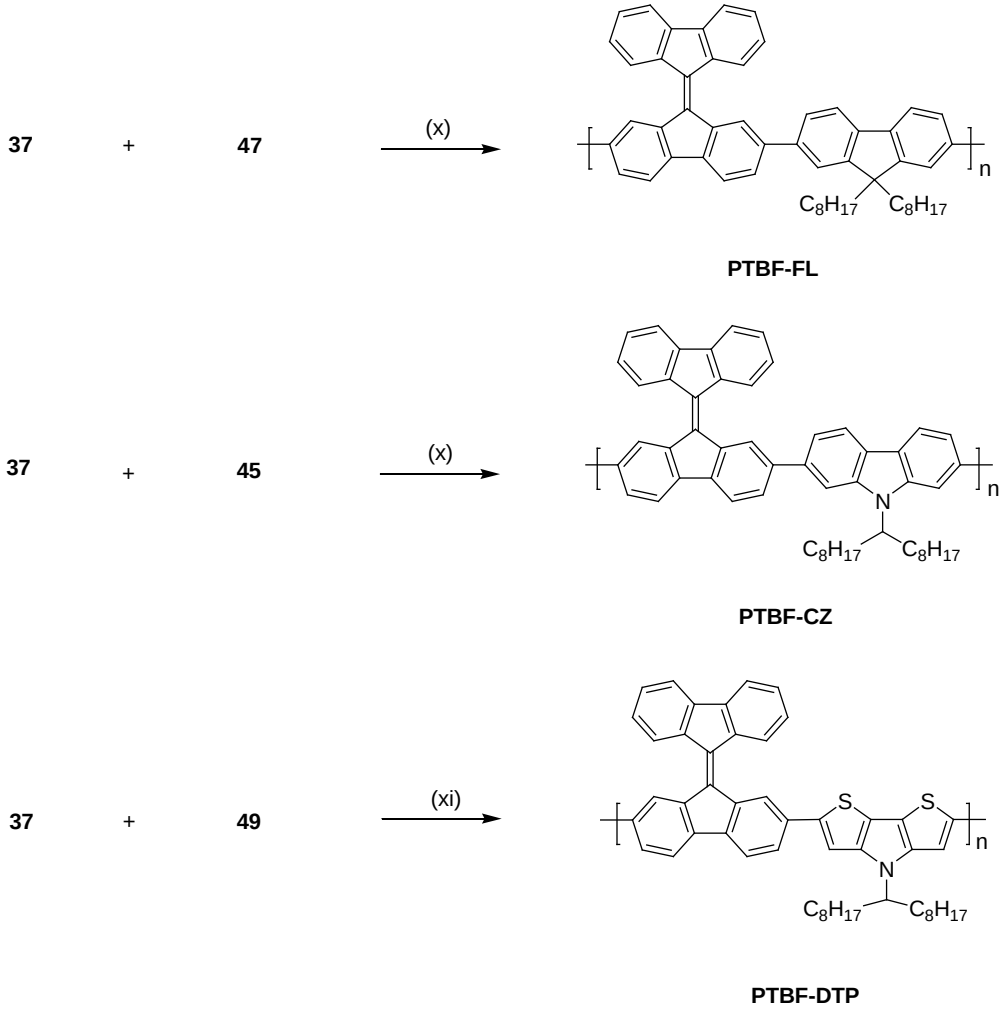

Reagents and conditions: (x) $Pd(PPh_3)_4$, 2 M Na_2CO_3, toluene, 120 ^oC, 48 h; (xi) $Pd(PPh_3)_2Cl_2$, THF, 90 ^oC, 48 h.

The Stille or Suzuki coupling reaction methods were used for the polymerization. The detail synthetic approach and experimental conditions are shown in **Scheme 7.2**. During the reaction, the solution became viscous and solution colour changed to dark brown, dark brown and dark green for **PTBF-FL**, **PTBF-CZ** and **PTBF-DTP** respectively. All polymerization proceeded smoothly and the target polymers were obtained as amorphous powders after Soxhlet extraction.

7.3.3 Polymer structure

The structures of **PTBF-FL**, **PTBF-CZ** and **PTBF-DTP** were confirmed by ^{1}H NMR spectroscopy and elemental analyses. For the three polymers, due to overlap of the broad resonance peaks of protons, the chemical shifts at the aromatic areas are not distinguishable. For the polymer **PTBF-CZ** and **PTBF-DTP**, broad peaks appearing at δ 4.0 and δ 4.5 are attributed to the proton connected to the tertiary carbon adjacent to the nitrogen atom. Chemical shifts from ca. δ 2.0 to δ 0.5 are assigned to the protons of the alkyl chains.

7.3 Results and discussion

7.3.1 Physical properties

All three TBF based polymers are soluble in common organic solvents such as $CHCl_3$, THF and toluene. **PTBF-FL**, **PTBF-CZ** and **PTBF-DTP** are obtained respectively as brown, brown and green powders. Their molecular weights as determined by GPC are summarized in **Table 7.1**. **PTBF-FL** and **PTBF-CZ** show similar molecular weights and PDIs while **PTBF-DTP** depicts a lower molecular weight in comparison. The number of aromatic rings which ranges from 47 to 47 can be calculated subsequently.

Table 7.1 GPC Results of Polymers **PTBF-FL**, **PTBF-CZ** and **PTBF-DTP**.

Polymer	M_n ($\times 10^3$)	M_w ($\times 10^3$)	PDI	n[a]
PTBF-FL	7.3	8.5	1.16	47
PTBF-CZ	7.3	8.3	1.14	45
PTBF-DTP	4.8	6.9	1.44	37

[a] Number of aromatic rings

7.3.2 Thermal properties

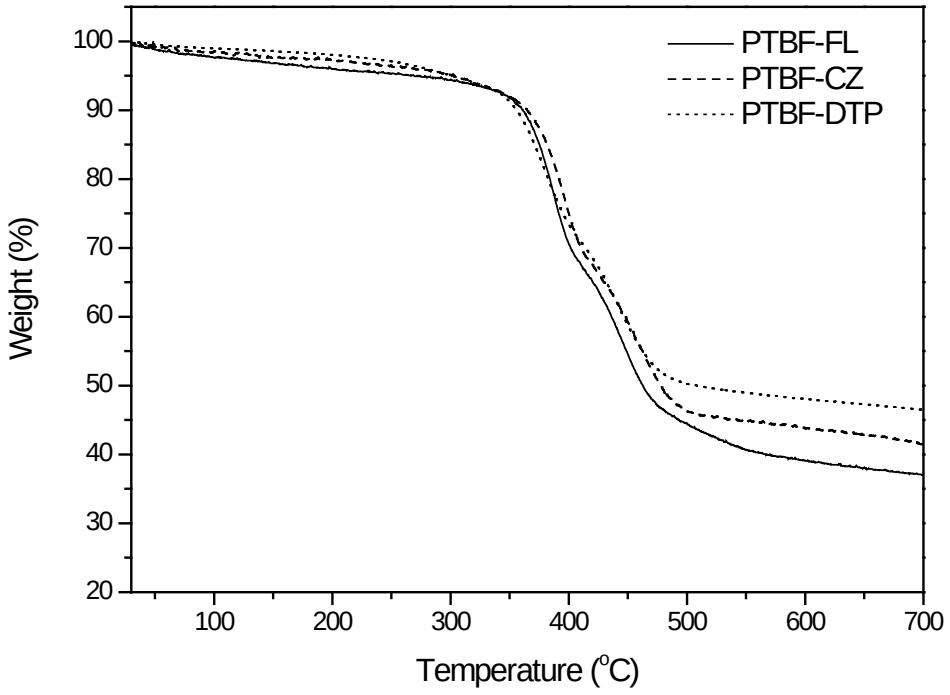

Figure 7.1 TGA curves of polymers **PTBF-FL**, **PTBF-CZ** and **PTBF-DTP** under nitrogen atmosphere.

The thermal stabilities of **PTBF-FL**, **PTBF-CZ** and **PTBF-DTP** were evaluated by TGA measurements over a temperature range of 25 to 700 ^oC under N_2 atmosphere.

Meanwhile, the glass transition behaviours of these polymers were investigated by DSC measurements over a temperature range of 25 to 200 ^{o}C again under N_2 atmosphere. The TGA curves are shown in **Figure 7.1**. In nitrogen atmosphere, the onset degradation temperatures (a weight loss ~ 5 %) of the three polymers are almost same and are higher than 350 ^{o}C. DSC measurements revealed that the glass transition temperatures of **PTBF-FL**, **PTBF-CZ** and **PTBF-DTP** are at 67, 75 and 52 ^{o}C respectively. TGA analyses thus indicate that these novel polymers are thermally stable under inert atmosphere. The results of thermal properties are summarized in **Table 7.2**.

Table 7.2 TGA and DSC Results of **PTBF-FL**, **PTBF-CZ** and **PTBF-DTP**.

Polymer	T_d [a] (^{o}C)	T_g (^{o}C)
PTBF-FL	358	67
PTBF-CZ	356	75
PTBF-DTP	352	52

[a] Weigth loss ~ 5 %

7.3.3 Optical properties

The optical properties of the polymer were investigated by UV-visible and photoluminescence spectroscopy at room temperature. The results are summarized in **Table 7.2**. In $CHCl_3$ dilute solution, the UV-visible absorption spectrum of **PTBF-DTP** show one absorption peak at 457 nm while both **PTBF-FL** and **PTBF-CZ** show two absorption peaks (**Figure 7.2**). The photoluminescence spectra of the polymers in dilute chloroform solution are depicted in **Figure 7.2**. **PTBF-FL**, **PTBF-CZ** and

PTBF-DTP display emission maxima (λ_{max}) at 403, 395 and 520 nm, which indicates a Stokes shift of 357143, 714286 and 158730 cm^{-1} respectively.

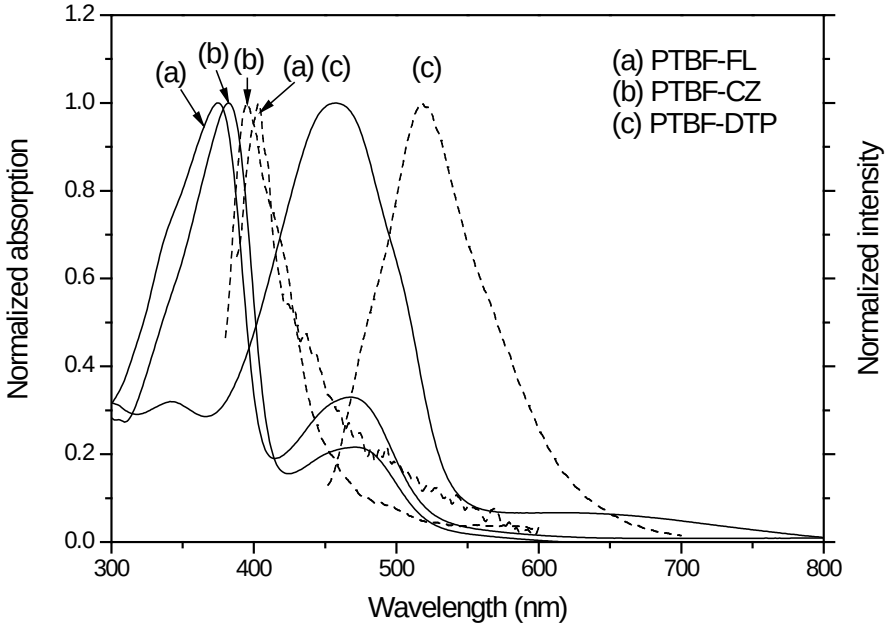

Figure 7.2 UV-vis (solid line) and PL (dash line) spectra of **PTBF-FL** (a), **PTBF-CZ** (b) and **PTBF-DTP** (c) in dilute $CHCl_3$ solution.

In addition, the optical absorption of the three polymers in solid states were also investigated (**Figure 7.3**). The polymers show broader absorption in solid states than when in solution. For **PTBF-FL** and **PTBF-CZ**, the absorption maxima are almost identical in film and when in dilute solution, implying weak inter-chain interactions in the solid states of these two polymers. The optical bandgaps calculated from UV-vis absorption in solid states show that **PTBF-DTP** has the smallest bandgap among these polymers, suggesting it may have better light-harvesting ability.

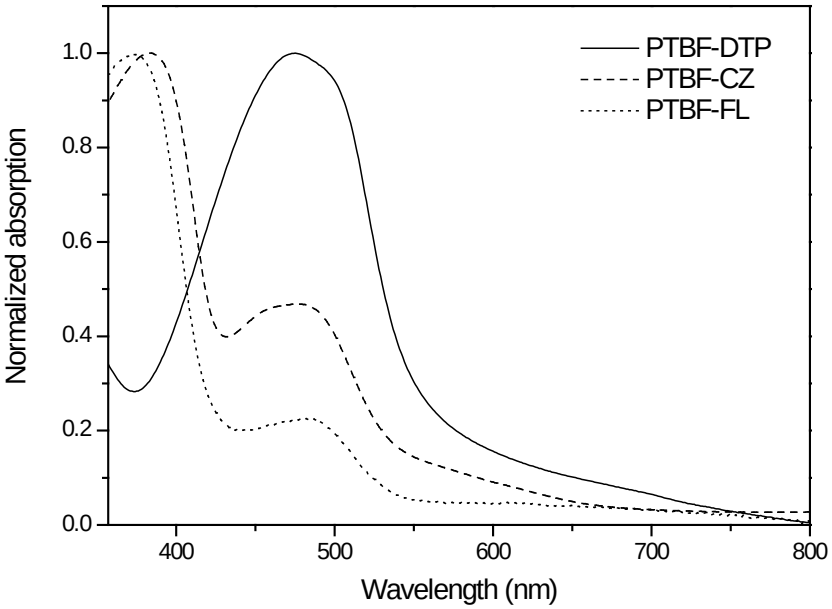

Figure 7.3 UV-vis spectra of **PTBF-FL**, **PTBF-CZ** and **PTBF-DTP** in solid states.

Table 7.3 Optical Properties of the Polymers in Solution and Film States.

Polymer	UV (solution) λ (nm)	PL (solution) λ (nm)	UV (film) λ (nm)	Stokes shift (cm^{-1})	Bandgap (opt.) ΔE (eV)
PTBF-FL	375, 470	403	374, 488	357143	2.25
PTBF-CZ	381, 466	395	382, 477	714286	2.14
PTBF-DTP	457	520	480	158730	1.89

7.3.4 Electrochemical properties

The electrochemical properties of **PTBF-FL**, **PTBF-CZ** and **PTBF-DTP** were determined by cyclic voltammetry (CV) and the voltammograms are shown in **Figure**

7.4. The measurements were performed in anhydrous acetonitrile solution of 0.1 M Bu_4NBF_4 under dry nitrogen atmosphere. A glassy carbon disk coated with a thin polymer film was used as work electrode, a silver wire as pseudo-reference electrode and a platinum wire as counter electrode. The redox potentials were calibrated against the ferrocene/ ferrocenium couple as an internal standard. **Table 7.4** summarises the electrochemical data of the polymers.

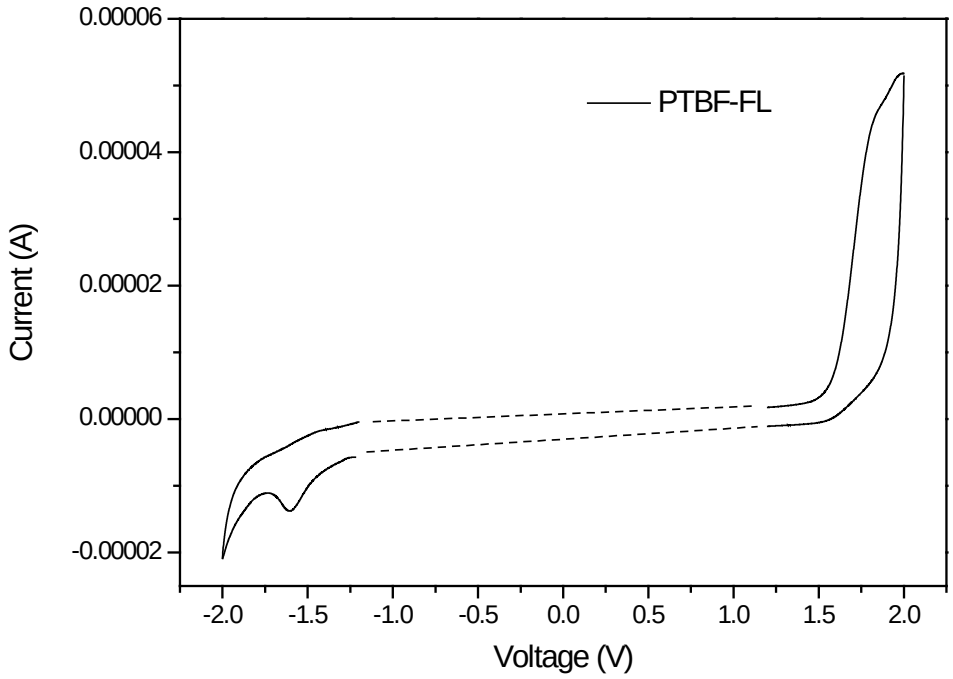

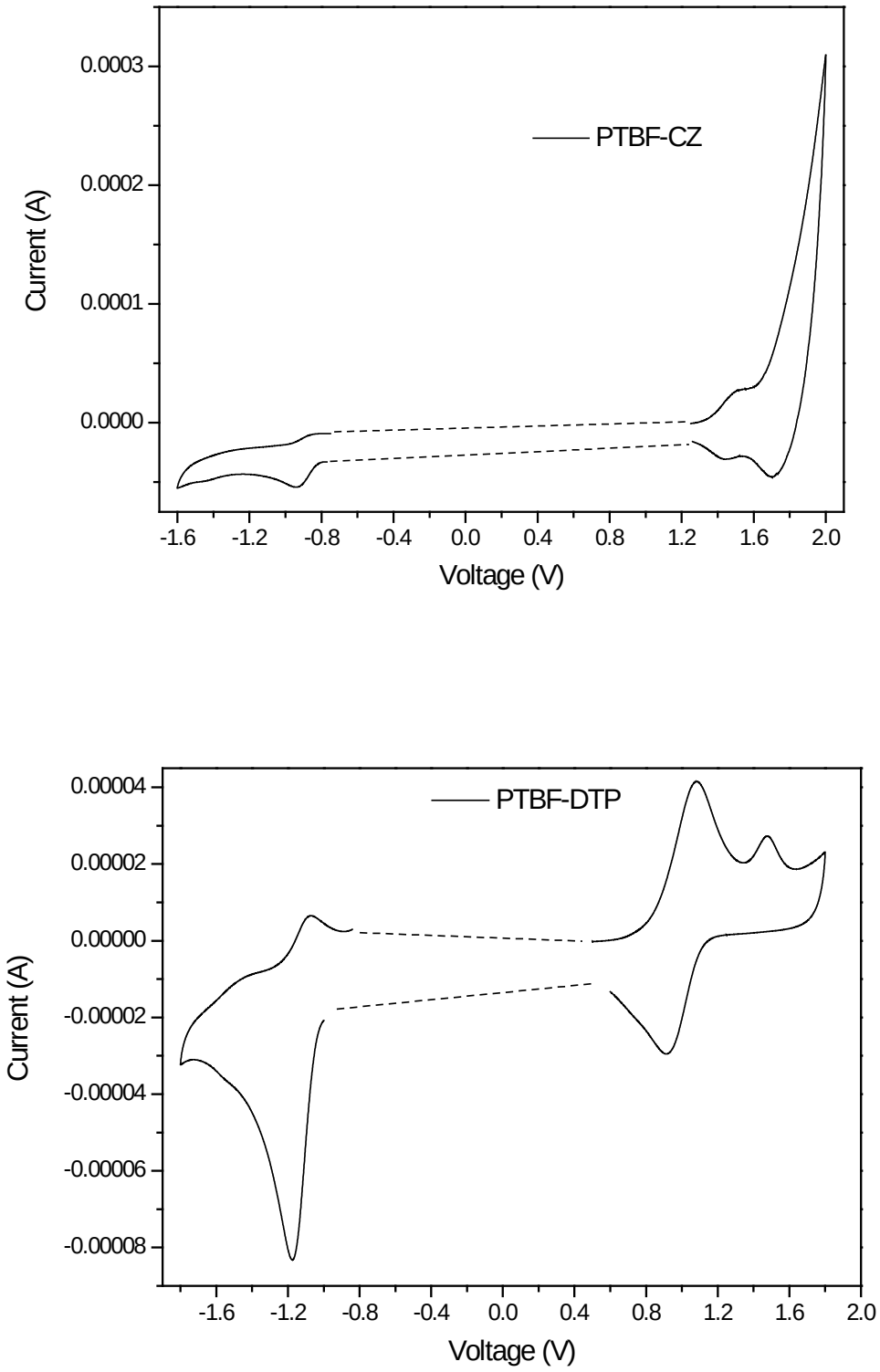

Figure 7.4 Cyclic voltammogram of **PTBF-FL**, **PTBF-CZ** and **PTBF-DTP** in solid states in Bu_4NBF_4/acetonitrile at a scan rate of 100 $mV \cdot s^{-1}$

Table 7.4 Onset and Peak Potentials of p- and n-Doping Processes of the Polymers.

Polymer	p-Doping			n-Doping			Bandgap
	E_{on} (V)	E_{pa} (V)	HOMO (eV)	E_{on} (V)	E_{pc} (V)	LUMO (eV)	ΔE (eV)[a]
PTBF-FL	1.41	1.80	-5.81	-1.05	-1.52	-3.35	2.46
PTBF-CZ	1.35	1.51, 1.95	-5.75	-0.88	-0.95	-3.57	2.23
PTBF-DTP	0.92	1.07, 1.49	-5.32	-0.95	-1.19	--3.45	1.87

[a] Electrochemical band gap

For polymer **PTBF-FL**, an onset oxidation potential of 1.41 V and an onset reduction potential of -1.05 V (versus SCE) were observed, which would correspond to a HOMO level of -5.81 eV and a LUMO level at -3.35 eV. Due to the electron-rich nitrogen atom in carbazole molecule, the polymer **PTBF-CZ** showed an onset oxidation potential at 1.35 V, which is 0.06 V lower than that of the polymer **PTBF-FL**. In addition, one of the two oxidation peaks of **PTBF-CZ** may be attributed to the oxidation of nitrogen atom. A HOMO level of -5.75 eV and a LUMO level of -3.57 eV are calculated for the polymer **PTBF-CZ**. Among the three polymers, **PTBF-DTP** has the lowest onset oxidation potential, which is 0.92 V and ca. 0.5 V lower than that of **PTBF-FL**. This can be attributed to the electron-rich thiophene ring structure as well as electron donation of the nitrogen atom in molecule of DTP. Furthermore, the electrochemical bandgaps of the three polymers can be calculated accordingly, which are 2.46, 2.23 and 1.87 eV, respectively. **PTBF-DTP** has the lowest bandgap among these three polymers.

In an OPV device, the LUMO level of donor material, such as the most widely used P3HT (LUMO = -3.0 eV), should be higher than that of the acceptor material for effective charge transport. The TBF based polymers thus satisfactorily meet this requirement when they are blended with P3HT to be of the active layer in BHJ devices. On the other hand, compared to the acceptor material PC61BM, whose LUMO level is -4.0 eV, TBF based polymers have much higher LUMO levels. Consequently, a higher open circuit voltage (V_{oc}) can be expected for OPV devices using P3HT:TBF blends as active layers compared to those devices using P3HT:PCBM as active layers.

7.3.5 Polymer microstructures

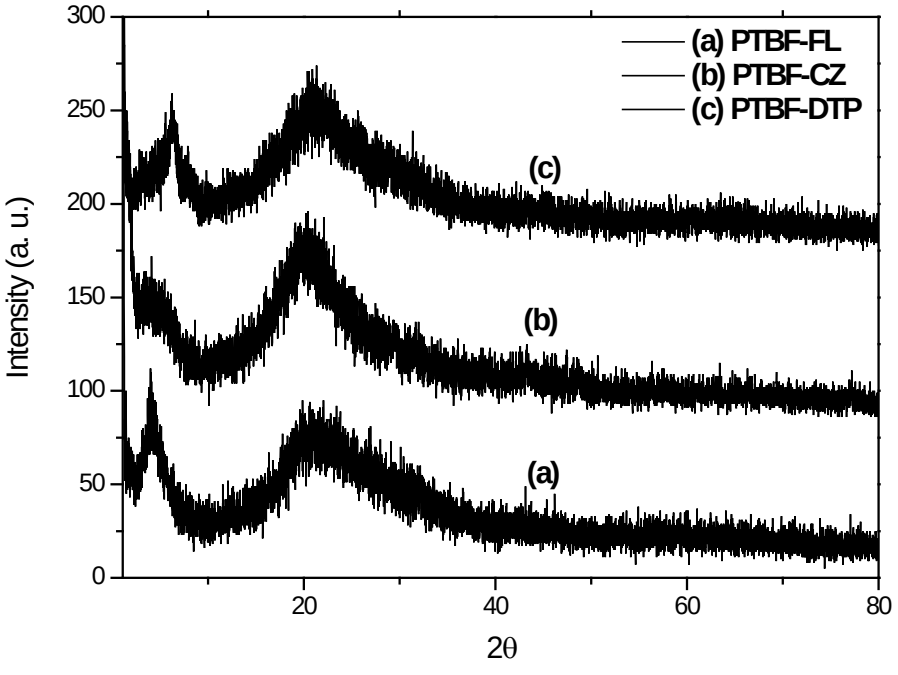

Figure 7.5 XRD spectrum of polymer **PTBF-FL**, **PTBF-CZ** and **PTBF-DTP**.

To investigate the microstructures of the polymers, X-ray diffraction (XRD) measurements of polymer films were performed at room temperature and the XRD spectra are shown in **Figure 7.5**. The 2θ scatting profile of the polymer films are shown in **Table 7.5**. The polymer sample films showed diffraction peak at 2θ = 4.1 ^{o} (d = 22.1 Å), 4.3 ^{o} (d = 21.6 Å) and 6.2 ^{o} (d = 14.1 Å) for **PTBF-FL**, **PTBF-CZ** and **PTBF-DTP** respectively, which would correspond to side to side distances between the side chains and the backbone main chains. Furthermore, there were additional broad peaks at around 2θ = 20 ^{o} for all the three polymers, which would correspond to the lamellar π-π stacking space of intermolecular polymer backbones. It can be concluded that the polymers **PTBF-FL**, **PTBF-CZ** and **PTBF-DTP** are partially crystalline which will be beneficial for the charge transfer in these polymers based OPV devices.

Table 7.5 XRD Diffraction Data of **PTBF-FL**, **PTBF-CZ** and **PTBF-DTP**.

Polymer	2θ peak (^{o})	Spacings (Å)
PTBF-FL	4.1	22.1
	20.8	4.1
PTBF-CZ	4.3	21.6
	20.2	4.35
PTBF-DTP	6.2	14.1
	20.7	4.25

7.5 Summary

A series of novel conjugated polymers based on TBF, **PTBF-FL**, **PTBF-CZ** and **PTBF-DTP**, have been successfully prepared by Suzuki coupling or Stille coupling reaction. These polymers are soluble in the common organic solvents and thermally stable under nitrogen atmosphere. Compared with PC61BM, these polymers have broader absorption in UV-vis light region and can thus potentially harvest more light in the solar spectrum. CV results show that **PTBF-FL**, **PTBF-CZ** and **PTBF-DTP** have the LUMO levels of -3.35, -3.57 and -3.45 eV, which is higher than the PC61BM LUMO level of -4.0 eV. Consequently, OPV devices based on **PTBF-FL**, **PTBF-CZ** and **PTBF-DTP** as acceptor materials can be expected to achieve a high V_{oc}. The investigation of polymers' micro-structures shows all the three polymers have partial crystalline structures, which could benefit charge transport in devices.

Chapter 8

Conjugated Polymers Based on Fluorene Derivatives and Alkoxyl Thiophene

8.1 Introduction

Interest in organic electronics (such as OPVs and OTFTs) and their use in various technological applications have grown significantly in recent years[159]. To realize the full potential of these applications, it is necessary to identify conjugated materials with high mobility and robust environmental stability. Empirically, an efficiently π-π stacking structure and polymer regioregularity are expected to facilitate carrier transport because both of these considerations are believed to help establish high interchain crystal orders, which are necessary for achieving high mobilities. As far as solution-processable polymeric semiconductors are concerned, impressive progress has been made in developing p-type materials such as P3HT, F8T2, and PQT, etc. However, the realization of high-performance, ambient-stable n-channel polymeric semiconductors remains challenging and the discovery of readily processable electron-transporting polymeric semiconductors would represent a major step towards polymeric complementary circuit technologies[160], where the combination of p- and n-channel transistors results in far greater circuit speeds, lower power dissipation and more stable operation. Currently, a conjugated polymer based on naphthalene-bis(dicarboximide)(NDI) polymer in combination with several polymeric dielectric materials has shown electron mobility up to 0.45 ~ 0.85 $cm^2V^{-1}s^{-1}$. The structure of the polymer is shown in **Figure 8.1**.

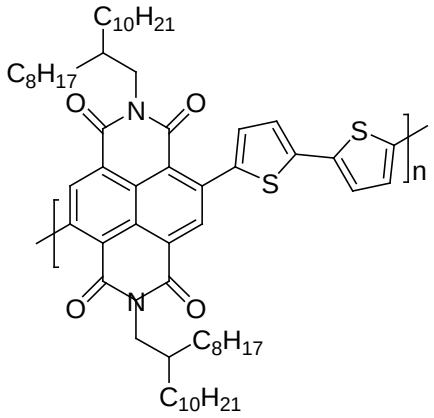

Figure 8.1 Polymer structure of poly{[N,N9-bis(2-octyldodecyl)-naphthalene-1,4,5,8 bis(dicarboximide)-2,6-diyl]-alt-5,59-(2,29-bithiophene)} (PNI2OD-T2)

Top-gate n-channel polymeric TFTs has been fabricated based on the polymer and the devices exhibit field-effect mobilities, processability, compatibility with various dielectric materials, and operational stability. Electron mobilities of > 0.1 $cm^2V^{-1}s^{-1}$ (up to 0.85 $cm^2V^{-1}s^{-1}$) in ambient conditions with $I_{on}/I_{off} > 10^6$ have been achieved by the top-gate bottom-contact transistors. In addition, this polymer can be processed by spin-coating as well as gravure, flexographic and inkjet printing the semiconducting layer, demonstrating great processing versatility. The TFT performances monitored in ambient conditions and under different relative humidities demonstrate remarkable. Herein, the combination of such n-channel material with previously developed high-performance p-channel polymers and optimized device architectures will open unprecedented opportunities for printed electronics.

Tetrabenzo[5.5]fulvalene (TBF) and fluorone molecules are both derivatives of fluorene molecules. The former one has the second fluorene unit linked with the patent fluorene at 9, 9’ positions by double bond while the later one has the oxygen atom linked with the patent fluorene at 9, 9’ positions by double bond. Therefore, electron withdrawing property while the similar rigidity is expected to be gained by

the two molecules compared to alkyl functionalized fluorene molecules. The crystalline structures have been demonstrated for the TBF based polymers prepared in the previous chapter.

On the other hand, a particular design need for organic electronics is in the area of n-channel (or n-type) conjugated materials, which conduct electrons. The motivation for seeking good n-channel materials is that they enable complementary circuit design that utilize both positive and negative gate voltages to switch transistors on and off. Consequently, the development of good n-channel OFFTs with performance comparable to that of p-channel OFETs is a major goal for organic electronics. It has been reported that TBF molecule possesses electron-accepting characteristics and is accordingly beneficial towards electron conduction. The fluorenone molecule is also characterized as having an electron deficient structure. Accordingly, polymers based on TBF and fluorenone units are potentially promising n-type materials for OFETs. In addition, substituted polythiophenes exhibited good OFET performance[139,161-163]. The alkoxyl chain would not only increase the polymer's solubility but also help to constitute hydrogen bonds in polymer's microstructure. In this chapter, we report the syntheses and characterization of novel polymers based on TBF or fluorone and alkoxyl substituted thiophene units.

8.2 Synthesis and characterization

8.2.1 Monomer synthesis

The synthesis of the compound **55** started from 3-bromothiophene and the detail synthetic steps are outlined in **Scheme 8.1**. Firstly, 3-methoxythiophene was prepared by reacting 3-bromothiophene with methanol in the presence of sodium methoxide. Subsequently compound **51** was reacted with 1-dodecanol in toluene solution and

converted to **52**, which was followed by bromination with NBS in chloroform to obtain compound **53**. An efficient palladium-catalyzed coupling reaction promoted by $AgNO_3$ and KF was utilized to transform compound **53** into the symmetrical bithiophene **54**. Subsequently, the tin reagent **55** was generated by lithiathing compound **54** followed by reaction with trimethyl tin chloride. TBF and fluorone were prepared as described in the preceding chapter.

Scheme 8.1 Synthetic approach of the monomers **55**, **57** and **58**.

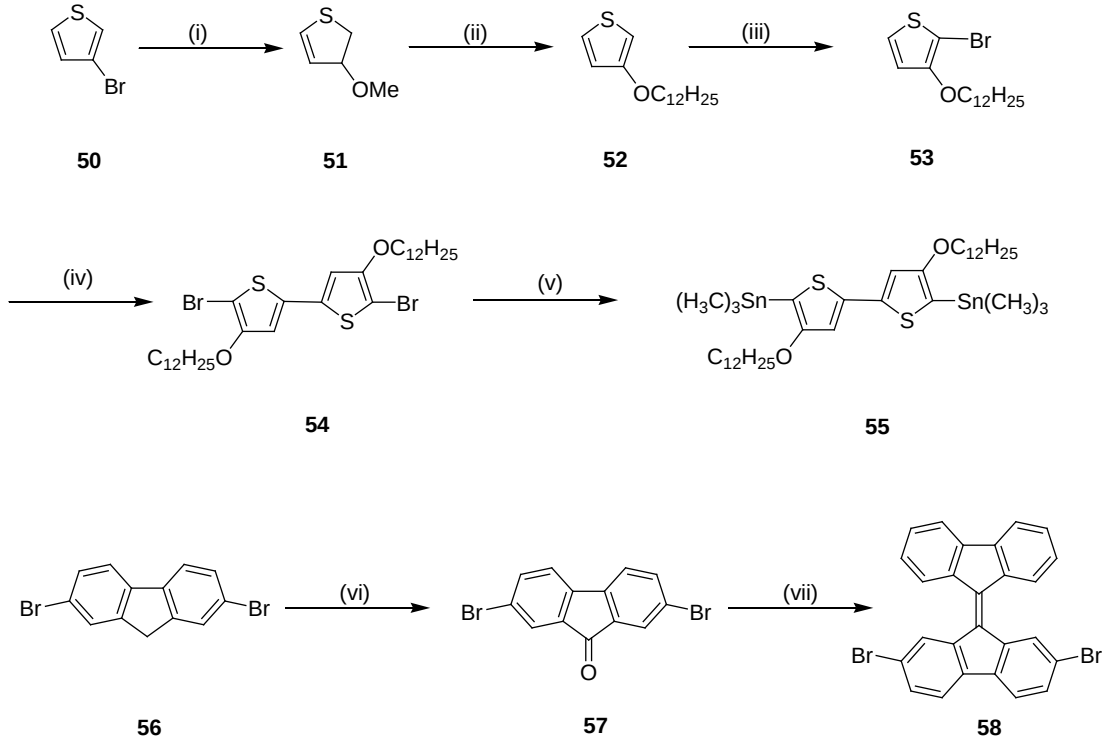

Reagents and conditions: (i) MeONa, CuBr, methanol; (ii) 1-dodecanol, p-toluenesulfonic acid monohydrate, toluene; (iii) NBS, $CHCl_3$; (iv) $PdCl_2(PhCN)_2$, KF, $AgNO_3$, DMSO; (v) n-BuLi, $(CH_3)_3SnCl$, -78 ^oC, anhydrous THF; (vi) CrO_3, DMSO; (vii) n-BuLi, $(CH_3)_3SiCl$, anhydrous THF.

8.2.2 Polymer synthesis

Polymerization was effected by the Stille coupling reaction in anhydrous THF (see **Scheme 8.2**). After reacting for 48 h, the crude polymer was precipitated in methanol

and collected by filtration. The purification of the polymers was performed by Soxhlet extraction and finally the target polymers were obtained as powdery solids.

Scheme 8.2 Synthetic approach of the polymer **PTBF-AOT** and **PFO-AOT**.

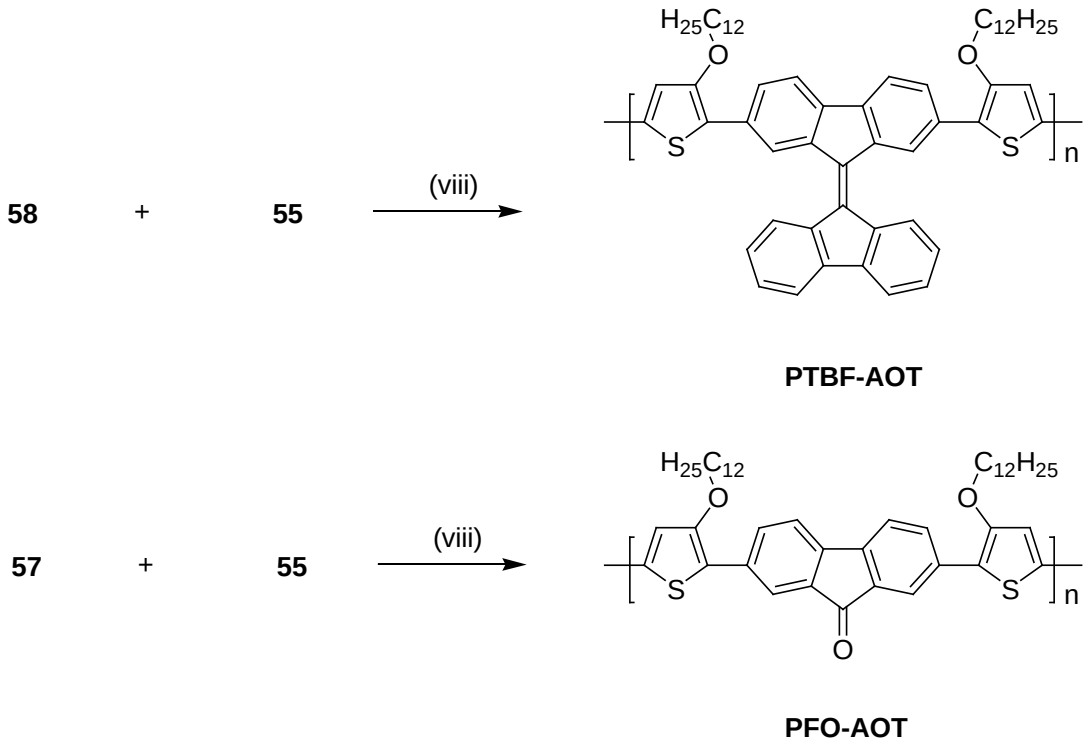

Reagents and conditions: (viii) $Pd(PPh_3)_2Cl_2$, THF, 90 ^oC, 48 h.

8.2.3 Polymer structures

The structure of **PTBF-AOT** and **PFO-AOT** were determined and confirmed by ^1H NMR spectroscopy and elemental analyses. The aromatic protons of the polymer **PTBF-AOT** appeared over δ 8.7 to 6.78 while those for **PFO-AOT** are from δ 7.9 to δ 6.8. Both the polymers show broad peaks appearing at around δ 4.0, which are attributed to the methylene protons adjacent to oxygen atom in the alkoxyl chain. Chemical shifts from ca. δ 2.0 to δ 0.5 arise from the protons of the methylene and terminal methyl units of the alkoxyl chains.

8.3 Results and discussion

8.3.1 Physical properties

Table 8.1 GPC Results of **PTBF-AOT** and **PFO-AOT**.

Polymer	M_n (10^3)	M_w (10^3)	PDI	n[a]
PTBF-AOT	6.1	8.5	1.39	40
PFO-AOT	9.3	11.5	1.24	65

[a] No. of aromatic rings

Both polymers are soluble in common organic solvents such as $CHCl_3$, THF and toluene. The polymers **PTBF-AOT** and **PFO-AOT** obtained are green and brown powders respectively. The GPC results are summarized in **Table 8.1**. The molecular weight of **PTBF-AOT** is lower than that of **PFO-AOT** arising from the sterically more encumbered TBF moiety compared to that of fluorone.

8.3.2 Thermal properties

The thermal properties of the polymers **PTBF-AOT** and **PFO-AOT** were investigated by TGA over a temperature range of 25 to 800 ^oC and DSC measurements over a temperature range of 25 to 200 ^oC under N_2 atmosphere. The TGA curves are shown in **Figure 8.2** and the corresponding values of T_d and T_g are listed in **Table 8.2**. The onset degradation temperatures for the polymers are similar and both are higher than 300 ^oC under nitrogen atmosphere. DSC measurements revealed a glass transition temperature of 152 ^oC for the polymer **PFO-AOT** (**Figure 8.2**). There was no discernible T_g for the polymer **PTBF-AOT** and this implied that the polymer **PFO-AOT** possesses a more rigid structure compared to the **PTBF-AOT**

polymer. TGA analyses demonstrated that **PTBF-AOT** and **PFO-AOT** are both thermally stable under inert atmosphere.

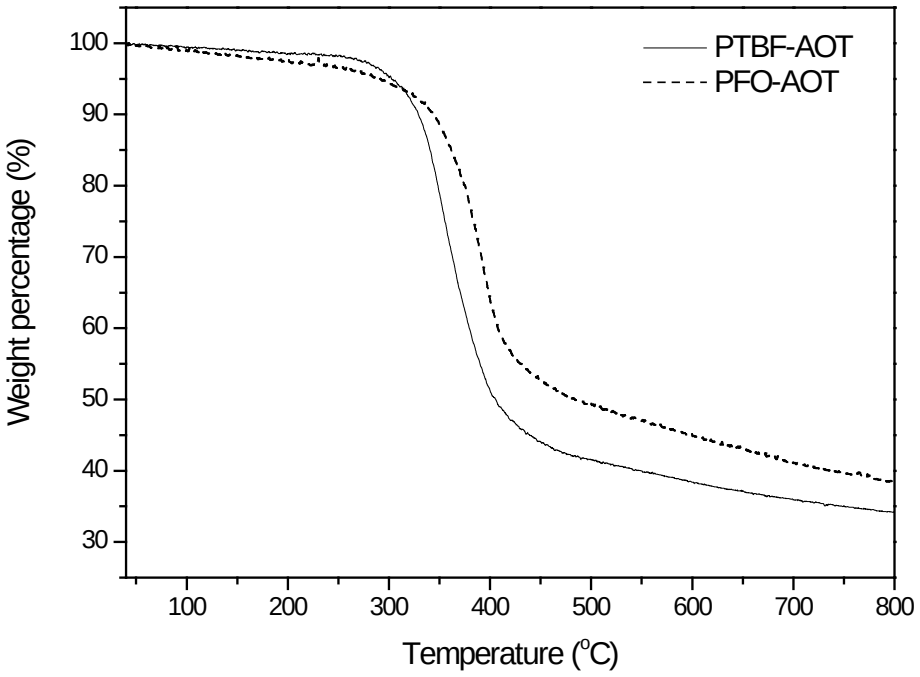

Figure 8.2 TGA curves of polymers **PTBF-AOT** and **PFO-AOT** under nitrogen atmosphere.

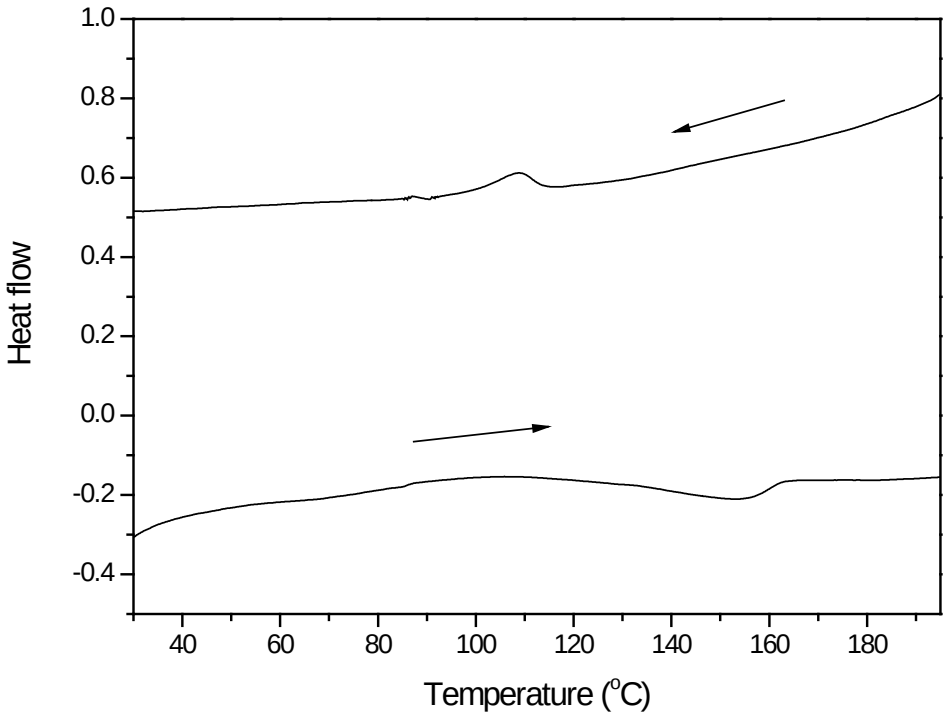

Figure 8.3 DSC curve of **PFO-AOT** at a heating rate of 10 °C/min under nitrogen atmosphere.

Table 8.2 TGA and DSC Results of **PTBF-AOT** and **PFO-AOT**.

Polymer	T_d [a] (°C)	T_g (°C)
PTBF-AOT	310	--
PFO-AOT	302	152

[a] Weigth loss ~ 5 %

8.3.3 Optical properties

The optical properties of the polymer were investigated by UV-vis and photoluminescence spectroscopy at room temperature (**Figure 8.4**). The results are summarized in **Table 8.3**. In dilute chloroform solution, the UV-visible absorption

maxima (λ_{max}) of **PTBF-AOT** is at 446 nm while the λ_{max} of **PTBF-AOT** is at 432 nm. The absorption maxima of the two polymers are almost identical as both are the fluorene derivatives, which have would have similar UV-vis absorption. The photoluminescence spectra of the polymers in dilute chloroform solution are depicted in **Figure 8.4**.

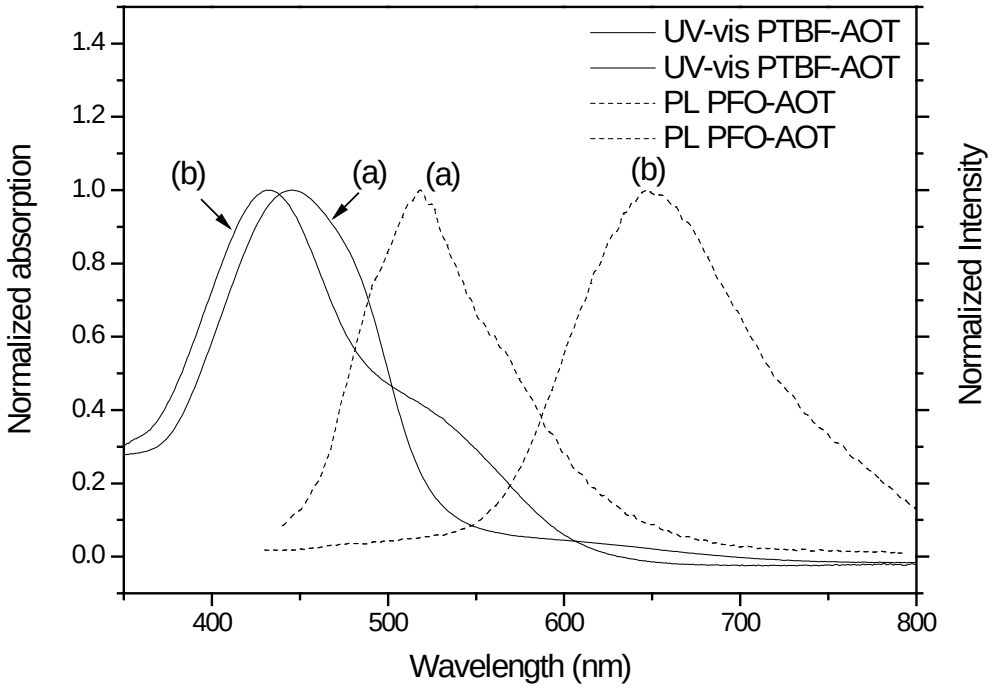

Figure 8.4 UV-vis (solid line) and PL (dash line) spectra of **PTBF-AOT** (a), **PFO-AOT** (b) in dilute $CHCl_3$ solution.

The polymer **PTBF-AOT** and **PFO-AOT** display maximum emission at λ = 518 and 648 nm with a calculated Stokes shift of 72 and 216 nm, respectively. The greater Stokes shifts of **PFO-AOT** indicate that a more effective charge transfer is afforded in comparison to that of the **PTBF-AOT** polymer.

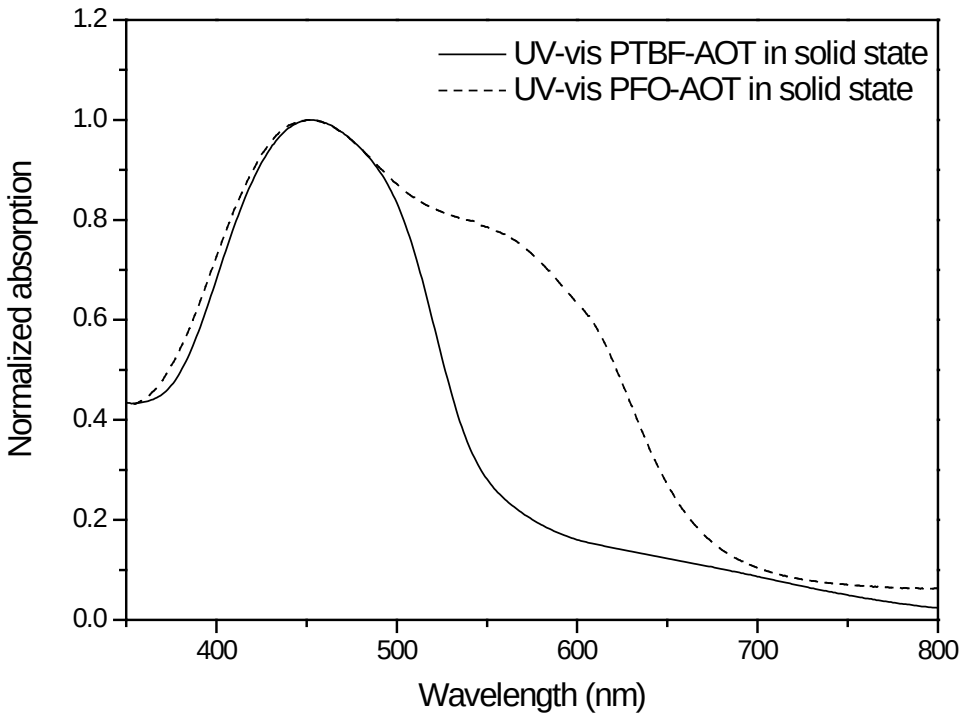

Figure 8.5 UV-vis spectra of **PTBF**-AOT and **PFO-AOT** in solid states.

Furthermore, the optical absorption of the polymers in solid states was also determined (**Figure 8.5**) by the UV-vis spectroscopy. Both polymers show much broader absorption in film states than that in solution. For polymer **PTBF-AOT**, the maximum absorption in film state is at 452 nm, which is 6 nm red-shifted compared to its absorption in dilute solution. This implies that there is no significant conformational change in the polymer chains between solution and film states for the polymer. Polymer **PFO-AOT** is about 20 nm red-shifted between the two states. Optical band gaps of 2.28 and 1.98 eV are calculated from UV-vis absorption in film states for **PTBF-AOT** and **PFO-AOT** respectively.

Table 8.3 The Optical Properties of the Polymers in Solution and Film States.

Polymer	UV (solution) λ (nm)	PL (solution) λ (nm)	UV (film) λ (nm)	Bandgap (opt.) ΔE (eV)
PTBF-AOT	446	518	452	1.95
PFO-AOT	432(518)	648	452(568)	1.98

8.3.4 Electrochemical properties

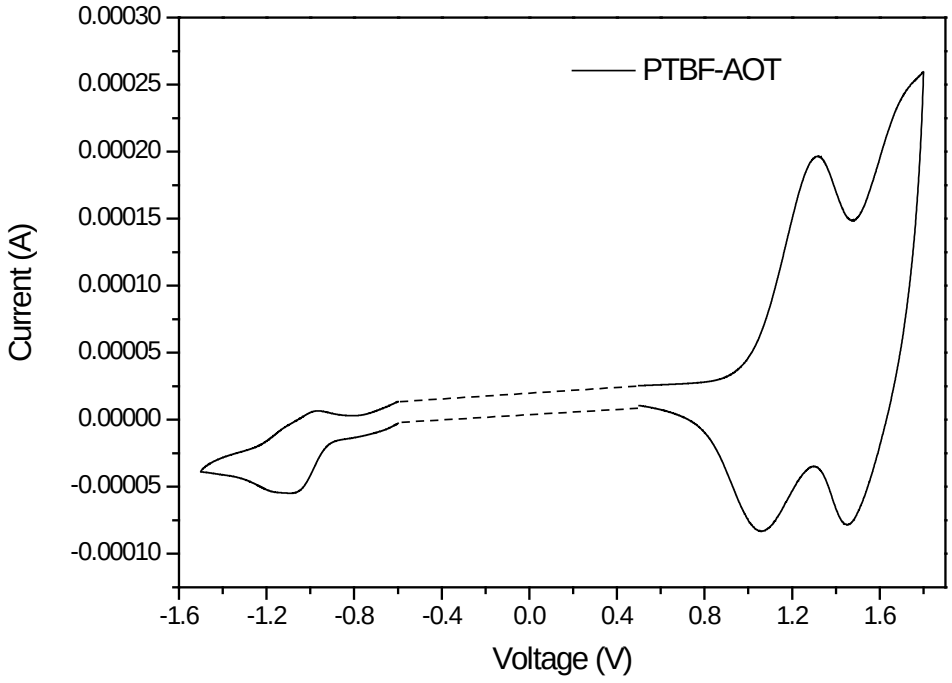

Figure 8.6 Cyclic voltammogram of **PTBF-AOT** in solid states in Bu_4NBF_4/acetonitrile at a scan rate of 100 $mV \cdot s^{-1}$.

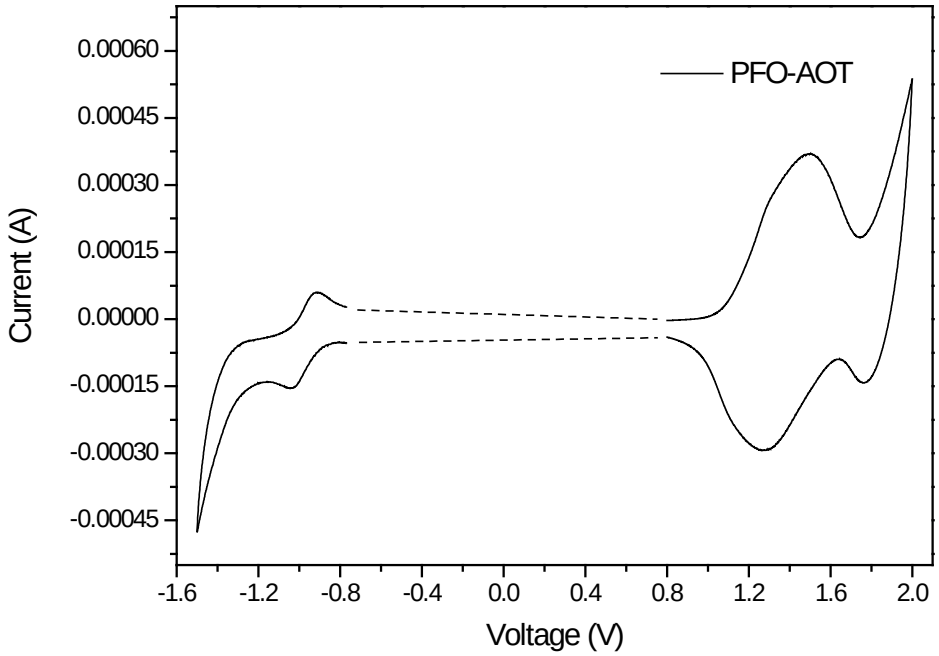

Figure 8.7 Cyclic voltammogram of **PFO-AOT** in solid states in Bu_4NBF_4/acetonitrile at a scan rate of 100 $mV \cdot s^{-1}$.

The electrochemical properties of **PTBF-AOT** and **PFO-AOT** were investigated by cyclic voltammetry (CV) and the voltammograms are shown in **Figure 8.6** and **Figure 8.7**. The measurements were performed in anhydrous acetonitrile solution of 0.1 M Bu_4NBF_4 under nitrogen atmosphere. A glassy carbon disk coated with a thin polymer film was used as working electrode, a silver wire as pseudo-reference electrode and a platinum wire as counter electrode. The redox potentials were calibrated against the ferrocene/ ferrocenium couple as an internal standard. The electrochemical data of the polymers are summarized in **Table 8.4**.

The onset oxidation potentials for the polymer **PTBF-AOT** and **PFO-AOT** are 1.07 V and 1.1 V (versus SCE), which would correspond to a HOMO level of -5.47 eV and a HOMO level of -5.5 eV, respectively. The two polymers have almost the same

oxidation onset potentials, due to both of them being oxidized at the alkoxyl substituted thiophene moiety first. The n-doping process (or electron accepting character) of both polymers can be obviously seen from the cyclic voltammograms. The onset reduction potential of **PTBF-AOT** is -0.96 V, which is 0.05 V lower than that of **PFO-AOT** whose onset reduction potential is -0.91 V. This may be contributed to a stronger electron accepting characteristic of fluorone unit compared to TBF. Furthermore, the electrochemical band gaps of the two polymers are calculated accordingly, which are 2.04 and 2.01 eV for the polymer **PTBF-AOT** and **PFO-AOT**, respectively.

Table 8.4 Onset and Peak Potentials of p- and n-Doping Processes of the Polymers.

Polymer	p-Doping			n-Doping			Bandgap
	E_{on} (V)	E_{pa} (V)	HOMO (eV)	E_{on} (V)	E_{pc} (V)	LUMO (eV)	ΔE (eV)[a]
PTBF-AOT	1.09	1.32, 1.74	-5.49	-0.96	-1.09	-3.45	2.04
PFO-AOT	1.1	1.50, 1.98	-5.5	-0.91	-1.05	-3.49	2.01

[a] Electrochemical band gap

8.3.5 Polymer microstructures

The investigation of the polymer microstructures was performed by X-ray diffraction (XRD) at room temperature (**Figure 8.8**). The θ - 2θ scatting profile of the polymer films are shown in **Table 8.5**. For **PTBF-AOT**, the diffraction peaks appear at 2θ = 3.1 ^{o} and 22.3 ^{o}, corresponding to spacings of 24.1 Å and 4.04 Å, respectively. For **PFO-AOT**, a very strong and sharp peak is shown at 2θ = 3.88 ^{o} which is assigned to the side to side distances between the side chains and the backbone main chains. From

these results, it can be concluded that **PFO-AOT** possesses high crystallinity while **PTBF-AOT** is only partially crystalline.

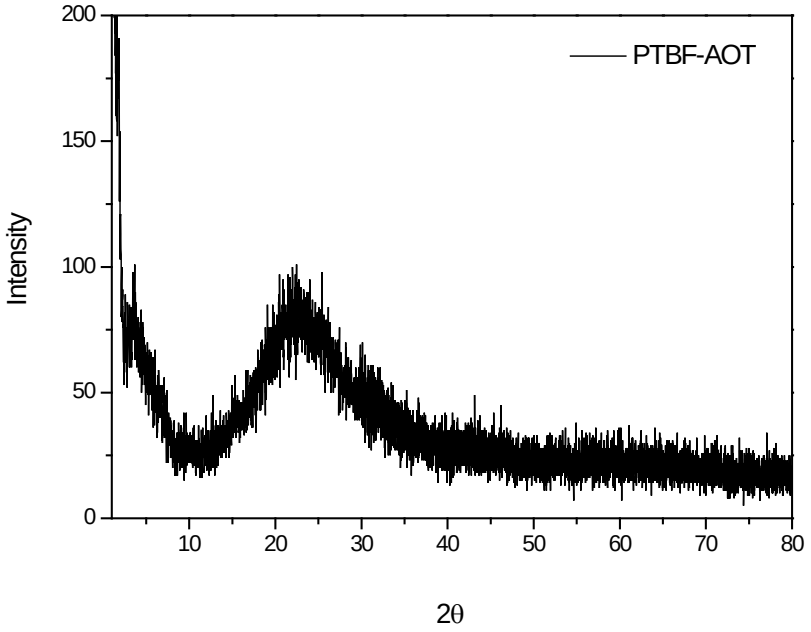

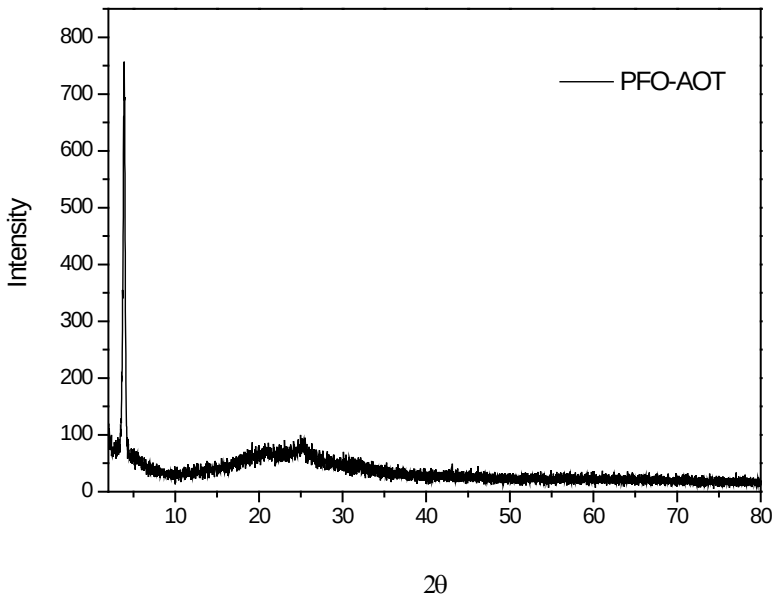

Figure 8.8 XRD spectrum of polymer **PTBF-AOT** and **PFO-AOT**.

Table 8.5 XRD Diffraction Data for **PTBF-AOT** and **PFO-AOT**.

Polymer	2θ peak (^{o})	Spacings (Å)
PTBF-AOT	3.1	24.1
	22.3	4.04
PFO-AOT	3.8	22.6
	20.8	4.2
	25.4	3.5

8.4 Summary

Novel conjugated polymers, **PTBF-AOT** and **PFO-AOT,** based on TBF and fluorone have been successfully prepared via Stille cross-coupling reactions. These new polymers are soluble in common organic solvents and thermally stable under inert atmosphere. The optical properties of polymers show that **PTBF-AOT** has UV-vis absorption maxima at 446 nm while that of **PFO-AOT** is at 432 nm. Optical band gaps of 1.95 and 1.98 eV are calculated for **PTBF-AOT** and **PFO-AOT** in film states. A Stokes shift more than 5×10^{4} cm^{-1} for **PFO-AOT** is observed from photoluminescence spectra. Notable p- and n-doping processes can be observed from the CV measurements for both polymers, inferring that hole and electron transports are thus possible. The results of XRD diffraction indicate that **PFO-AOT** has a high crystalline order whilst **TBF-AOT** has only a partial crystalline structure. Such crystalline structures will benefit for alignments of the polymer chains and imply that the polymers might be potential materials with desirable mobility.

Chapter 9
Conclusions and Suggestions for Future Work

9.1 Conclusions

In this dissertation , novel dithieno[3,2-b:2',3'-d]pyrroles (DTP)/fluorene derivatives conjugated molecules/macromolecules (both p-type and n-type, **Figure 9.1**) have been successfully prepared and characterized. The physical, optical, electrochemical and structural properties of these materials were investigated. The findings presented in this dissertation show that these new materials have interesting optical and electrochemcial characteristics which make them promising for applications in organic electronics.

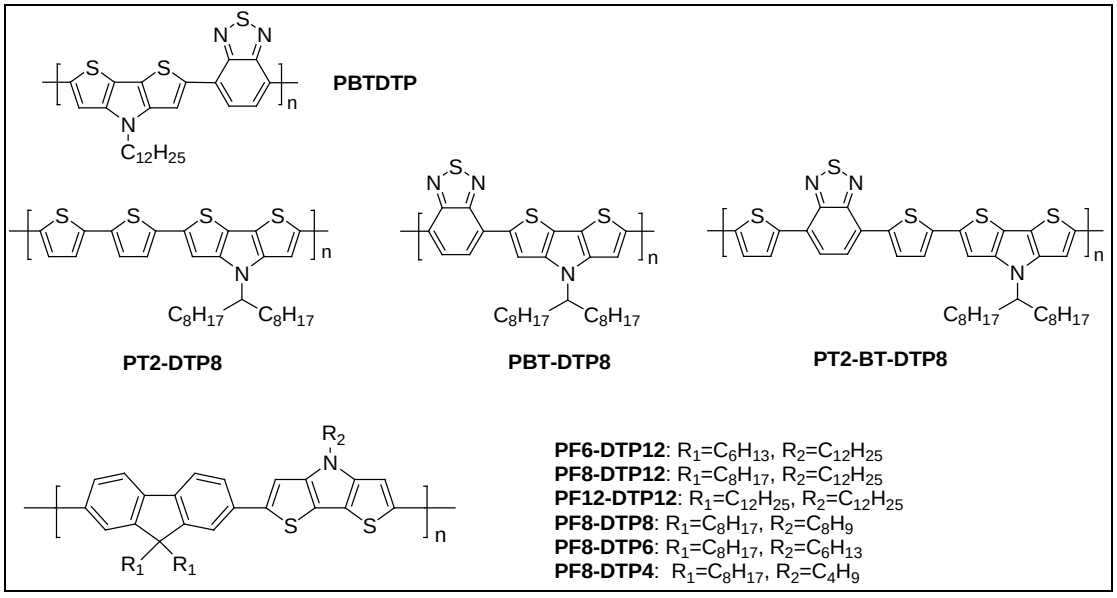

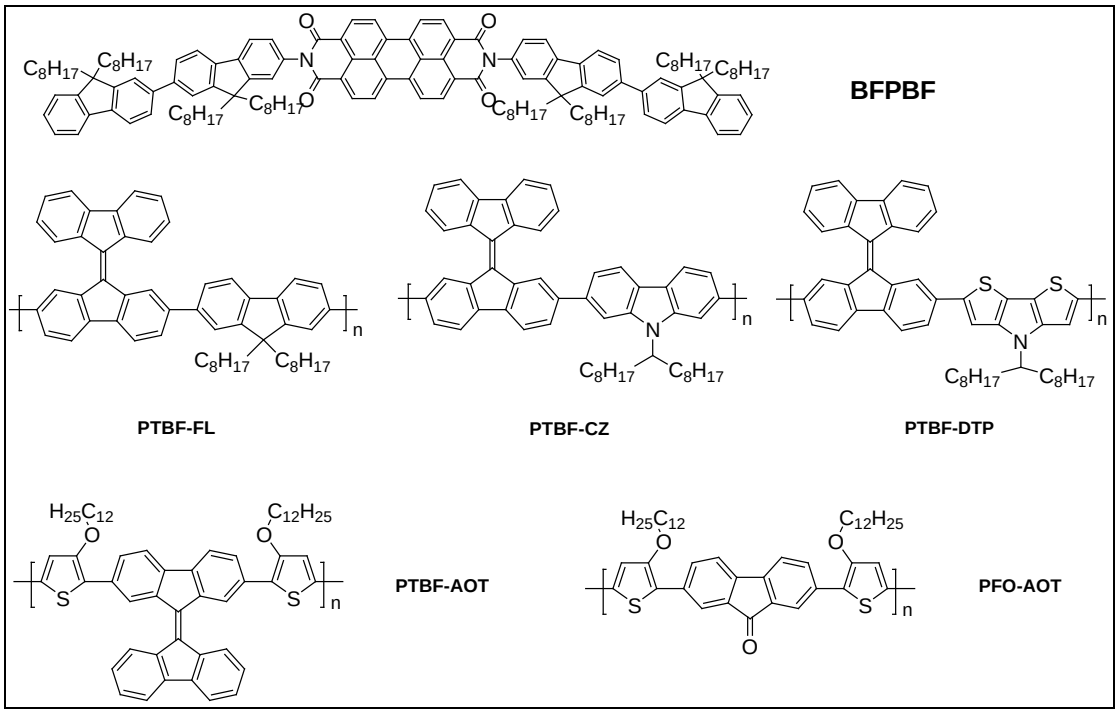

Figure 9.1 Novel p-type and n-type materials prepared in the dissertation.

In Chapter 3, a N-1-octyldithieno[3,2-b:2',3'-d]pyrrole based donor-acceptor polymer (**PBTDTP**) was synthesized and characterized. The preparation of the polymer was effected by using a Stille coupling polymerization and the structure of the polymer was confirmed by NMR spectroscopy. The polymer was further characterized with UV-vis spectroscopy and cyclic voltammetry. An optical band gap of around 1. 4 eV and a HOMO level of -5.0 eV and a LUMO level of -3.3 eV were determined. Spectroscopic investigation showed that **PBTDTP** afforded a broad absorption beyond 800 nm in the visible light region. In addition, the polymer's energy level matches with that of the common acceptor PCBM. These results are indicative that **PBTDTP** can serve as donor (p-type) material in organic electronics.

In Chapter 4 with a view to tune the polymer energy level on a molecular level, N-1-octylnonyldithieno[3,2-b:2',3'-d]pyrrole was copolymerized with units of different

electron-donating/accepting characteristics. A new series of DTP polymers (**PT2-DTP8, PBT-DTP8 and PT2-BT-DTP8**) containing bithiophene, benzothiadiazole and bisthiophenylbenzothiadiazole units were prepared via Stille coupling reaction. The synthesized polymers were found to be soluble in common organic solvents and thermally stable. UV-vis spectroscopy investigations indicate that **PBT-DTP8** and **PT2-BT-DTP8** depicted a band gap as low as 1.4 and ca 1.7 eV for **PT2-DTP8**. Electrochemical results revealed that HOMO energy levels of -5.02, -4.97 and -5.00 eV are respectively calculated for **PT2-DTP8**, **PBT-DTP8** and **PT2-BT-DTP8**. BHJ OPV devices using a blend of the polymers and PCBM as active layers were fabricated and their photovoltaic characteristics were determined. Amongst the devices, the active layer comprising a blend of **PT2-BT-DTP8**/PCBM exhibited the highest power conversion efficiency of 0.51%. The results indicate that these N-1-octylnonyldithieno[3,2-b:2',3'-d]pyrrole based polymers can be used as p-type materials in organic BHJ solar cells.

In Chapter 5, a series of alternative fluorene dithieno[3,2-b:2',3'-d]pyrrole copolymers (**PF-DTP**s) were prepared. With a view of investigating the pendant chain's influences on the polymers' properties, copolymers with various lengths of alkyl subsituents attached to fluorene and DTP units have been prepared. The lengths of substituted alkyl chains on fluorene and DTP units affect the polymers' solubility as well as their optical properties. Minor UV-vis absorption shifts which were observed between the solution and film phase indicate that structural rigidity are gained arising from the **PF-DTP**s backbone and further corroborated by the presence of vibronic features in their film phase. It is generally believed that structural planarity and rigidity could facilitate charge transfer and accordingly such polymers would thus

be potential candidates for applications in organic electronics such as OFETs. Reproducible cyclic voltammetry measurements revealed that **PF-DTP**s have prominent electron donating behaviour. At the same time, a HOMO energy level below than -5.45 eV can be calculated for the polymers, indicating that they are fairly stable electrochemically.

In Chapter 6, N, N' – Bis(9, 9, 9', 9'-tetraoctyl-bisfluoren-2-yl)-3, 4 : 9, 10-perylene bisimide (**BFPBF)**, which is n-type material, was prepared and investigated. **BFPBF** was found to be soluble in common organic solvents and thermally stable. In comparison to the N,N'-dialkyl functionalized perylene bisimides, the incorporation of alternative bisfluorenyl chromophores moieties improves the light harvesting ability of **BFPBF**. An optical band gap of 2.0 eV can be calculated and the intramolecular fluorescence quenching implies a photoinduced electron transfer occurring from the fluorenyl group to the perylene core. The LUMO level of **BFPBF** is -4.07 eV, which is comparable to that of **PCBM**. Organic BHJ photovoltaic device was fabricated by using the blend of P3HT/**BFPBF** as the active layer. Power conversion efficiency of 0.13% and a V_{oc} of 0.66 V was achieved for an non-optimised solar cell device.

In Chapter 7, a series of novel tetrabenzo[5,5']fulvalene (TBF) based polymers (**PTBF-FL**, **PTBF-CZ** and **PTBF-DTP**) were synthesized and their potentials as acceptor materials in BHJ OPV evaluated and discussed. These polymers were soluble in the commonly used organic solvents and thermally stable under nitrogen atmosphere. Compared with **PCBM**, these polymers have much more broader absorption in UV-vis light region. CV results showed that **PTBF-FL**, **PTBF-CZ** and

PTBF-DTP have LUMO levels at -3.35, -3.57 and -3.45 eV, which is higher than the **PCBM** LUMO level at -4.0 eV. Accordingly, a high V_{oc} can be expected for OPV devices using TBF based polymers as acceptor materials. The investigation of micro-structures indicated that the polymers are partially crystalline and this would be beneficial to charge transfer in devices.

In Chapter 8, novel conjugated polymers (**PTBF-AOT** and **PFO-AOT**) were prepared via Stille cross-coupling reactions. The new polymers incorporate alternative tetrabenzo[5,5]fulvalene or fluorone unit with alkoxyl chain substituted thiophene units in polymer backbones. **PTBF-AOT** and **PFO-AOT** were found to be thermally stable in inert atmosphere with a T_d above 300 ^oC. UV-vis spectroscopic investigations depicted the UV-vis absorption maxima at 446 nm for **PTBF-AOT** and 432 nm for **PFO-AOT**. A notable Stokes shift more than 200 nm for **PFO-AOT** can be observed in the photoluminescence spectra, indicating that effective charge transfer can occur in the polymer. The electron-accepting behaviours of the polymers are clearly displayed through the CV measurements and thus they can potentially be used as n-type materials. The results of XRD diffraction indicate that a high crystalline structure is achieved for **PFO-AOT** and a partial crystalline structure for **TBF-AOT**. The structural planarity and regularity of these polymers would facilitate their electron transporting properties.

9.2 Suggestions for future work

On the basis of findings in this dissertation, the following are suggested for the future work.

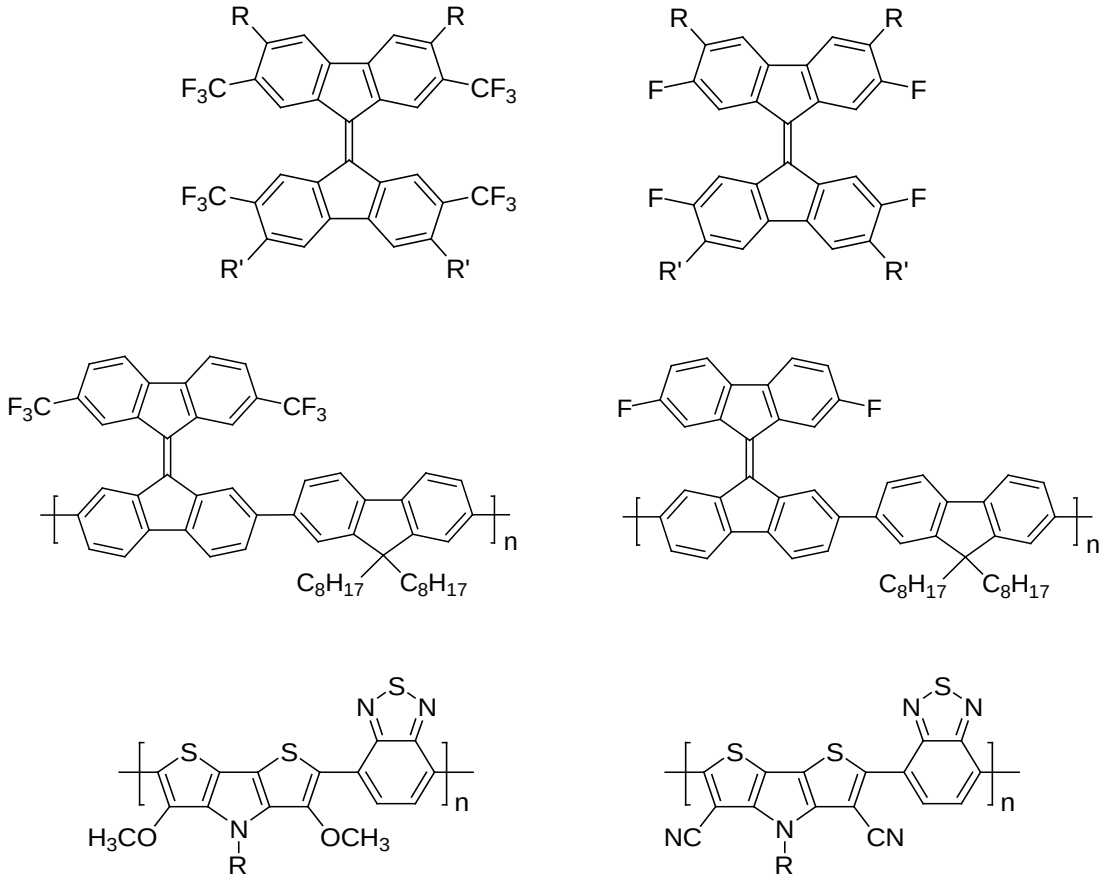

Figure 9.2 Examples of proposed molecules/polymers containing DTP or TBF moieties for organic electronics applications.

N-functionalized dithieno[3,2-b:2’,3’-d]pyrroles (DTPs) have flat molecular structures with good electron-donating character. Hence, DTPs can be promising building blocks for achieving donor-acceptor polymers. Polymers containing DTP and appropriate acceptor moieties are expected to have a low band gap and able to harvest sunlight effectively, so they are good candidates as donor materials in OPVs. Additionally, DTP molecule can still be modified by electron donating and electron withdrawing groups to tune the polymers properties and bandgaps. Subsequently, in comparison with P3HT, higher V_{oc} and PCE (> 5%) are expected to achieve in the

device based on the blend of the polymer containing DTP moiety and PC60BM (or PC70BM). Some examples of DTP based polymers with modification by electron-donating or electron-accepting groups are shown in **Figure 9.2** and these polymers might be potential candidates for application of different organic electronics.

On the other hand, the molecule tetrabenzo[5,5']fulvalene (TBF) were recently noticed for its electron-accepting characteristics, because of the steric strain relief and the gained in aromaticity after addition of one electron. Compared to another acceptor molecule C_{60}, one of advantages for TBF is versatile functionalization and thus the energy level as well as the solubility of materials can be easily tuned on a molecular level. Novel acceptor materials based on TBF can be prepared by careful design of molecular structures of target oligomers/polymers. These materials may be a new generation of electron acceptors in organic electronics with good qualities and are expectable to be processed from solution. For example, BHJ OPV devices using the active layer formed by blend of P3HT and the TBF type material are expected to have a high open circuit voltage which might be beyond 1.0 V. Some examples of TBF based oligomers/polymers are demonstrated in **Figure 9.2** and they are potential suitable candidates as n-type materials in organic electronics.

Reference:

(1) Chiang, C. K.; Jr. Fincher, C. R.; Park, Y. W.; Heeger, A. J. S. H.; Louis, E. J.; Gau, S. C.; MacDiarmid, A. G. "Electrical-Conductivity in Doped Polyacetylene" *Phys. Rev. Lett.* **1977**, *39*, 1098.

(2) Harrison, W. A. *Solid State Theory*; Dover, New York, 1979.

(3) Kittel, C. *Introduction to Solid State Physics*; John Wiley & Sons: New York, 1976.

(4) Chapin, D. M.; Fuller, C. S.; Pearson, G. L. "A New Silicon P-N Junction Photocell for Converting Solar Radiation Into Electrical Power" *J. Appl. Phys.* **1954**, *25*, 676.

(5) Green, M. A.; Emery, K.; King, D. L.; Igari, S.; Warta, W. "Solar Cell Efficiency Tables" *Prog. Photovolt.: Res. Appl.* **2003**, *11*, 347.

(6) Goetzberger, A.; Hebling, C.; Chock, H. W. "Photovoltaic Materials, History, Status and Outlook " *Mater. Sci. Eng. R* **2003**, *40*, 1.

(7) Johnson, J. C. *Chem. Eng. News* **2004**, *82*, 25.

(8) Frohne, H.; Shaheen, S.; Brabec, C.; Müller, D.; Sariciftci, N. S.; Meerholz, K. "Influence of The Anodic Work Function on The Performance of Organic Solar Cells" *Chem. Phys. Chem.* **2002**, *9*, 795.

(9) Allemand, P. M.; Koch, A.; Wudl, F.; Rubin, Y.; Diederich, F.; Alvarez, M. M.; Anz, S. J.; Whetten, R. L. "2 Different Fullerenes Have The Same Cyclic Voltammetry"*J. Am. Chem. Soc.* **1991**, *113*, 1050.

(10) Wudl, F. "The Chemical-Properties of Buckminsterfullerene (C-60) And The Birth and Infancy of Fulleroids" *Acc. Chem. Res.* **1992**, *25*, 157.

(11) Lee, S. K.; Zu, Y.; Herrmann, A.; Geerts, Y.; Müllen, K.; Bard, A. " Electrochemistry, Spectroscopy and Electrogenerated Chemiluminescence of Perylene, Terrylene, and Quaterrylene Diimides in Aprotic Solution" *J. Am. Chem. Soc* **1999**, *121*, 3513.

(12) Tang, C. W. "2-Layer Organic Photovoltaic Cell" *Appl. Phys. Lett.* **1986**, *48*, 183.

(13) Tsuzuki, T. T.; Shirota, Y.; Rostalski, J.; Meissner, D. "The Effect of Fullerene Doping on Photoelectric Conversion Using Titanyl Phthalocyanine and A Perylene Pigment " *Sol. Energy Mater. Sol. Cells* **2000**, *61*, 1.

(14) Zhou, X.; Blochwitz, J.; Pfeiffer, M.; Nollau, A.; Fritz, T.; Leo, K. "Enhanced Hole Injection into Amorphous Hole-Transport Layers of Organic Light-Emitting Diodes Using Controlled p-Type Doping" *Adv. Funct. Mater.* **2001**, *11*, 310.

(15) Wöhrle, D.; Meissner, D. "Organic Solar-Cells" *Adv. Mater.* **1991**, *3*, 129.

(16) Winder, C.; Sariciftci, N. S. "Low Bandgap Polymers for Photon Harvesting in Bulk Heterojunction Solar Cells" *J. Mater. Chem* **2004**, *14*, 1077.

(17) Harrison, M. G.; Gruener, J.; Spencer, G. C. W. "Analysis of The Photocurrent Action Spectra of MEH-PPV Polymer Photodiodes" *Phys. Rev. B* **1997**, *55*, 7831.

(18) Petterson, L. A. A.; Roman, L. S.; Inganas, O. "Modeling Photocurrent Action Spectra of Photovoltaic Devices Based on Organic Thin Films" *J. Appl. Phys.* **1999**, *86*, 487.

(19) Hoppe, H.; Sariciftci, N. S. "Organic Solar Cells: An Overview" *J. Mater. Chem.* **2004**, *19*, 1924.

(20) Peumans, P.; Uchida, S.; Forrest, S. "Efficient Bulk Heterojunction Photovoltaic Cells Using Small-Molecular-Weight Organic Thin Films" *Nature* **2003**, *425*, 158.

(21) Yu, G.; Heeger, A. J. "Charge Separation and Photovoltaic Conversion in Polymer Composites With Internal Donor-Acceptor Heterojunction" *J. Appl. Phys.* **1995**, *78*, 4510.

(22) Miranda, P. B.; Moses, D.; Heeger, A. J. "Ultrafast Photogeneration of Charged Polarons in Conjugated Polymers" *Phys. Rev. B* **2001**, *64*, 81201.

(23) Mozer, A.; Sariciftci, N. S. "Conjugated Polymer Photovoltaic Devices and Materials" C. R. *Chimie* **2006**, *9*, 568.

(24) Hoppe, H.; Sariciftci, N. S. "Organic Solar Cells: An overview" *J. Mater. Chem.* **2004**, *19*, 1924.

(25) Rostalski, J.; Meissner, D. "Monochromatic Versus Solar Efficiencies of Organic Solar Cells" *Sol. Energy Mater. Sol. Cells* **2000**, *61*, 87.

(26) Brabec, C. J.; Cravino, A.; Meissner, D.; Sariciftci, N. S.; Fromherz, T.; Minse, M.; Sanchez, L.; Hummelen, J. C. "Origin of The Open Circuit Voltage of Plastic Solar Cells" *Adv. Funct. Mater.* **2001**, *11*, 374.

(27) Scharber, M. C,; Mühlbacher, D.; Koppe, M.; Denk, P.; Waldauf, C.; Heeger, A. J.; Brabec, C. "Design Rules for Donors in Bulk-Heterojunction Solar Cells - Towards 10 % Energy-Conversion Efficiency" *Adv. Mater.* **2006**, *18*, 789.

(28) Mallairas, G. G.; Salem, J. R.; Brock, P. J.; Scott, J. C. "Photovoltaic Measurement of The Built-in Potential in Organic Light Emitting Diodes and Photodiodes" *J. Appl. Phys.* **1998**, *84*, 1583.

(29) Liu, J.; Shi, Y.; Yang, Y. "Solvation-Induced Morphology Effects on The Performance of Polymer-based Photovoltaic Devices" *Adv. Funct. Mater.* **2001**, *11*, 420.

(30) Van Duren, J. J.; Loos, J.; Morissey, F.; Leewis, C. M.; Kivits, K. P.; Vanzendoorn, L. J.; Rispens, M. T.; Hummelen, J. C.; Janssen, R. A. J. "In-situ Compositional and Structural Analysis of Plastic Solar Cells" *Adv. Funct. Mater.* **2002**, *12*, 665.

(31) Van Duren, J.; Yang, X.; Loos, J.; Bulle-Lieuwma, C. W. T.; Sievel, A. B.; Hummelen, J. C.; Janssen, R. A. J. "Relating The Morphology of Poly(p-phenylene vinylene)/Methanofullerene Blends to Solar-cell Performance" *Adv. Funct. Mater.* **2004**, *14*, 425.

(32) Hoppe, H.; Niggemann, M.; Winder, C.; Kraut, J.; Hiesgh, R.; Hinsch, A.; Meissner, D.; Sariciftci, N. S. "Nanoscale Morphology of Conjugated polymer/fullerene-based Bulk-heterojunction Solar Cells" *Adv. Funct. Mater.* **2004**, *14*, 1005.

(33) Martens, T.; Hoen, J. D.; Munters, T.; Beelen, Z.; Goris, L.; Monca, J.; Oliesloeger, M. D.; Vanderzende, D.; De Schopper, L.; Andriessen, R. "Disclosure of The Nanostructure of MDMO-PPV : PCBM Bulk Hetero-junction Organic Solar Cells by a Combination of SPM and TEM" *Synth. Met.* **2003**, *138*, 243.

(34) Arias, A. C.; MacKenzie, J. D.; Stevenson, R.; Halls, J. M.; Inbasekaran, M.; Woo, E. P.; Richards, D.; Friend, R. H. "Photovoltaic Performance and Morphology of Polyfluorene Blends: A Combined Microscopic and Photovoltaic Investigation" *Macromolecules* **2001**, *34*, 6005.

(35) Gadisa, A.; Svensson, M.; Andersson, M. R.; Inganäs, O. "Correlation Between Oxidation Potential and Open-circuit Voltage of Composite Solar Cells Based on Blends of Polythiophenes/fullerene Derivative" *Appl. Phys. Lett.* **2004**, *84*, 1609.

(36) Van Duren, J.; Yang, X.; Loos, J.; Bulle-Lieuwma, C. W. T.; Sievel, A. B.; Hummelen, J. C.; Janssen, R. A. J. "Relating the Morphology of Poly(p-phenylene vinylene)/methanofullerene Blends to Solar-cell Performance" *Adv. Funct. Mater.* **2004**, *14*, 425.

(37) Lilienfeld, J. E. *U. S. patent No 1545175* **1930**.

(38) Tsumura, A.; Koezuka, H.; Ando, T. "Macromolecular Electronic Device - Field-Effect Transistor with A Polythiophene Thin-film" *Appl. Phys. Lett.* **1986**, *49*, 1210.

(39) Koezuka, H.; Tsumura, A.; Ando, T. "Field-effect Transistor with Polythiophene Thin-Film" *Synth. Met.* **1987**, *18*, 669.

(40) Ong, B. S.; Wu, Y.; Liu, P.; Gardner, S. "High-performance Semiconducting Polythiophenes for Organic Thin-film Transistors" J. Am. Chem. Soc. **2004**, *126*, 3378.

(41) Sirringhaus, H.; Tessler, N.; Friend, R. H. "Integrated Optoelectronic Devices Based on Conjugated Polymers" *Science* **1998**, *280*, 1741.

(42) Dimitrakopoulos, C. D.; Malenfant, P. R. L. "Organic Thin Film Transistors for Large Area Electronics" *Adv. Mater.* **2002**, *14*, 99.

(43) Halik, M.; Klauk, H.; Zschieschang, U.; Schmid, G.; Ponomarenko, S.; Kirchmeyer, S.; Weber, W. "Relationship Between Molecular Structure and

Electrical Performance of Oligothiophene Organic Thin Film Transistors" *Adv. Mater*. **2003**, *15*, 917.

(44) Dinelli, F.; Murgia, M.; Levy, P.; Cavallini, M.; Biscarini, F.; De Leeuw, D. M. "Spatially Correlated Charge Transport in Organic Thin Film Transistors" *Phys. Rev. Lett.* **2004**, *92*, 116802.

(45) Peisert, H.; Knupfer, M.; Fink, J. *Recent Res. Dev. Appl. Phys.* **2002**, *5*, 129.

(46) Bredas, J. L.; Calbert, J. P.; da Silva, D. A.; Cornil, J. "Organic Semiconductors: A Theoretical Characterization of the Basic Parameters Governing Charge Transport" *Proc. Natl. Acad. Sci. U.S.A.* **2002**, *99*, 5804.

(47) Horowitz, G.; Hajlaoui, R.; Bourguiga, R.; Haijlaoui, M. "Theory of the Organic Field-effect Transistor" *Synth. Met.* **1999**, *101*, 401.

(48) Katz, H. E.; Bao, Z. "The Physical Chemistry of Organic Field-effect Transistors" *J. Phys. Chem. B* **2000**, *104*, 671.

(49) Shaheen, S. E.; Brabec, C. J.; Sariciftci, N. S.; Padinger, F.; Fromherz, T.; Hummelen, J. C. "2.5% Efficient Organic Plastic Solar Cells" *Appl. Phys. Lett.* **2001**, *78*, 841.

(50) Van Duren, J.; Yang, X.; Loos, J.; Bulle-Lieuwma, C. W. T.; Sievel, A. B.; Hummelen, J. C.; Janssen, R. A. J. "Relating the Morphology of Poly(p-phenylene vinylene)/methanofullerene Blends to Solar-cell Performance" *Adv. Funct. Mater*. **2004**, *14*, 425.

(51) Ibrahim, M. A.; Roth, H. K.; Schroedner, M.; Kalvin, A.; Zhokhavets, U.; Gobsch, G.; Scharff, P.; Sensfuss, S. "The Influence of the Optoelectronic Properties of Poly(3-alkylthiophenes) on the Device Parameters in Flexible Polymer Solar Cells" *Org. Electron.* **2005**, *6*, 65.

(52) Coppo, P.; Turner, M. L. "Cyclopentadithiophene Based Electroactive Materials" *J. Mater. Chem.* **2005**, *15*, 1123.

(53) Hutchison, G. R.; Ratner, M. A.; Marks, T. J. "Hopping Transport in Conductive Heterocyclic Oligomers: Reorganization Energies and Substituent Effects" *J. Am. Chem. Soc.* **2005**, *127*, 2339.

(54) Chirvaze, D.; Chiguvare, Z.; Knipper, M.; Parisi, J.; Dyakonov, V.; Hummelen, J. C. "Temperature Dependent Characteristics of Poly(3 hexylthiophene)-fullerene Based Heterojunction Organic Solar Cells" *J. Appl. Phys.* **2003**, *93*, 3376.

(55) Reyes, R. R.; Kim, K.; Carroll, D. L. "High-efficiency Photovoltaic Devices Based on Annealed Poly(3-hexylthiophene) and 1-(3-methoxycarbonyl)-Propyl-1-phenyl-(6,6)C-61 Blends" *Appl. Phys. Lett.* **2005**, *87*, 083506

(56) McCullough, R. D.; Lowe, R. D. "Enhanced Electrical-Conductivity in Regioselectively SynthesizedD Poly(3-Alkylthiophenes)" *J. Chem. Soc., Chem. Commun.* **1992**, 70.

(57) McCullough, R. D.; Lowe, R. D.; Jarayaman, M.; Anderson, D. L. "Design, Synthesis, and Control of Conducting Polymer Aachitectures - Structurally Homogeneous Poly(3-Alkylthiophenes)" *J. Org. Chem.* **1993**, *58*, 904.

(58) Loewe, R. S.; Ewbank, P. C.; Liu, J.; Zhai, L.; McCullough, R. D. "Regioregular, Head-to-tail Coupled Poly(3-alkylthiophenes) Made Easy by the GRIM Method: Investigation of the Reaction and the Origin of Regioselectivity" *Macromolecules* **2001**, *34*, 4324.

(59) Prosa, T. J.; Winokur, M. J.; Moulton, M. M.; Smith, P.; Heeger, A. J. "X-Ray Structural Studies of Poly(3-Alkylthiophenes) - an Example of an Inverse Comb" *Macromolecules* **1992**, *25*, 4364.

(60) Kim, J.; Kim, S.; Lee, H.; Lee, K.; Ma, W.; Huong, X.; Heeger, A. J. "New Architecture for High-efficiency Polymer Photovoltaic Cells Using Solution-based Titanium Oxide as an Optical Spacer" *Adv. Mater.* **2006**, *18*, 572.

(61) Schuler, S. *Appl. Phys. A* **2003**, *79*, 37.

(62) Padinger, F.; Rittberger, R.; Sariciftci, N. S. "Effects of Postproduction Treatment on Plastic Solar Cells" *Adv. Funct. Mater.* **2003**, *13*, 85.

(63) Ahn, T.; Sein Holta, H. L. "Effect of Annealing of Polythiophene Derivative for Polymer Light-emitting Diodes" *Appl. Phys. Lett.* **2002**, *80*, 392.

(64) Al Ibrahim, M.; Roth, H. K.; Zhokhavets, U.; Gobsch, G.; Sensfuss, S. "Flexible Large Area Polymer Solar Cells Based on Poly(3-hexylthiophene)/fullerene" *Sol. Energy Mater. Sol. Cells* **2005**, *85*, 13.

(65) Koeckelberghs, G.; Cremer, L. D.; Vanormelingen, W.; Verbiest, T.; Persoons, A.; Samyn, C. "Synthesis and Properties of Polydithieno[3,2-b : 2 ',3 '-d]pyrroles: A Class of Soluble (chiral) Conjugated Polymers with a Stable Oxidized State" *Macromolecules* **2005**, *38*, 4545.

(66) Odom, S. A.; Lancaster, K.; Beverina, L.; Lefler, K. M.; Thompson, N. J.; Coropceanu, V.; Bredas, J. L.; Marder, S. R.; Barlow, S. "Bis[bis-(4-alkoxyphenyl) amino] Derivatives of Dithienylethene, Bithiophene, Dithienothiophene and Dithienopyrrole: Palladium-catalysed Synthesis and Highly Delocalised Radical Cations" *Chem. Euro. J.* **2007**, *13*, 9637.

(67) Radke, K. R.; Ogawa, K.; Rasmussen, S. C. "Highly Fluorescent Oligo thiophenes Through the Incorporation of Central Dithieno[3,2-b:2',3'-d]pyrrole Units" *Org. Lett.* **2007**, *7*, 5253.

(68) Ogawa, K.; Rasmussen, S. C. "N-Functionalized Poly(dithieno[3,2-*b*:2',3'-*d*]pyrrole)s: Highly Fluorescent Materials with Reduced Band Gaps" *Macromolecules* **2006**, *39*, 1771.

(69) K.Ogawa; Radke, K. R.; Rothstein, S. D.; Rasmussen, S. C. "A Simple and Efficient Route to N-Functionalized Dithieno[3,2-*b*:2',3'-*d*]pyrroles: Fused-Ring Building Blocks for New Conjugated Polymeric Systems" *J. Org. Chem.* **2001**, *66*, 9067.

(70) Liu, J. Y.; Zhang, R.; Sauvé, G.; Kowalewski, T.; McCullough, R. D. "Highly Disordered Polymer Field Effect Transistors: N-Alkyl Dithieno[3,2-b : 2 ',3 '-d]pyrrole-based Copolymers with Surprisingly High Charge Carrier Mobilities" *J. Am. Chem. Soc.* **2008**, *130*, 13167.

(71) Chang, J.; Sun, B.; Breiby, D. W.; Nielsen, M. M.; Sölling, T. I.; Giles, M.; McCulloch, I.; Sirringhaus, H. "Enhanced Mobility of Poly(3-hexylthiophene) Transistors by Spin-coating from High-boiling-point Solvents" *Chem. Mater.* **2004**, *23*, 4772.

(72) Grell, M.; Redecker, M.; Whitehead, K. S.; Bradley, D. D. C.; Inbasekaran, M.; Woo, E. P.; Wu, W. "Monodomain Alignment of Thermotropic Fluorene Copolymers" *Liq. Cryst.* **1999**, *26*, 1403.

(73) Sirringhaus, H.; Wilson, R. J.; Friend, R. H.; Inbasekaran, M.; Wu, W.; Woo, E. P.; Grell, M.; Bradley, D. D. C. "Mobility Enhancement in Conjugated

Polymer Field-effect Transistors through Chain Alignment in a Liquid-crystalline Phase" *Appl. Phys. Lett.* **2000**, *77*, 406.

(74) Riklin, M.; Zelewsky, A. v.; Bashall, A.; McPartlin, M.; Baysal, A.; Connor, J. A.; Wallis, J. D. "Synthesis, Structure and Chemistry of a Twisted Olefinic Bis-didentate Proligand: 5,5'-bi-5H-Cyclopenta[2,1-b: 3,4-b ']dipyridinylidene" *Helv. Chim. Acta* **1999**, *82*, 1666.

(75) Cohen, Y.; Klein, J.; Rabinovitz, M. "Stable Polycyclic Anions - Dianions from Overcrowded Ethylenes" *J. Chem. Soc. Chem. Commun.* **1986**, 1071.

(76) Brunetti, F. G.; Gong, X.; Tong, M.; Heeger, A. J.; Wudl, F. "Strain and Huckel Aromaticity: Driving Forces for a Promising New Generation of Electron Acceptors in Organic Electronics" *Angew. Chem. Int. Ed.* **2010**, *49*, 532.

(77) Riklin, M.; Zelewsky, A. v.; Bashall, A.; McPartlin, M.; Baysal, A.; Connor, J. A.; Wallis, J. D. "Synthesis, Structure and Chemistry of a Twisted Olefinic Bis-didentate Proligand: 5,5'-bi-5H-Cyclopenta[2,1-b :3,4-b ']dipyridinylidene" *Helv. Chim. Acta* **1999**, *82*.

(78) Khor, E.; Ng, S. C.; Li, H. C.; Chai, S. "Selective Functionalization of 2,2'-Bithiophenes" *Heterocycles* **1991**, *32*, 1805.

(79) Koeckelberghs, G.; Cremer, L. D.; Persoons, A.; Verbiest, T. "Influence of the Substituent and Polymerization Methodology on the Properties of Chiral Poly(dithieno[3,2-b : 2',3'-d]pyrrole)s" *Macromolecules* **2007**, *40*, 4173.

(80) Neto, B. A. D. S.; Lopes, A. S.; Wuest, M.; Costa, V. E. U.; G. Ebeling, J. D. "Reductive Sulfur Extrusion Reaction of 2,1,3-benzothiadiazole Compounds:

A New Methodology Using $NaBH_4/CoCl_2$ Center Dot $6H(_2)O((cat))$ as the Reducing System" *Tetrahedron. Lett.* **2005**, *46*, 6843.

(81) Kim, J. J.; Choi, H.; Lee, J. W.; Kang, M. S.; Song, K.; Kang, S. O.; Ko, J. "A Polymer Gel Electrolyte to Achieve ≥6% Power Conversion Efficiency with a Novel Organic Dye Incorporating a Low-band-gap Chromophore" *J. Mater. Chem* **2008**, *18*, 5223.

(82) Moulé, A. J.; Tsami, A.; Bünnagel, T. W.; Forster, M.; Kronenberg, N. M.; Scharber, M.; Koppe, M.; Morana, M.; Brabec, C. J.; Meerholz, K.; Scherf, U. "Two Novel Cyclopentadithiophene-Based Alternating Copolymers as Potential Donor Components for High-Efficiency Bulk-Heterojunction-Type Solar Cells" *Chem. Mater.* **2008**, *20*, 4045.

(83) Ranger, M.; Rondeau, D.; Leclerc, M. "Molecular Design and Characterization of Chromic Polyfluorene Derivatives" *Macromolecules* **1997**, *30*, 7686.

(84) Yu, W. L.; Pei, J.; Cao, Y.; Huang, W.; Heeger, A. J. "New Efficient Blue Light Emitting Polymer for Light Emitting Diodes" *Chem.Comm.* **1999**, 1837.

(85) Belfield, K. D.; Schafer, K. J.; Mourad, W.; Reinhardt, B. A. "Synthesis of New Two-photon Absorbing Fluorene Derivatives via Cu-Mediated Ullmann Condensations" *J. Org. Chem.* **2000**, *65*, 4475.

(86) Dudek, S. P.; Pouderoijen, M.; Abbel, R.; Schenning, A. P. H. J.; Meijer, E. W. "Synthesis and Energy-transfer Properties of Hydrogen-bonded Oligofluorenes" *J. Am. Chem. Soc.* **2005**, *127*, 11763.

(87) Ahrens, M. J.; Tauber, M. J.; Wasielewski, M. R. "Bis(n-octylamino)perylene-3,4 : 9,10-bis(dicarboximide)s and Their Radical Cations: Synthesis, Electrochemistry, and ENDOR Spectroscopy" *J. Org. Chem.* **2006**, *71*, 2107.

(88) Rathnayake, H. P.; Cirpan, A.; Karasz, F. Z.; Odoi, M. Y.; Hammer, N. I.; Barnes, M. D.; Lahti, P. M. "Luminescence of Molecular and Block Copolymeric 2,7-bis(phenylethenyl)-fluorenones; Identifying Green-band Emitter Sites in a Fluorene-based Luminophore" *Chem. Mater.* **2007**, *19*, 3265.

(89) Mills, N. S.; Burns, E. E.; Hodges, J.; Gibbs, J.; Esparza, E.; Malandra, J. L.; Koch, J. "Dications of Fluorenylidenes. Electronic Effects on the Paratropicity/antiaromaticity of 2,7-Disubstituted Fluorenyl Cations" *J. Org. Chem.* **1998**, *63*, 3017.

(90) Zhou, E.; Yamakawa, S.; Tajima, K.; Yang, C.; Hashimoto, K. "Synthesis and Photovoltaic Properties of Diketopyrrolopyrrole-Based Donor−Acceptor Copolymers" *Chem. Mater.* 2009, *21*, 4055.

(91) Sonntag, M.; Strohriegl, P. "Novel 2,7-Linked Carbazole Trimers as Model Compounds for Conjugated Carbazole Polymers" *Chem. Mater.* **2004**, *16*, 4736.

(92) Guo, X.; Watson, M. D. "Conjugated Polymers from Naphthalene Bisimide" *Org. Lett.* **2008**, *10*, 5333.

(93) Takahashi, M.; Masui, K.; Sekiguchi, H.; Kobayashi, N.; Mori, A.; Funahashi, M.; Tamaoki, N. "Palladium-catalyzed C-H Homocoupling of Bromothiophene Derivatives and Synthetic Application to Well-defined Oligothiophenes" *J. Am. Chem. Soc.* **2006**, *128*, 10930.

(94) Campos, L. M.; Tontcheva, A.; Guenes, S.; Sonmez, G.; Neugebauer, H.; Sariciftci, N. S.; Wudl, F. "Extended Photocurrent Spectrum of A Low Band gap Polymer in A Bulk Heterojunction Solar Cell" *Chem. Mater.* **2005**, *17*, 4031.

(95) Sonmez, G.; Meng, H.; Wudl, F. "Extended Photocurrent Spectrum of A Low Band Gap Polymer in A Bulk Heterojunction Solar Cell" *Chem. Mater.* **2003**, *15*, 4923.

(96) Ajayaghosh, A. "Donor–acceptor Type Low Band Gap Polymers:polysquaraines and Related Systems" *Chem. Soc. Rev.* 2003, *32*, 181.

(97) Neef, C. J.; Brotherston, I. D.; Ferraris, J. P. "Synthesis and Electronic Properties of Poly(2-phenylthieno[3,4-b]thiophene): A New Low Band Gap Polymer" *Chem. Mater.* **1999**, *11*, 1957.

(98) Lakshmikantham, M. V.; Lorcy, D.; Scordilis-Kelley, C.; Wu, X.; Parakka, J. P.; Metzger, R. M.; Cava, M. P. "Poly(Naphtho[2,3-c]thiophene-alt-bithiophene) - A Novel Low-band-gap Polymer" *Adv. Mater.* **1993**, *5*, 723.

(99) Pomerantz, M.; Chaloner-Gill, B.; Harding, L. O.; Tseng, J. J.; Pomerantz, W. J. "Poly(2,3-dihexylthieno[3,4-B]pyrazine) - A New Processable Low Band-gap Polyheterocycle" *J. Chem. Soc. Chem. Commun.* **1992**, *1992*, 1672.

(100) Brabec, C. J.; Sariciftci, N. S.; Hummelen, J. C. "Plastic Solar Cells" *Adv. Funct. Mater.* **2001**, *11*, 15.

(101) Coakley, K. M.; McGehee, M. D. "Conjugated Polymer Photovoltaic Cells" *Chem. Mater.* **2004**, *16*, 4533.

(102) Bundgaard, E.; Krebs, F. C. "Low Band Gap Polymers for Organic Photovoltaics" *Sol. Energy Mater. Sol. Cells* **2007**, *91*, 954.

(103) Roncali, J. "Synthetic Principles for Bandgap Control in Linear pi-Conjugated Systems" *Chem. Rev.* **1997**, *97*, 173.

(104) Chen, H. Y.; Hou, J.; Zhang, S.; Liang, Y.; Yang, G.; Yang, Y.; Yu, L.; Wu, Y.; Li, G. " Polymer Solar Cells with Enhanced Open-circuit Voltage and Eefficiency" *Nat. Photonics* **2009**, *13*, 649.

(105) Kovacic, P.; Jones, M. B. "Dehydro Coupling of Aromatic Nuclei by Catalyst Oxidant Systems - Poly(para-phenylene)" *Chem. Rev.* **1987**, *87*, 357.

(106) Pan, X. Y.; Liu, S. P.; Chan, H. S. O.; Ng, S. C. "Novel Fluorescent Carbazolyl-pyridinyl Alternating Copoloymers: Synthesis, Characterization, and Properties" *Macromolecules* **2005**, *38*, 7629.

(107) Kroon, R.; Lenes, M.; Hummelen, J. C.; Blom, P. W. M.; DeBoer, A. B. "Small Bandgap Polymers for Organic Solar Cells (polymer material development in the last 5 years)" *Poly. Rev.* **2008**, *48*, 531.

(108) Kitamura, C.; Tanaka, S.; Yamashita, Y. "Design of Narrow-bandgap Polymers. Syntheses and Properties of Monomers and Polymers Containing Aromatic-donor and o-Quinoid-acceptor Units" *Chem. Mater.* **1996**, *8*, 570.

(109) Jayakannan, M.; Hal, P. A. V.; Jannsen, R. A. J. *J.* "Synthesis and Structure-property Relationship of New Donor-acceptor-type Conjugated Monomers and Polymers on the Basis of Thiophene and Benzothiadiazole" *Polym. Sci. Polym. Chem.* **2002**, *40*, 251.

(110) Koppe, M.; Scharber, M.; Brabec, C.; Duffy, W.; Heeney, M.; McCulloch, I. "Polyterthiophenes as Donors for Polymer Solar Cells" *Adv. Funct. Mater.* **2007**, *17*, 1371.

(111) Shi, C. J.; Yao, Y.; Yang, Y.; Pei, Q. B. "Regioregular Copolymers of 3-Alkoxythiophene and Their Photovoltaic Application" *J. Am. Chem. Soc.* **2006**, *128*, 8980.

(112) Schilinsky, P.; Asawapirom, U.; Scherf, U.; Biele, M.; Brabec, C. J. "Influence of the Molecular Weight of Poly(3-hexylthiophene) on the Performance of Bulk Heterojunction Solar Cells" *Chem. Mater.* **2005**, *17*, 2175.

(113) He, M. Q.; Zhang, F. X. "Synthesis and Structure of Alkyl-substituted Fused Thiophenes Containing up to Seven Rings" *J. Org. Chem.* **2007**, *72*, 442.

(114) Xiao, K.; Liu, Y. Q.; T. Qi, W. Z.; Wang, F.; Gao, J. H.; Qiu, W. F.; Ma, Y. Q.; Cui, G. L.; Chen, S. Y.; Zhan, X. W.; Yu, G.; Qin, J. G.; Hu, W. P.; Zhu, D. B. "A Highly pi-Stacked Organic Semiconductor for Field-effect Transistors Based on Linearly Condensed Pentathienoacene" *J. Am. Chem. Soc.* **2005**, *127*, 13281.

(115) M, X. J.; Chan, H. S. O.; Ng, S. C.; Chung, N. T. S. "Polymers Synthesized from (3-Alkylthio)thiophenes by the FeCl3 Oxidation Method" *Synth. Met.* **2002**, *132*, 63.

(116) Chen, Z. K.; Zheng, Y.; Yan, H.; Facchetti, A. "Naphthalenedicarboximide- vs Perylenedicarboximide-Based Copolymers. Synthesis and Semiconducting Properties in Bottom-Gate N-Channel Organic Transistors" *J. Am. Chem. Soc.* **2009**, *131*, 8.

(117) Tang, W. H.; Ke, L.; Chen, Z. K. "Incorporating Perylene Moiety into Poly(phenothiazine-co-bithiophene) Backbone for Higher Charge Transport" *J. Phys. Chem. B* **2008**, *112*, 3590.

(118) Ogawa, K.; Rasmussen, S. C. "N-functionalized poly(dithieno[3,2-b : 2 ',3 '-d]pyrrole)s: Highly Fluorescent Materials with Reduced Band Gaps" *Marcromolecules* **2006**, *39*, 1771.

(119) Guy, K.; Lieven, D. C.; André, P.; Thierry, V. "Influence of the Substituent and Polymerization Methodology on the Properties of Chiral Poly(dithieno[3,2-*b*:2‘,3‘-*d*]pyrrole)s" *Marcromolecules* **2007**, *40*, 4173.

(120) Steckler, T. T.; Zhang, X.; Hwang, J.; Honeyager, R.; Ohira, S.; Zhang, X. H.; Grant, A.; Ellinger, S.; Odom, S. A.; Sweat, D.; Tanner, D. B.; Rinzler, A. G.; Barlow, S.; Bredas, J. L.; B, K.; Marder, S. R.; Reynolds, J. R. "A Spray-Processable, Low Bandgap, and Ambipolar Donor-Acceptor Conjugated Polymer" *J. Am. Chem. Soc.* **2009**, *131*, 2824.

(121) Karla, R. R.; Katsu, O.; Seth, C. R. "Highly Fluorescent Oligothiophenes through the Incorporation of Central Dithieno[3,2-b:2¢,3¢-d]pyrrole Units" *Org. Lett.* **2005**, *7*, 5253.

(122) Mühlbacher, D.; Scharber, M.; Morana, M.; Zhu, Z.; Waller, D.; Gaudiana, R.; Brabec, C. "High Photovoltaic Performance of A Low-bandgap Polymer" *Adv. Mater.* **2006**, *18*, 2884.

(123) Brabec, C. J.; Winder, C.; Sariciftci, N. S.; Hummelen, J. C.; Dhanabalan, A.; Hal, P. A. v.; Janssen, R. A. J. "A Low-bandgap Semiconducting Polymer for Photovoltaic Devices and Infrared Emitting Diodes" *Adv. Funct. Mater.* **2002**, *12*, 709.

(124) Kim, J. Y.; Lee, K.; Coates, N. E.; Moses, D.; Nguyen, T. Q.; M. Dante, A. J. H. "Efficient Tandem Polymer Solar Cells Fabricated by All-solution Processing" *Science* **2007**, *317*, 222.

(125) Bundgaard, E.; Krebs, F. C. "Low-band-gap Conjugated Polymers Based on Thiophene, Benzothiadiazole, and Benzobis(thiadiazole)" *Marcromolecules* **2006**, *39*, 2823.

(126) Connelly, N. G.; Geiger, W. E. "Chemical Redox Agents for Organometallic Chemistry" *Chem. Rev.* **1996**, *96*, 877.

(127) Roncali, J. "Molecular Engineering of the Band Gap of pi-Conjugated Systems: Facing Technological Applications" *Macromol. Rapid Commun.* **2007**, *28*, 1761.

(128) Hu, X.; Shi, M.; Zuo, L.; Nan, Y.; Liu, Y.; Fu, L.; Chen, H. "Synthesis , Characterization, and Photovoltaic Property of A Low Band Gap Polymer Alternating Dithienopyrrole and Thienopyrroledione Units" *Polymer.* **2011**, *52,* 2559.

(129) Shi, M.; Deng, D.; Chen, L.; Ling, J.; Fu, L.; Hu, X.; Chen, H. "Design and synthesis of Dithieno[3,2-b:2'3'-d]pyrrole-Based Conjugated Polymers for Photovoltaic Applications: Consensus between Low Band Gap and Low HOMO Energy Level" *J.Poly.Sci. A, Poly. Chem.* **2011**, *49*, 1453.

(130) Sahu, D.; Padhy, H.; Patra, D.; Huang, J.; Chu, C.; Lin, H. "Synthesis and Characterization of Novel Low-Bandgap Triphenylamine-Based Conjugated Polymers with Main-Chain Donors and Pendent Acceptors for Organic Photovoltaics" *J.Poly.Sci. A, Poly. Chem.* **2010**, *48*, 5812.

(131) Bao, Z.; Rogers, J. A.; Katz, H. E. "Printable Organic and Polymeric Semiconducting Materials and Devices" *J. Mater. Chem.* **1999**, *9*, 1895.

(132) Locklin, J.; Li, D.; Mannsfeld, S.; Borkent, E.; Meng, H.; Advincula, R.; Bao, Z. "Organic Thin Film Transistors Based on Cyclohexyl-substituted Organic Semiconductors" *Chem. Mater.* **2005**, *17*, 3366.

(133) McCullough, R. D.; Lowe, R. D.; Jayaraman, M.; Anderson, D. L. "Design, Synthesis, and Control of Conducting Polymer Architectures - structurally Homogeneous Poly(3-alkylthiophene)" *J. Org. Chem.* **1993**, *58*, 904.

(134) Heeney, M.; Bailey, C.; Genevicius, K.; Shkunov, M.; Sparrowe, D.; Tierney, S.; McCulloch, I. "Stable Polythiophene Semiconductors Incorporating Thieno[2,3-b]thiophene" *J. Am. Chem. Soc.* **2005**, *127*, 1078.

(135) Blouin, N.; Michaud, A.; Leclerc, M. "A Low-bandgap Poly(2,7-carbazole) Derivative for Use in High-performance Solar Cells" *Adv. Mater.* **2007**, *19*, 2295.

(136) Soci, C.; Hwang, I.-W.; Moses, D.; Zhu, Z.; Waller, D.; Gaudiana, R.; Brabec, C. J.; Heeger, A. J. "Organic Field-effect Devices as Tool to Characterize the Bipolar Transport in Polymer-fullerene Blends: The Case of P3HT-PCBM" *Adv. Funct. Mater.* **2007**, *17*, 632.

(137) Winder, C.; Sariciftci, N. S. "Low Bandgap Polymers for Photon Harvesting in Bulk Heterojunction Solar Cells" *J. Mater. Chem.* **2004**, *14*, 1077.

(138) Pan, H.; Li, Y.; Wu, Y.; Liu, P.; Ong, B. S.; Zhu, S.; X., G. "Low-temperature, Solution-processed, High-mobility Polymer Semiconductors for Thin-film Transistors" *J. Am. Chem. Soc.* **2007**, *129*, 4112.

(139) Zhang, M.; Tsao, H. N.; Pisula, W.; Yang, C.; Mishra, A. K.; Müllen, K. "Field-effect Transistors Based on a Benzothiadiazole-cyclopentadithiophene Copolymer" *J. Am. Chem. Soc.* **2007**, *129*, 3472.

(140) Sirringhaus, H. "Device physics of Solution-processed Organic Field-effect Transistors" *Adv. Mater.* **2005**, *17*, 2411.

(141) Malik, S.; K., N. A. "Crystallization Mechanism of Regioregular Poly(3-alkyl thiophene)s" *J. Polym. Sci., Part B: Polym. Phys.* **2002**, *40*, 2073.

(142) Piliego, C.; Holcombe, T. W.; Douglas, J. D.; Woo, C. H.; Beaujuge, P. M.; Frechet, J. M. J. "Synthetic Control of Structural Order in N-Alkylthieno[3,4-c]pyrrole-4,6-dione-Based Polymers for Efficient Solar Cells" *J. Am. Chem. Soc.* **2010**, *132*, 7595.

(143) Bronstein, H.; Leem, D. S.; Hamilton, R.; Woebkenberg, P.; King, S.; Zhang, W.; Ashraf, R. S.; Heeney, M.; Anthopoulos, T. D.; Mello, J.; McCulloch, I. "Indacenodithiophene-co-benzothiadiazole Copolymers for High Performance Solar Cells or Transistors via Alkyl Chain Optimization" *Macromolecules* **2011**, *44*, 6649.

(144) Krebs, F. C.; Spanggaard, H. "Antibatic Photovoltaic Response in Zinc-porphyrin-linked Oligothiophenes" *Sol. Energy Mater. Sol. Cells* **2005**, *88*, 363.

(145) Krebs, F. C.; Hagemann, O. "Directional Synthesis of A Dye-linked Conducting Homopolymer" *J. Org. Chem.* **2003**, *68*, 2463.

(146) Hagemann, O.; Jørgensen, M.; Krebs, F. C. "Synthesis of An All-in-one Molecule (for Organic Solar Cells)" *J. Org. Chem.* **2006**, *71*, 5546.

(147) Krebs, F. C.; Hagemann, O.; Jørgensen, M. "Synthesis of Dye Linked Conducting Block Copolymers, Dye Linked Conducting Homopolymers and

Preliminary Application to Photovoltaics" *Sol. Energy Mater. Sol. Cells* **2004**, *83*, 211.

(148) Würthner, F. "Plastic Transistors Reach Maturity for Mass Applications in Microelectronics" *Angew. Chem., Int. Ed.* **2001**, *40*, 1037.

(149) Würthner, F. "Perylene Bisimide Dyes as Versatile Building Blocks for Functional Supramolecular Architectures" *Chem. Commun.* 2004, 1564.

(150) Debije, M. G.; Chen, Z.; Piris, J.; Neder, R. B.; Watson, M. M.; Müllen, K.; Würthner, F. "Dramatic Increase in Charge Carrier Lifetime in a Liquid Crystalline Perylene Bisimide Derivative upon Bay Substitution with Chlorine" *J. Mater. Chem.* **2005**, *15*, 1270.

(151) Shin, W. S.; Jeong, H. H.; Kim, M. K.; Jin, S. H.; Kim, M. R.; Lee, J. K.; Lee, J. W.; Gal, Y. S. "Effects of Functional Groups at Perylene Diimide Derivatives on Organic Photovoltaic Device Application" *J. Mater. Chem.* **2006**, *16*, 384.

(152) Langhals, H. "Cyclic Carboxylic Imide Structures as Structure Elements of High-stability - Novel Developments in Perylene Dye Chemistry" *Heterocycles* **1995**, *40*, 477.

(153) Choi, H.; Paek, S.; Song, J.; Kim, C.; Cho, N.; Ko, J. "Synthesis of Annulated Thiophene Perylene Bisimide Analogues: Their Applications to Bulk Heterojunction Organic Solar Cells" *Chem. Commun.* 2011, *47*, 5509.

(154) Dias, F. B.; Pollock, S.; Hedley, G.; Pålsson, L. O.; Monkman, A.; Perepichka, I. I.; Perepichka, I. F.; Tavasli, M.; Bryce, M. R. "Intramolecular Charge Transfer Assisted by Conformational Changes in the Excited state of

Fluorene-dibenzothiophene-S,S-dioxide co-oligomers" *J. Phys. Chem. B* **2006**, *110*, 19329.

(155) Givishi, R.; Resifeld, R.; Burshtein, Z. "Spectroscopy and Laser Action of the “Red Perylimide Dye” in Various Solvents" *Chem. Phys. Lett.* **1993**, *213*, 338.

(156) Holman, M. W.; Yan, P.; Ching, K. C.; Liu, R.; Ishak, F. I.; Adams, D. M. "A Conformational Switch of Intramolecular Electron Transfer" *Chem. Phys. Lett.* **2005**, *413*, 501.

(157) Shin, W. S.; Jeong, H. H.; Kim, M. K.; Jin, S. H.; Kim, M. R.; Lee, J. K.; Leec, J. W.; Gal, Y. S. "Effects of Functional Groups at Perylene Diimide Derivatives on Organic Photovoltaic Device Application" *J. Mater. Chem.* **2006**, *16*. 384.

(158) Hummelen, J. C.; Knight, B. W.; LePeq, F.; Wudl, F.; Yao, J.; Wilkins, C. L. "Preparation and Characterization of Fulleroid and Methanofullerene Derivatives" *J. Org. Chem.* **1995**, *60*, 532.

(159) Mitzi, D. B.; Kosbar, L. L.; Murray, C. E.; Copel, M.; Afzali, A. "High-mobility Ultrathin Semiconducting Films Prepared by Spin Coating" *Nature* **2004**, *428*, 299.

(160) Klauk, H.; Zschieschang, U.; Pflaum, J.; Halik, M. "Ultralow-power Organic Complementary Circuits" *Nature* **2007**, *445*, 745.

(161) Ong, B. S.; Wu, Y.; Liu, P.; Gardner, S. "High-performance Semiconducting Polythiophenes for Organic Thin-film Transistors" *J. Am. Chem. Soc.* **2004**, *126*, 3378.

(162) Usta, H.; Facchetti, A.; Marks, T. J. "Air-stable, Solution-processable n-Channel and Ambipolar Semiconductors for Thin-film Transistors Based on

the Indenofluorenebis(dicyanovinylene) Core" *J. Am. Chem. Soc.* **2008**, *130*, 8580.

(163) Mcculloch, I.; Heeney, M.; Bailey, C.; Genevicius, K.; Macdonald, I.; Shkunov, M.; Sparrowe, D.; Tierney, S.; Wagner, R.; Zhang, W.; Chabinyc, M. L.; Kline, R. J.; Mcgehee, M. D.; Toney, M. F. "Liquid-crystalline Semiconducting Polymers with High Charge-carrier Mobility" *Nat. Mater.* **2006**, *5*, 328.

Appendix I ^{1}H NMR spectra of the synthesized molecules and polymers

NMR spectra of molecules and polymers in Chapter 3

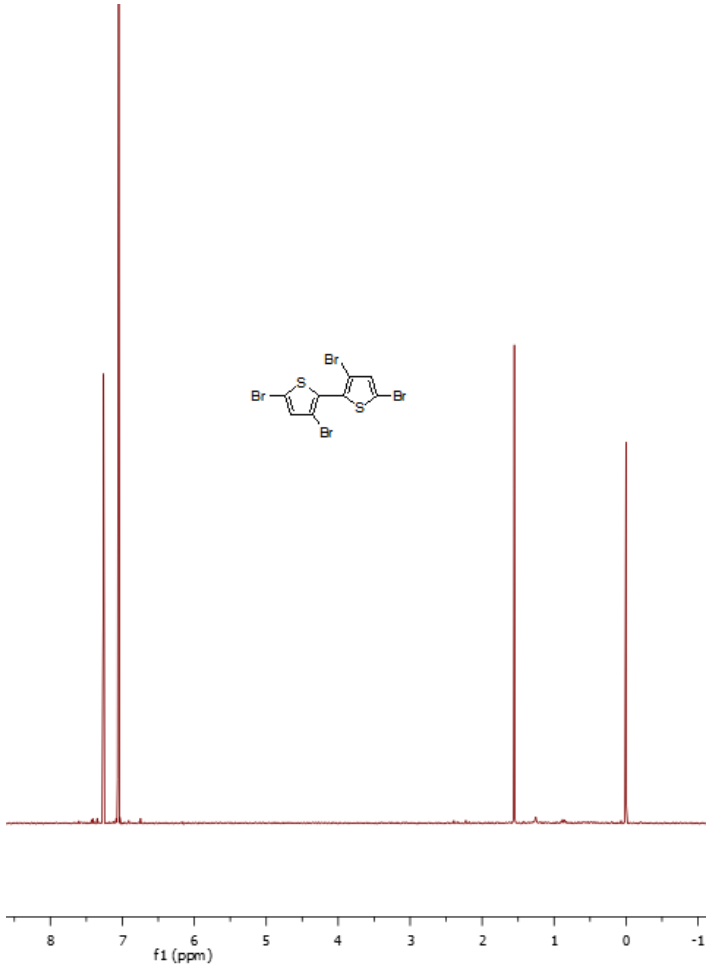

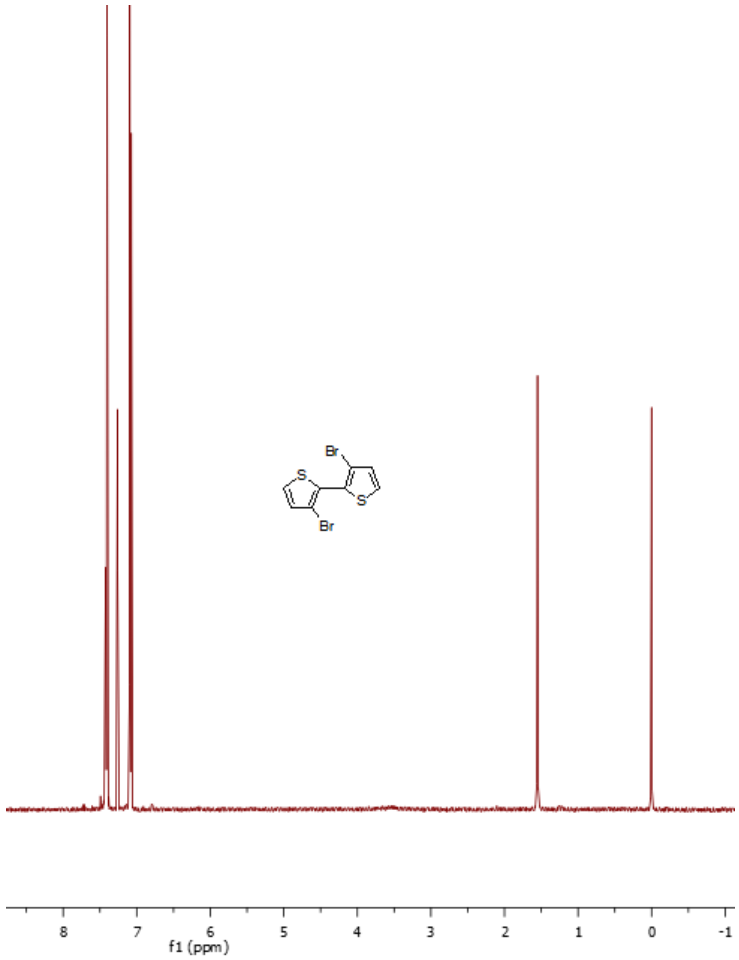

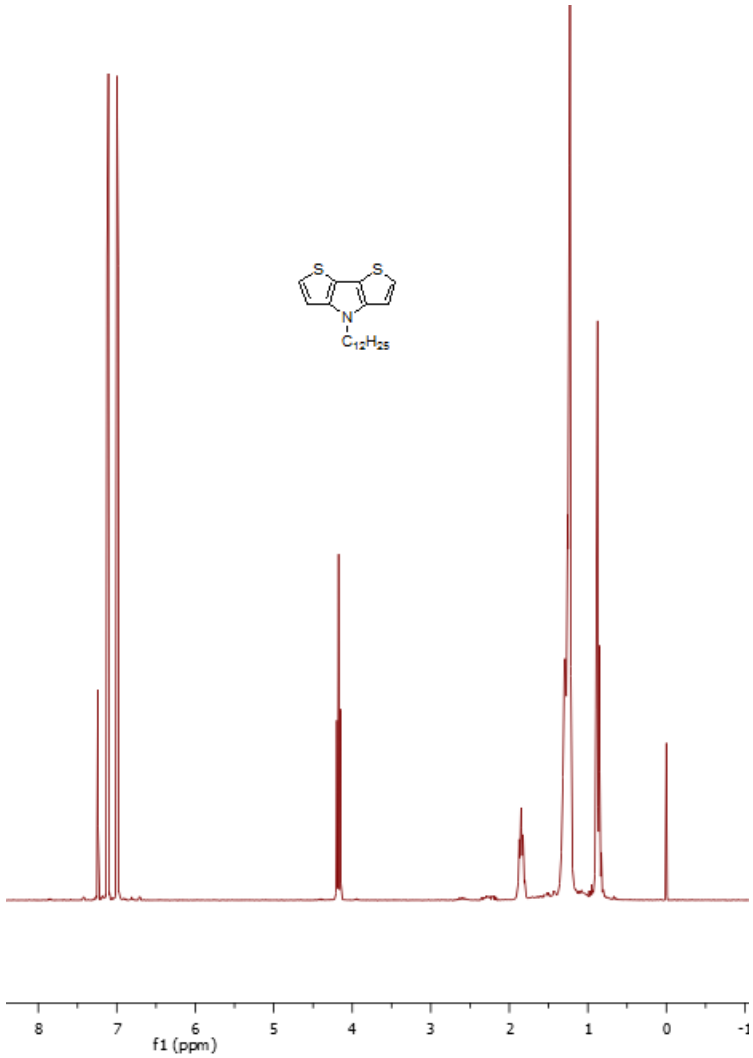
S
S
N
C12H25
8
7
6
5
4
3
2
1
0
-1
f1 (ppm)

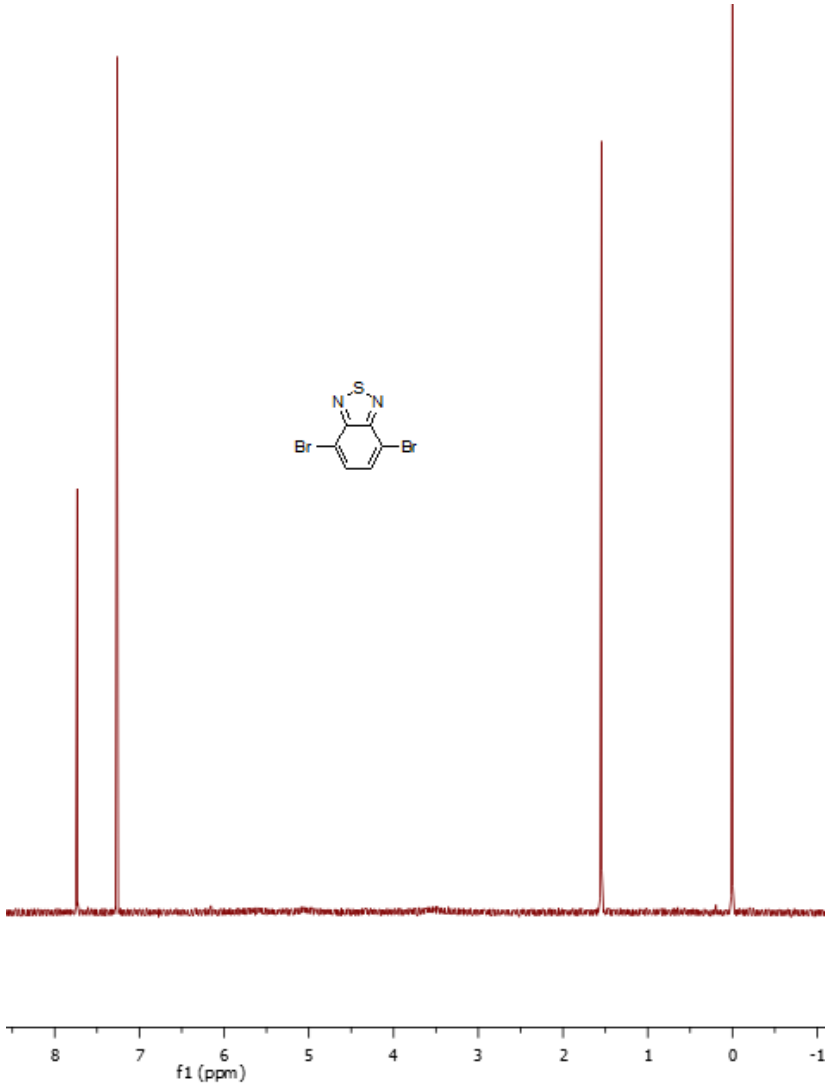
S
N
N
Br
Br
8
7
6
5
4
3
2
1
0
-1
f1 (ppm)

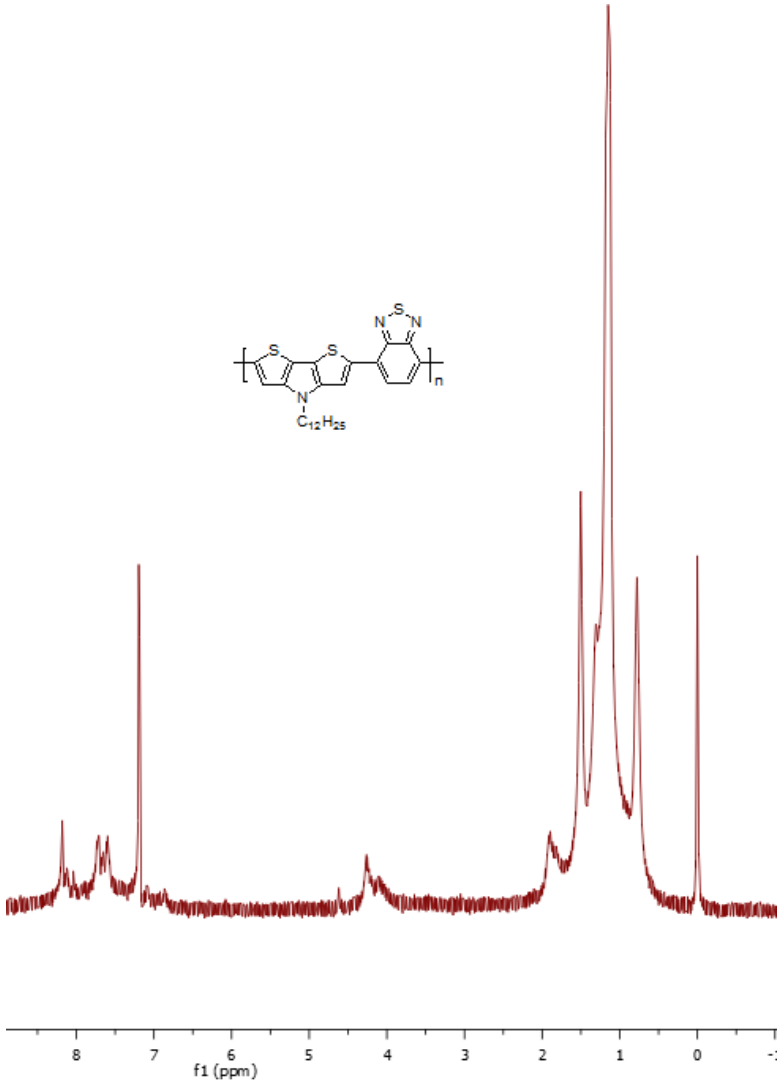
S
S
N
S
N
n
N
C12H25
8
7
6
5
4
3
2
1
0
f1 (ppm)

NMR spectra of molecules and polymers in Chapter 4

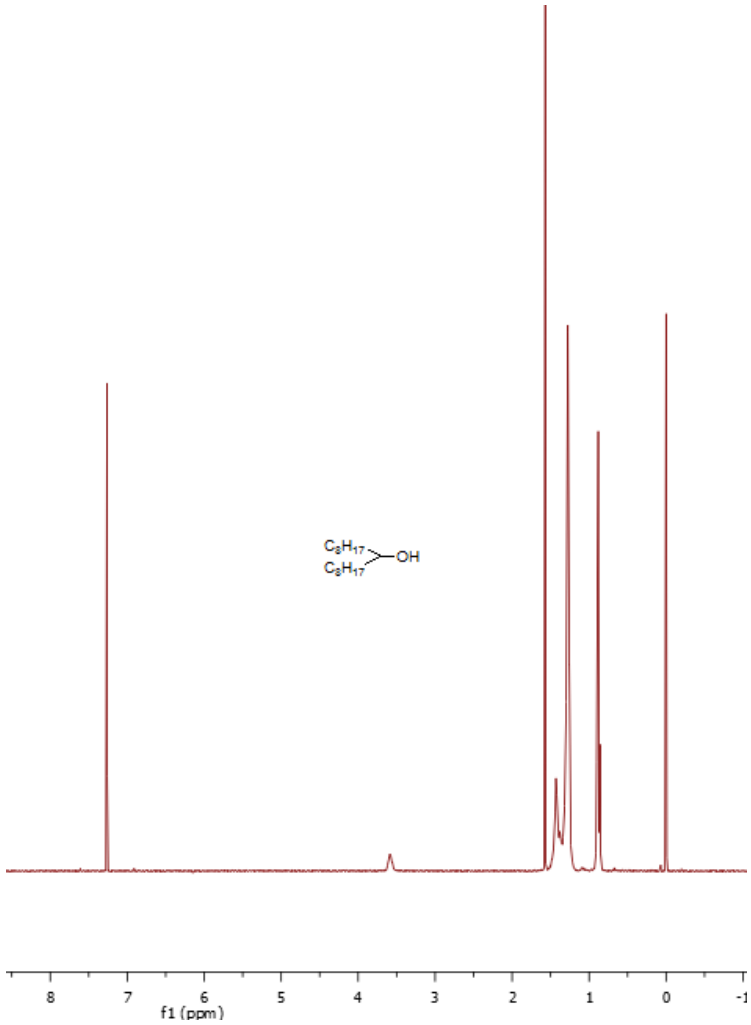

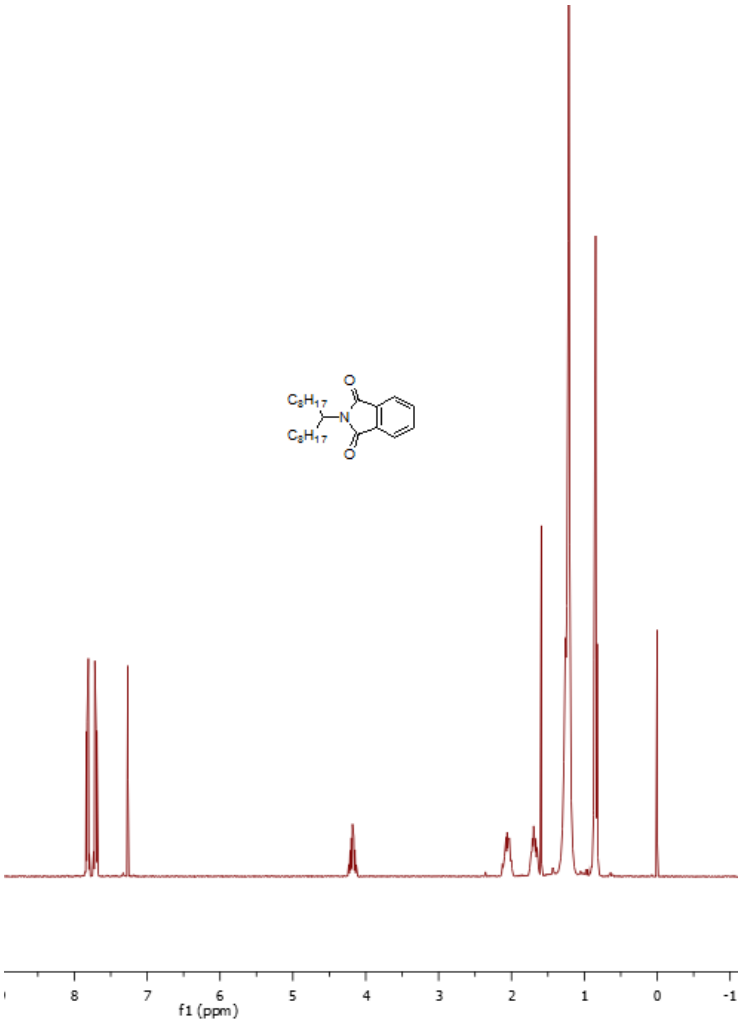

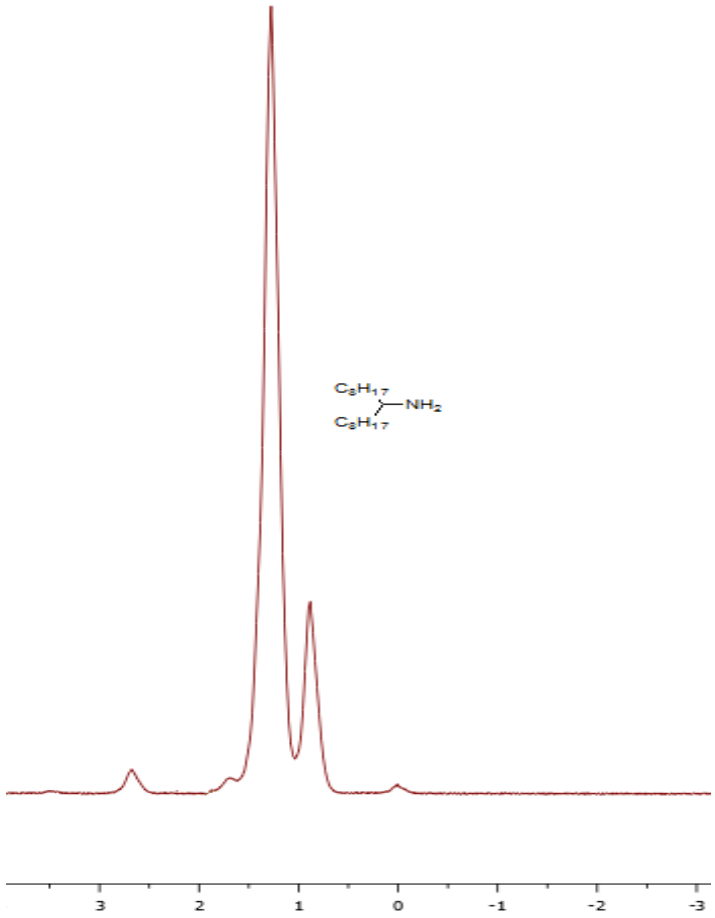
C_8H_{17}
C_8H_{17}
NH_2
3
2
1
0
-1
-2
-3

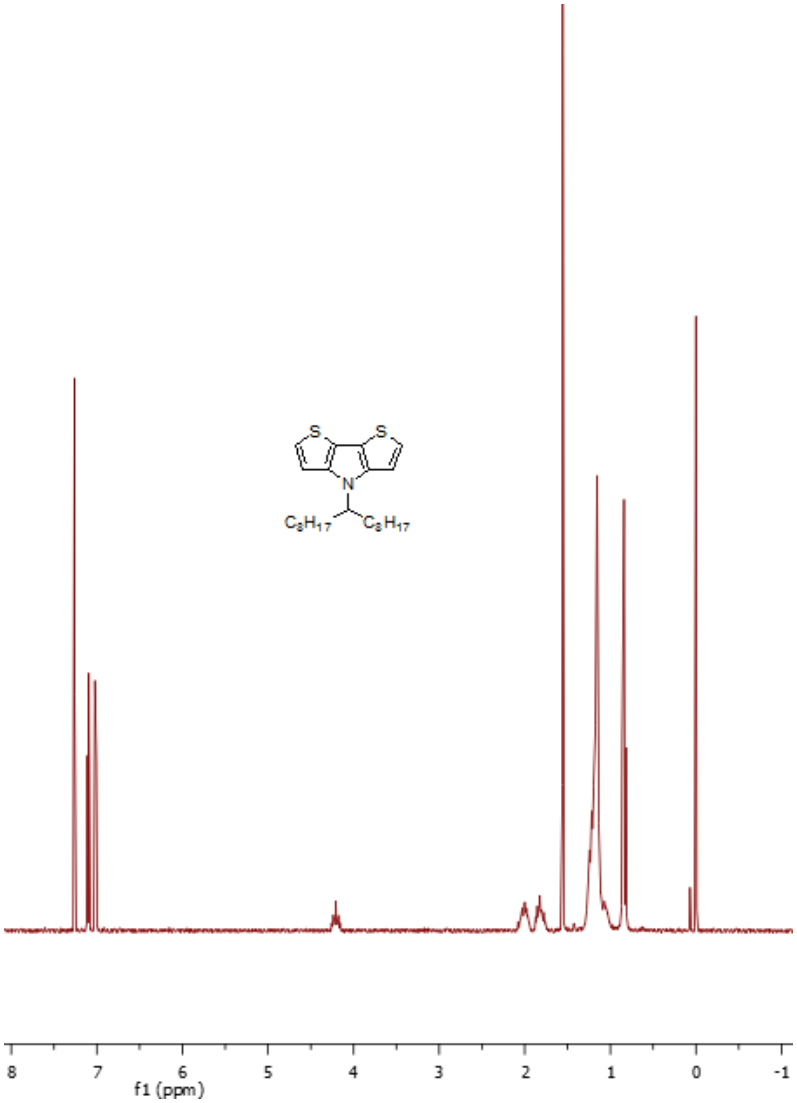
S
S
N
C_8H_{17}
C_8H_{17}
8
7
6
5
4
3
2
1
0
-1
f1 (ppm)

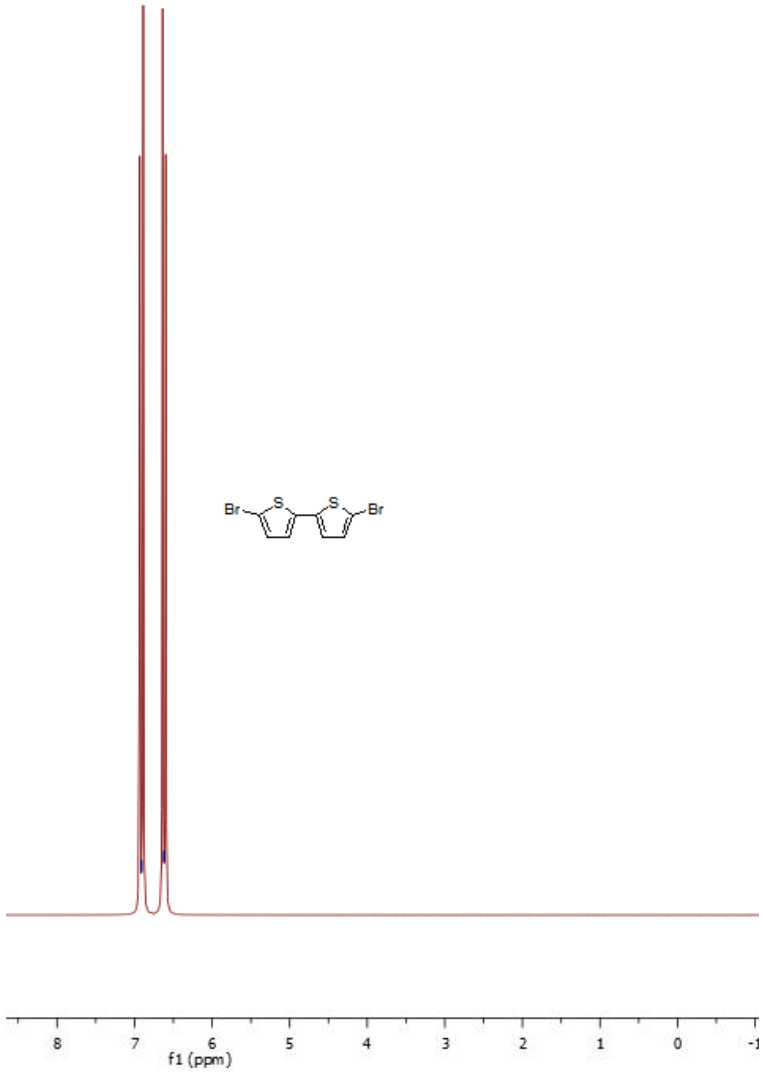
Br
S
S
Br
8
7
6
5
4
3
2
1
0
-1
f1 (ppm)

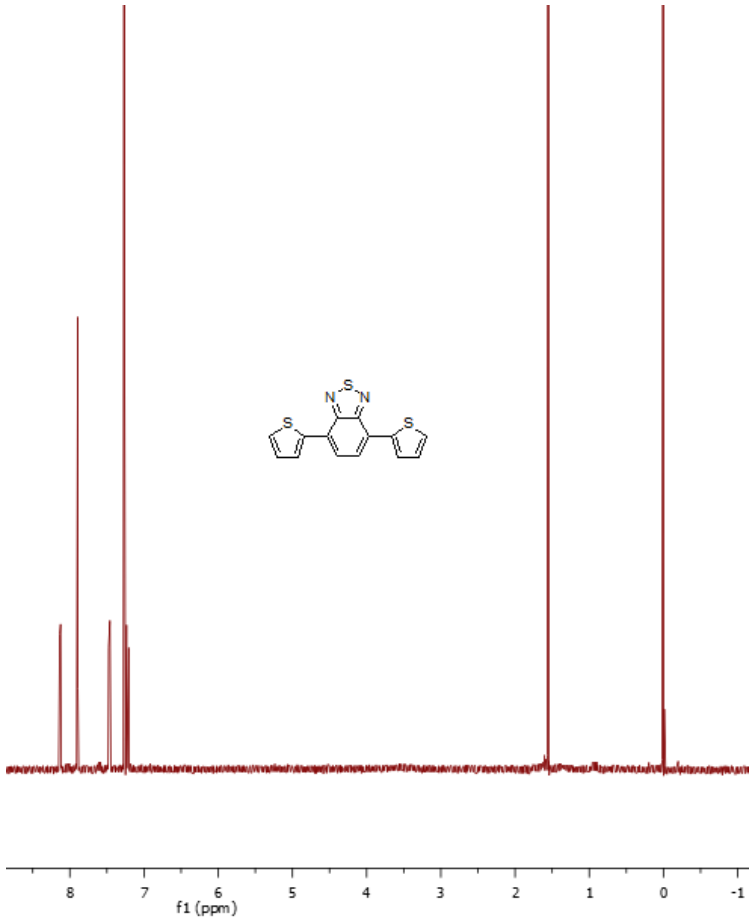
N
S
N
S
S
8
7
6
5
4
3
2
1
0
-1
f1 (ppm)

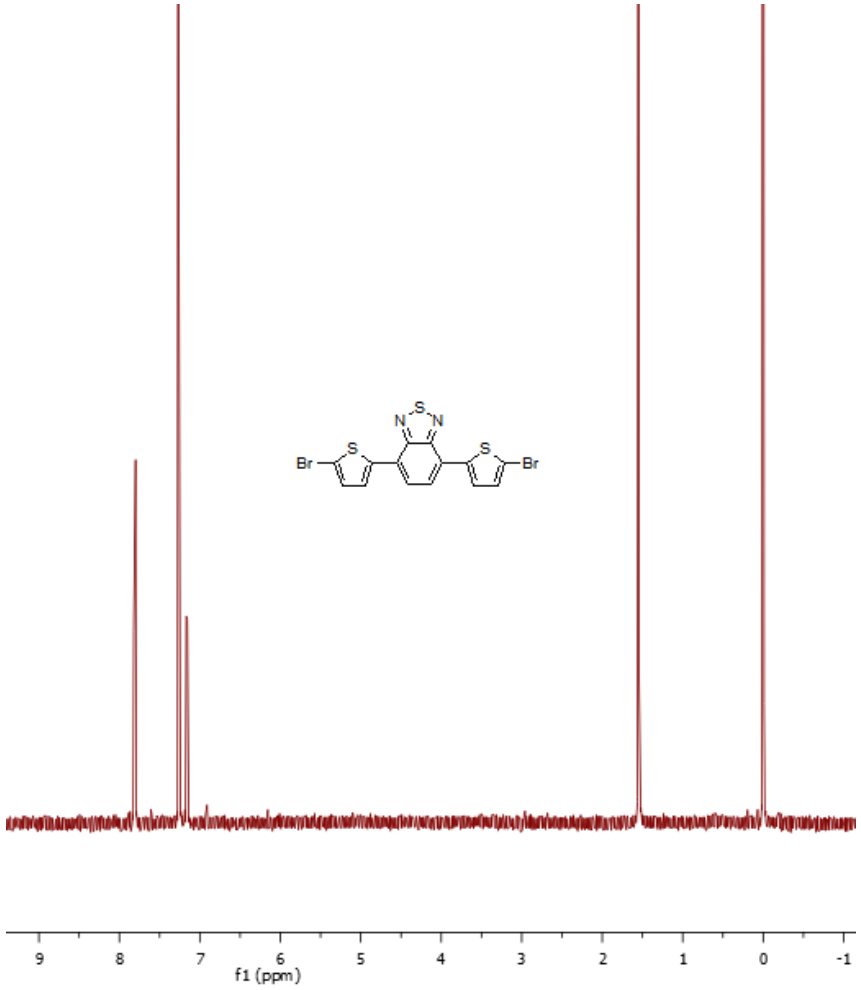
Br
S
N
S
N
S
Br
9
8
7
6
5
4
3
2
1
0
-1
f1 (ppm)

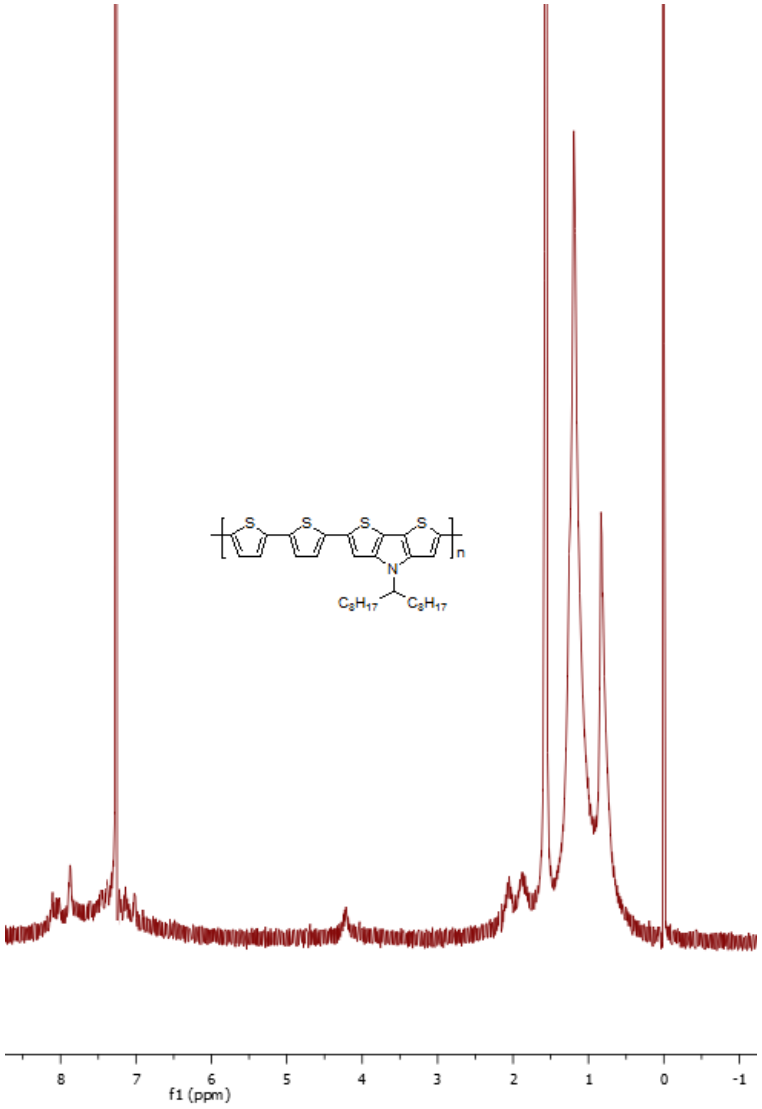
S
S
S
S
n
N
C8H17
C8H17
8
7
6
5
4
3
2
1
0
-1
f1 (ppm)

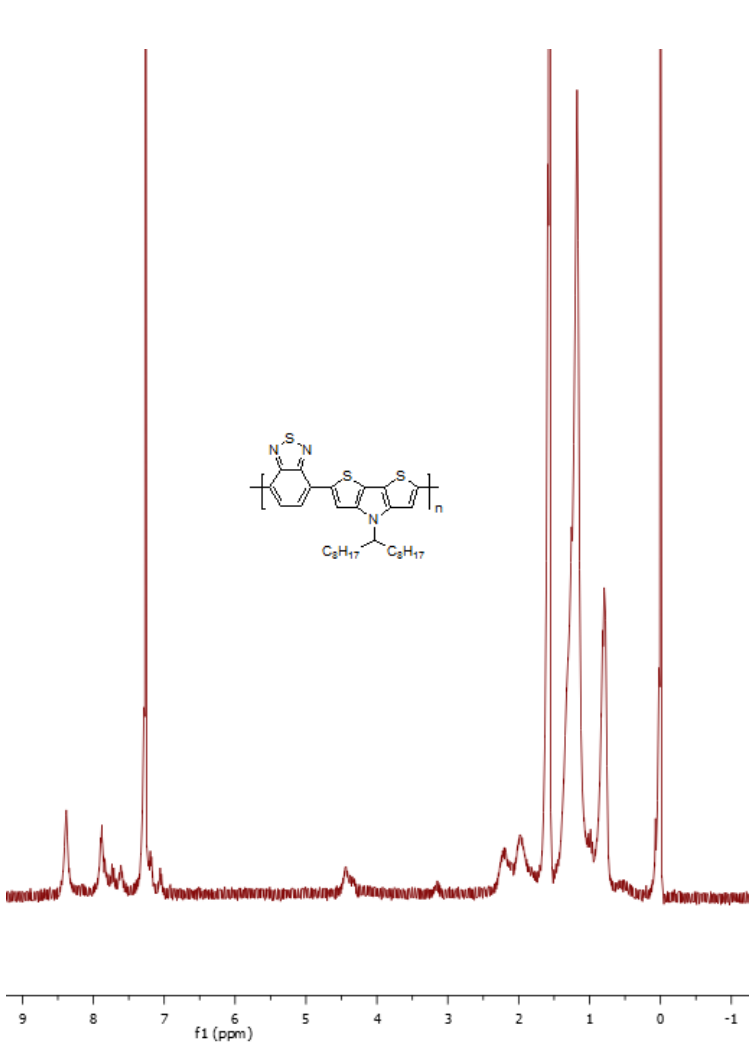
N
S
N
S
S
S
N
n
C8H17
C8H17
9
8
7
6
5
4
3
2
1
0
-1
f1 (ppm)

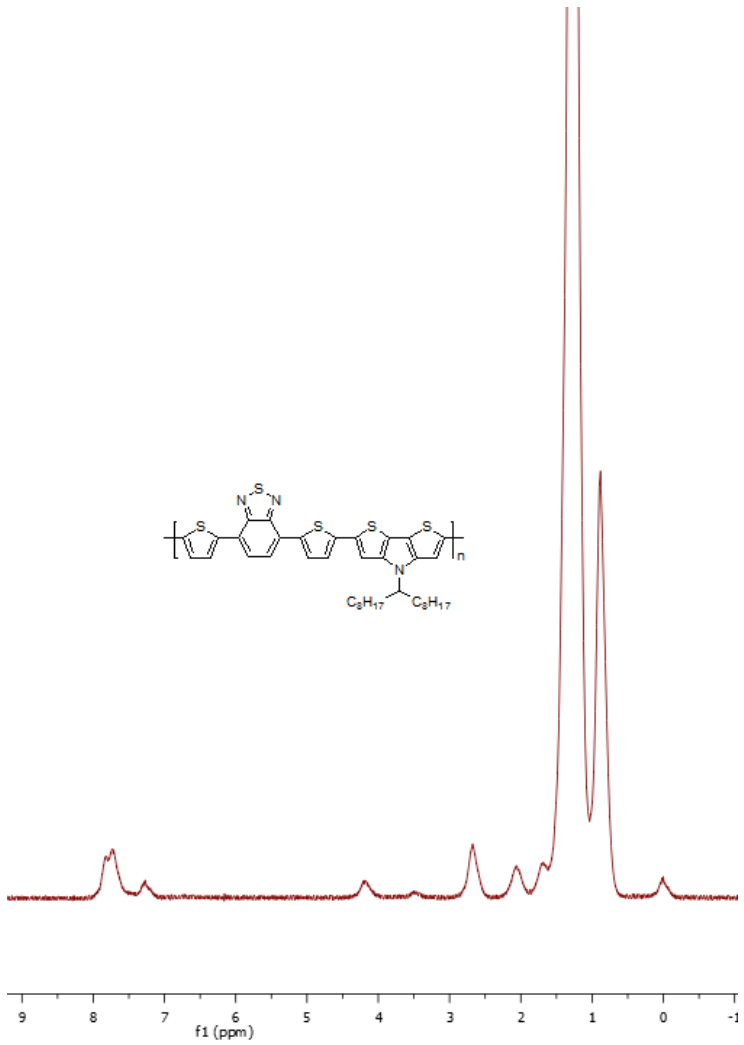
N
S
N
S
S
S
S
N
n
C8H17
C8H17
9
8
7
6
5
4
3
2
1
0
-1
f1 (ppm)

NMR spectra of molecules and polymers in Chapter 5

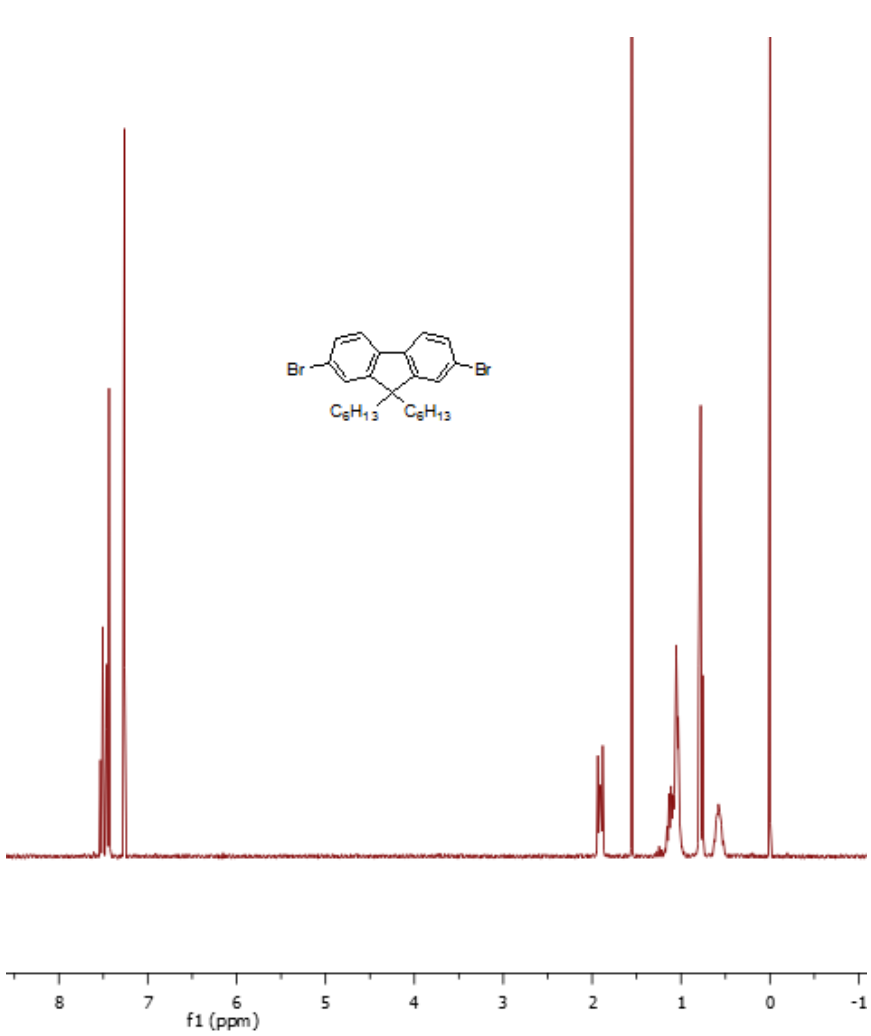

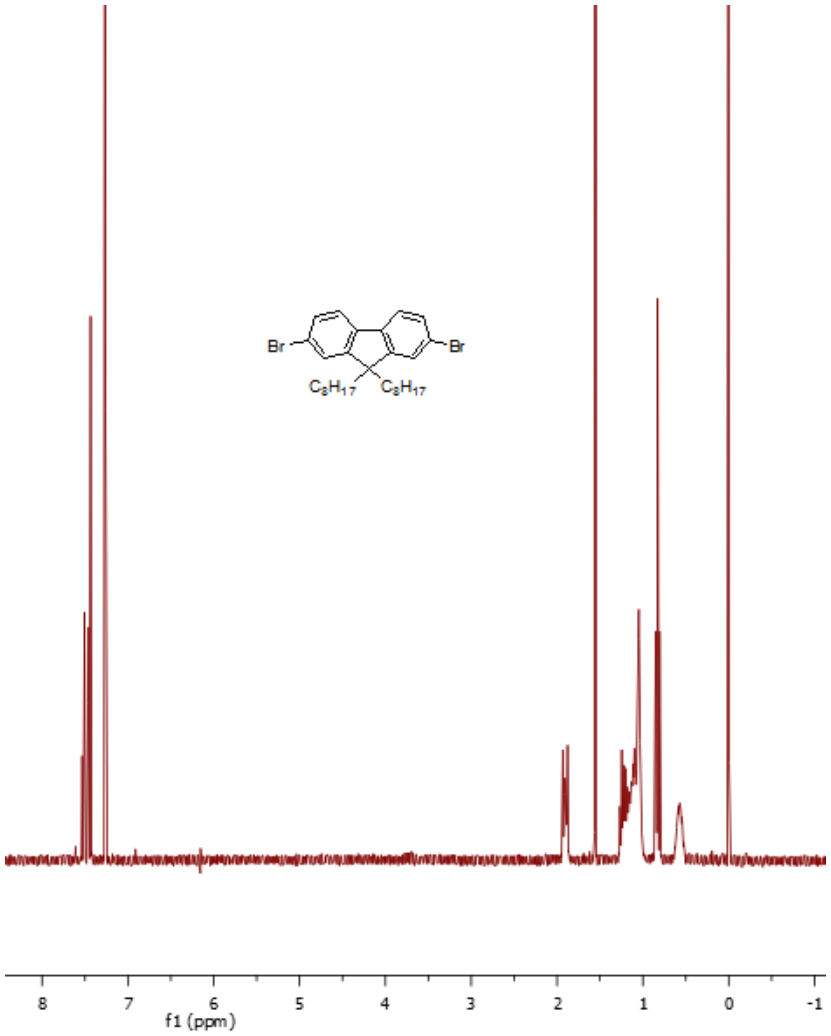

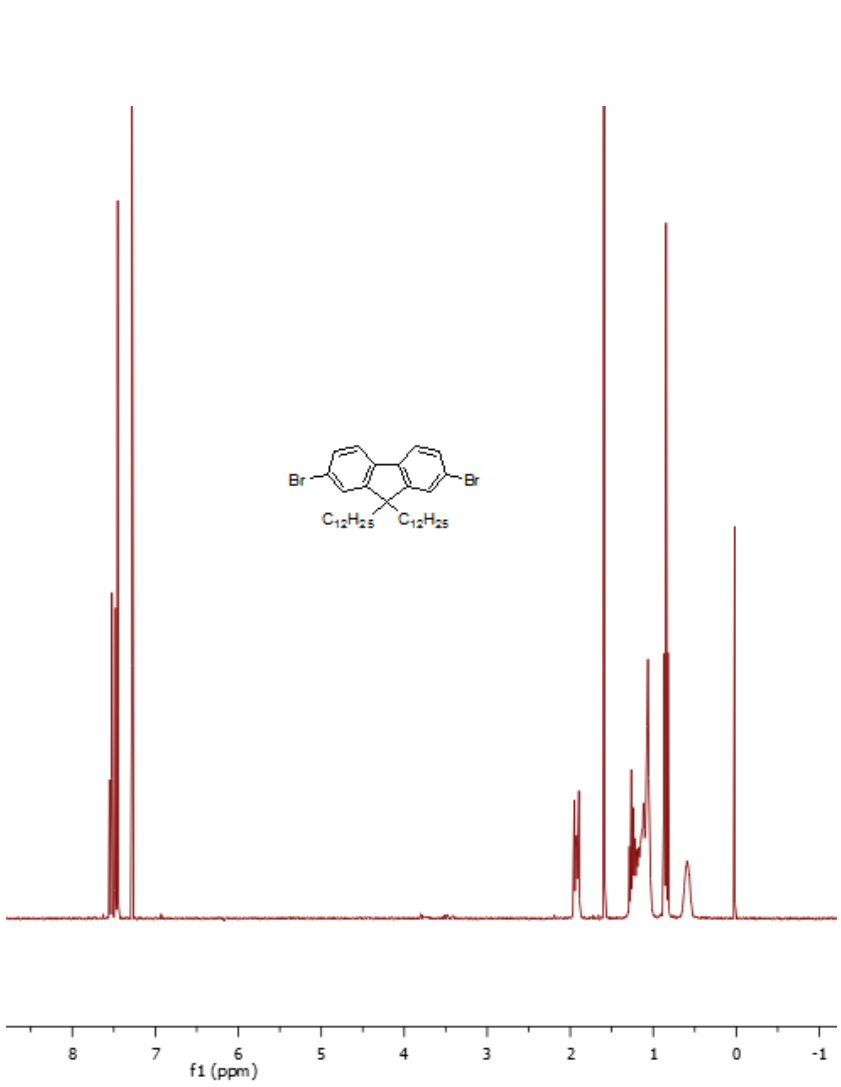
Br
Br
C12H25
C12H25
8
7
6
5
4
3
2
1
0
-1
f1 (ppm)

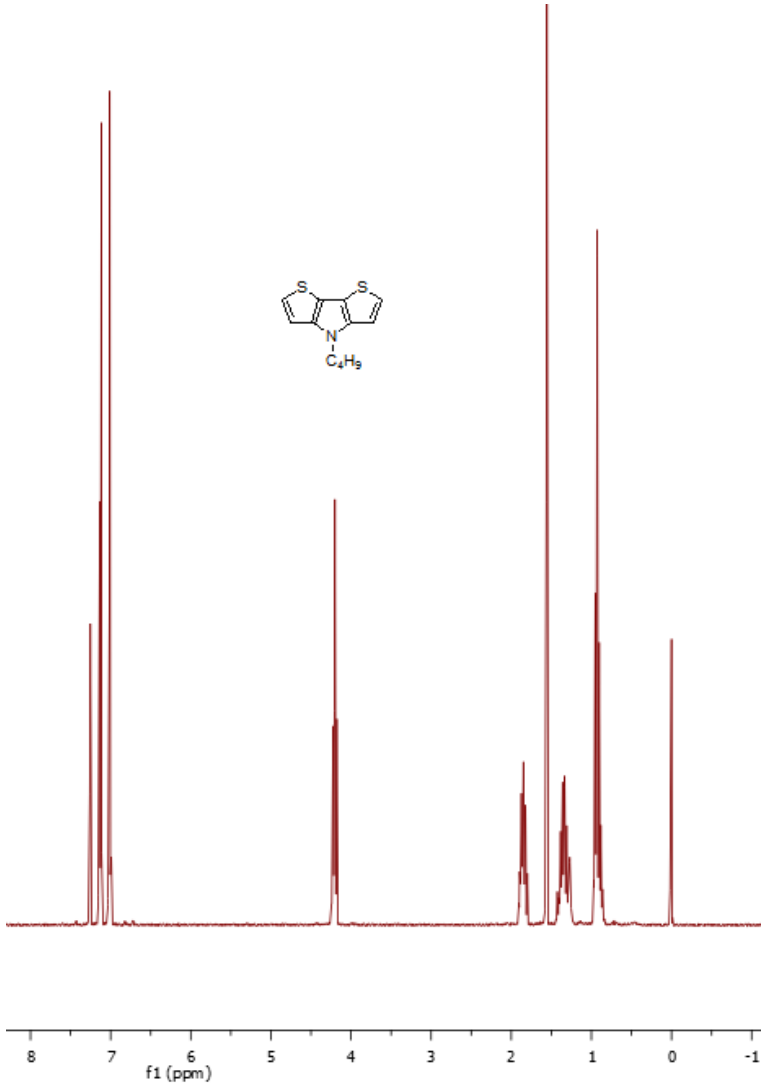
S
S
N
C4H9
8
7
6
5
4
3
2
1
0
-1
f1 (ppm)

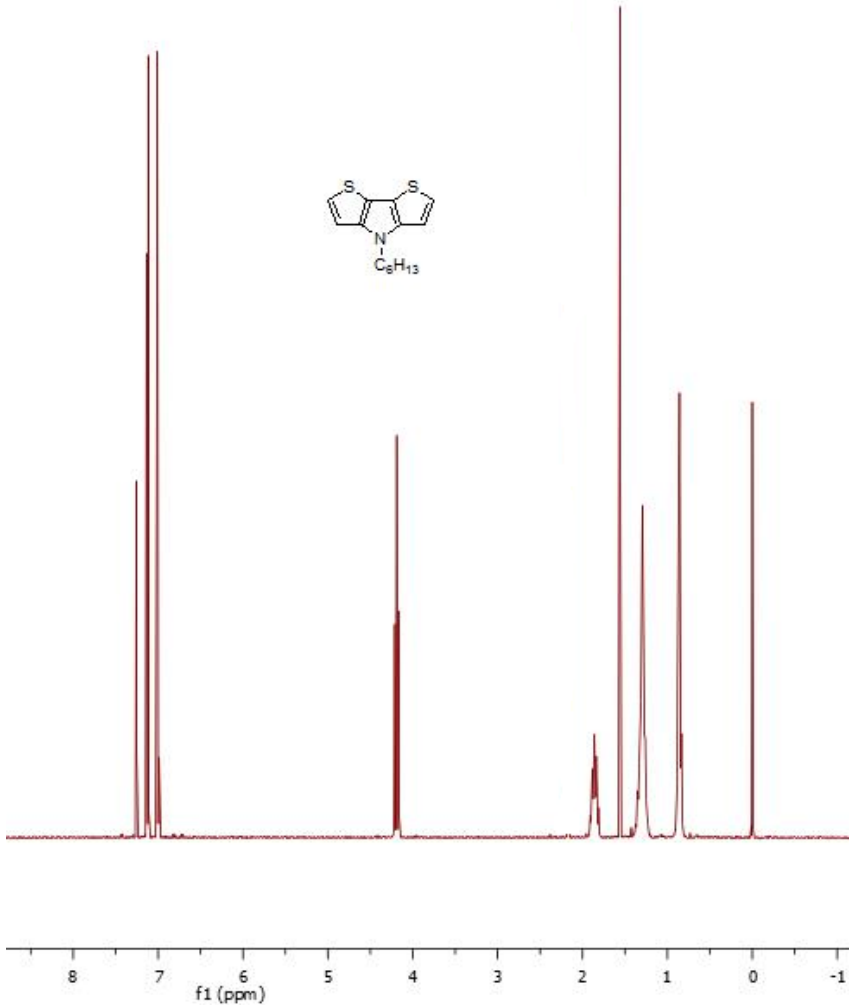
S
S
N
C8H13
8
7
6
5
4
3
2
1
0
-1
f1 (ppm)

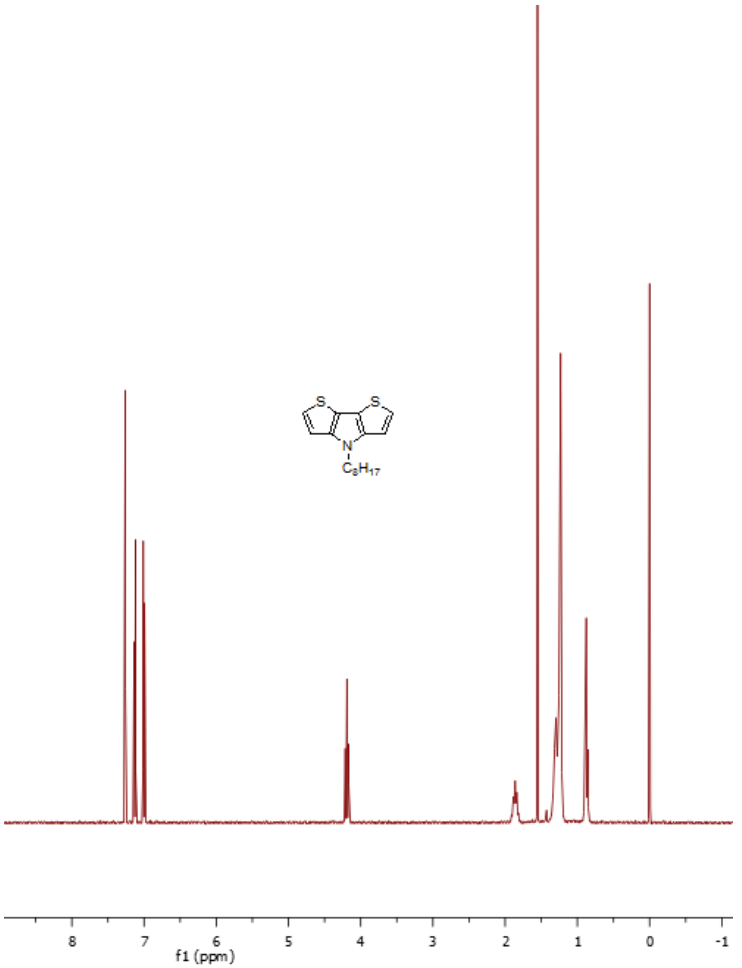
S
S
N
C8H17
8
7
6
5
4
3
2
1
0
-1
f1 (ppm)

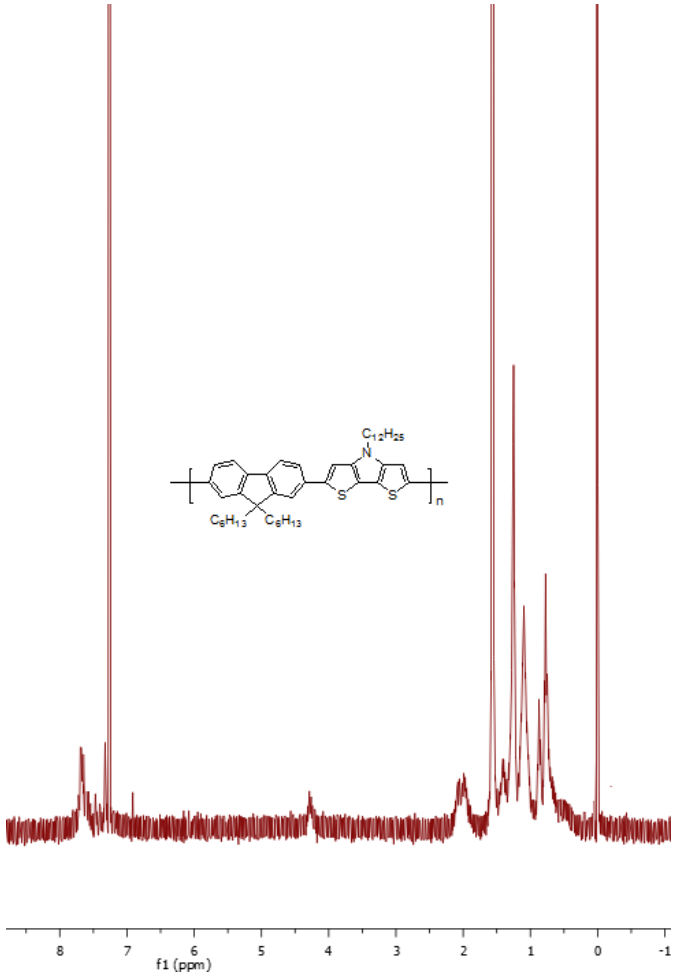
C12H25
N
S
S
n
C8H13
C8H13
8
7
6
5
4
3
2
1
0
-1
f1 (ppm)

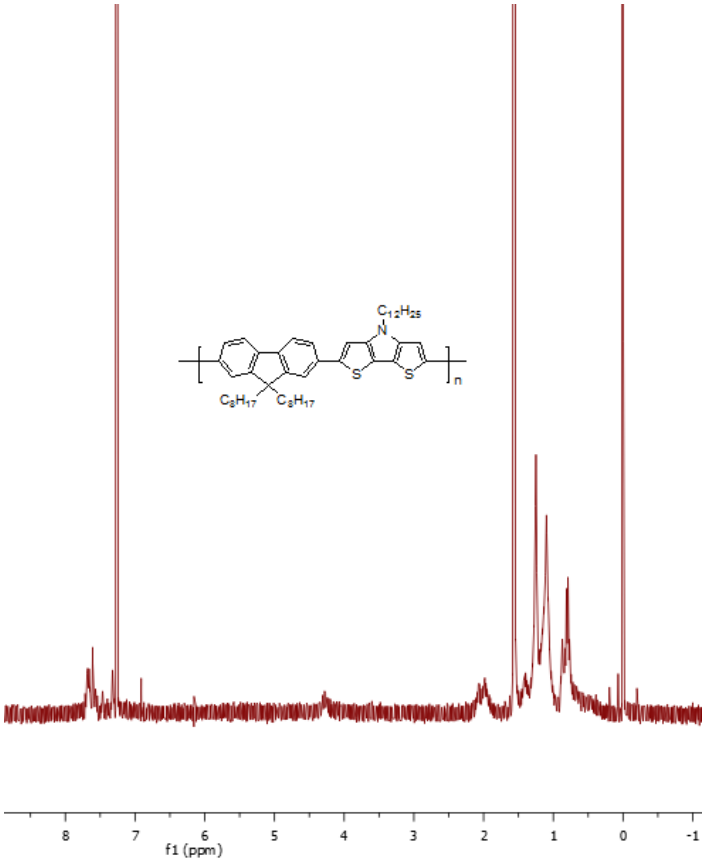
C12H25
N
S
S
n
C8H17
C8H17
8
7
6
5
4
3
2
1
0
-1
f1 (ppm)

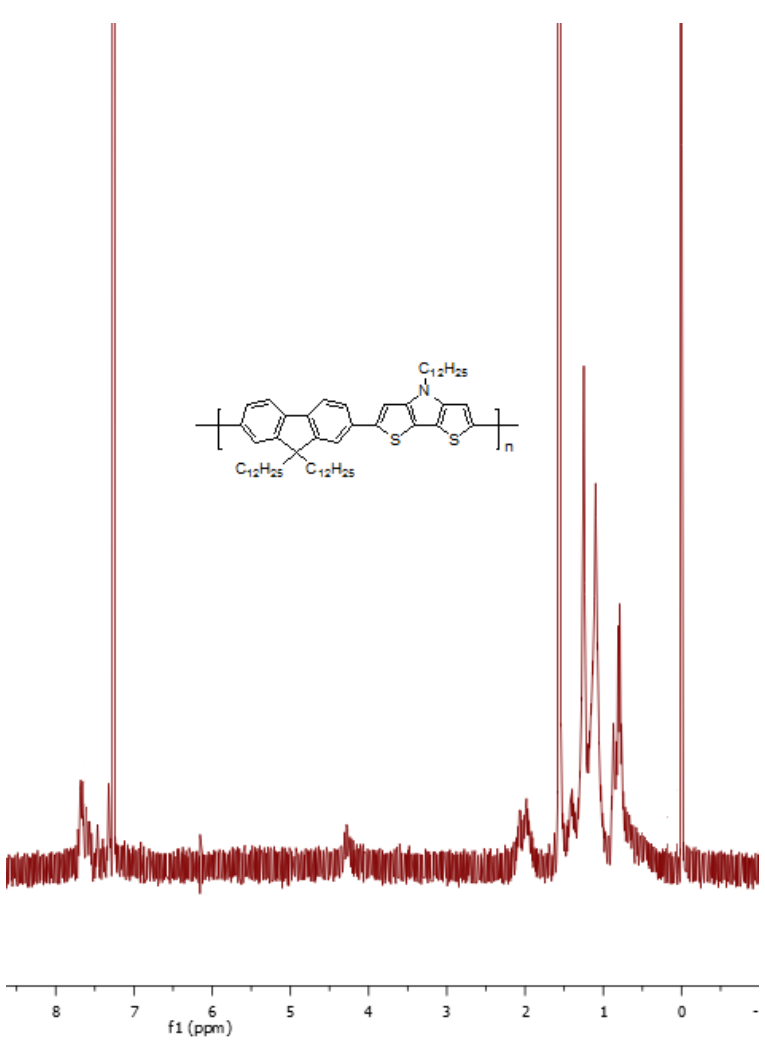
C12H25
N
S
S
n
C12H25
C12H25
8
7
6
5
4
3
2
1
0
-
f1 (ppm)

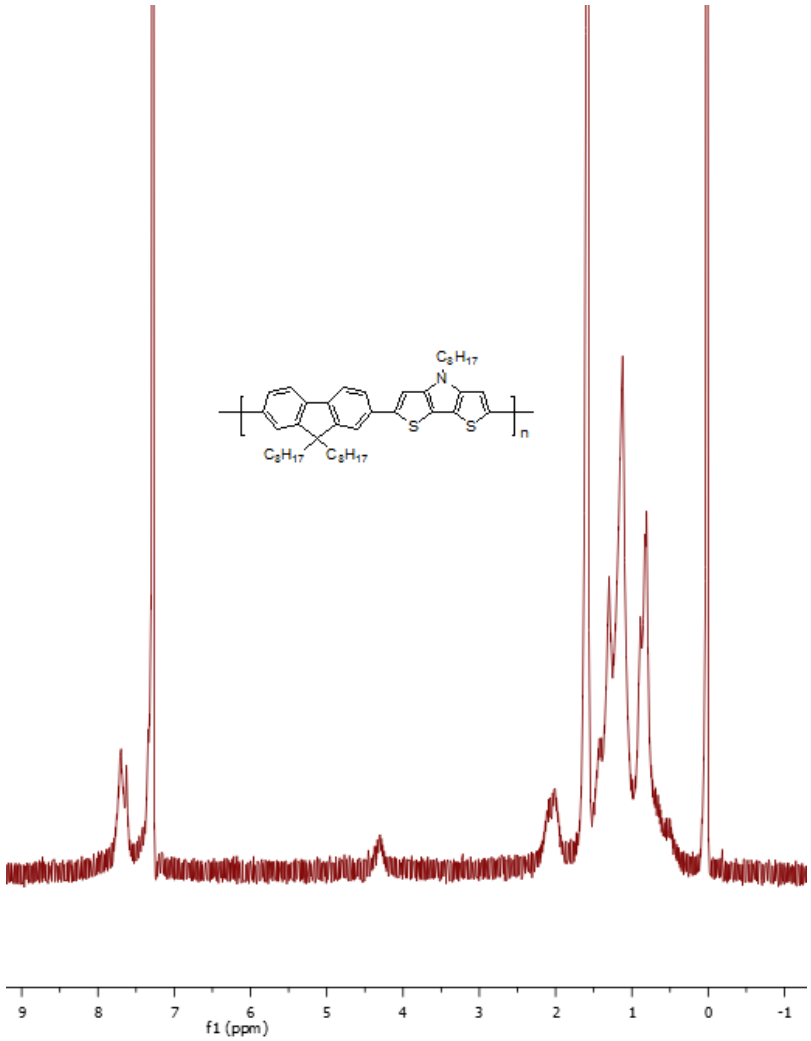
C8H17
N
S
S
n
C8H17
C8H17
9
8
7
6
5
4
3
2
1
0
-1
f1 (ppm)

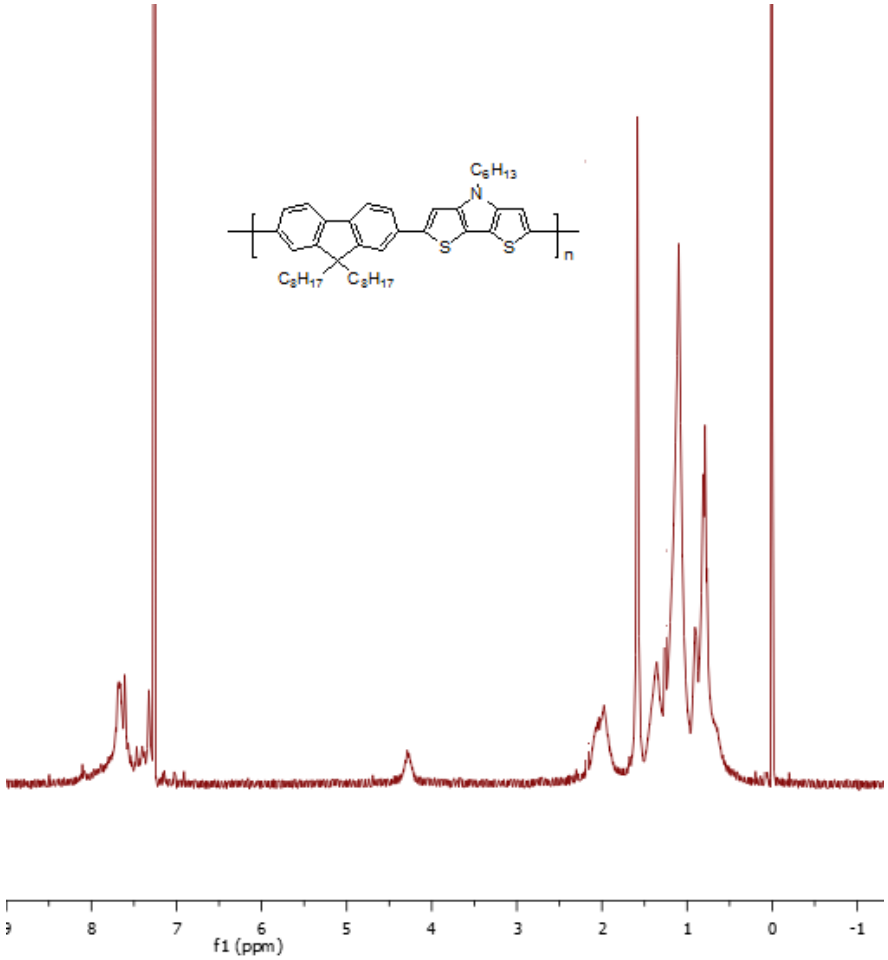
C6H13
N
S
S
n
C8H17
C8H17
9
8
7
6
5
4
3
2
1
0
-1
f1 (ppm)

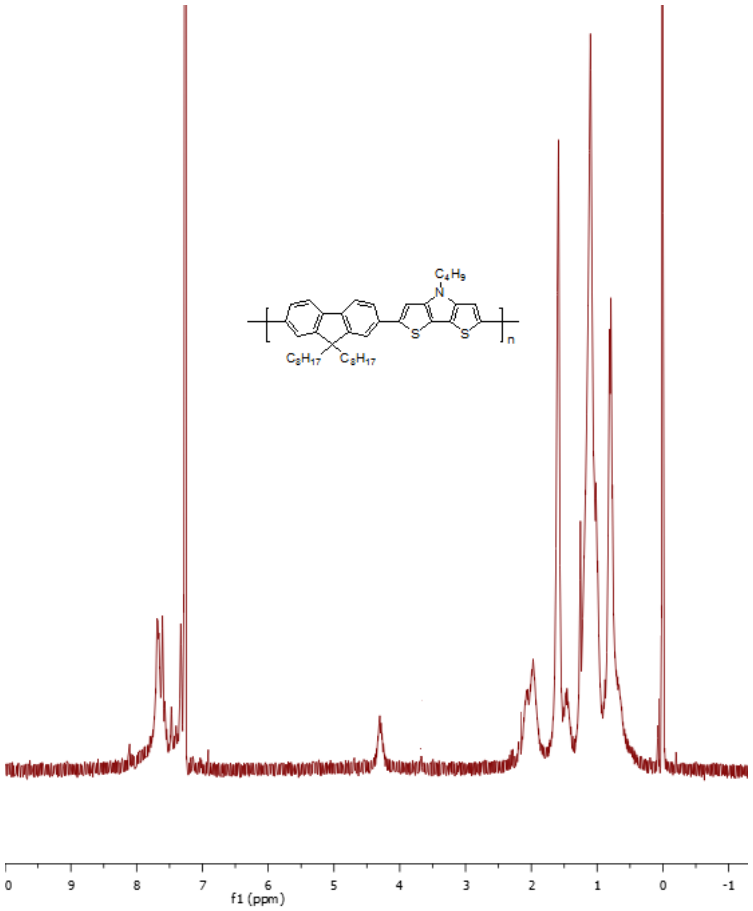
C4H9
N
S
S
n
C8H17
C8H17
0
9
8
7
6
5
4
3
2
1
0
-1
f1 (ppm)

NMR spectra of molecules and polymers in Chapter 6

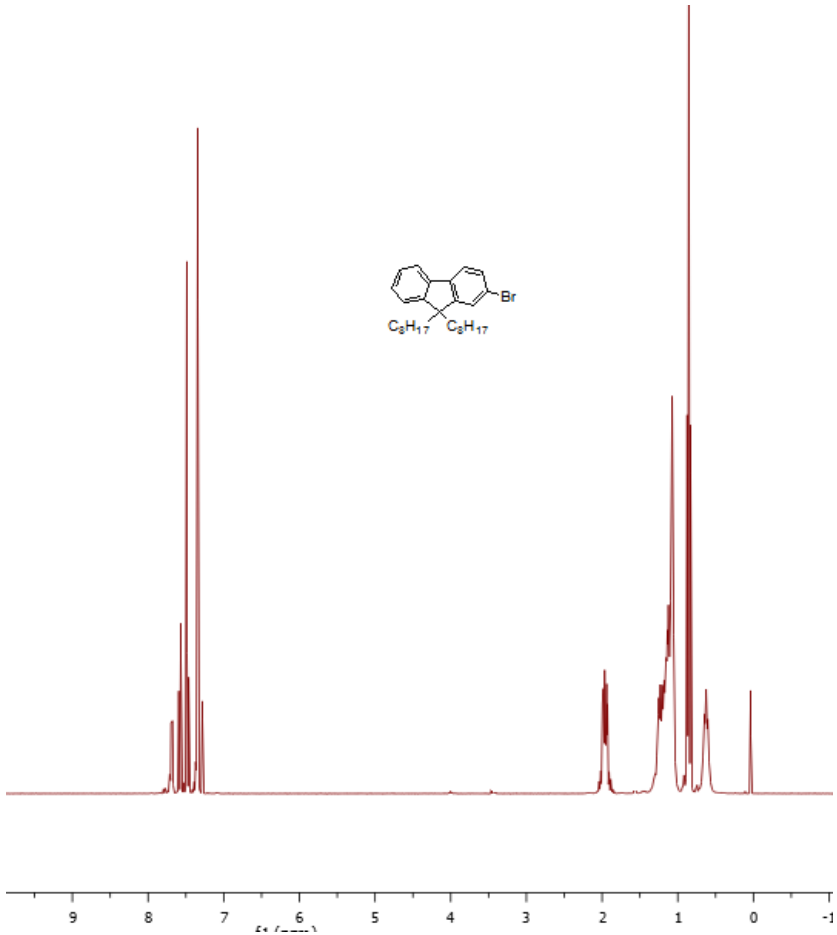

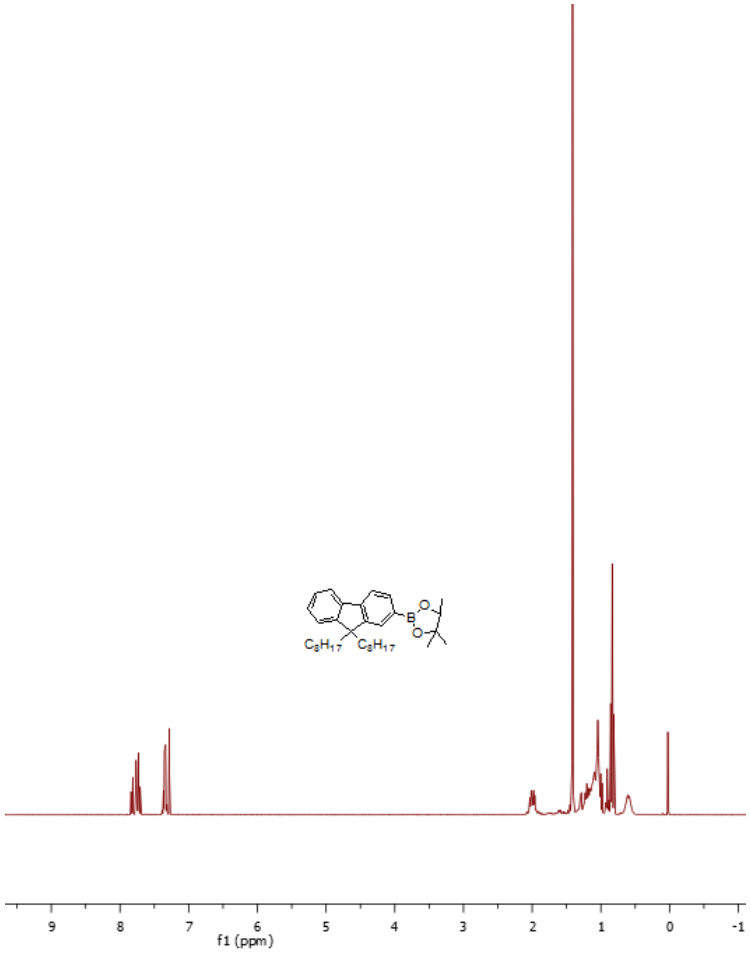

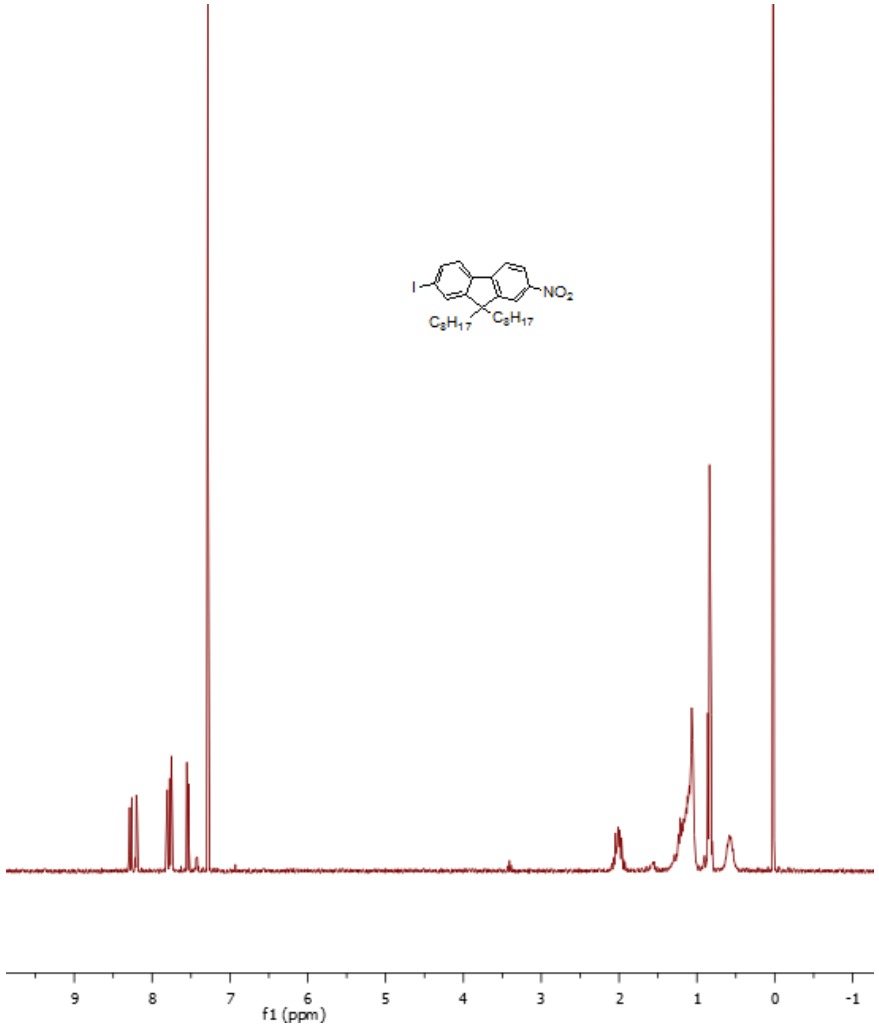
I
NO2
C8H17
C8H17
9
8
7
6
5
4
3
2
1
0
-1
f1 (ppm)

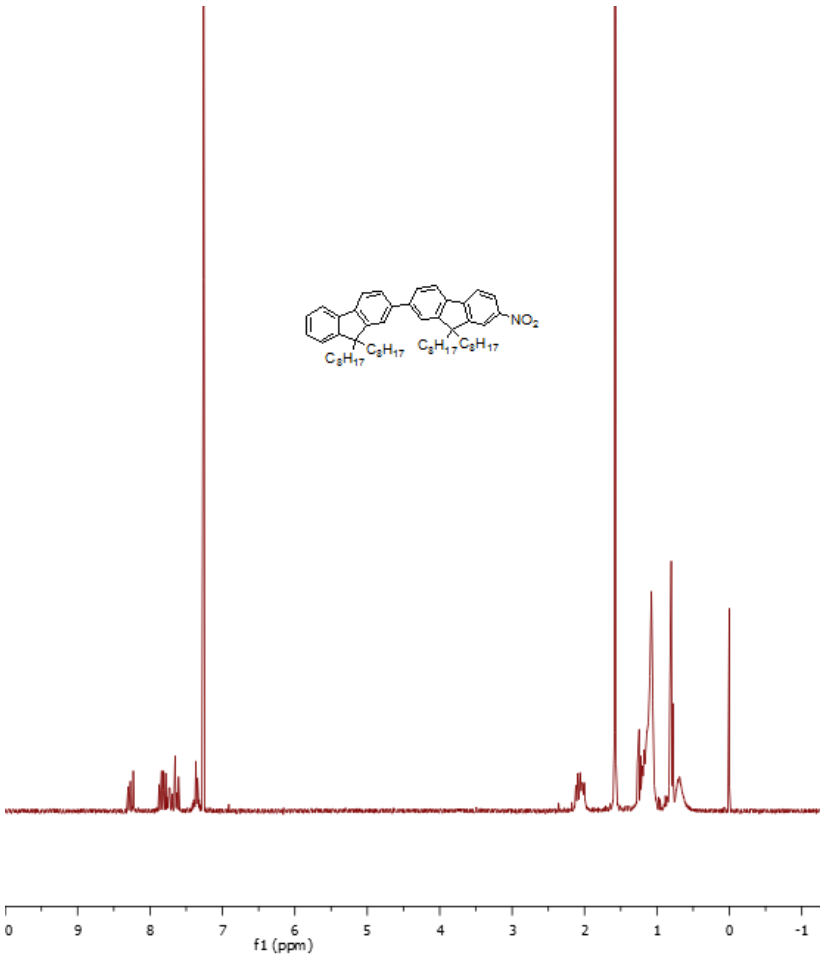
NO2
C8H17
C8H17
C8H17
C8H17
0
9
8
7
6
5
4
3
2
1
0
-1
f1 (ppm)

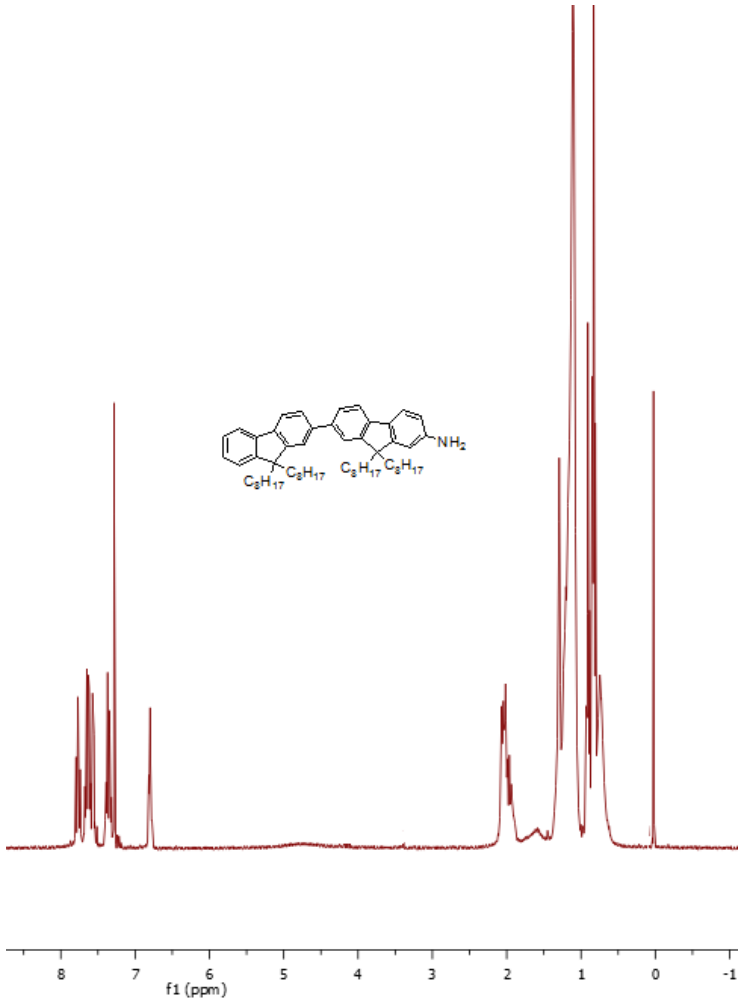
NH2
C8H17
C8H17
C8H17
C8H17
8
7
6
f1 (ppm)
5
4
3
2
1
0
-1

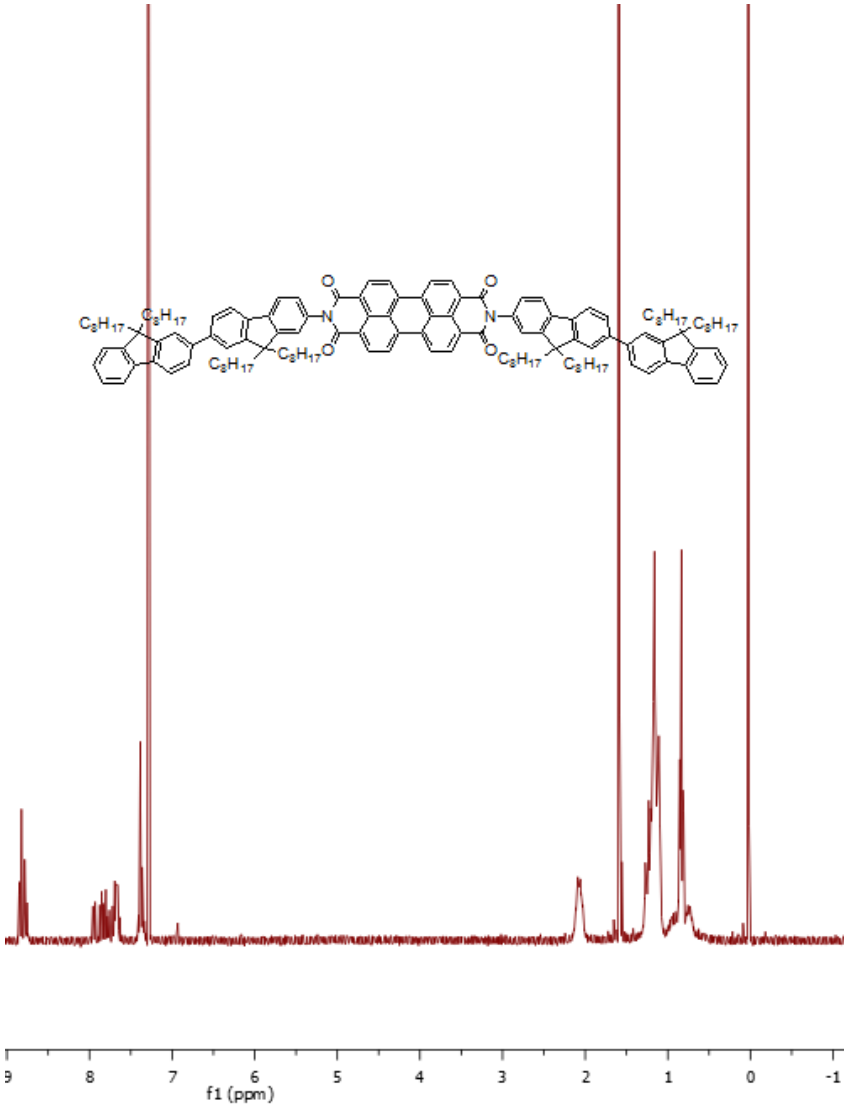
O
O
N
N
O
O
C8H17
C8H17
C8H17
C8H17
C8H17
C8H17
C8H17
C8H17
9
8
7
6
f1 (ppm)
5
4
3
2
1
0
-1

NMR spectra of molecules and polymers in Chapter 7

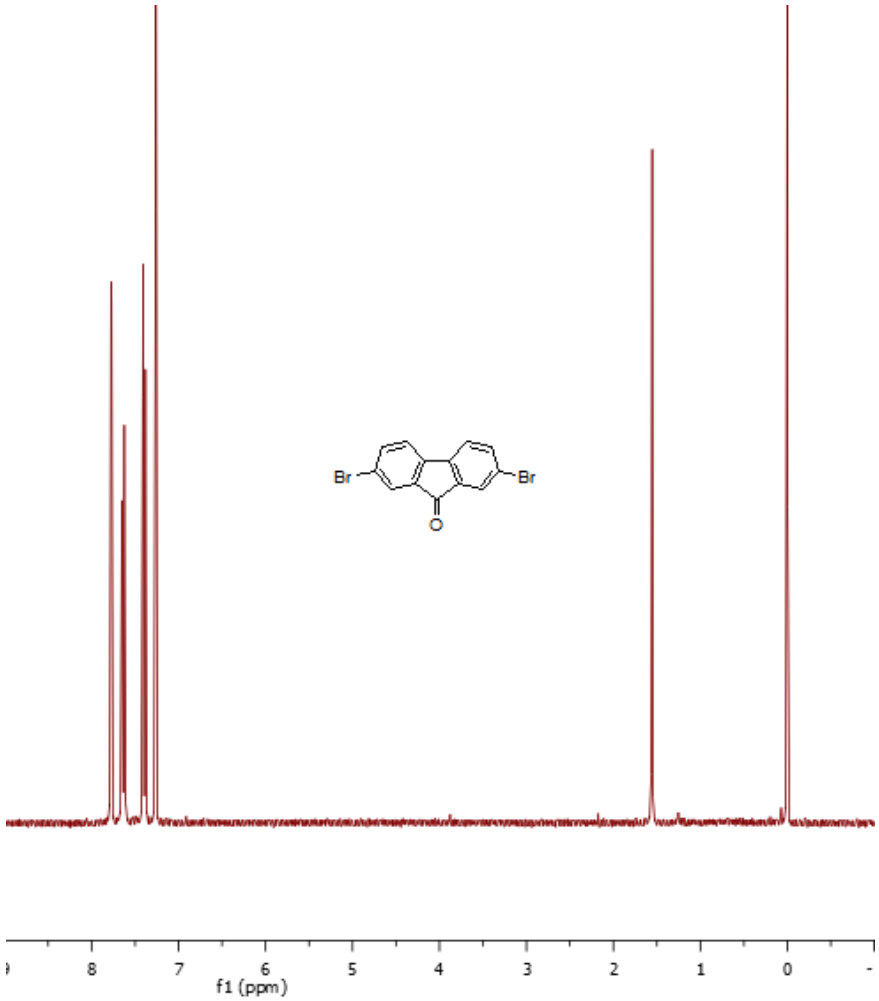

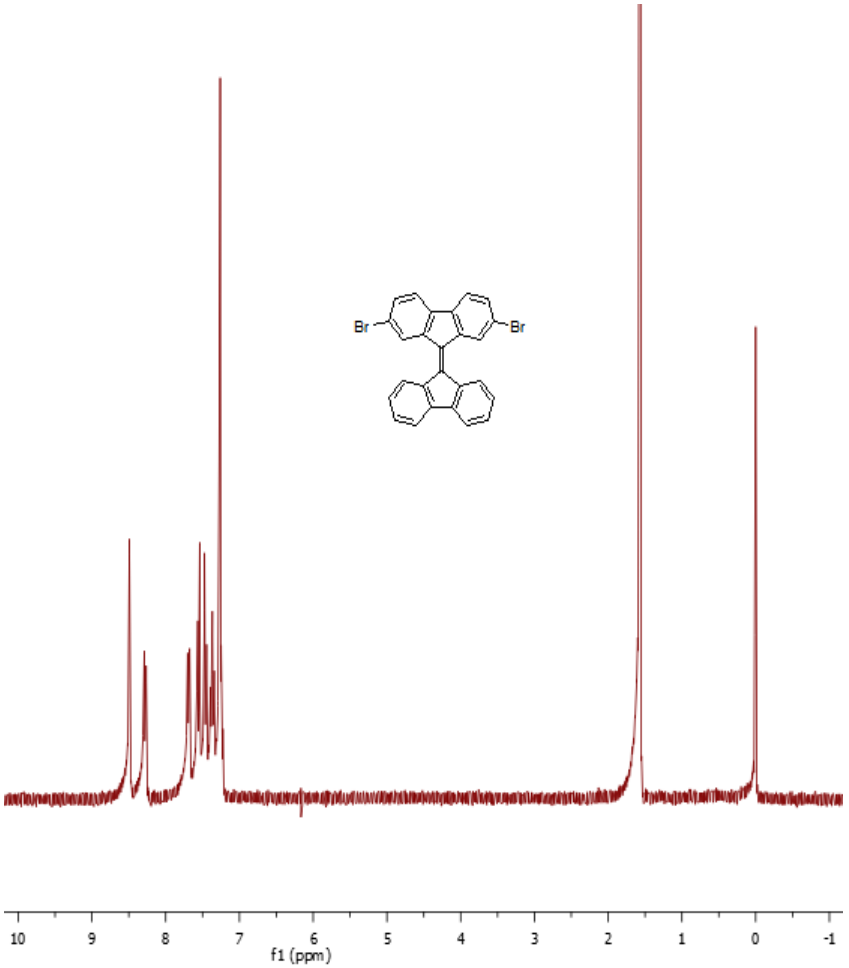

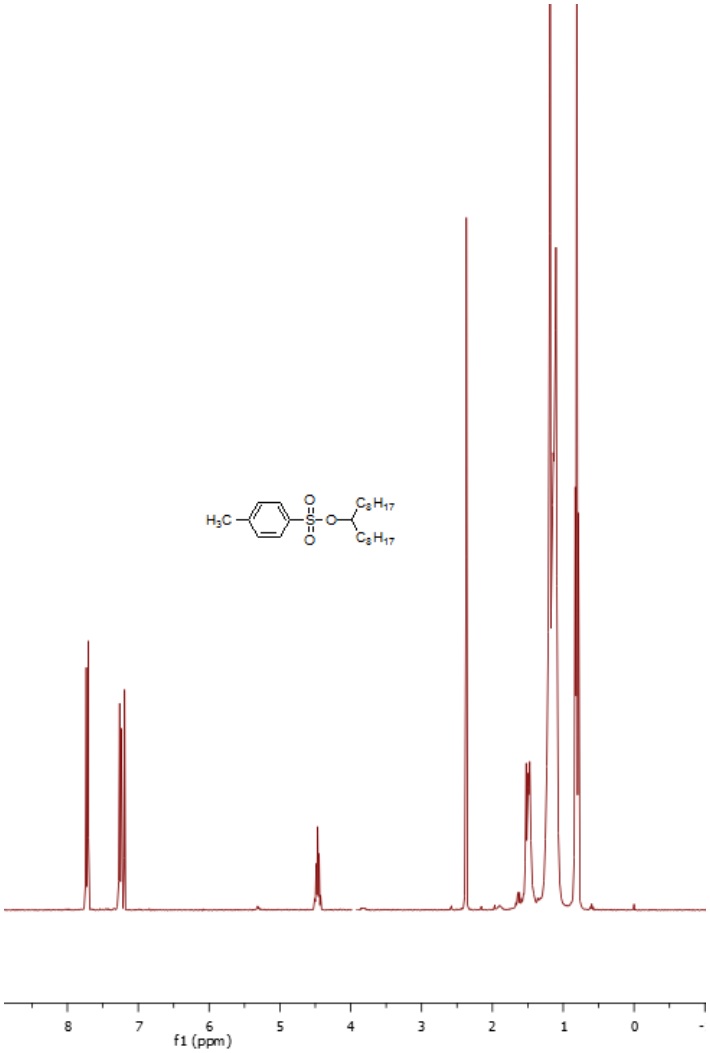
H3C
O
O
O
O
C8H17
C8H17
8
7
6
5
4
3
2
1
0
f1 (ppm)

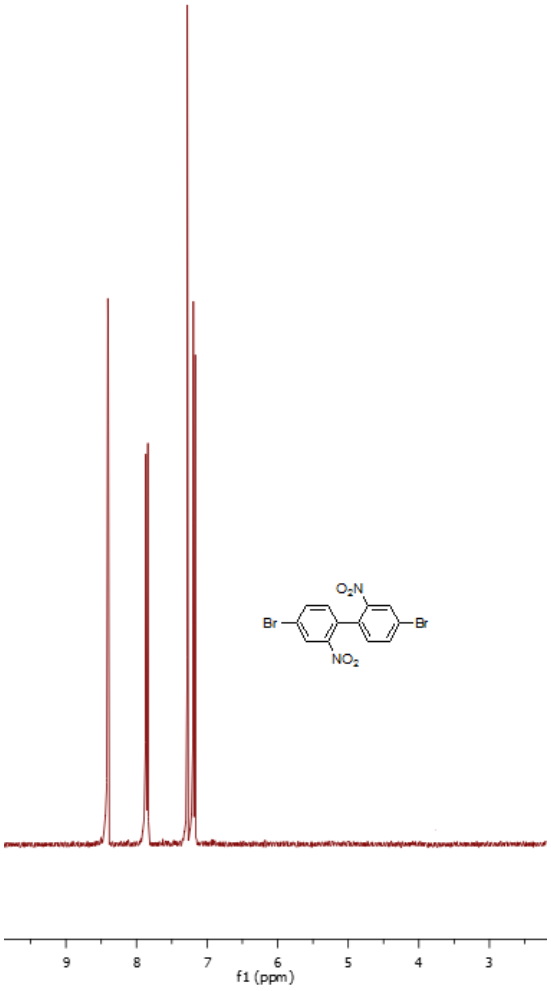
O2N
Br
Br
NO2
9
8
7
6
5
4
3
f1 (ppm)

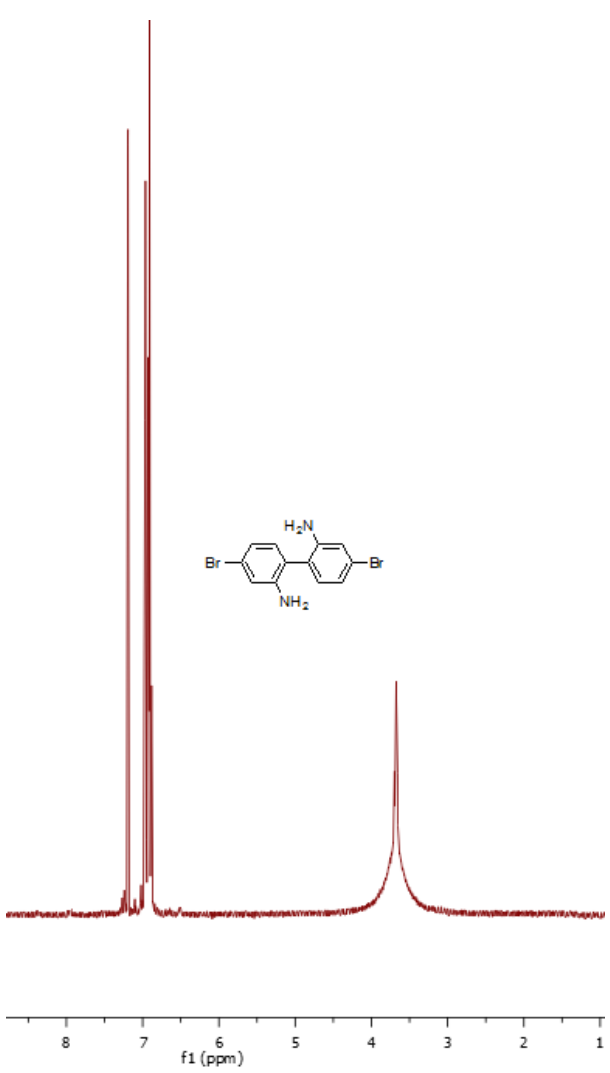
H2N
Br
Br
NH2
8
7
6
5
4
3
2
1
f1 (ppm)

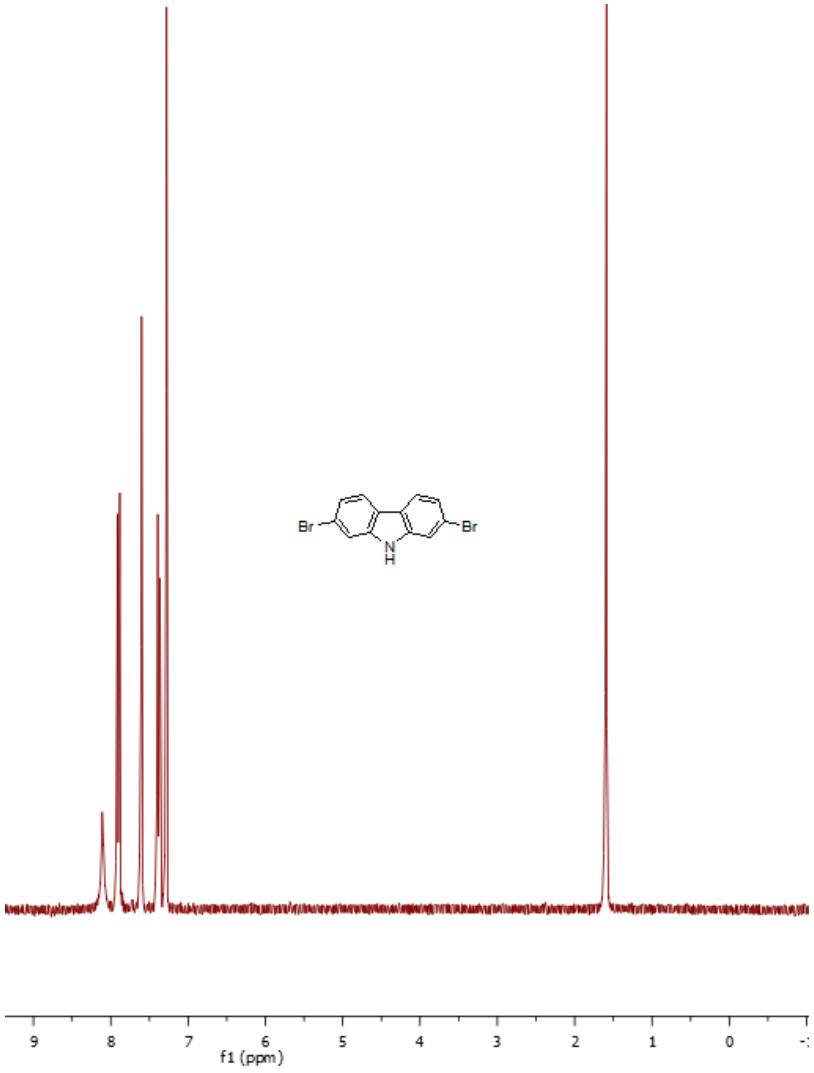
Br
Br
N
H
9
8
7
6
5
4
3
2
1
0
f1 (ppm)

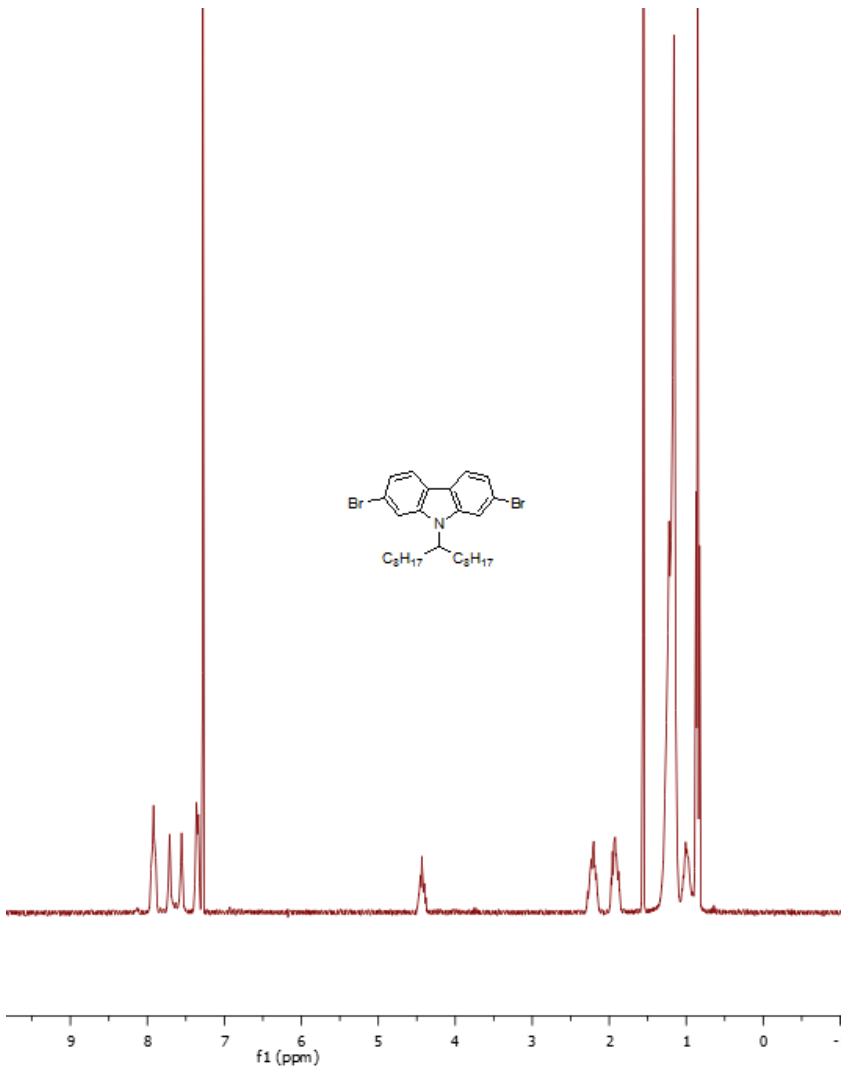
Br
Br
N
C8H17
C8H17
9
8
7
6
5
4
3
2
1
0
f1 (ppm)

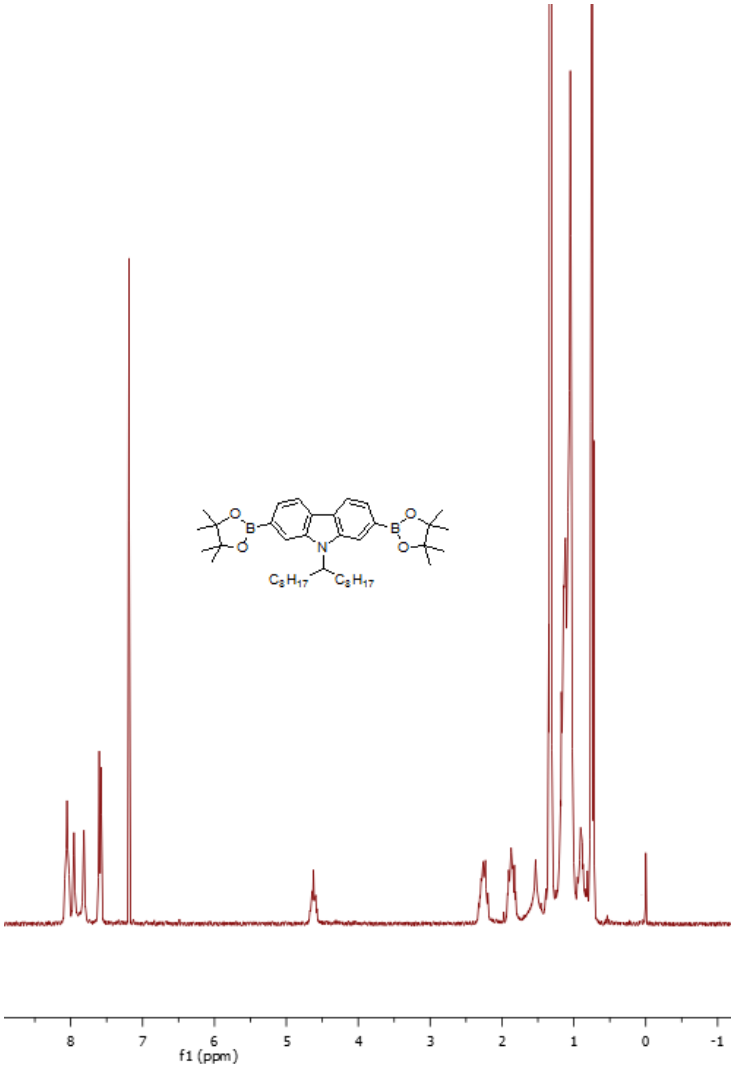
O
B
O
O
B
O
N
C8H17
C8H17
8
7
6
5
4
3
2
1
0
-1
f1 (ppm)

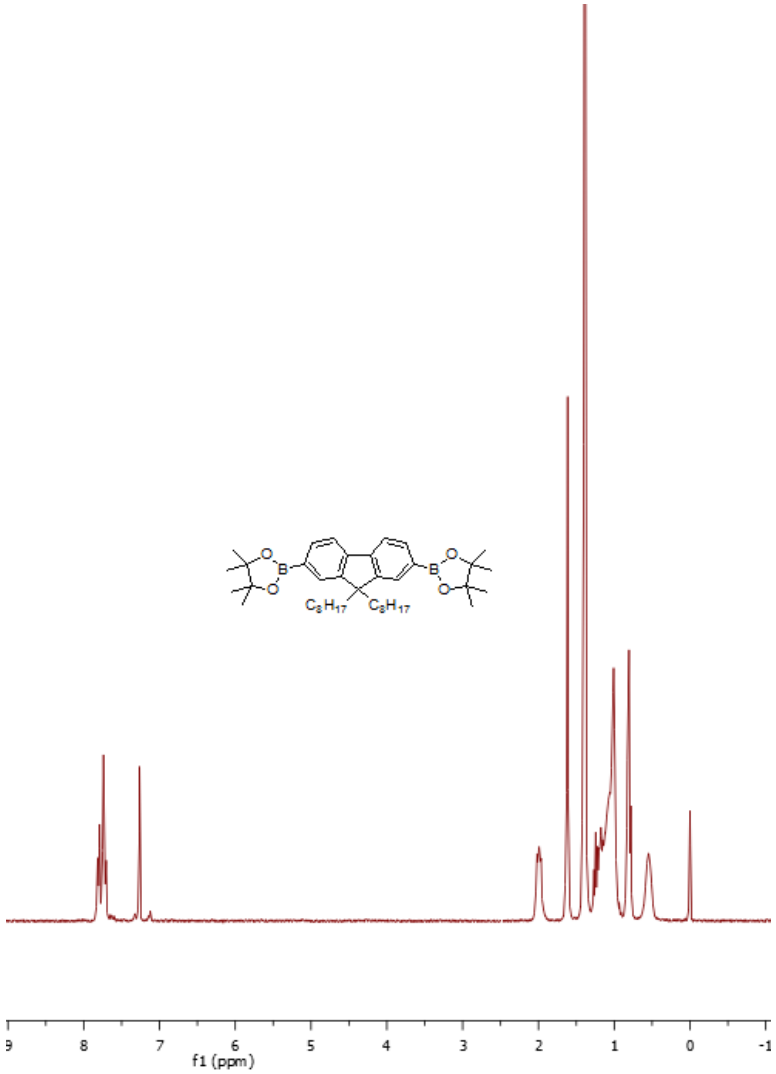
O
B
O
O
B
O
C_8H_{17} C_8H_{17}
9 8 7 6 5 4 3 2 1 0 -1
f1 (ppm)

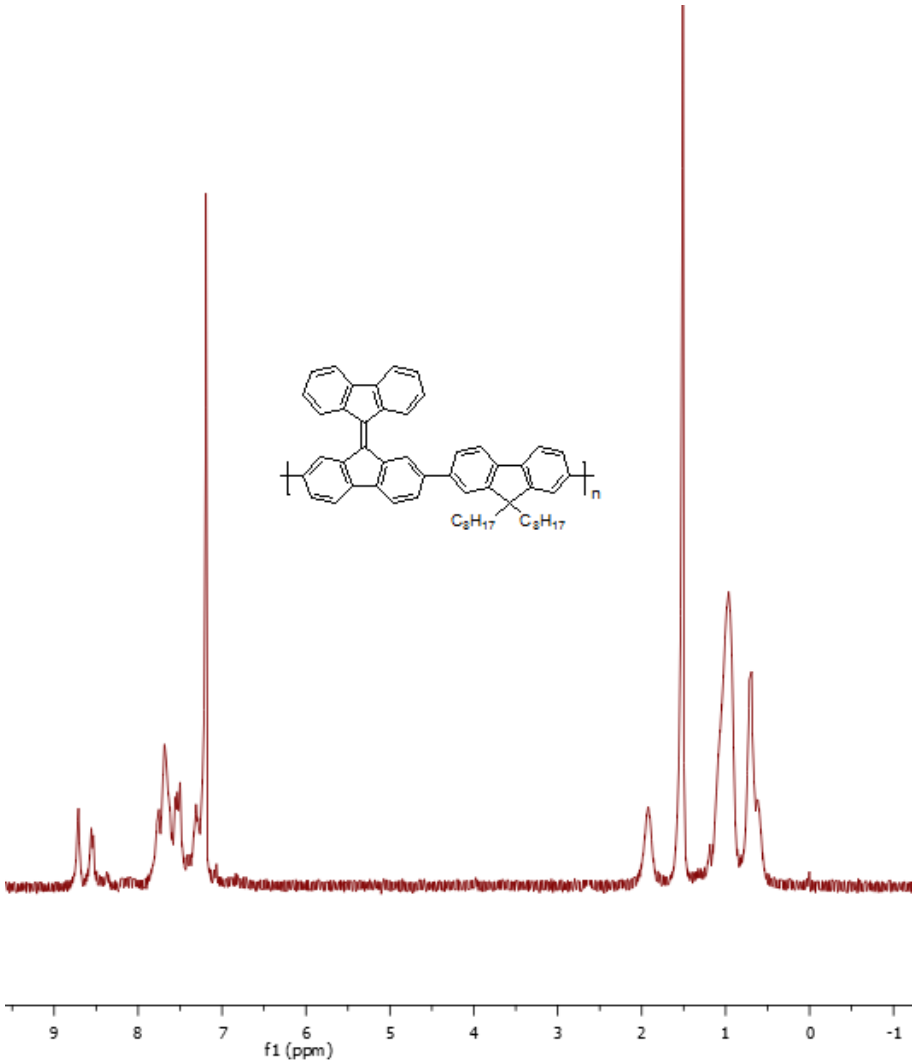
n
C_8H_{17} C_8H_{17}
9 8 7 6 5 4 3 2 1 0 -1
f1 (ppm)

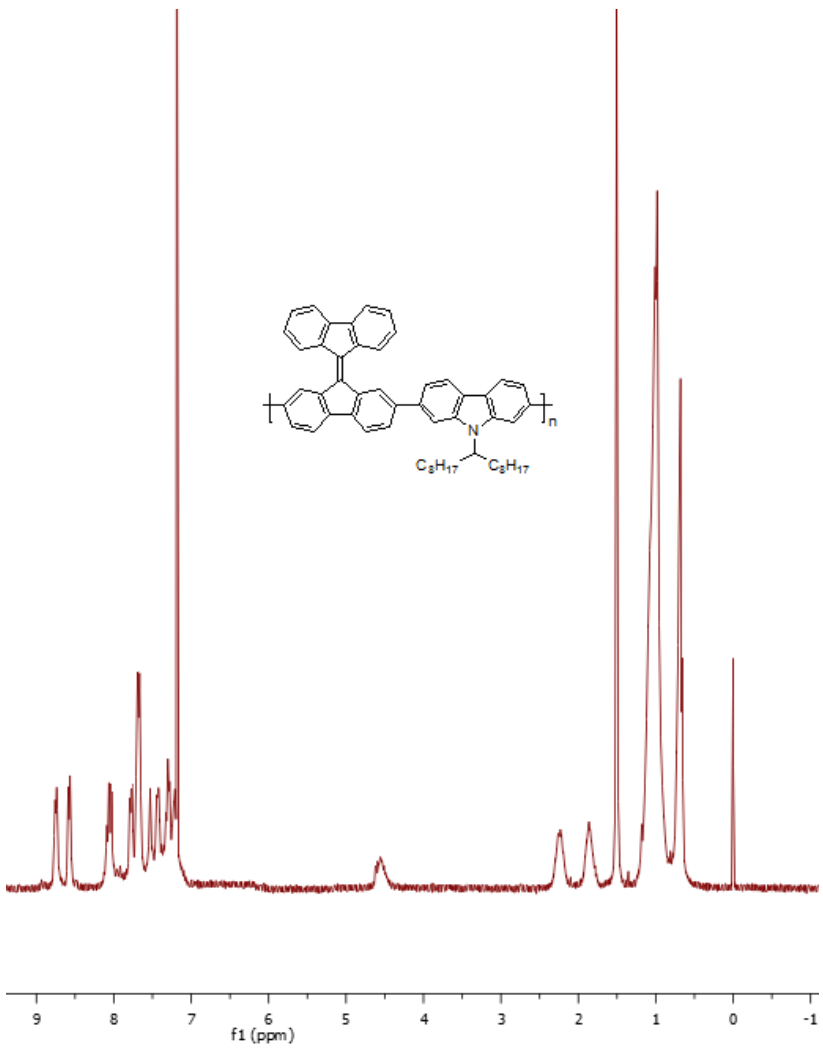
N
C_8H_{17}
C_8H_{17}
n
9
8
7
6
5
4
3
2
1
0
-1
f1 (ppm)

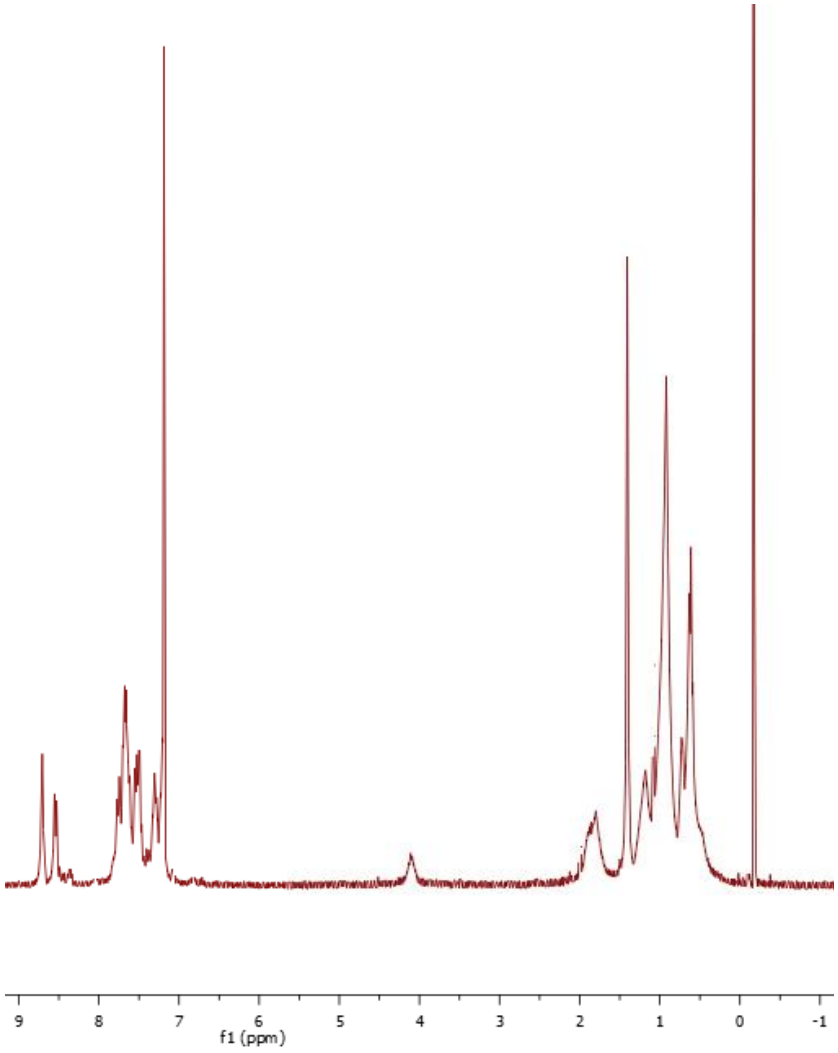
9
8
7
6
5
4
3
2
1
0
-1
f1 (ppm)

NMR spectra of molecules and polymers in Chapter 8

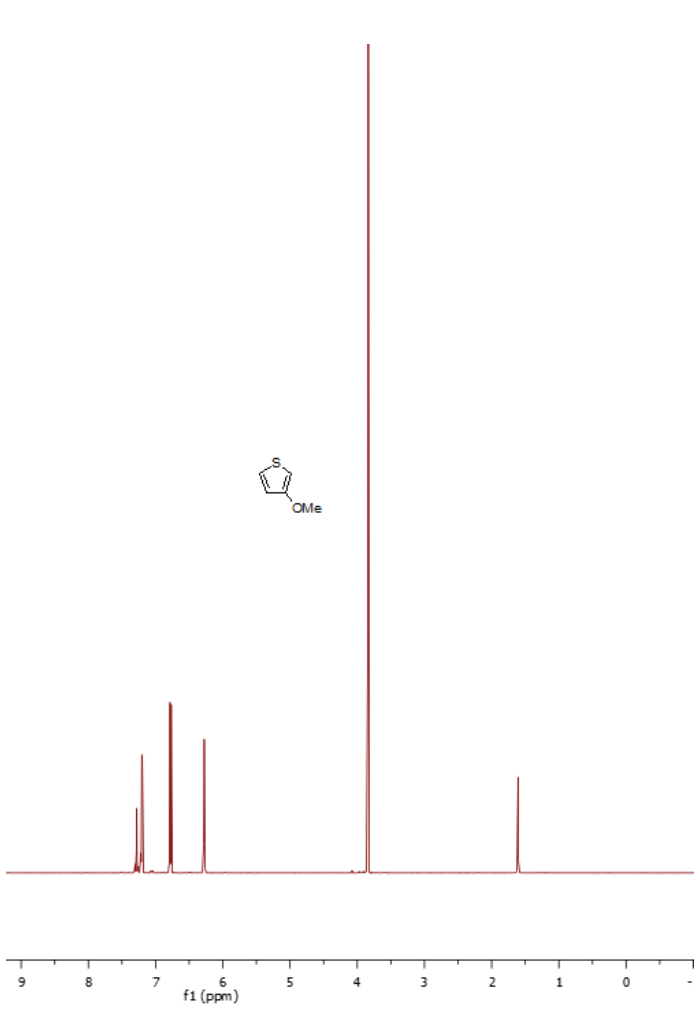
S
OMe
9
8
7
6
5
4
3
2
1
0
f1 (ppm)

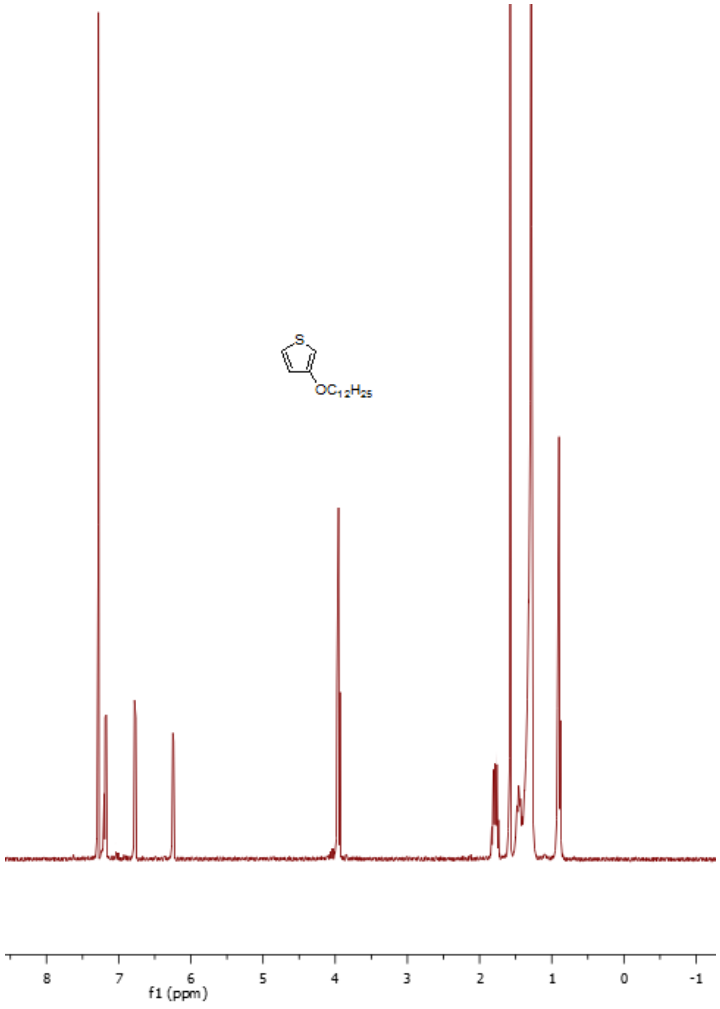
S
OC12H25
8
7
6
5
4
3
2
1
0
-1
f1 (ppm)

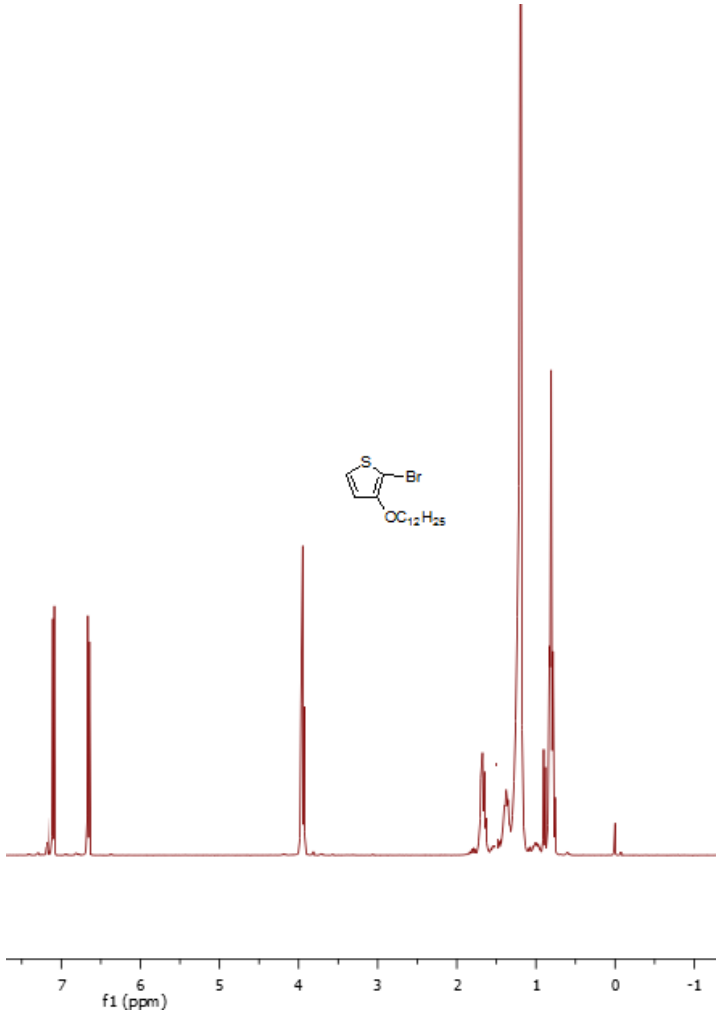
S
Br
OC12H25
7
6
5
4
3
2
1
0
-1
f1 (ppm)

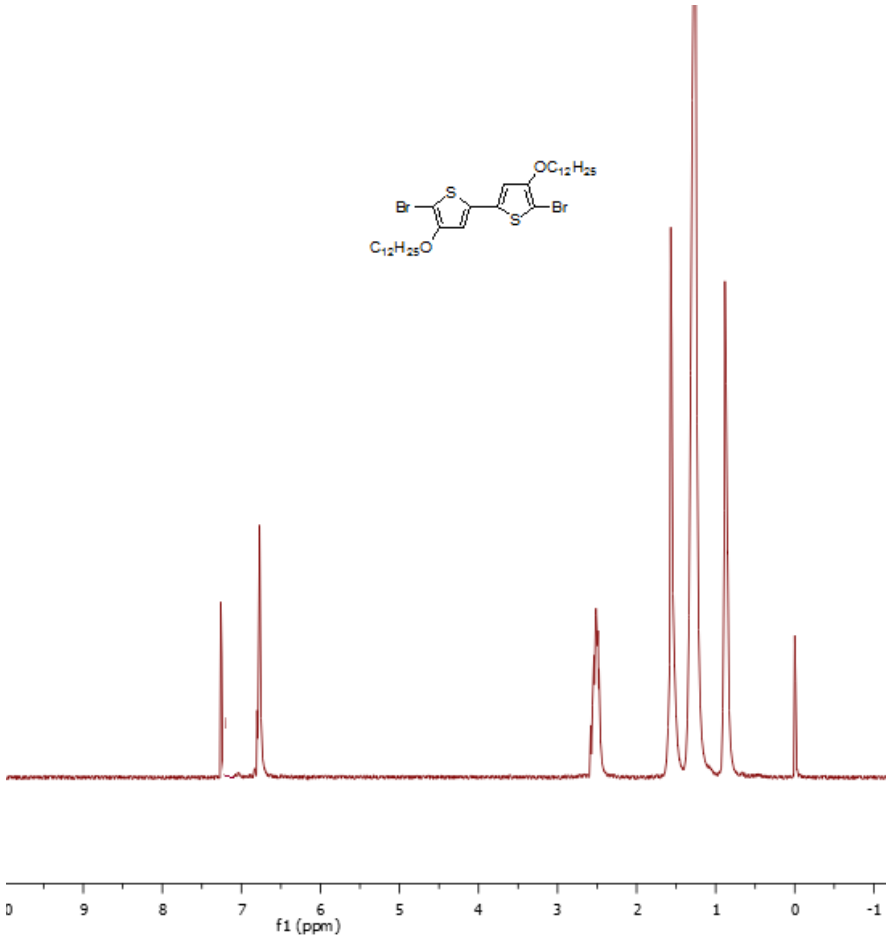
OC12H25
S
Br
Br
C12H25O
S
0
9
8
7
6
5
4
3
2
1
0
-1
f1 (ppm)

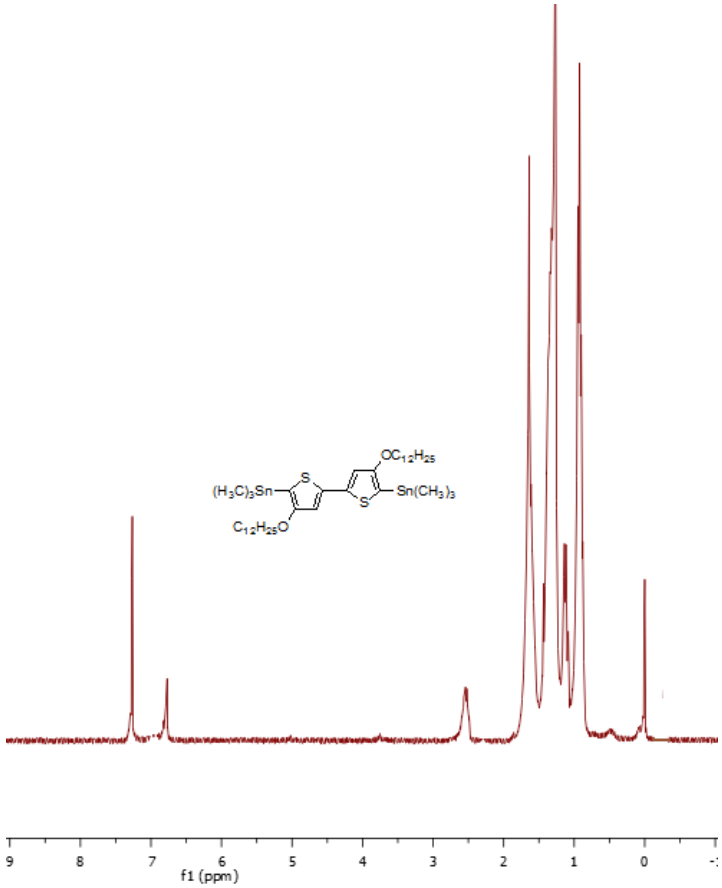
$OC_{12}H_{25}$
$(H_3C)_3Sn$
$Sn(CH_3)_3$
$C_{12}H_{25}O$
S
S
9 8 7 6 5 4 3 2 1 0 -1
f1 (ppm)

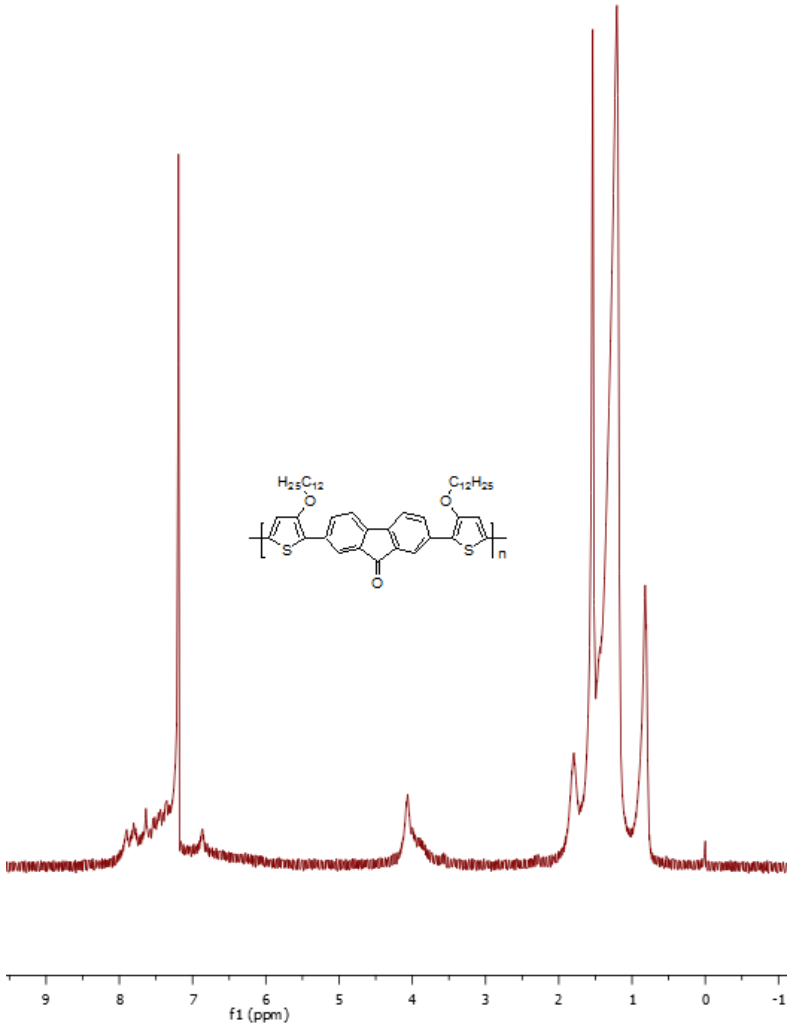
$H_{25}C_{12}$
$C_{12}H_{25}$
O
O
S
S
O
n
9 8 7 6 5 4 3 2 1 0 -1
f1 (ppm)

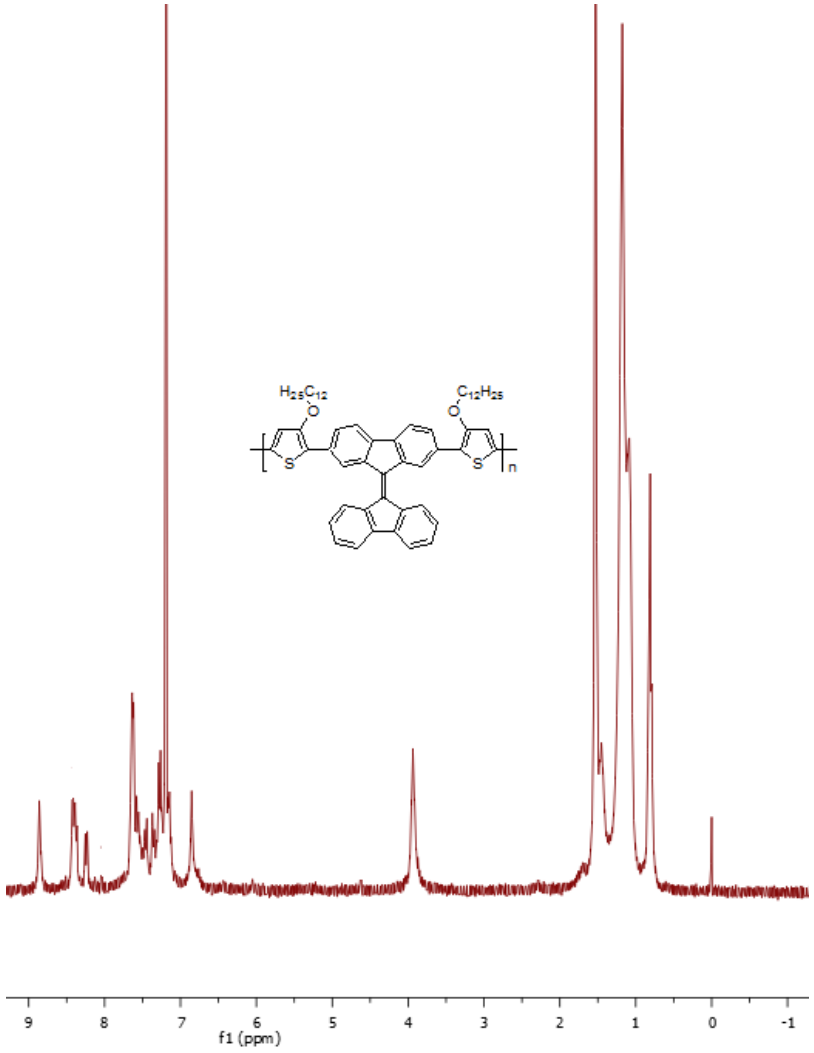
H25C12
O
C12H25
O
S
S
n
9
8
7
6
5
4
3
2
1
0
-1
f1 (ppm)

Appendix II GPC traces of the synthesized polymers

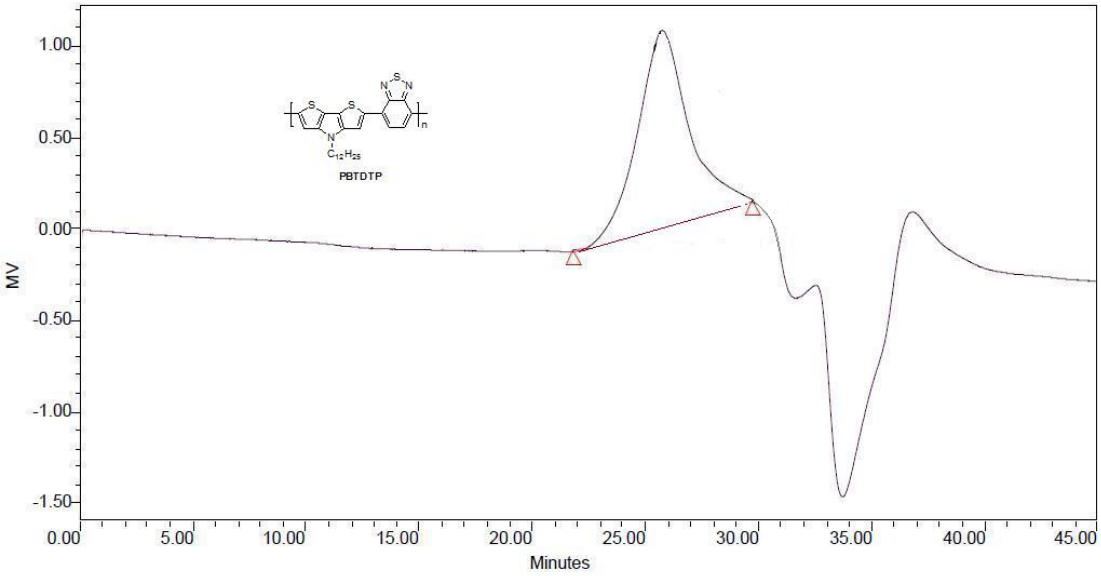

GPC Results

	Dist Name	Elution Volume (ml)	Retention Time (min)	Adjusted RT (min)	Mn	Mw	MP	Mz	Mz+1	Mz/Mw
1		25.687	25.687	25.687	4126	4546	3769	5712	8635	1.256439

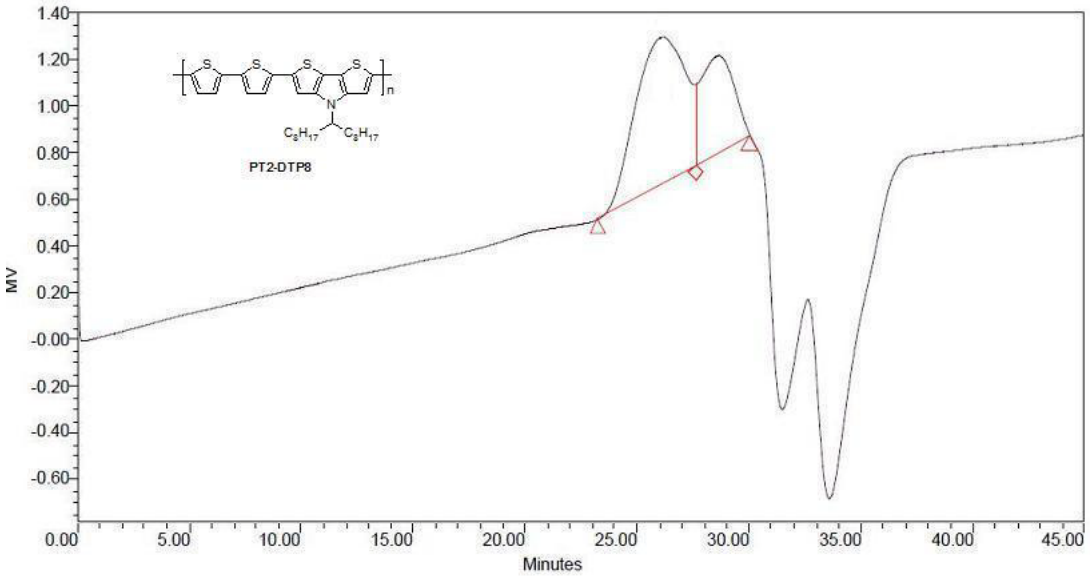

GPC Results

	Dist Name	Elution Volume (ml)	Retention Time (min)	Adjusted RT (min)	Mn	Mw	MP	Mz	Mz+1	Mz/Mw
1		26.017	26.017	26.017	6961	8847	8032	11237	15527	1.270215

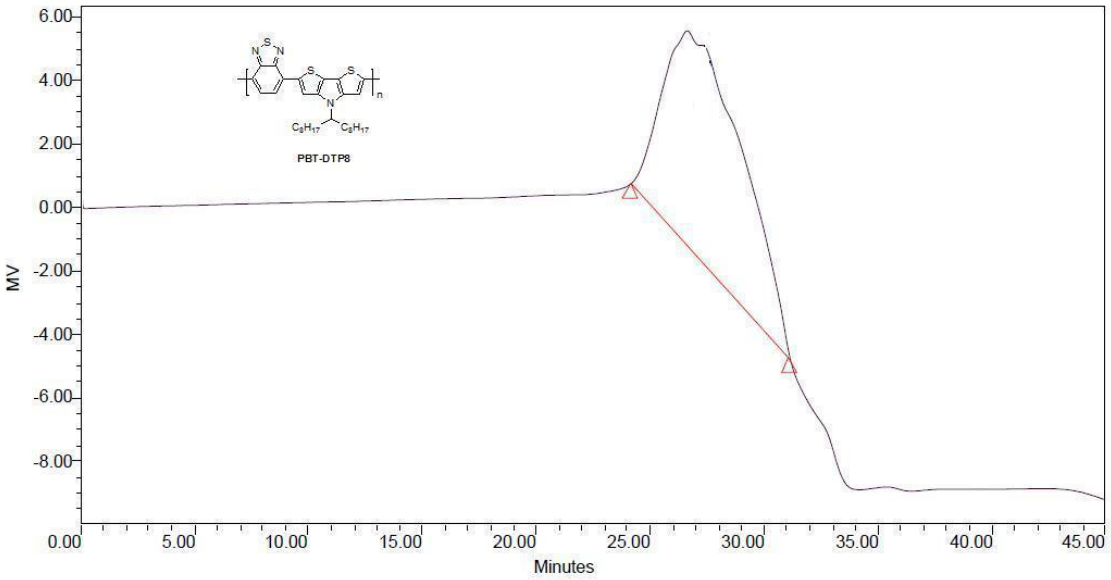

GPC Results

	Dist Name	Elution Volume (ml)	Retention Time (min)	Adjusted RT (min)	Mn	Mw	MP	Mz	Mz+1	Mz/Mw
1		27.333	27.333	27.333	4785	7348	5616	11421	14745	1.555439

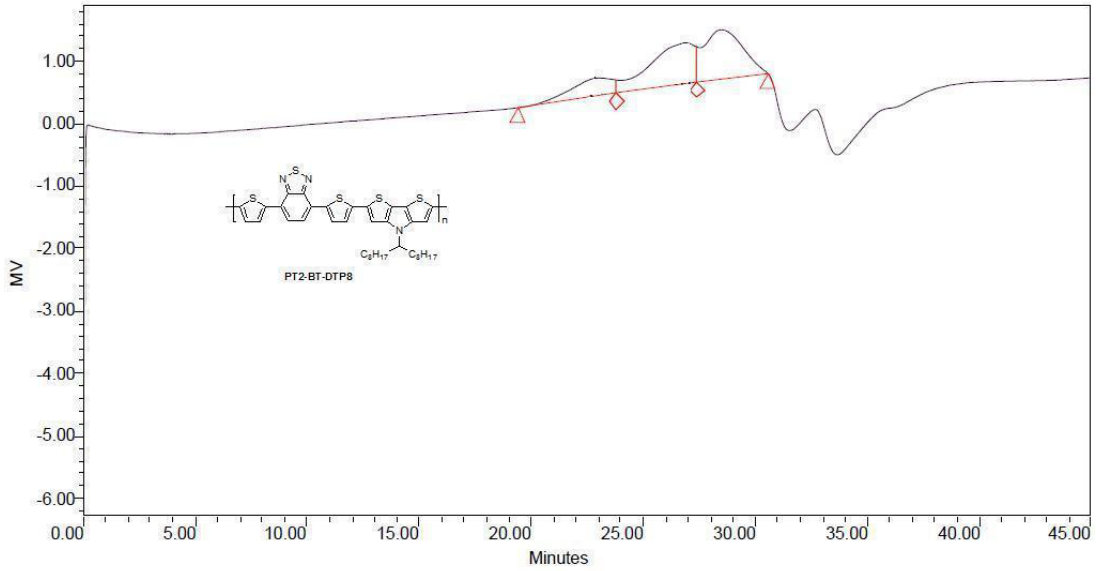

GPC Results

	Dist Name	Elution Volume (ml)	Retention Time (min)	Adjusted RT (min)	Mn	Mw	MP	Mz	Mz+1	Mz/Mw
1		22.800	22.800	14545	21645	19645	15621	26413	33093	1.344538

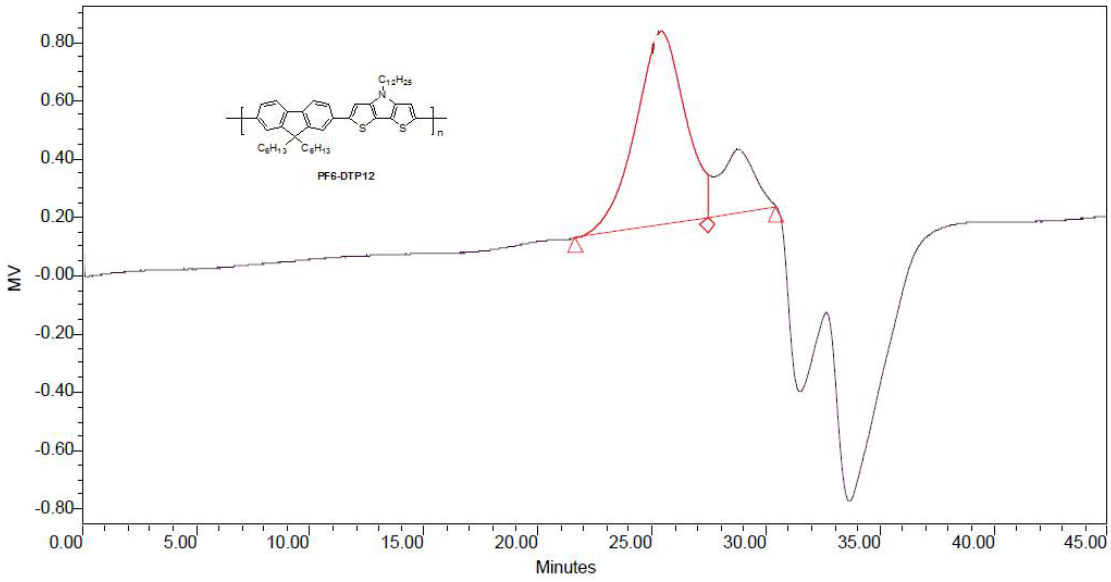

GPC Results

	Dist Name	Elution Volume (ml)	Retention Time (min)	Adjusted RT (min)	Mn	Mw	MP	Mz	Mz+1	Mz/Mw
1		25.317	25.317	25.317	4664	6378	5427	8776	11914	1.375944

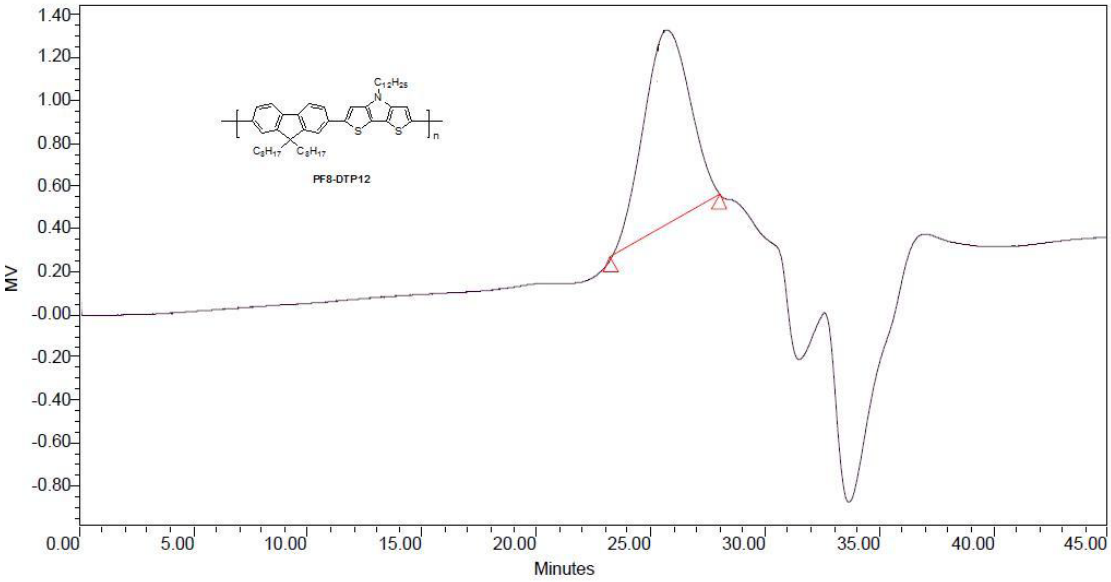

GPC Results

	Dist Name	Elution Volume (ml)	Retention Time (min)	Adjusted RT (min)	Mn	Mw	MP	Mz	Mz+1	Mz/Mw
1		25.583	25.583	25.583	4534	5818	4699	7193	9380	1.236323

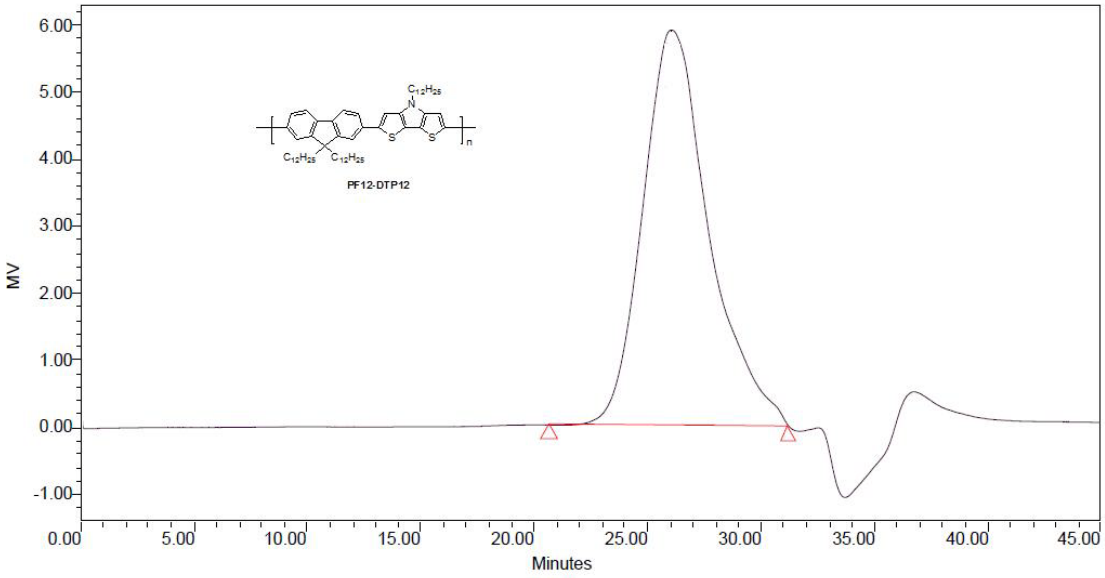

GPC Results

	Dist Name	Elution Volume (ml)	Retention Time (min)	Adjusted RT (min)	Mn	Mw	MP	Mz	Mz+1	Mz/Mw
1		26.017	26.017	26.017	3193	5170	4688	8092	9206	1.565220

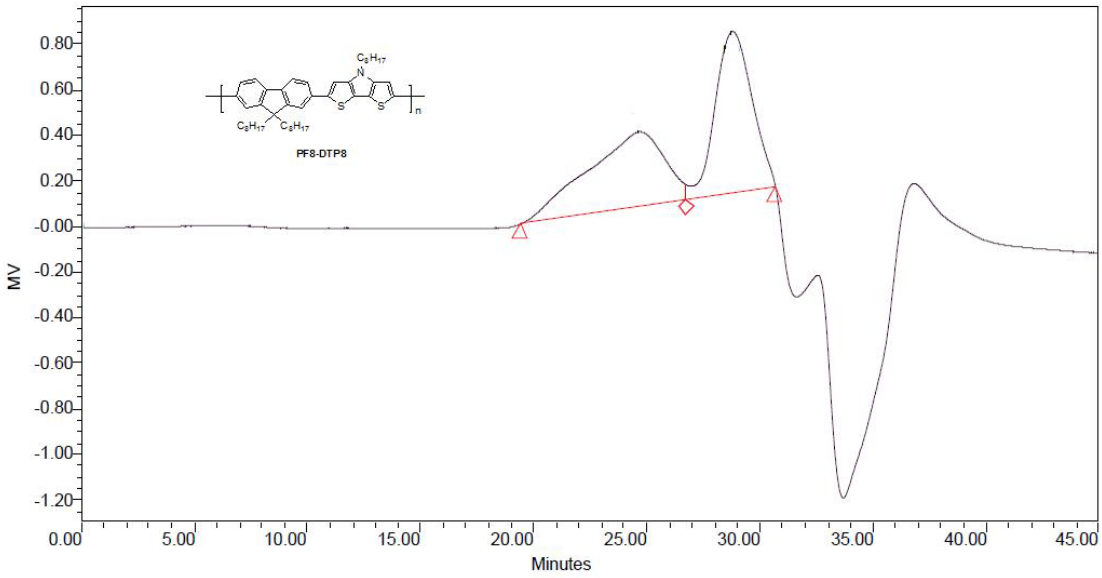

GPC Results

	Dist Name	Elution Volume (ml)	Retention Time (min)	Adjusted RT (min)	Mn	Mw	MP	Mz	Mz+1	Mz/Mw
1		24.600	24.600	24.600	6157	12132	7880	25337	62079	2.088470

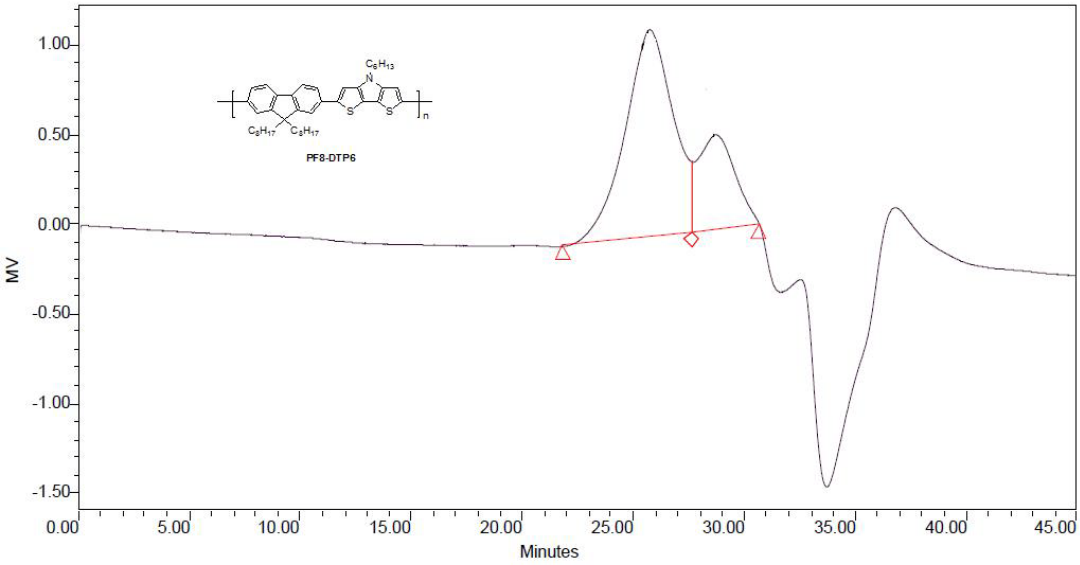

GPC Results

	Dist Name	Elution Volume (ml)	Retention Time (min)	Adjusted RT (min)	Mn	Mw	MP	Mz	Mz+1	Mz/Mw
1		25.687	25.687	25.687	3796	5268	4438	7330	9925	1.391534

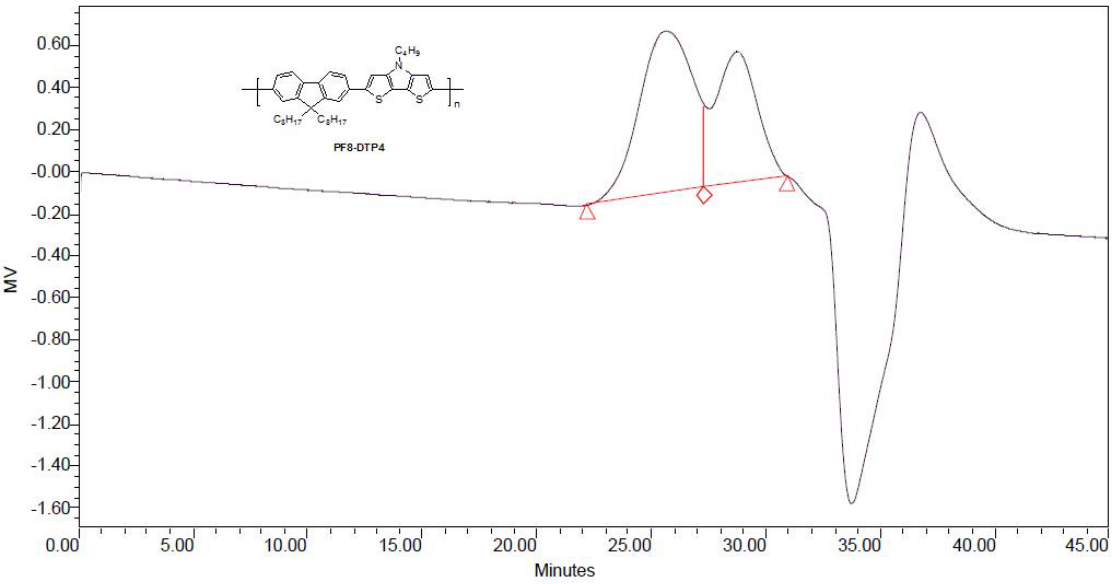

GPC Results

	Dist Name	Elution Volume (ml)	Retention Time (min)	Adjusted RT (min)	Mn	Mw	MP	Mz	Mz+1	Mz/Mw
1		25.500	25.500	25.500	4066	5429	4917	7257	9413	1.336624

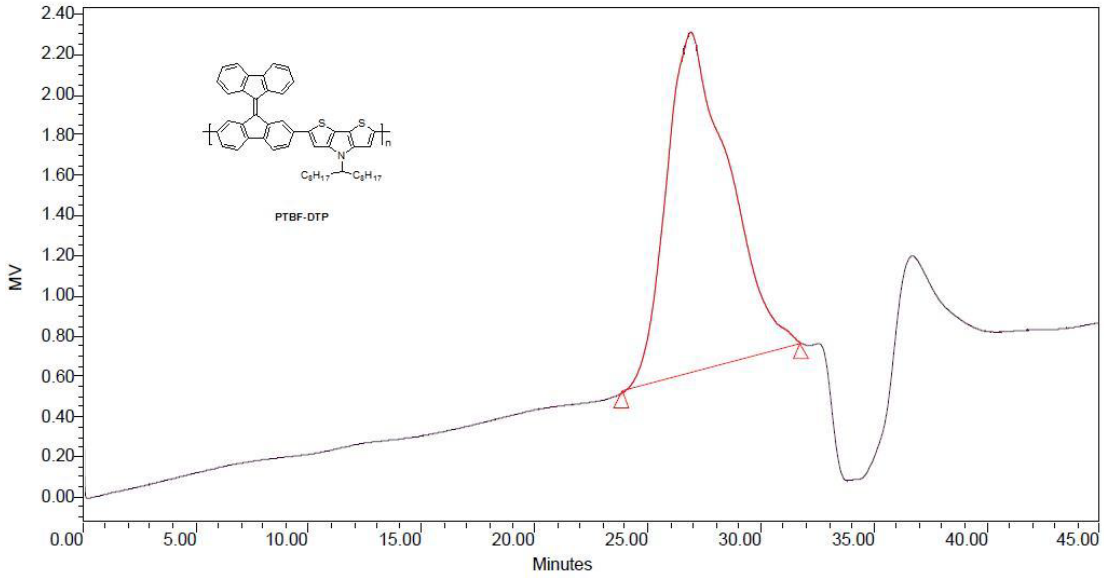

GPC Results

	Dist Name	Elution Volume (ml)	Retention Time (min)	Adjusted RT (min)	Mn	Mw	MP	Mz	Mz+1	Mz/Mw
1		26.833	26.833	26.833	4762	6786	5952	9934	14332	1.464767

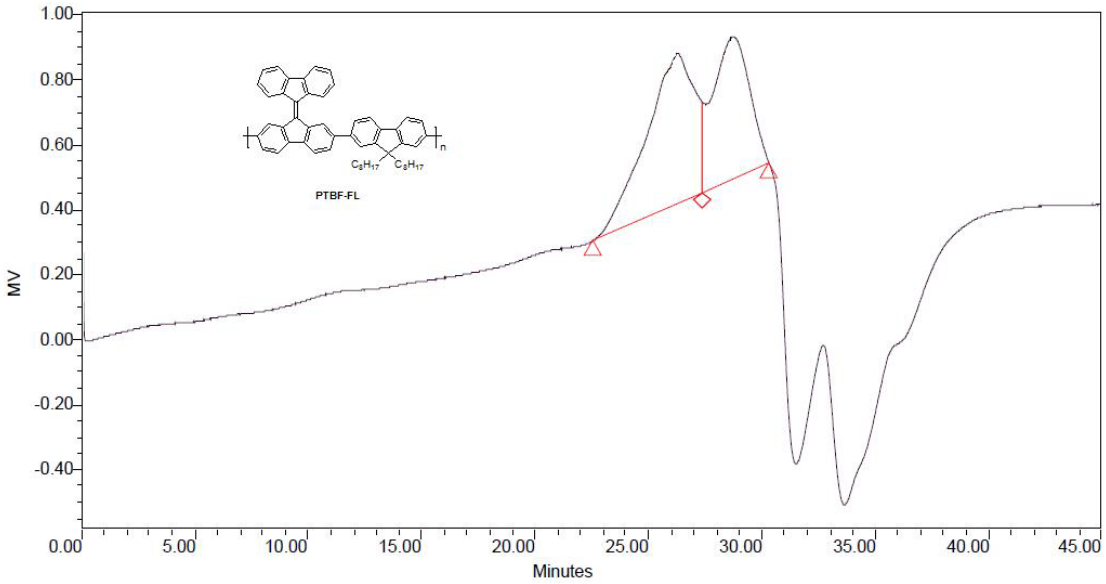

GPC Results

	Dist Name	Elution Volume (ml)	Retention Time (min)	Adjusted RT (min)	Mn	Mw	MP	Mz	Mz+1	Mz/Mw
1		26.183	26.183	26.183	7335	8528	7749	11815	14032	1.385406

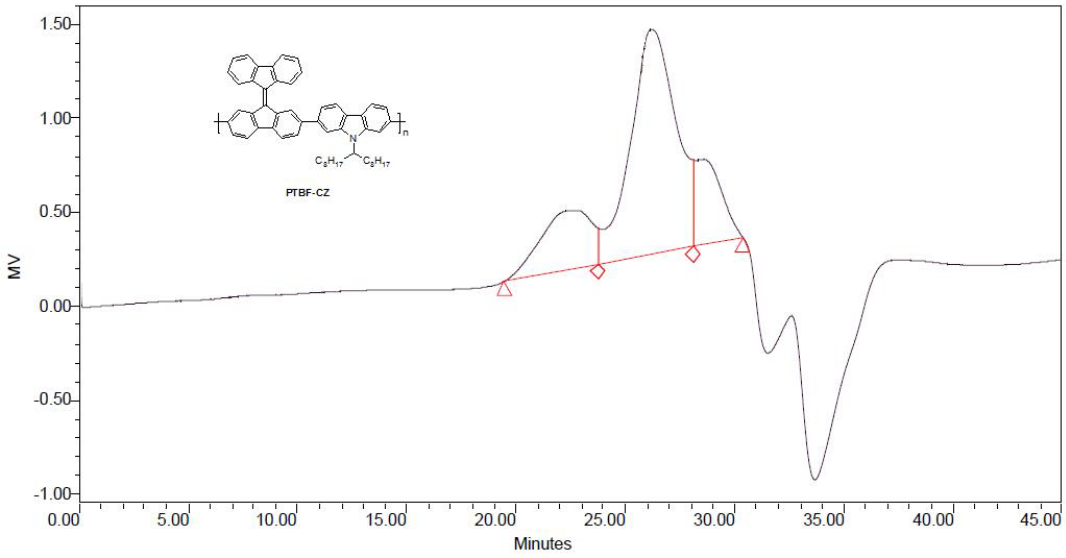

GPC Results

	Dist Name	Elution Volume (ml)	Retention Time (min)	Adjusted RT (min)	Mn	Mw	MP	Mz	Mz+1	Mz/Mw
1		22.250	22.250	22.250	7311	8325	7599	11312	14508	1.358882

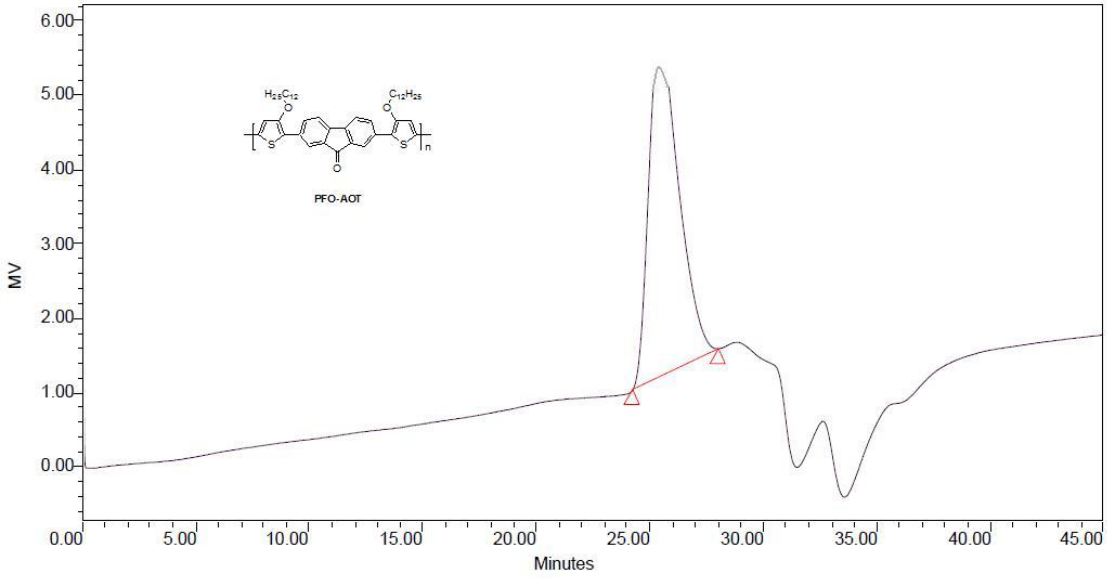

GPC Results

	Dist Name	Elution Volume (ml)	Retention Time (min)	Adjusted RT (min)	Mn	Mw	MP	Mz	Mz+1	Mz/Mw
1		23.546	23.546	23.546	9336	11535	9231	13675	16785	1.185462

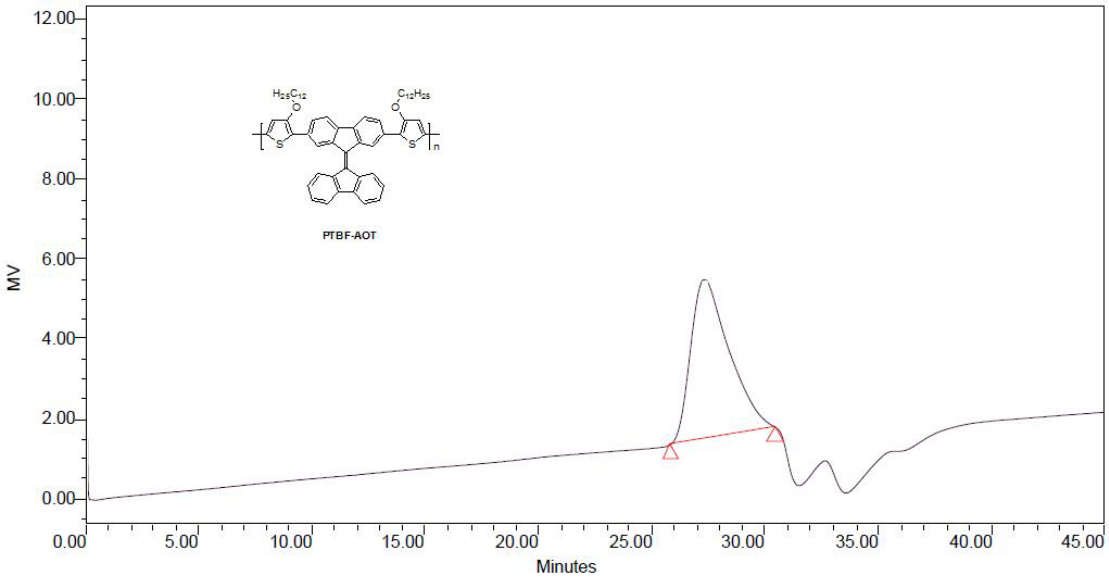

GPC Results

	Dist Name	Elution Volume (ml)	Retention Time (min)	Adjusted RT (min)	Mn	Mw	MP	Mz	Mz+1	Mz/Mw
1		24.788	24.788	24.788	6128	8539	7738	11345	14862	1.562832